THE UNIVERSITY OF CHICAGO

IDENTIFYING LOCOMOTOR ADAPTATIONS IN THE HOMINOID CLAVICLE AND THE IMPLICATIONS FOR INTERPRETING HOMININ BEHAVIOR

A DISSERTATION SUBMITTED TO

THE FACULTY OF THE DIVISION OF THE BIOLOGICAL SCIENCES

AND THE PRITZKER SCHOOL OF MEDICINE

IN CANDIDACY FOR THE DEGREE OF

DOCTOR OF PHILOSOPHY

GRADUATE PROGRAM IN INTEGRATIVE BIOLOGY

BY

HANNAH NICOLE FARRELL

CHICAGO, ILLINOIS

JUNE 2024

For my parents,

with your love and support anything is possible.

“One tiny step at a time. Baby steps.”

- *What About Bob? (1991)*

Contents

List of Figures

List of Tables

Acknowledgments

This dissertation would not have been possible without the kindness and support of so many people – thank you.

To my advisor, Zeray Alemseged, thank you for taking a chance on a timid undergraduate and for helping me grow into the confident researcher I am today. From my first day in the lab, you have encouraged me to think independently and find my own 'niche' within paleoanthropology. Thank you for creating an environment where I was encouraged to explore methods you were not always familiar with, and where I always felt comfortable to ask for help. Your guidance (and patience) over the last five years has been invaluable, and I feel incredibly fortunate to have you as a mentor.

Thank you to my committee, Callum Ross, Zhe-Xi Luo, and Zewdi Tsegai for your unwavering support throughout these last five years. Callum, thank you for always making me feel like a welcomed member of the Ross lab. Being able to sit in during lab meetings and learn from the research projects your lab was working on inspired me to think more broadly about how to investigate form and function. Luo, thank you for being impressed with how fast and efficiently I can CT scan bones and for always giving your honest opinion about my figure aesthetics – these beautiful figures are for you. Zewdi, despite joining the team a couple of years later than everyone else, you have taught me so much. Thank you for showing me how to batch process my trabecular data, the real reason why this dissertation was able to be completed in five years, and for being an incredible mentor as I applied for fellowships.

To my lab mates, thank you for making work feel like a second home. Yared, thank you for showing me the ropes. It was intimidating to join such a small, quiet lab but you made me

feel welcomed right away. Maddie and Laura, thank you for the yearly AABA slumber parties, coffee hours, endless laughs, many public outreach events, and the occasional well-aimed jab and/or frivolous argument. You three are truly the best 'lab siblings' I could have asked for. To the wonderful postdocs I overlapped with during my time in the lab, Dr. Peter Stamos, Dr. Faye McGeechie, and Dr. Austin Lawrence, thank you for always being willing to share your nuggets of wisdom. Whether I was freaking out about my first conference talk, how to cold email an intimidating faculty member, or even getting through these last few months – you have all guided and supported me along this journey. Last, but not least, I must say a humungous thank you to our lab manager Rebecca. You have CT scanned for me, 3D printed bones, and solved almost every tech issue I have come across in the last three years – a simple thank you is not enough; you are amazing, and I hope you know it.

Thank you to so many OBA faculty and staff, who helped me troubleshoot chapters, pay bills, and get the important paperwork done. Specifically, thank you to Audrey Aronowsky for all your help with everything from A to Z during this dissertation. And thank you to the IB, CEB, and EE students that I have had the pleasure of getting to know over these last five years.

To all of my collaborators and colleagues, thank you for supporting my research. Thank you for your assistance with CT scanning (April Neander, Greg Lin, Heiko Temming, and Gideon Chinamatira), extant specimen access (Marisa Surovy, AMNH; Christine Bailey, CMNH; Adam Ferguson, Bruce Patterson, and Larry Heaney, FMNH; Darrin Lunde and Megan Viera, USNM; Mark Omura, Harvard MCZ; Roman Wittig and Catherine Crockford, Taï Chimpanzee Project; Tracy Kivell and Philipp Gunz; MPI), and access to fossil hominin data (Bernhard Zipfel, Yohannes Haile-Selassie, and Lee Berger). Thank you also to the National

Science Foundation, the Leakey Foundation, Margaret and Will Hearst, the Committee on Evolutionary Biology Hind's Fund, and the Alemseged Lab for funding this research.

The road to completing this dissertation was not always easy, so I must thank my friends and family (and my therapist) for their continuous emotional support. Thank you to Alec Wilken and Emily Hillan for listening to me kvetch over a pitcher of Miller High Life at Jimmy's, going on Broadway adventures with me, and for just always being there when I needed it. Alec also deserves a special shout out for the countless hours he spent with me running the analyses for Chapter 4 (and checking it for errors at the last minute) – I am eternally grateful for your friendship. Beyond the office, I must also thank my amazing friends Alannah, Tara, Wyatt, Leslie, and Sophia. Thank you to Alannah and Tara for never getting mad at me for not responding to their texts and for our biannual facetimes where we pretend like no time has passed at all; to Wyatt for reminding me what a little inspiration can do to change someone's life – I cannot wait to celebrate you next; to Leslie for supporting my dreams since we were 16 years old working at Starbucks and I was saving up with the hope of going to college; and to Sophia for being my first friend in Chicago and creating the core memory of walking 14 miles down a flat trait in Joliet while waiting for my dog to be done at the vet.

Finally, to my family – my parents, husband, in-laws, and pup. Thank you for always listening, even if you did not always understand what I was talking about. This is for you.

Abstract

One of the hallmarks of the emergence of hominins is a transition to bipedalism, but debates continue on the importance of arboreal behaviors including climbing trees for food, shelter, and safety during and after this evolutionary transition. The australopithecines, a diverse group of early hominins living in Africa from 4.2 to 1.98 million years ago, exhibit a mosaic of novel lower limb adaptations tied to bipedality and largely primitive upper limb features, providing a unique opportunity to explore the evolving role of the upper limb and shoulder as hominins became obligate bipeds. To assess the integrated function of the shoulder, I explore the morphology of the clavicle in living hominoids via four approaches: a 3D geometric morphometrics analysis of shape throughout ontogeny, quantification of diaphysis cross-sectional geometry through ontogeny, an investigation of trabecular structure in adults, and identifying how morphological variation affects bone strain during locomotion using finite element modeling. The fossil hominins *Australopithecus afarensis* (KSD-VP-1/1; DIK-1-1), *Australopithecus africanus* (StW 431g; StW 573f, StW 582), *Australopithecus sediba* (UW 88-38), and *Homo naledi* (UW 101-258; UW 101-1229) were then analyzed and compared to the extant apes. Together, the results from all analyses stress the importance of continued arboreality and support extending hypotheses of locomotor diversity amongst the early, habitually bipedal hominins to include variation in arboreal behaviors. No fossil individuals included show the same combined trend in cortical geometry, trabecular structure, and external shape, but the similarities and differences amongst them most likely reflect the impact of the surrounding environmental conditions on locomotor behavior. The results presented here also provide a potential explanation for why modern humans and chimpanzee clavicles are so alike despite very

different uses of the upper limb and positioning of the shoulder girdle. Analyses considering external shape (Chapters 1 and 4) highlight the evolutionary time and magnitude of imposed bone strain it takes to cause external changes in clavicle shape. Additionally, since the release of the upper limb from strictly locomotor demands likely decreased the magnitude of strain habitually faced by the clavicle, any modification in clavicular morphology reflective of this transition are identifiable in the internal structure of the bone (Chapters 2 and 3) long before any changes in external shape. In sum, this research has provided novel insight into the locomotor regime of *Australopithecus*, supporting arboreal behaviors as a critical component of daily life and highlighting the variation in upper limb loading even between relatively contemporaneous hominins. Most importantly, the results presented here provide evolutionary context for the similarity between modern human and chimpanzee clavicular morphology, allowing for a better interpretation of the fossil material moving forward.

Introduction

The evolutionary history of vertebrates is full of monumental functional transitions preserved in the fossil record. Over the last 400 million years, vertebrates have moved from water to land, changed their limb posture from sprawling to parasagittal, and become obligate bipeds at least once depending on one's own definition of obligate bipedality. But these transitions did not happen instantaneously nor was there directionality, resulting in fossil taxa that exhibit a mixture of morphological traits related to both adaptations, making it difficult to categorize them into distinct groups. This complicates our understanding of the relationship between form and function especially in the fossil record as we do not always have modern analogues for the combinations of morphological traits observed in fossil taxa. Hominins are no exception to this. For these reasons, locomotor adaptations in early hominins and the role of the upper limb and shoulder have long been of interest to paleoanthropologists as the group's mosaic morphology combines primitive features (so called ape-like) hypothesized to be indicative of arboreal behaviors whereas derived traits (human-like) suggesting increased use of bipedalism.

It is widely accepted that *Australopithecus* was habitually bipedal when terrestrial (Stamos and Alemseged, 2023). The taxon displays numerous derived musculoskeletal modifications indicating directional selection for bipedality such as an anteriorly placed foramen magnum, a short, broad, and robust weight bearing pelvis, and a pronounced bicondylar angle at the knee, among others (Ward, 2013). However, these same australopiths also possess higher intermembral and brachial indices, longer and more curved phalanges, an ape-like semicircular canal, and a more cranially oriented glenoid of the scapula – all traits that are encountered in suspensory apes and therefore are suggested to be primitive retentions from a more arboreal ancestor (Ward, 2013). In *Australopithecus afarensis*, in particular, the combination of largely

novel traits in the pelvis, lower limb, and the foot indicative of habitual bipedalism (*sensu* Stamos and Alemseged, 2023) and ape-like features in the upper limb and shoulder potentially implying arborealism has led to unresolved debate regarding the nature and extent of the latter in the species.

Current disagreement over the functional significance of the ape-like morphology in the upper limb of *Australopithecus* has led to questions regarding both the use of arboreal behaviors as a component of daily life and the adaptive significance of those behaviors. Some view the persistence of these 'ancestral' traits as evidence of their continued and significant use – by which continued arboreal behaviors (e.g., sleeping, sourcing food, avoiding predators) positively impacted fitness via stabilizing selection (Jungers, 1982; Jungers and Stern, 1983; Stern and Susman, 1983; Stern, 2000; Green and Alemseged, 2012; Kappelman et al., 2016; Ruff et al., 2016; Stamos and Alemseged, 2023). Stamos and Alemseged (2023) make a convincing argument in favor of stabilizing selection as one of the mechanisms behind the preservation of the ape-like traits. They suggest that given the clear craniodental morphological diversity in *Australopithecus* that emerges over the course of about 2 million years, the fact that similar changes are not seen in the climbing-related morphology supports the traits as targets of stabilizing selection. Moreover, the retention of primitive traits over such a length of time alongside clear directional selection towards bipedality makes it difficult to conclusively disprove their adaptive value (Ward, 2002; Stamos and Alemseged, 2023). Others argue that the primitive features were non-adaptive retentions occurring alongside morphological traits clearly indicative of strong directional selection for bipedality at the expense of arboreality (Lovejoy et al., 1973; Latimer et al., 1987; Lovejoy, 1988; Latimer and Lovejoy, 1989; Ward, 2002, 2013; Harcourt-Smith and Aiello, 2004).

This enduring debate emphasizes the need to identify morphological features in the hominoid shoulder that can be saliently used to tease out the functional significance of the so-called ape-like features, likely through the application of new methodological approaches to existing extant and fossil taxa. Existing research on the humerus and scapula have highlighted the potential for these new avenues, such as investigating the developmental plasticity of the morphological features (e.g., Green and Alemseged, 2012) and exploring internal bone structure (e.g., Kivell et al., 2018), to further inform our understanding of the form-function relationship in the hominin shoulder. These efforts support the application of such approaches to the remaining elements in the upper limb and shoulder, especially the clavicle. In this dissertation, I perform a multipronged analysis of the hominoid clavicle to establish an integrative framework for exploring locomotor adaptations in both extant apes and fossil hominin, with the explicit objective of contributing to the body of knowledge addressing this long-standing debate and shed light on the role of arboreality in *Australopithecus*.

Our current understanding of the hominin shoulder

The shoulder girdle (clavicle, scapula, and humerus) of *Australopithecus* is often investigated to gain insight into adaptations for arboreality given that shoulder morphology distinguishes extant monkeys from apes and non-human apes from modern *Homo sapiens* (Larson, 2013). Most analyses have found that *Australopithecus* generally had a primitive, ape-like shoulder. In extant apes, clavicular shape is hypothesized to be related to scapular position on the thorax (Voisin, 2006a). In comparison to monkeys, ape clavicles are typically described as longer relative to overall body size which is suggested to be necessary to facilitate their more dorsal scapular position (Le Gros Clark, 1959; Martin, 1986; Ciochon, 1987; Harrison, 1987).

Further, the curvatures in the craniocaudal plane are hypothesized to provide information on scapular position with human clavicles having only a single, inferior curvature related to the low position of the scapula, while non-human apes have a superior curvature to facilitate their higher scapular position (Voisin, 2006; Squyres and DeLeon, 2015; but see Melillo et al., 2019). Clavicular length is also often compared using indices relating it to humeral length (Schultz, 1930) and second rib area (Roach and Richmond, 2015). The claviculohumeral ratio is most commonly used to compare relative clavicle length and it been suggested that there is a common isometric scaling relationship in all primates, likely representing the primitive condition (Larson, 2013). Out of the extant primates, only orangutans and modern humans consistently fall above the linear relationship (Figure 0.1; also see Larson, 2013), suggesting they have a derived condition of longer clavicles than would be expected given their humeral length. In orangutans, this signal is likely being driven by a relatively long clavicle while in modern humans it is the result of short humeri.

Although found in the fossil record, most early hominin clavicles are small fragments, making it difficult to compare their morphology with that of extant apes. Out of the larger known fragments, A.L. 333x 6/9 (Lovejoy et al., 1982), the most complete *Au. afarensis* clavicle, is described to not have the single inferior curvature, which Voisin (2006a) associates with a low scapular position, suggesting a high dorsal scapular position that was likely inherited from the *Pan-Homo* most recent common ancestor. Given that most known fragments contain the lateral curvature of the clavicle, a lot of emphasis has been placed on describing the morphology of the conoid tubercle. Between modern *Pan* and *Homo, Pan* typically has a more flange-like conoid tubercle manifesting as a continuation of the edge where the cranial and dorsal surfaces of the clavicle meet at the lateral curvature. In *Homo,* on the other hand, the conoid tubercle is either

missing entirely or is present as a lump near the dorsal edge of the inferior surface of the lateral curvature. Most *Australopithecus* clavicles are described as having a relatively small or non-existent conoid tubercle, more like the modern human condition (*Au. afarensis*: AL 288-1bz, Johanson et al., 1982; AL 333-94, Lovejoy et al., 1982; *Au. africanus*: StW 431g, Toussaint et al., 2003; StW 582, Partridge et al., 2003; Green, 2020). The one exception is StW 606 which is described as having a pronounced conoid flange as in chimpanzees (Partridge et al., 2003). Despite considerable morphological variation in conoid tubercle placement and pronouncement amongst early hominins, the significance of this diversity remains unclear.

Extant apes are also unlike monkeys in their scapular proportions. Apes have scapulae that are much taller craniocaudally than they are mediolaterally broad, while the opposite is the case in other primates (Ashton and Oxnard, 1964; Roberts, 1974; Young, 2008). The reduced mediolateral breadth in apes may be related to the need for the vertebral column to not impede scapular movement, given the more dorsal position of the scapulae on the thorax relative to monkeys (Roberts, 1974). Another possibility is that the increased craniocaudal length may act to provide more surface area for the attachment of the rotator cuff muscles (Roberts, 1974; however, see Larson and Stern, 2013), critical for both stabilizing the highly mobile shoulder and producing the wide diversity of behaviors the increased range of motion permits. Humans are unique from the other apes in having a relatively small supraspinous fossa and a large infraspinous fossa, potentially reflecting the increased use of medial and lateral rotary movements by modern humans during manipulatory behaviors (Roberts, 1974). The juvenile *Au. afarensis* individual DIK-1-1 has scapulae that are described to be *Gorilla*-like (Alemseged et al., 2006), with a supraspinous to infraspinous fossa length ratio more like extant apes than modern humans (Alemseged et al., 2006; Green and Alemseged, 2012). The orientation of the

scapular spine also distinguishes modern humans from the other apes. Non-human apes tend to have an oblique scapular spine, although not as prominent in orangutans, and the glenoid fossa faces cranially – both features associated with the use of the upper limb in suspensory, overhead postures (Stern and Susman 1983, Larson 2012, Alemseged et al 2006, Ward 2013, 2015). Humans, on the other hand, have a nearly horizontal scapular spine and laterally facing glenoid fossae. All known early hominin fossils have ape-like cranially oriented glenoid fossae (*Au. afarensis*: AL 288-11, Stern and Susman, 1983; DIK-1-1, Alemseged et al., 2006; KSD-VP-1/1g, Melillo, 2016; *Au. africanus*: Sts 7, Green, 2020; *Au. sediba*: UW88-56, Berger et al., 2010; U.W. 101-1301 (Feuerriegel et al., 2017) and all but KSD-VP-1/1g display ape-like oblique scapular spines (Green and Alemseged, 2012; Melillo, 2016).

More extant ape-like features in the *Australopithecus* shoulder are found in the humerus. Apes have a bony ridge separating the insertion sites for the infraspinatus and supraspinatus muscles on the greater tubercle, while modern humans have a relatively continuous region of attachment for the two muscles. An ape-like bony ridge has been described in *Au. africanus* (Sts7, Robinson, 1972), *Au. afarensis* (AL 288-1r., Johanson et al., 1982; AL 333-107, Lovejoy et al., 1982), and *Au. sediba* (Churchill et al., 2013, 2018), but a human-like surface has been described in *Homo naledi* (U.W. 102a-257, Feuerriegel et al., 2019). Humeral torsion also varies amongst the apes. Only African great apes and modern humans have a high degree of humeral torsion; lesser apes have a low degree of torsion and orangutans are somewhere intermediate (Evans and Krahl, 1945; Larson, 1988, 2013). Such high humeral torsion in modern humans is hypothesized to have evolved in response to a more habitually medially rotated arm posture during the manipulation of objects, and in apes it is argued to be necessary to facilitate the sagittal elbow orientation required during knuckle walking (Larson, 2013). Interestingly, fossil

hominins have a relatively low degree of humeral torsion, suggesting that high torsion evolved in the hominin lineage recently and is convergent with the condition seen in extant African apes. This absence of torsion in early hominins has been used as evidence against the hypothesis that the most recent common ancestor of humans and chimpanzees was a knuckle walker that has been championed by many (Senut, 1985; Sarmiento, 1994; Gebo, 1996; Richmond and Strait, 2000; Richmond et al., 2001; but see Kivell et al, 2006).

Overall, the early hominin shoulder girdle has retained many features considered to represent the ancestral condition, and therefore largely resembles extant apes. The combination of traits described in the *Australopithecus* clavicle, scapula, and humerus suggest these hominins had a highly positioned scapula on a funnel shaped thorax. Moreover, their shoulder morphology suggests that early hominins maintained adaptations for arboreal locomotion such as cranially oriented glenoid fossae, dorsal scapulae with fossae that are still ape-like in size, and obliquely oriented clavicles (Stern and Susman, 1983; Green and Alemseged, 2012; Larson, 2013). Although some early hominin humeri are described as having a shallow bicipital groove, more like modern *Homo*, they also notably lack many of the derived features that distinguish modern humans and later *Homo* from apes. Given that the derived features are suggested to be related to the release of the upper limb from locomotor demands and its more frequent use to manipulate objects, and hominins were at least habitually bipedal by about 4 million years ago (Stamos and Alemseged, 2023), it is notable that their shoulder morphology appears to hold no signal of the functional shift and further underscores the potential functional relevance of the primitive traits.

The clavicle as a source of new information

The clavicle is developmentally unique amongst the elements comprising the shoulder. It is the only long bone to ossify intramembranously via its primary ossification centers, and endochondrally at the epiphyses (O'Rahilly and Gardner, 1972; Ogata and Uhthoff, 1990; Black and Scheuer, 1996). Additionally, it is one of the first bones to ossify *in utero* (Ogata and Uhthoff, 1990) and the last to fully fuse its epiphyses in modern humans (Black and Scheuer, 1996), suggesting the bone may have a larger window in which to plastically respond to environmental stimuli.

Moreover, despite being positioned far from direct contact with the substrate, the clavicle is critical in shoulder stability during locomotion. The ape clavicle is commonly described as a bony strut that keeps the highly mobile shoulder propped away from the thorax (Mivart and Huxley, 1867; Schultz, 1930; Howell, 1937; Ljunggren, 1979; Barros, 2014) yet the documented external morphological variation amongst primates (Figure 0.2, Ashton and Oxnard, 1964; Voisin, 2006) suggests the shape may be optimized for certain locomotor regimes or shoulder configurations. As the only bony articulation between the upper limb and thorax, the clavicle contributes greatly to the range of motion available to the scapula and therefore the upper limb during locomotion (Figure 0.3; Levangie and Norkin, 2011). The clavicle is also an attachment site for powerful arm flexors, medial rotators, and head stabilizers used during hominoid locomotion (Figure 0.4). In most apes, the deltoid, trapezius, and pectoralis major muscles all have heads that originate on the clavicle (Swindler and Wood, 1973; Diogo and Wood, 2011, 2012). There are minor variations amongst the apes regarding how far medially or laterally an attachment region stretches, but the only significant difference is that in *Pongo* the pectoralis major only attaches to the sternum and not the clavicle (Diogo and Wood, 2011; Diogo et al., 2013b). Moreover, electromyography (EMG) analyses have demonstrated the activity of these

muscles during knuckle walking (Tuttle and Basmajian, 1978; Larson and Stern, 1987), suspension (Larson and Stern, 1986; Larson et al., 1991), and vertical climbing (Larson and Stern, 1986; Larson et al., 1991).

The relatively understudied nature of the clavicle further makes it an interesting source of new insight into osteological correlates of locomotor behavior. Its external morphology has only been quantitatively compared in a few studies (Voisin, 2006a; Barros, 2014; Squyres and DeLeon, 2015), but there is still ambiguity around the functional significance of the variation in curvature amongst extant hominoids. Other types of morphological analyses, made possible with the increasing accessibility to novel imaging techniques, may contribute to a better understanding of the form-function relationship in the ape clavicle. Because the clavicle is a long bone (Black and Scheuer, 1996), functionally relevant traits can be discerned through the investigation of its structural properties via the quantification of its cross-sectional geometry (Ruff and Runestad, 1992; Ruff et al., 2006; Habib and Ruff, 2008; Kilbourne and Hutchinson, 2019; Parsi-Pour and Kilbourne, 2020). The cortical geometry of a long bone can also provide insight into the bending and torsional loads incurred by the element (Ruff and Runestad, 1992; Ruff et al., 2006). Additionally, there is a trabecular network running through the entire diaphysis in most ape clavicles (Harrington et al., 1993), meaning the trabecular structure can also be explored in relation to locomotion as has become increasingly popular in form-function analyses (e.g., Shaw and Ryan, 2012; Ryan and Shaw, 2013; Tsegai et al., 2013, 2017, 2018; Kivell, 2016; Kivell et al., 2018; Dunmore et al., 2020, 2023). Furthermore, the clavicle's robusticity allows for relatively good preservation in the fossil record. Fragmentary clavicles have been associated with hominin taxa as old as *Ar. ramidus*, are present amongst *Australopithecus*, and increase in number in the younger taxa.

In this dissertation, I include eight fossil hominin clavicles representing four different species and two genera (*Au. afarensis, Au. africanus, Au. sediba,* and *H. naledi*). A review of the description and current interpretations of each can be found below. Ultimately, if features in the clavicle are demonstrated to be relevant to interpret locomotion, we will be better positioned to explore the link between form and function and to address the aforementioned debate regarding the significance of arborealism in early hominins.

A review of fossil hominin clavicles included in this dissertation (Table 0.1; Figure 0.5)

Australopithecus afarensis

DIK-1-1 (Alemseged et al., 2006; Farrell and Alemseged, 2023): both the left and right clavicles associated with the DIK-1-1 juvenile partial skeleton (est. 2.5 years old, Gunz et al., 2020). The right clavicle measures approximately 67.8 mm and the left measures 68.2 mm. Both have taphonomic damage around the lateral curvature, slightly altering curvature in that region, but generally the shape of the element is intermediate of *Pan* and *Homo*.

KSD-VP-1/1f (Haile-Selassie et al., 2010; Melillo, 2016): most of a left clavicle estimated to have originally measured 156 mm and is associated with the KSD-VP-1/1 partial skeleton. Its length most closely aligns it with modern *Homo*.

Australopithecus africanus

StW 431g (Berger, 1994; Toussaint et al., 2003; Green, 2020): lateral half of a right clavicle measuring approximately 71.5 mm and is associated with the StW 431 skeleton, an adult individual. The specimen is described to have an enlarged deltoid ridge and poorly developed conoid tubercle.

StW 573f (Carlson et al., 2021): a complete right clavicle measuring 142.9 mm associated with the 'Little Foot' skeleton. The clavicle is described as absolutely long and has a high claviculohumeral ratio exceeding that of all apes except orangutans. Curvatures in the dorsoventral plane are described as most like *Pan*, while those in the craniocaudal plane are intermediate of *Pan* and *Homo*. Although attributed by some to *Australopithecus prometheus*, here this specimen is grouped with *Au. africanus* in line with other interpretations of the 'Little Foot' morphology as within the potential range of intraspecific variation of *Au. africanus* (Alemseged, 2023).

StW 582 (Green, 2020): 70 mm of a right clavicle with most of the medial and lateral curvature preserved. Both the conoid tubercle and deltoid crest are described as weak.

Australopithecus sediba

UW 88-38 and UW 88-142 (Churchill et al., 2013, 2018): two fragments that together represent a complete right clavicle associated with the MH2 adult partial skeleton. They are described as both relatively and absolutely short, and relatively gracile. The curvatures and morphology of the sternoclavicular joint surface suggest the clavicle was obliquely oriented and the shoulder sat high on the thorax. The deltoid crest is described as more anteriorly oriented like in modern humans, but the conoid tubercle is prominent and flange-like similar to *Pan*.

Homo naledi

UW 101-258 (Feuerriegel et al., 2017): right clavicle midshaft fragment measuring 63.3 mm. The deltoid crest is described as sharp and anteriorly placed, and the conoid tubercle is prominent and centrally located on the inferior aspect of the diaphysis.

UW 101-1229 (Feuerriegel et al., 2017): partial right clavicle formed from several refitted fragments totaling 73.1 mm when assembled. A small portion of the sternal metaphysis is preserved, but even though the sternal epiphysis is not present this element is presumed to belong to an adult individual. The subclavian groove is described as a distinct sulcus and there is a groove on the inferior aspect assumed to eventually lead to where the conoid tubercle would have been.

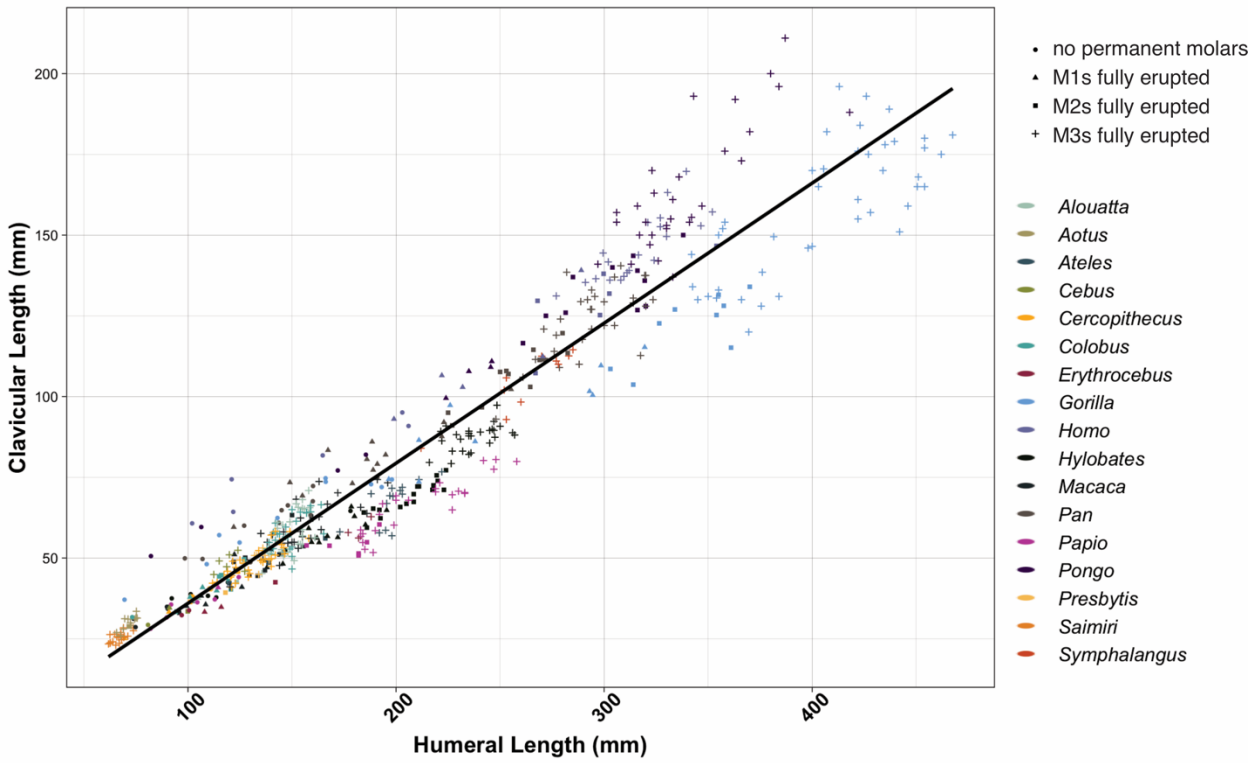

Figure 0.1. Claviculohumeral ratio measured in seventeen primate taxa (*Alouatta, Aotus, Ateles, Cebus, Cercopithecus, Colobus, Erythrocebus, Gorilla, Homo, Hylobates, Macaca, Pan, Papio, Pongo, Presbytis, Saimiri,* and *Symphalangus*). The shape of the point on the plot represents the age group of the individual, and the color of the point indicates the genus. All data was collected by H.N. Farrell.

Figure 0.2. External shape variation in the extant hominoid clavicle. The clavicles are viewed from ventral on the left and cranial on the right. The lateral end is always on the left, and medial end on the right.

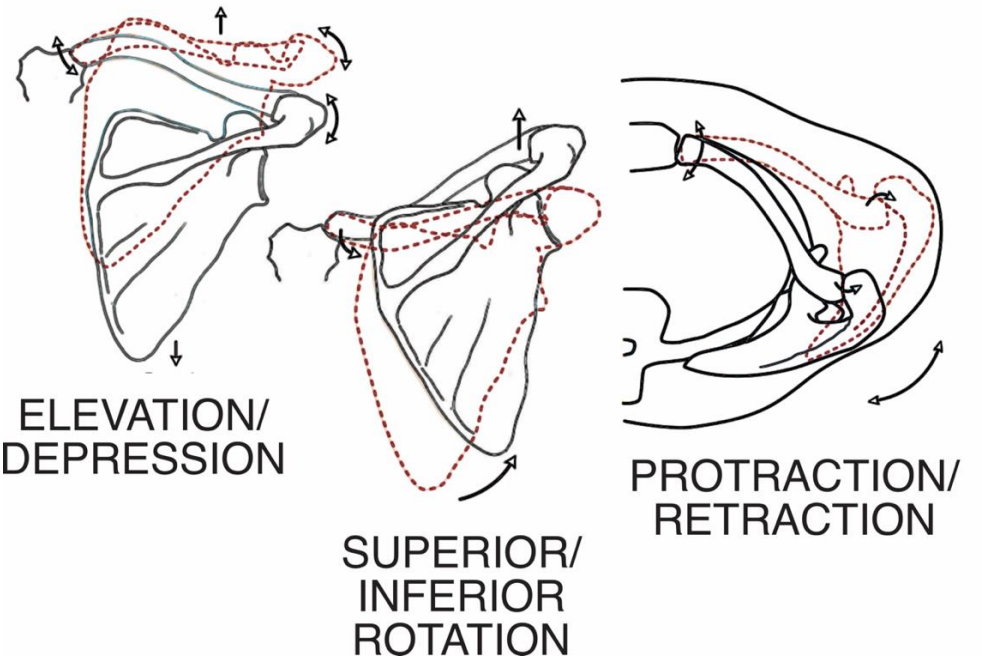

Figure 0.3. Clavicular contributions to scapular motion.

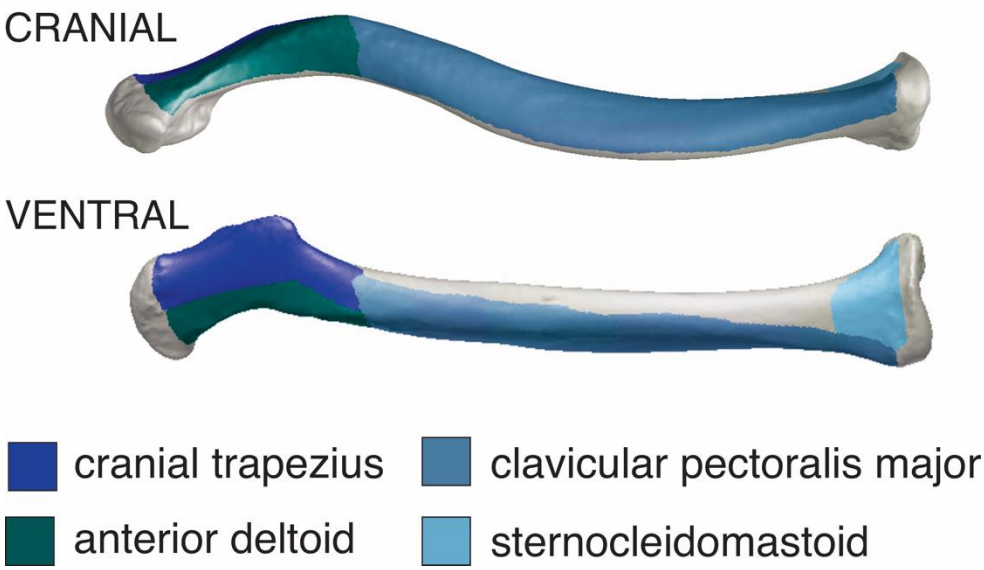

Figure 0.4. External shape variation in the extant hominoid clavicle. The clavicles are viewed from ventral on the left and cranial on the right. The lateral end is always on the left, and medial end on the right.

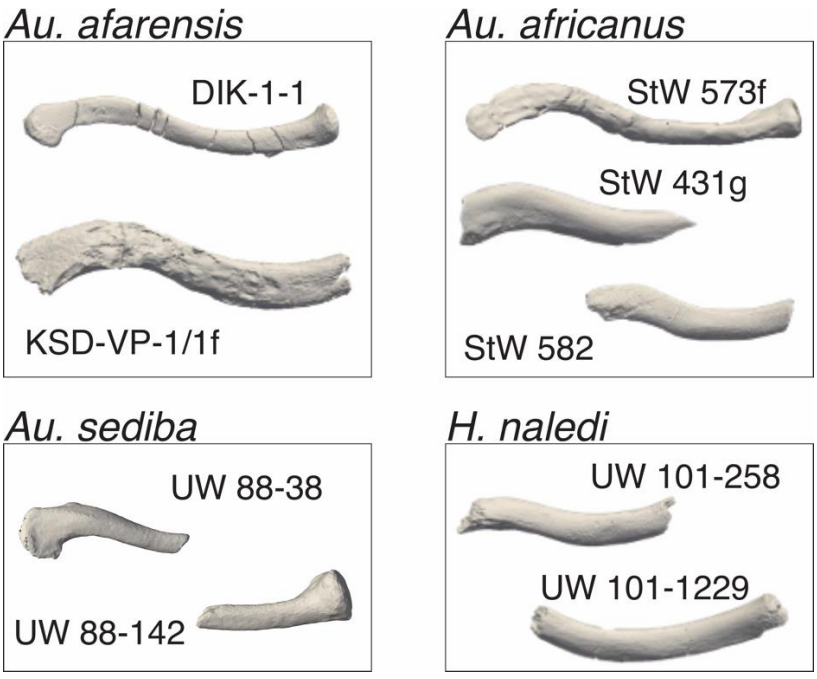

Figure 0.5. Fossil specimens included in this dissertation grouped by hypothesized taxonomic affiliations, viewed from above (cranial).

Table 0.1. Geologic provenance and estimated dates for fossil hominin taxa included in this dissertation. The references are for the geologic site information and estimated dates, not necessarily for the original fossil description.

Fossil Specimen	Site	Date	Reference
DIK-1-1	Sidi Hakoma Member of the Hadar Formation	3.31 – 3.35 MA	Alemseged et al., 2006
KSD-VP-1/1f	Korsi Dora vertebrate locality 1, Woranso-Mille	3.6 – 3.58 MA	Haile-Selassie et al., 2010
StW 431g	Sterkfontein Member 4, Bed 2, from Q/45 21'11"-22'11"	4.17 – 2.1 MA	Toussaint et al., 2003; Zipfel et al., 2020
StW 573f	Sterkfontein Member 2, from Silberberg Grotto	ca. 3.67 MA	Carlson et al., 2021
StW 582	Sterkfontein Member 4, from D/8	4.17 – 2.1 MA	Zipfel et al., 2020
UW 88-38 (88-142)	Malapa South Africa, Facies D	1.8 – 1.9 MA	Dirks et al., 2010
UW 101-258	Dinaledi chamber, Rising Star cave system	414 – 236 KA	Dirks et al., 2017
UW 101-1229	Dinaledi chamber, Rising Star cave system	414 – 236 KA	Dirks et al., 2017

1. Exploring Clavicular Ontogeny in Apes through Geometric Morphometrics

Introduction

To advance our understanding of arboreality in *Australopithecus*, more clarity is needed regarding the relationship between form and function in the shoulder of extant apes. We currently have a good sense of what morphological features distinguish the shoulder of apes from those of monkeys, since apes require further adaptations for suspensory arboreal behaviors and their orthograde posture. However, it is less obvious how the observed morphological variation in the ape shoulder reflects generic or species level differences in locomotion.

Ape locomotor and postural behaviors are incredibly diverse; even when the animals are known for predominantly performing one locomotor style, there is always still some level of variation. For this reason, ape locomotion is best viewed as a suite or 'regime' of behaviors. *Pongo* best exemplifies this idea as its locomotion is often described as a continuum of complex postures and movements (Sugardjito and Hooff, 1986; Thorpe and Crompton, 2005, 2006). In a single locomotor bout lasting no longer than twenty seconds, an adult orangutan was reported to perform more than five distinct locomotor modes (Thorpe and Crompton, 2006). Despite the wide range of observed behaviors, orangutans are most often classified as almost exclusively arboreal, performing predominantly orthograde suspension when locomoting (Thorpe and Crompton, 2005, 2006; Fleagle, 2013). *Hylobates*, on the other hand, represent the opposite end of the variability spectrum. Gibbons use brachiation as their main mode of locomotion (around 75% of the time) and are even observed to use suspension as a static posture when foraging and feeding (Gittins, 1983; Fleagle, 2013).

Gorilla and *Pan* have a significant amount of substrate flexibility, as they both have been observed to travel terrestrially and arboreally (Hunt, 1991; Doran, 1992, 1993, 1997; Sarringhaus et al., 2014). Also, unlike orangutans, which have little differences in locomotor behavior between juveniles and adults (Sugardjito and Hooff, 1986; Thorpe and Crompton, 2005, 2006), gorillas and chimpanzees have clear shifts in their locomotor regimes through ontogeny (Doran, 1992, 1993, 1997; Sarringhaus et al., 2014). As adults, *Gorilla beringei* rarely climbs trees and builds their sleeping nests on the ground (Rothman et al., 2006; Fleagle, 2013), but as juveniles, gorillas spend up to 50% of their locomotor bouts arboreally climbing (Doran, 1997). *Gorilla gorilla* is slightly more arboreal, especially the females and younger individuals, but is still predominantly terrestrial by adulthood (Mehlman and Doran, 2002; Fleagle, 2013). In comparison to the other apes, and even as juveniles, *Gorilla* rarely uses suspensory postures and behaviors (Fleagle, 2013). Chimpanzees (*Pan troglodytes*) also become increasingly more terrestrial during ontogeny, however, adults are more suspensory and arboreal than *Gorilla* (Doran, 1992, 1993, 1997) – although less so than *Pongo* and *Hylobates* (Fleagle, 2013). As juveniles, *Pan* can spend up to 80% of its time in the trees, predominantly climbing and using suspensory behaviors (Doran 1992, 1993, 1997). Juvenile chimpanzees are also more active than adults, spending about 10 – 15% more time locomoting (Sarringhaus et al., 2014).

Such locomotor diversity and the variation in structural support required by each behavioral regime is hypothesized to be related to the clavicular morphology of each taxon (Voisin, 2006a; Squyres and DeLeon, 2015). The curvatures of the clavicle generally differentiate *Hylobates* from the great apes and variably distinguish amongst the other taxa. The current consensus is that the ventrally projecting curvature in the dorsoventral plane is beneficial for powerful arm flexion during suspension, and the curvatures in the craniocaudal plane are related

to the position of the scapula on the thorax (Voisin, 2006a; Squyres and DeLeon, 2015). However, work by Melillo and colleagues (2019) has not supported the latter form-function relationship; although, there exist concerns about the effect of the supine posture of the sampled individuals during data collection on the results of the study. Additionally, these functional hypotheses leave several trends in clavicular morphology unexplained. First, Voisin (2006a) emphasizes the role of ventral curvature as the attachment for the clavicular head of the pectoralis major in generating strong flexion for suspension, however this would not account for the present of such a curvature in *Pongo* as they do not have a clavicular attachment of the pectoralis major (Diogo and Wood, 2011, 2012; Diogo et al., 2013b). Moreover, the strong similarities in clavicular curvature observed by Squyres and DeLeon (2015) between *Homo* and *Pan* further calls into question the relationship between inferior curvature and scapular position on the thorax. Therefore, any new analyses of clavicular shape should strive to more clearly connect curvature with its locomotor significance.

Previous investigations aiming to connect form and function in the hominoid skeleton have highlighted the use of an ontogenetic sample to identify developmentally plastic traits (e.g., Mitteroecker et al., 2004; Cowgill, 2007; Green and Alemseged, 2012; Green, 2013; Barros, 2014; Morimoto et al., 2018; Nalley et al., 2019, 2024; Stamos and Weaver, 2020). The infraspinous fossa of the scapula increases in breadth in *Pan* and *Gorilla* through ontogeny alongside their increase in knuckle-walking frequency as they become more terrestrial (Green and Alemseged, 2012). The morphology of the juvenile *Au. afarensis* DIK-1-1 clavicle suggests the *Au. afarensis* shoulder followed a developmental trajectory more similar to the extant African apes than modern humans, supporting the importance of arboreality for this species (Green and Alemseged, 2012). Additionally, humeral torsion is developmentally plastic in modern *Homo sapiens* (Cowgill, 2007) and extant hominoids (Barros, 2014), supporting the interpretation of humeral torsion in the

hominin fossil record as a functionally informative trait (Larson, 2013). Clavicular curvature has been suggested by some to be ontogenetically conserved (Corrigan, 1960) and by others to be developmentally plastic (Barros, 2014). However, the statistical significance of the results supporting the latter hypothesis varies depending on the method used to quantify curvature (Barros, 2014), leaving the developmental trajectory of this element unresolved.

Since we have not yet been able to identify clear signals of morphological adaptation for locomotion in the adult hominoid clavicle, it is possible that a larger-scale ontogenetic analysis via an established shape quantification method may reveal informative characteristics as they gradually establish themselves alongside the adult locomotor regime. Moreover, using 3D geometric morphometrics allows for the comparison of shape change and variation concomitantly across the entire element as opposed to each 2D curvature in isolation or compared to other linear measurements in a bivariate manner. If salient features can be identified in the extant ape clavicle tied to locomotor adaptation through ontogeny, or if more support can be provided for features suggested through previous investigations, we would be better positioned to interpret the significance of the presence or absence of such traits in the hominin fossil record. Further, the existence of preserved clavicles from juvenile early hominins, such as DIK-1-1, offers the opportunity to directly examine the plasticity of these features in fossil hominins through ontogeny. In this study, I analyze one of the largest datasets of hominoid clavicular shape through ontogeny to test hypotheses concerning curvature plasticity during development and pinpoint traits indicative of locomotor adaptation in the fossil hominin shoulder. Specifically, I evaluate three hypotheses: (1) morphological variation across the entire hominoid sample will overshadow any nuanced intraspecific changes in curvature through ontogeny, thus plasticity can only be identified through independent generic analyses; (2) ontogenetic changes in curvature will occur in *Pan* and

Gorilla alongside their shift from arboreality to terrestriality, and modern humans as they become obligate bipeds; (3) given the similarities between modern *Homo* and *Pan* clavicles, fossil hominins will not exhibit distinguishable differences in shape from either taxon.

Materials and Methods

Sample:

In total, 326 extant hominoids were sampled (*Homo sapiens*, N = 37; *Gorilla gorilla*, N = 53; *Gorilla beringei*, N =22; *Pan troglodytes*, N = 85; *Pongo abelii*, N = 15; *Pongo pygmaeus*, N = 40; *Hylobates lar*, N = 68; and *Hylobates concolor*, N = 6; Table 1.1); the Appendix details the composition of the sample. To enable generic comparisons, both species of *Gorilla* were combined, as were both species of *Pongo*. To facilitate comparisons amongst individuals of similar age, dental developmental stages were used to divide the ontogenetic sample into four age groups: infants (no permanent molars erupted), juveniles (M1 erupted), adolescents (M1 and M2 erupted), and adults (M3 erupted) (Smith et al., 1994). Although the resolution of these age bins does not allow for the separate analysis of apes pre-locomotor independence, or before the animal navigates its environment without parental assistance, a sufficient sample size of those individuals could not be attained given their limited availability in domestic museum collections. The extant ape sample includes specimens housed in the American Museum of Natural History (AMNH), Cleveland Museum of Natural History (CMNH), Field Museum of Natural History (FMNH), Harvard Museum of Comparative Zoology (MCZ), Max Planck Institute for Evolutionary Anthropology (MPI), and Smithsonian Institution (USNM, formerly National Museum of Natural History). The modern *Homo sapiens* sample is sourced from the Hammond Todd Collection and includes post-industrial individuals of known age and sex. Non-pathological right clavicles, free from external

damage were preferentially sampled. Left clavicles were occasionally sampled when the right one was missing or damaged but were mirrored prior to analysis. Fossil hominin specimens (N = 8) included in the analyses represent *Australopithecus afarensis, Australopithecus africanus, Australopithecus sediba*, and *Homo naledi* (Table 1.2). Prior to analyses, the two fragments from *Au. sediba* (U.W. 88-38, from the same individual) were refitted to form one complete clavicle and two partial clavicles from *H. naledi* (U.W. 101-1229 and 101-258, from different individuals but estimated to be the same size) were aligned and reconstructed to form a nearly complete clavicle missing the sternal and acromial extremities.

Microcomputed tomographic scans (μCT) of the extant individuals were generated at the University of Chicago using a Phoenix|x-ray Nanotom and v|tome|x combination (RRID:SCR_024763) and at the Center for Nanoscale Systems at Harvard University using an HMXST Micro-CT x-ray imaging system. Due to the variation in specimen size and density, voltage ranged from 70 – 110 kV, current ranged from 150 – 320 μA, and resolution ranged from 27.38 – 89.20 μm for the extant sample. DIK-1-1 was scanned on the ID17 beamline at the European Synchrotron Radiation Facility (ESRF) in Grenoble, France, at a resolution of 30.30 μm. Scans of KSD-VP-1/1f were generated at Penn State University using a GE v|tome|x at a resolution of approximately 62.0 μm. All other fossil specimens were scanned at the University of the Witwatersrand, Johannesburg using a Nikon Metrology XTH 225/320 LC micro-CT system.

Surface models, landmarks, and analyses:

All specimens were manually segmented (*Avizo Lite 2020.2*, Visualizations Sciences Group, 2017) to create a solid surface for landmarking. If a specimen was a left clavicle, it was

mirrored using *Geomagic DesignX* (oqton, 2023). When needed, *Geomagic DesignX* was also used to smooth surfaces to prevent landmarks from being skewed based on taphonomic damage.

To quantify external shape 3 true landmarks and 4 curves of 13 sliding semi-landmarks each were placed on each complete specimen (*Checkpoint*, Stratovan Corporation, 2018). The chosen landmarking scheme followed previous quantifications of clavicular shape (Squyres and DeLeon, 2015; Melillo, 2016; Melillo et al., 2019) that best capture the curvatures of the element in the dorsoventral plane and was further elaborated upon to better capture the variation in the craniocaudal plane (Figure 1.1; Table 1.3). In the extant and complete fossil analyses of shape, all 55 landmarks are represented. To accommodate the fragmentary hominin clavicles for shape comparison, any landmarks missing from the fossils were omitted from the entire dataset, meaning additional analyses were performed on a subset of 23 and 29 landmarks from the original configuration (Table 1.4).

All analyses were run on 9 different subsets of the full dataset: the full extant hominoid ontogenetic series, each extant hominoid taxon individually to test hypothesis (1), and the full extant ontogenetic series with different combinations of fossils included based on preservation (details of specimen inclusion can be found in Table 1.4). Prior to multivariate analysis of each data subset, the semi-landmarks were slid to minimize bending energy (Bookstein, 1997; Gunz et al., 2005; Zelditch et al., 2012), and all landmarks were subjected to a generalized Procrustes analysis (GPA) which corrects for differences in rotation, translation, and isometric size between individuals (O'Higgins, 2000; Zelditch et al., 2012) using the function *gpagen* from the 'geomorph' R package 4.0.6 (Adams et al., 2020). A principal components analysis (PCA) was performed on the corrected landmark coordinate data matrix using the *gm.prcomp* function from 'geomorph', and the resulting principal coordinate (PC) scores and Procrustes distances between

individual landmark configurations were then used as the inputs for the tests of morphological disparity. Using *morphol.disparity* (Foote, 1993; Zelditch et al., 2012), two tests of morphological disparity were run. The first quantified how much each group contributed to the overall morphological disparity in the dataset (partial disparity *sensu* Foote, 1993), and the second analysis performed pairwise comparisons amongst the defined groups to test for significant differences in shape. In both analyses, the Procrustes coordinates were regressed against centroid size to account for the effects of allometry ($p < 0.0001$; Figure 1.2). Significance was determined at $p = 0.05$ for all analyses. All morphological and statistical tests described above were carried out using R 4.3.2 (R Core Team, 2023).

Results

Extant Hominoids:

Full Sample

The first three PCs from the principal components analysis are shown in Figure 1.3. Together, these three PC axes describe approximately 75% of the total variance in the dataset. PC1 (55.74%) primarily describes the prominence of the ventral curvature of the clavicle with the negative end of the axis occupied by *Hylobates* with very prominent curvature, and *Gorilla,* having little to no ventral curvature, falling along the positive end of the axis. *Homo* and *Pan* cluster tightly along PC1 and have some overlap with *Pongo*, although *Pongo* falls further towards the negative end of the axis. PC2 (10.92%) weakly separates the taxa based on the magnitude of curvature in the dorsoventral plane and the presence or absence of a cranially projecting curvature on the lateral end. Those on the positive end of PC2, such as *Homo* and *Pan*, display both the ventrally projecting curvature around midshaft and the dorsally projecting curvature found

laterally, while the negative end of PC2 is occupied by individuals with a straighter diaphysis in dorsoventral view, as can be seen most often in *Pongo* and *Gorilla*. Taxa with one dorsoventral curvature fall closer to the middle of PC2, such as *Hylobates* with a ventrally directed curvature at midshaft. Although the separation is weak, PC2 distinguishes *Homo* from the non-*Pan* apes because *Homo* often has a weaker inferior curvature, as described by Voisin (2006). There is also substantial overlap amongst *Gorilla, Pongo,* and *Hylobates* along PC2. PC3 (8.69%) to some extent also reflects the variation in dorsoventral curvature captured by PC1 and PC2, and craniocaudal curvature more medially than PC2. The negative end of PC3 contains taxa such as *Gorilla* and *Hylobates,* which variably have an inferiorly directed curvature midshaft in combination with less prominent curvatures in the dorsoventral plane, while the positive end of PC3 has taxa with both prominent dorsoventral curvatures and a strong superiorly directed curvature on the lateral end like *Pan* and some individuals in *Homo* and *Pongo*. Although individuals from the same age group do not cluster intraspecifically in the morphospace, statistical comparisons of shape indicate that *Gorilla* infants and juveniles are significantly different from the adolescents and adults (Table 1.7).

Tests of generic contribution to overall morphological disparity (Foote, 1993; Zelditch et al., 2012), suggest that in this dataset, *Gorilla* and *Hylobates* contribute the most to overall disparity while *Homo* contributes the least (Table 1.5). Based on the first 3 PC axes, this result is expected as morphologically "extreme" or peripheral subgroups tend to make a greater contribution to overall group disparity compared to more centralized groups in morphospace (Foote, 1993). It should be noted, however, that partial disparity is not analogous to intra-group variance and therefore is not intended to measure morphological disparity within a group on its own (Foote, 1993; Zelditch et al., 2012). Consequently, the reported contributions to overall

disparity should not be interpreted as relative measures of intra-genus variation. Pairwise comparisons of shape support the differences seen along the PC axes (Table 1.6). After accounting for allometry, *Gorilla* is significantly different in shape from all other great apes, and *Pan* and *Pongo* are significantly different from all other apes except *Homo*. Comparing the intra-group variances calculated when overall disparity versus partial disparity is used, all apes have a higher raw group variance than partial group variance (Table 1.8). This indicates that there is substantial shape variation in the dataset overall, but much of the observed shape variation can be explained by generic affiliations as a grouping variable. Therefore, clavicles randomly sampled from the same genus will be more similar in shape than two clavicles sampled from the entire dataset.

Genus Subsamples

Because the clavicles have been demonstrated to be more variable within hominoids as a whole than within a specific genus, it is possible that any potential signal of shape change through ontogeny at the generic level is being overridden by the morphological variation differentiating amongst the hominoids. Therefore, the same analyses were also run on each hominoid genus separately. Notably, results are very similar amongst the apes – there are practically no significant differences in shape change through ontogeny (Figure 1.4; Table 1.9) and the adults of each taxon contribute the most to morphological disparity (Table 1.10). Interestingly, the significant differences in shape among *Gorilla* age categories in the interspecific analysis are no longer significant. The only significant pairwise comparison in the intraspecific analyses is between infant and adult *Hylobates.* Looking at intra-group variance, all age categories of all taxa have a higher value when generated from overall morphological disparity compared to that calculated from partial disparity (Table 1.11). This again means that two clavicles from the same age bin, within the same genus, will be more similar in shape than two randomly chosen clavicles.

Fossil Hominins:

None of the hominin genera significantly contribute to overall morphological disparity (i.e., more than 0.5%) in any of the three analyses including fossils (Table 1.12). As all fossil specimens plot along PC1-PC3 within the distribution already covered by extant hominoids (Figures 1.5 – 1.7) and given the small number of individuals sampled per genus, they would not be expected to greatly contribute to disparity.

In the analysis including complete hominin fossils, the resulting morphospace and variation captured along the first 3 PC axes was practically identical to that resulting from the extant analysis (Figure 1.5). After accounting for centroid size, no pairwise differences in shape emerge between the fossil hominins and extant apes (Table 1.13). All three fossil specimens, representing *Au. afarensis, Au. africanus,* and *Au. sediba,* plot firmly within the overlapping regions of *Pan* and *Homo*. There is also some similarity in shape with *Pongo* along PC1 and PC3.

When KSD-VP-1/1f and the UW 101 composite are added and their missing landmarks are removed from the analysis, hominoid taxa begin to cluster more closely in the morphospace with notably more overlap amongst *Pongo*, *Pan*, and *Homo* (Figure 1.6) although they still remain significantly different in shape. There are still no significant differences in shape between the fossil hominin and extant ape taxa after accounting for centroid size (Table 1.14). The variation captured along the first three PC axes are again similar to that seen in the extant analysis. PC1 reflects variation in the ventral curvature at midshaft, PC2 is driven by the combination of a ventral midshaft curvature and a lateral superior curvature, and PC3 captures more of a sigmoid shape along its minimum end and a diaphysis with one predominant curve along the positive end – reflecting relatively how medially along the diaphysis the lateral curvature begins. The fossil

sample, now also including *H. naledi,* clusters closely along PC1 but is more spread out along PC2 with *Au. sediba* falling along the negative end, *Au. africanus* and *H. naledi* around zero, and *Au. afarensis* plotting slightly more positively. DIK-1-1 falls within the range of *Homo* but not the *Pan*, while KSD-VP-1/1f falls just beyond the distribution of *Pan* within the region occupied by both *Pongo* and *Hylobates*. *Au. sediba, Au. africanus,* and *H. naledi* fall within the overlap of shape distribution of *Pan* and *Pongo*. Along PC3, the australopiths cluster together just slightly below zero while *H. naledi* plots alone on the positive end within the distribution of *Pongo*. DIK-1-1 falls within the area of morphospace occupied by both *Pan* and *Homo,* but KSD-VP-1/1f is plotting outside of that range and within the *Pongo* range of variation along the negative end of PC3.

Adding in the final fossil specimens and omitting their missing landmarks from the dataset again appears to have reduced the separation of genera in the morphospace (Figure 1.7), but most statistically significant differences in shape between extant taxa are preserved (Table 1.15). Even though more shape variation is being captured by PC1, PC2 clusters the taxa better in the morphospace. None of the *Australopithecus* specimens have significantly different shapes than the other sampled taxa after accounting for centroid size. In contrast to *Australopithecus, H. naledi* is significantly different in shape from *H. sapiens.* Here, PC1 appears to represent the degree of superior curvature and dorsoventral expansion seen laterally, with both features more present on the minimum end of the axis and less present on the maximum end. PC2 predominantly captures the variation in lateral curvature in the dorsoventral plane with the negative end showing more of the dorsally projecting portion and the positive end showing more of the ventrally projecting portion of the curvature. Along PC3, despite not differentiating among the extant taxa very well, generally negative scores are associated with a combination of a more dorsal and superiorly

projecting lateral curvature and positive scores are driven by dorsoventral expansion in this region of curvature at the positive end. Fossil hominins are spread along PC1 with *Au. sediba* falling on the negative end, *Au. africanus* and *H. naledi* plotting right around zero, and *Au. afarensis* on the positive end. All fossil hominin taxa are roughly lumped along PC2, but *Au. sediba* is just slightly more positive than the others. Again, PC3 appears to differentiate *H. naledi* from the australopiths with it separating on the positive end while the others fall just negative of zero. Plotting PCs 1 and 2, *Au sediba* falls within the region of overlap of *Pan* and *Pongo*. DIK-1-1 falls within the overlap of *Homo* and *Pan*, but KSD-VP-1/1f is on the boarder of the *Pan* and *Hylobates* shape space while being firmly within the range of *Pongo*. *H. naledi* is within the region of overlap of *Homo, Pan, Pongo,* and *Gorilla*. Plotted along PCs 1 and 3, *Au. sediba* falls within an area of overlap with *Pan, Pongo* and *Gorilla*. StW 573 and 582 fall within the range of variation of all extant apes except *Hylobates*, while the other *Au. africanus* specimen StW 431g falls within the distribution of *Homo* and *Gorilla*. Both *Au. afarensis* individuals fall within the range of *Homo, Gorilla, Pongo,* and *Hylobates*. *H. naledi* is unique relative to the other fossil hominins once again, occupying a region of the morphospace where *Hylobates, Pan, Pongo,* and *Gorilla* overlap but notably not *Homo sapiens*.

Discussion

Neither the analysis on the full ontogenetic dataset nor those at the generic level revealed any developmentally plastic traits in the clavicle that could be linked to changes in locomotor behavior. While the interspecific morphological variation is clearly greater than what would be expected intraspecifically either within an age category or ontogenetically, even when explored independently, no hominoid taxon exhibited developmental trends in clavicular morphology. This

is in line with descriptions of the human clavicle by (Corrigan, 1960) and hypotheses by Lovejoy et al. (2003) that claim skeletal morphology is entirely the result of positional information from mesenchymal cells during early growth. However, this is in contrast to the developmental plasticity identified in the other shoulder girdle elements (Cowgill, 2007; Green and Alemseged, 2012; Green, 2013; Barros, 2014) and many other regions of the skeleton (e.g., Mitteroecker et al., 2004; Morimoto et al., 2018; Nalley et al., 2019, 2024; Stamos and Weaver, 2020).

Adult apes contribute the most to the total disparity described by the morphospace, occupying the areas also covered by the sub-adult individuals. This suggests that the clavicle may show subtle, non-significant, changes in external shape through ontogeny, but these changes are not predictable and ultimately produce a wider range of morphological variation. This is further supported by the comparison of intra-group variance calculated both with and without consideration of partial variance: sub-adults have a tenfold lower intra-group variance when age is considered, while adults have very similar measured variance. This means that, within a genus, two randomly selected adults are likely to be just as similar (or different) in shape as two randomly selected clavicles from across the ontogenetic stages, while two randomly selected juveniles would be more similar in shape than two random clavicles from the entire sample. Such ambiguity in the significance of shape variation in extant hominoids greatly lessens the utility of quantifying clavicular shape for identifying locomotor adaptation in the hominin evolutionary record.

External shape analysis partially supports previous groupings of extant hominoid clavicles (Voisin, 2006a; Squyres and DeLeon, 2015) but does not fully support previous characterizations of modern human clavicular morphology as distinct (Voisin, 2006a, 2006b, 2008). Instead, the human and chimpanzee ranges of morphological variation heavily overlap. Additionally, despite practicing relatively similar locomotor behaviors, *Pan* and *Gorilla* are statistically different in

shape in all analyses. This, in combination with the absence of ontogenetic change, suggests that while variation in locomotor behavior may be the primary influence on clavicular shape, the morphology is genetically constrained, and any changes would require considerable evolutionary time to become evident without the action of strong directional selection.

Fossil hominins most often fall within the *Homo-Pan* distribution, and occasionally fall into the range of *Pongo* shape space. This supports previous characterizations of these clavicles as 'primitive' (Churchill et al., 2013, 2018; Melillo, 2016; Feuerriegel et al., 2017; Carlson et al., 2021), yet it raises doubts regarding the reliability of a single inferior curvature as a definitive indicator of a lower scapular position on the thorax, supporting conclusions by Melillo and colleagues (2019). To varying extents, *Australopithecus* morphologically aligns with modern *Homo, Pan*, and *Pongo*, and *H. naledi* most closely aligns with *Pongo*. DIK-1-1 is unique among the fossil hominin individuals in that it always plots with modern *Homo* along the first three PCs in all analyses, in contrast to other descriptions of *Au. afarensis* clavicular morphology as more ape-like (Voisin, 2015; Melillo, 2016). *Au. sediba* does fall firmly within the range of variation of *Pan*, supporting previous descriptions of its morphology as *Pan*-like (Churchill et al., 2013, 2018; Voisin, 2015). However, it also firmly falls within the distribution of *Homo*, which stresses the challenge in distinguishing between *Pan* and *Homo* clavicles based solely on curvature and underscores the limitations of using this dichotomy as the context for interpreting fossil hominin morphology. This analysis also captures the morphological similarities between both *Au. sediba*, as represented by UW 88-38, and *Au. afarensis*, as represented by KSD-VP-1/1f, with modern *Pongo* as reported by Melillo (2016). Despite being implied by Voisin (2015) to not fit within the paradigm of *Au. afarensis* clavicular morphology, KSD-VP-1/1f clusters well with the other *Australopithecus* specimens along the major axes of variation.

Notably, *H. naledi* is significantly different from modern humans in the analysis of acromial fragments. Despite previous characterizations of the *H. naledi* shoulder likening it more to *Australopithecus* than to other contemporaneous *Homo* (Feuerriegel et al., 2017, 2019), here *H. naledi* is different, though not significantly so, from *Australopithecus* in shape along PC3 in both the acromial fragment analysis and the nearly complete analysis. This is partially in contrast to the description of the nearly complete *H. naledi* clavicle, UW 102a-021, by Voisin and colleagues (2020), in which it is said to be most similar to modern chimpanzees. The results of these analyses are likely to differ from other descriptions of the material due to the capacity of a principal components analysis (PCA) of landmark data to consider multiple axes of variation in concert. This enables the identification of more nuanced differences in overall shape than could be discerned by assessing each morphological feature independently, as is often done for the original descriptions and interpretations of the fossils. Based on the shape variation captured by PC3 in the analyses here, it appears that the lateral clavicular curvature of this *H. naledi* individual inflects more laterally on the preserved diaphysis relative to the conoid tubercle than the sampled *Australopithecus* individuals. However, the functional significance of this is still unclear. Even though *Gorilla* spans almost the full range of PC3, such a high degree of variation in this trait is not seen in the other extant apes, so the difference between *H. naledi* and the australopithecines may be meaningful to some extent. This dissimilarity with *Australopithecus*, coupled with the clear differences in morphology with modern humans, suggests that *H. naledi* clavicular morphology reflects adaptation to selective pressures not strongly acting on the *H. sapiens* lineage.

Significance

This analysis both supports and challenges previous characterizations of clavicular shape in extant apes and fossil hominins. Although *Gorilla* and *Hylobates*, two apes with very different locomotor behaviors, are easily distinguished by shape, there is substantial overlap among the other ape taxa (*Pongo*, *Pan*, and *Homo*), all of which also use a variety of behaviors and postures. The quantification and comparison of shape presented here suggests that the frequent comparison of fossil hominin clavicles to modern *Pan* and *Homo* has created a false dichotomy of shape variation between the two genera, when of the five modern ape taxa, *Homo* and *Pan* are arguably the most similar in shape. Instead, this analysis highlights some morphological similarities between fossil hominins and *Pongo*, alongside previous recognition of similarities with *Homo* and *Pan*. The conclusions reached here also challenge previous reports of developmental plasticity in clavicular curvature through ontogeny, suggesting that biomechanically meaningful connections should not be made regarding subtle variations in clavicular morphology between individuals of the same genus – such as the differences present between DIK-1-1 and KSD-VP-1/1f. Ultimately, external shape as measured through the presence and degree of clavicular curvature alone should not be used to taxonomically assign clavicular fragments to any fossil hominin species nor confidently convey morphological affinity with any modern ape taxon.

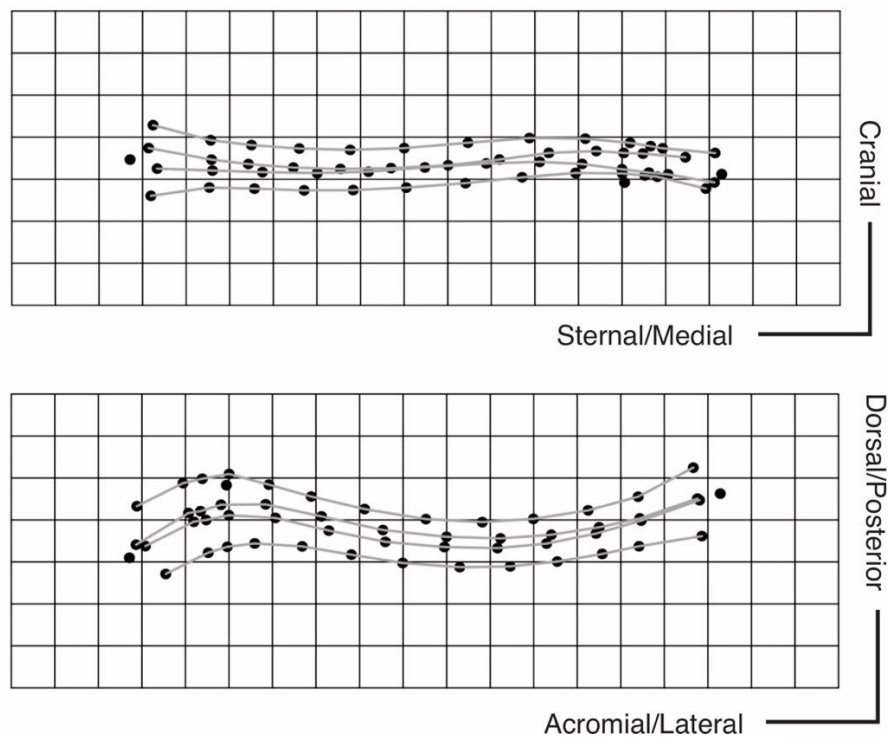

Figure 1.1. Landmark scheme displayed on the mean shape of the extant dataset.

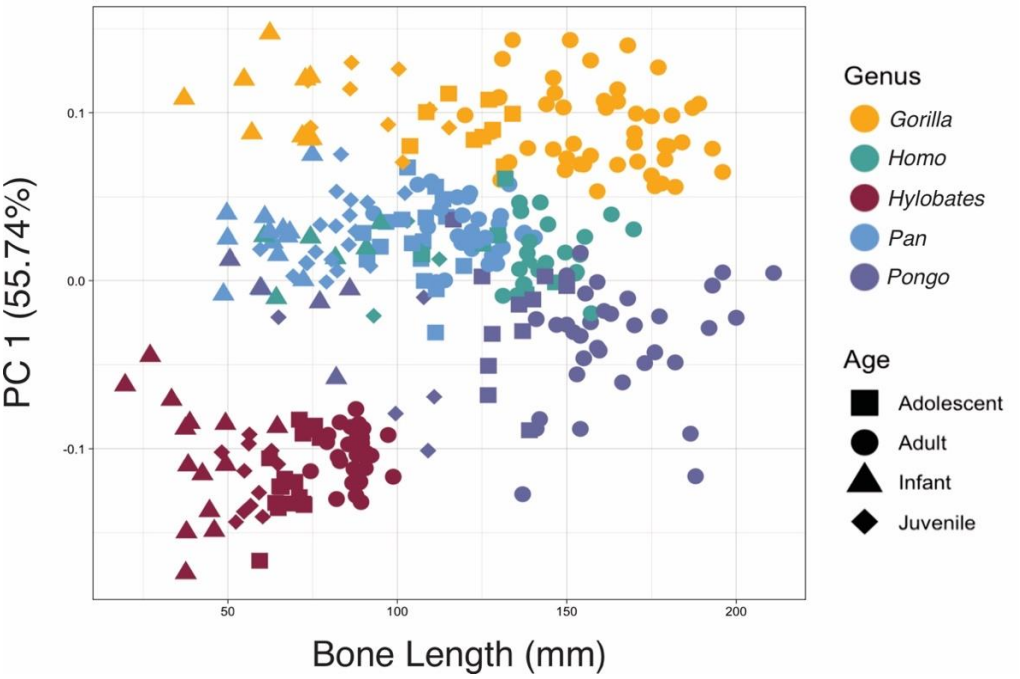

Figure 1.2. Effects of allometry in the dataset. Plot of bone length in millimeters against PC1.

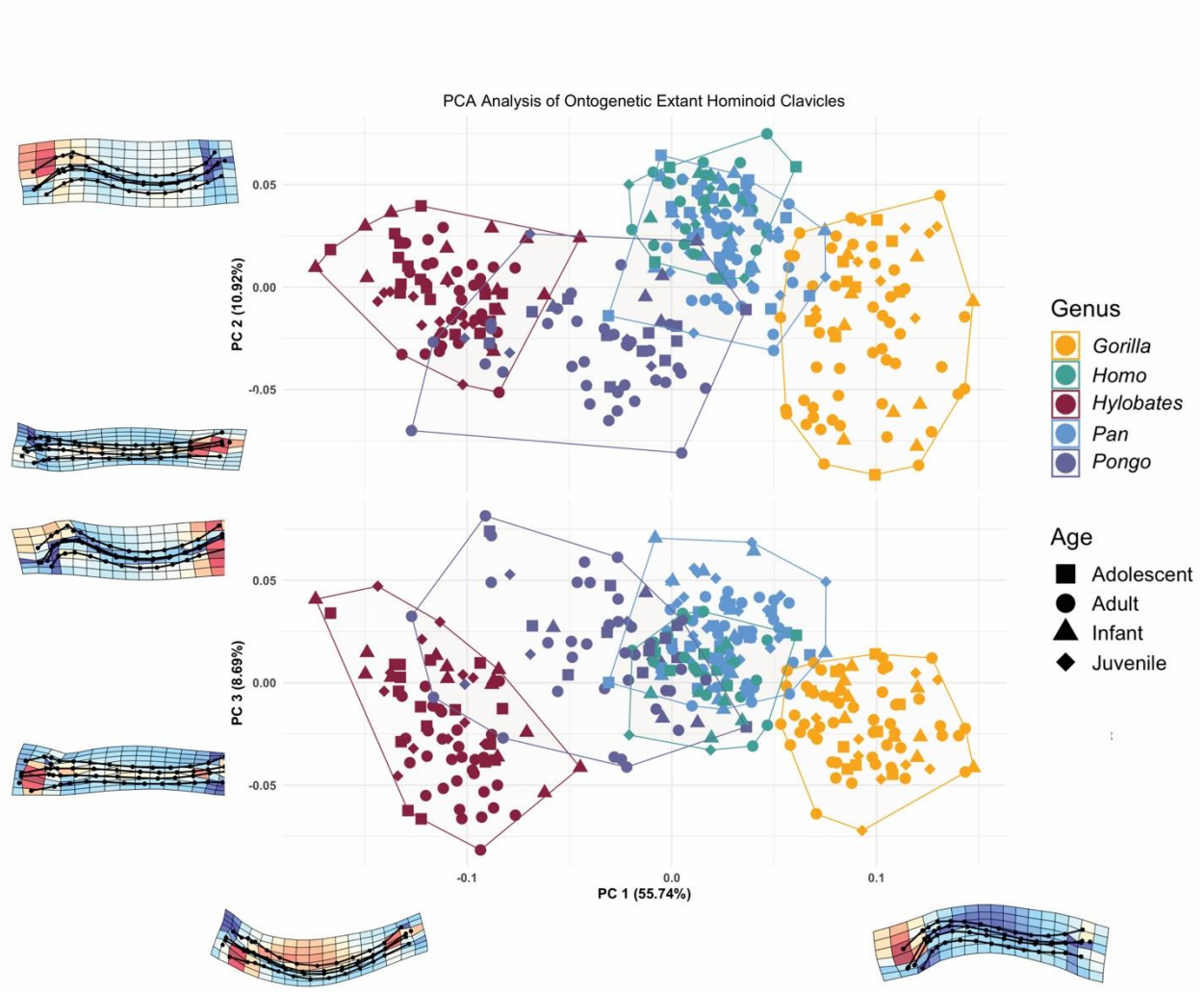

Figure 1.3. Variation along the first three PC axes: extant ontogenetic sample.

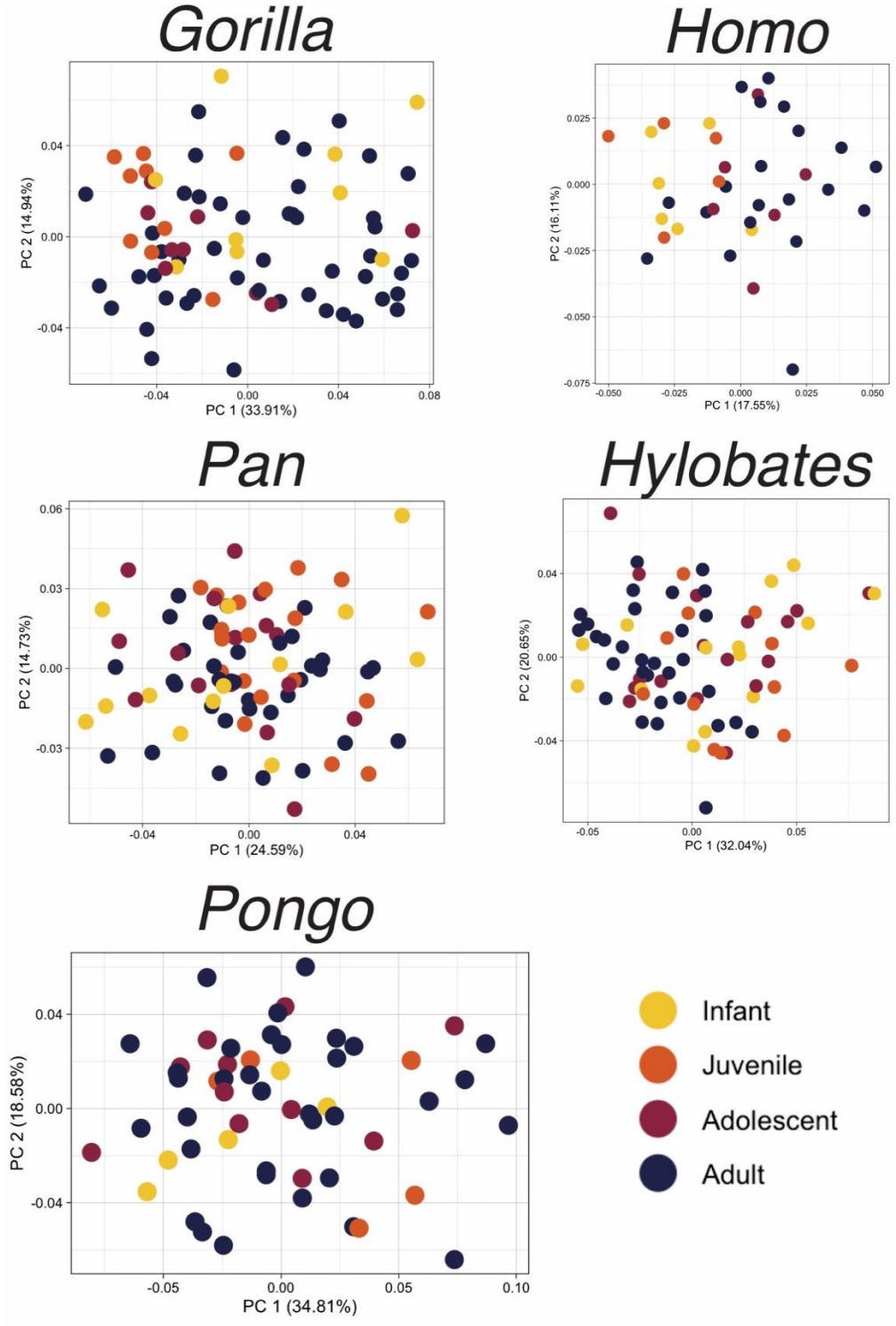

Figure 1.4. Variation along the first two PC axes: intraspecific samples.

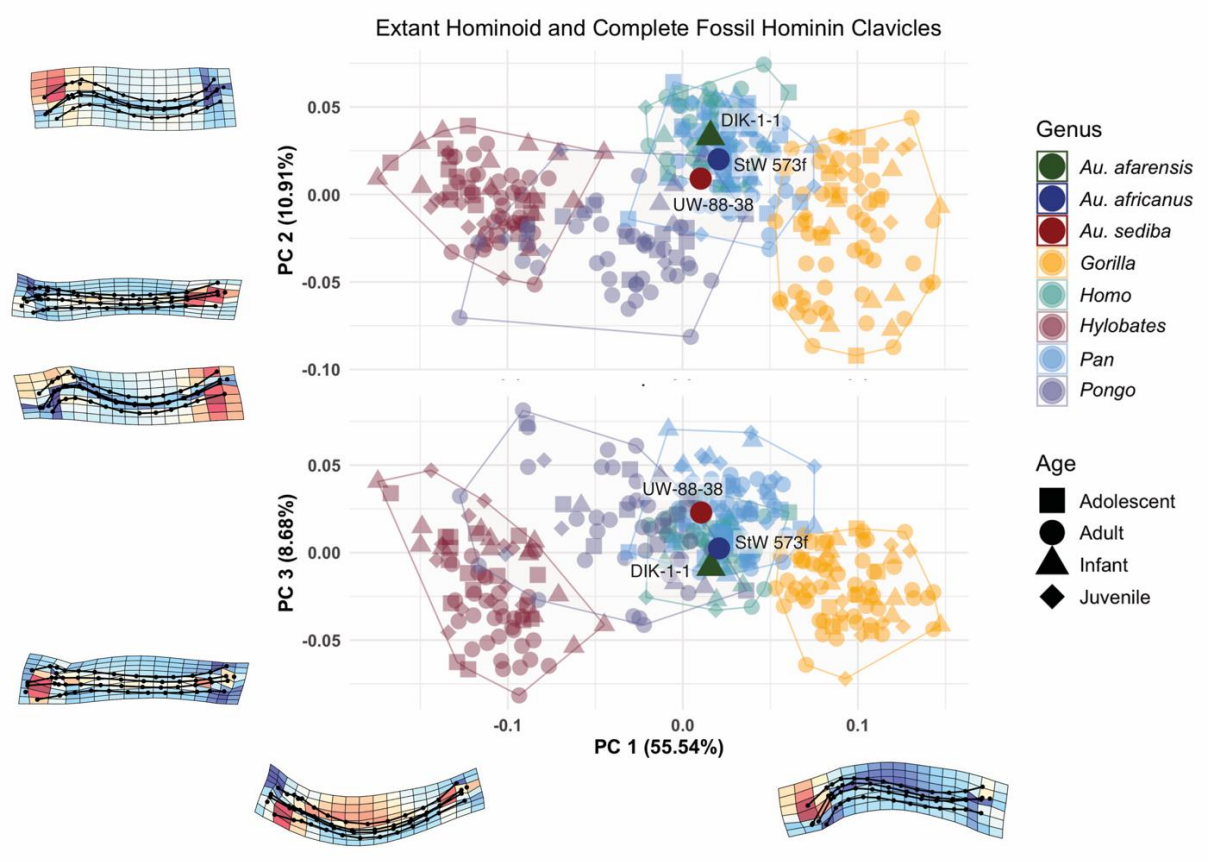

Figure 1.5. Variation along the first three PC axes with complete landmark set: extant ontogenetic sample and complete fossil hominins (*Au. afarensis*, DIK-1-1; *Au. africanus*, StW 573f; *Au. sediba*, UW 88-38).

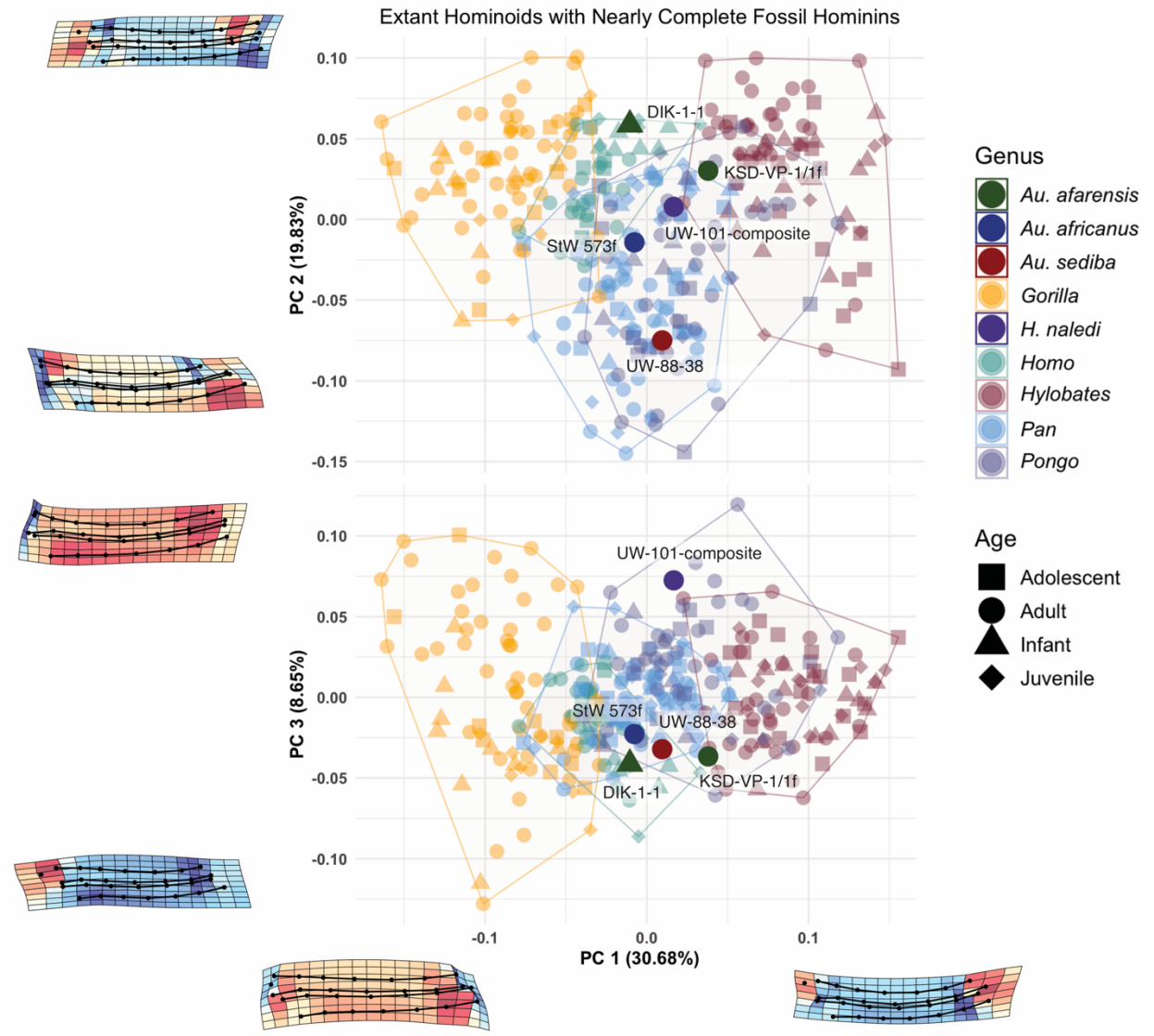

Figure 1.6. Variation along the first three PC axes with a partial set of landmarks for the nearly complete fossil analysis: extant ontogenetic sample, complete, and nearly complete fossil hominins (*Au. afarensis*, DIK-1-1 and KSD-VP-1/1f; *Au. africanus*, StW 573f; *Au. sediba*, UW 88-38; *H. naledi*, UW 101-1229 and -258 composite).

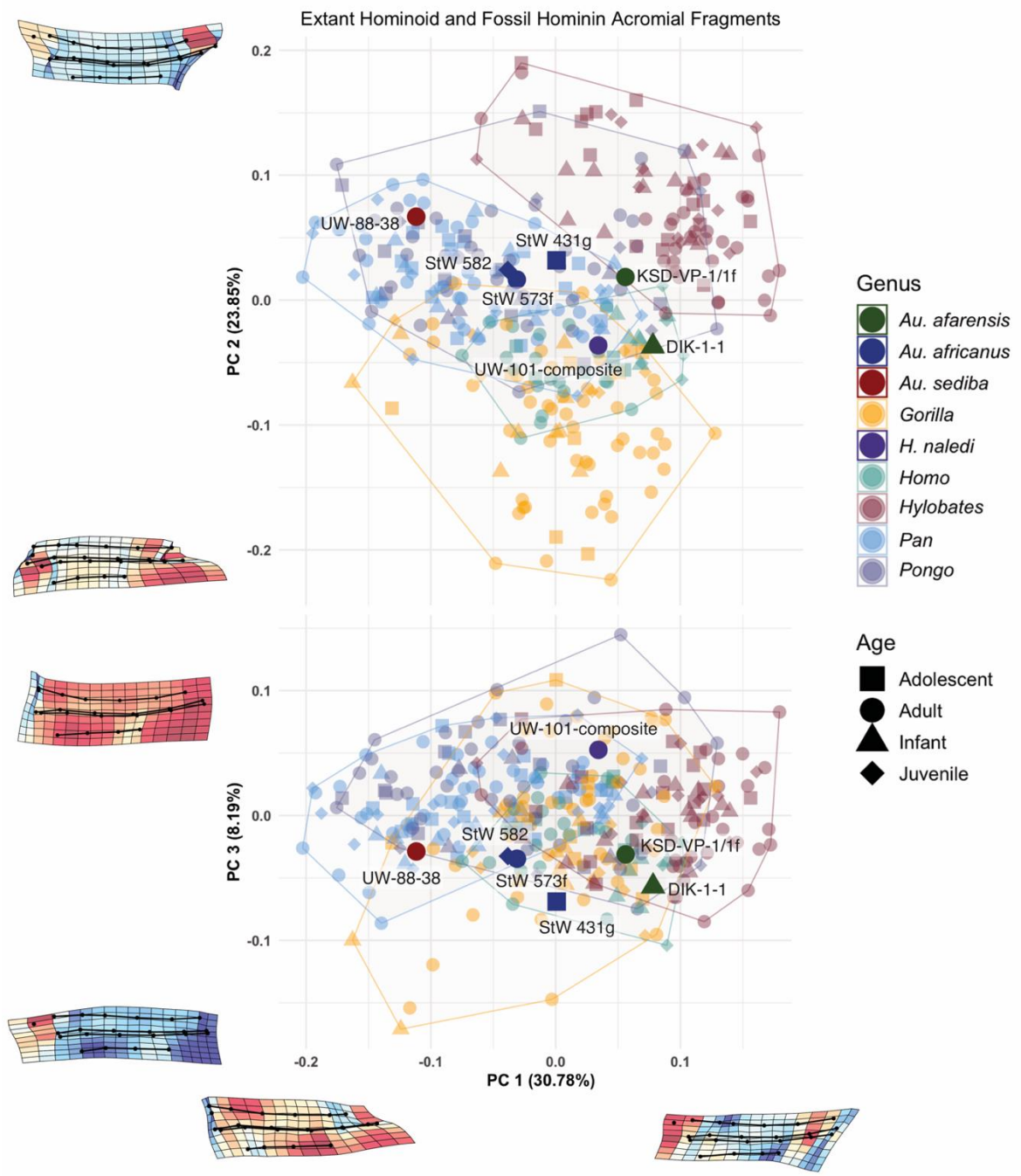

Figure 1.7. Variation along the first three PC axes with a partial set of landmarks for the fragmentary fossil analysis: extant ontogenetic sample and all fossil hominins (*Au. afarensis*, DIK-1-1 and KSD-VP-1/1f; *Au. africanus*, StW 431g, StW 573f, and StW 582; *Au. sediba*, UW 88-38; *H. naledi*, UW 101-1229 and -258 composite).

Table 1.1. Extant sample

Genus	Age	N
Gorilla	Infant	9
	Juvenile	9
	Adolescent	9
	Adult	48
Homo	Infant	6
	Juvenile	5
	Adolescent	6
	Adult	20
Hylobates	Infant	14
	Juvenile	12
	Adolescent	17
	Adult	31
Pan	Infant	13
	Juvenile	20
	Adolescent	17
	Adult	35
Pongo	Infant	5
	Juvenile	5
	Adolescent	11
	Adult	34

Table 1.2. Fossil sample.

Genus	Individual	Est. Age	Description	Reference
Au. afarensis	DIK-1-1	Infant	Complete left and right clavicles	Alemseged et al. (2006)
	KSD-VP-1/1f	Adult	Nearly complete left clavicle, missing the epiphyseal extremities	Haile-Selassie et al. (2010)
Au. africanus	StW 431g	Adult	Lateral half of a right clavicle missing the acromial extremity	Toussaint et al. (2003)
	StW 573f	Adult	Entire right clavicle	Carlson et al. (2021)
	StW 582	Juvenile	Lateral fragment containing both the medial and lateral curvatures, and conoid tubercle	Zipfel, Ward, and Richmond (2020)
Au. sediba	UW 88-38	Adult	Two fragments representing an entire right clavicle	Churchill et al. (2013)
H. naledi	UW 101-258	Adult	Lateral fragment containing both the medial and lateral curvatures, and conoid tubercle	Feuerriegel et al. (2016)
	UW 101-1229	Adult	Midshaft and sternal metaphysis section composed of three refitted fragments	Feuerriegel et al. (2016)

Table 1.3. Landmarks.

Number	Type	Description
1	II	Center of the sternal/medial articular surface.
2	II	Center of the acromial/lateral articular surface.
3	II	Most inferior point on the conoid tubercle/flange.
4 – 16	curve semi-landmarks	Cranial surface midline.
17 – 29	curve semi-landmarks	Ventral surface midline.
30 – 42	curve semi-landmarks	Caudal surface midline.
43 – 55	curve semi-landmarks	Dorsal surface midline.

Table 1.4. Individual inclusion in analyses

Analysis	N	Description
Extant Apes	326	Entire ontogenetic sample of extant *Gorilla, Homo, Hylobates, Pan,* and *Pongo*
Gorilla Ontogenetic Series	75	Infant, juvenile, adolescent, and adult *Gorilla gorilla* and *Gorilla beringei*
Homo Ontogenetic Series	37	Infant, juvenile, adolescent, and adult *Homo sapiens*
Hylobates Ontogenetic Series	74	Infant, juvenile, adolescent, and adult *Hylobates lar* and *Hylobates concolor*
Pan Ontogenetic Series	85	Infant, juvenile, adolescent, and adult *Pan troglodytes*
Pongo Ontogenetic Series	55	Infant, juvenile, adolescent, and adult *Pongo pygmaeus* and *Pongo abelii*
Complete Hominin Fossils	329	Entire ontogenetic sample of extant apes, DIK-1-1, StW 573f, and UW 88-38
Nearly Complete Hominin Fossils	331	Entire ontogenetic sample of extant apes, DIK-1-1, KSD-VP-1/1f, StW 573f, UW 88-38, and UW 101 composite
Fragmentary Hominin Fossils	333	Entire ontogenetic sample of extant apes, DIK-1-1, KSD-VP-1/1f, StW 431g, StW 573f, StW 582, UW 88-38, and UW 101 composite

Table 1.5. Extant Morphospace: Contributions to Morphological Disparity

Genus	Contribution to Overall Disparity	Age	Contribution to Genus Disparity
Gorilla	33.16%	Infant	4.85%
		Juvenile	4.35%
		Adolescent	3.43%
		Adult	20.53%
Homo	6.29%	Infant	1.02%
		Juvenile	0.66%
		Adolescent	0.95%
		Adult	3.65%
Hylobates	35.14%	Infant	6.40%
		Juvenile	6.05%
		Adolescent	8.66%
		Adult	14.02%
Pan	13.21%	Infant	2.47%
		Juvenile	3.28%
		Adolescent	2.40%
		Adult	5.05%
Pongo	12.21%	Infant	0.66%
		Juvenile	1.25%
		Adolescent	1.83%
		Adult	8.47%

Table 1.6. Extant Morphospace: Pairwise Comparisons by Genus.

	Gorilla	*Homo*	*Hylobates*	*Pan*
Gorilla	1	**0.0001**	0.3878	**0.0001**
Homo	**0.0001**	1	**0.0001**	0.5056
Hylobates	0.3878	**0.0001**	1	**0.0001**
Pan	**0.0001**	0.5056	**0.0001**	1
Pongo	**0.0001**	0.1655	**0.0001**	**0.0156**

Table 1.7. Extant Morphospace: Pairwise Comparisons by Genus and Age Group.

	***Gorilla* Adolescent**	***Gorilla* Adult**	***Gorilla* Infant**	***Gorilla* Juvenile**	***Homo* Adolescent**	***Homo* Adult**	***Homo* Infant**	***Homo* Juvenile**	***Hylobates* Adolescent**	***Hylobates* Adult**	***Hylobates* Infant**	***Hylobates* Juvenile**
***Gorilla* Adolescent**	1.0000	0.8216	0.0001	0.0003	0.0634	0.0439	0.1618	0.0753	0.3603	0.3379	0.7645	0.5023
***Gorilla* Adult**	0.8216	1.0000	0.0001	0.0001	0.0335	0.0059	0.1177	0.0421	0.1033	0.0555	0.8754	0.2438
***Gorilla* Infant**	0.0001	0.0001	1.0000	0.4469	0.0001	0.0001	0.0001	0.0001	0.0002	0.0001	0.0001	0.0001
***Gorilla* Juvenile**	0.0003	0.0001	0.4469	1.0000	0.0001	0.0001	0.0001	0.0001	0.0020	0.0014	0.0001	0.0015
***Homo* Adolescent**	0.0634	0.0335	0.0001	0.0001	1.0000	0.7018	0.6506	0.9839	0.0049	0.0042	0.0761	0.0111
***Homo* Adult**	0.0439	0.0059	0.0001	0.0001	0.7018	1.0000	0.8694	0.7037	0.0004	0.0001	0.0486	0.0031
***Homo* Infant**	0.1618	0.1177	0.0001	0.0001	0.6506	0.8694	1.0000	0.6536	0.0234	0.0168	0.2039	0.0394
***Homo* Juvenile**	0.0753	0.0421	0.0001	0.0001	0.9839	0.7037	0.6536	1.0000	0.0076	0.0080	0.0873	0.0172
***Hylobates* Adolescent**	0.3603	0.1033	0.0002	0.0020	0.0049	0.0004	0.0234	0.0076	1.0000	0.9520	0.1516	0.8094
***Hylobates* Adult**	0.3379	0.0555	0.0001	0.0014	0.0042	0.0001	0.0168	0.0080	0.9520	1.0000	0.1310	0.8315
***Hylobates* Infant**	0.7645	0.8754	0.0001	0.0001	0.0761	0.0486	0.2039	0.0873	0.1516	0.1310	1.0000	0.2821
***Hylobates* Juvenile**	0.5023	0.2438	0.0001	0.0015	0.0111	0.0031	0.0394	0.0172	0.8094	0.8315	0.2821	1.0000
***Pan* Adolescent**	0.0085	0.0005	0.0001	0.0001	0.8067	0.3781	0.4373	0.8448	0.0001	0.0001	0.0057	0.0006
***Pan* Adult**	0.0043	0.0001	0.0001	0.0001	0.7550	0.2607	0.3733	0.7980	0.0001	0.0001	0.0023	0.0002
***Pan* Infant**	0.0962	0.0383	0.0001	0.0001	0.5764	0.7964	0.9675	0.5847	0.0027	0.0014	0.1246	0.0127
***Pan* Juvenile**	0.0428	0.0056	0.0001	0.0001	0.7050	0.9907	0.8655	0.7117	0.0003	0.0002	0.0490	0.0043
***Pongo* Adolescent**	0.0363	0.0097	0.0001	0.0001	0.9348	0.7116	0.6636	0.9177	0.0010	0.0007	0.0403	0.0040
***Pongo* Adult**	0.3331	0.2138	0.0001	0.0001	0.1551	0.1086	0.3912	0.1713	0.0127	0.0052	0.4603	0.0482
***Pongo* Infant**	0.0450	0.0239	0.0001	0.0001	0.8272	0.5365	0.5140	0.8433	0.0046	0.0043	0.0518	0.0098
***Pongo* Juvenile**	0.3495	0.3488	0.0001	0.0005	0.4124	0.5320	0.6925	0.4236	0.0727	0.0650	0.4450	0.1202

Table 1.7. continued

	Pan Adolescent	*Pan* Adult	*Pan* Infant	*Pan* Juvenile	*Pongo* Adolescent	*Pongo* Adult	*Pongo* Infant	*Pongo* Juvenile
***Gorilla* Adolescent**	0.0085	0.0043	0.0962	0.0428	0.0363	0.3331	0.0450	0.3495
***Gorilla* Adult**	0.0005	0.0001	0.0383	0.0056	0.0097	0.2138	0.0239	0.3488
***Gorilla* Infant**	0.0001	0.0001	0.0001	0.0001	0.0001	0.0001	0.0001	0.0001
***Gorilla* Juvenile**	0.0001	0.0001	0.0001	0.0001	0.0001	0.0001	0.0001	0.0005
***Homo* Adolescent**	0.8067	0.7550	0.5764	0.7050	0.9348	0.1551	0.8272	0.4124
***Homo* Adult**	0.3781	0.2607	0.7964	0.9907	0.7116	0.1086	0.5365	0.5320
***Homo* Infant**	0.4373	0.3733	0.9675	0.8655	0.6636	0.3912	0.5140	0.6925
***Homo* Juvenile**	0.8448	0.7980	0.5847	0.7117	0.9177	0.1713	0.8433	0.4236
***Hylobates* Adolescent**	0.0001	0.0001	0.0027	0.0003	0.0010	0.0127	0.0046	0.0727
***Hylobates* Adult**	0.0001	0.0001	0.0014	0.0002	0.0007	0.0052	0.0043	0.0650
***Hylobates* Infant**	0.0057	0.0023	0.1246	0.0490	0.0403	0.4603	0.0518	0.4450
***Hylobates* Juvenile**	0.0006	0.0002	0.0127	0.0043	0.0040	0.0482	0.0098	0.1202
***Pan* Adolescent**	1.0000	0.9520	0.2812	0.3827	0.6834	0.0131	0.9743	0.2289
***Pan* Adult**	0.9520	1.0000	0.2086	0.2695	0.6065	0.0019	0.9921	0.1853
***Pan* Infant**	0.2812	0.2086	1.0000	0.7860	0.5641	0.2693	0.4366	0.6842
***Pan* Juvenile**	0.3827	0.2695	0.7860	1.0000	0.7215	0.1057	0.5458	0.5351
***Pongo* Adolescent**	0.6834	0.6065	0.5641	0.7215	1.0000	0.0897	0.7512	0.4046
***Pongo* Adult**	0.0131	0.0019	0.2693	0.1057	0.0897	1.0000	0.1042	0.7531
***Pongo* Infant**	0.9743	0.9921	0.4366	0.5458	0.7512	0.1042	1.0000	0.3217
***Pongo* Juvenile**	0.2289	0.1853	0.6842	0.5351	0.4046	0.7531	0.3217	1.0000

Table 1.8. Extant Morphospace: Intra-group Variance

	Raw Variance	Partial Variance
Gorilla	0.0142	0.00346
Homo	0.0064	0.00066
Hylobates	0.0133	0.00367
Pan	0.0055	0.00138
Pongo	0.0082	0.00127

Table 1.9. Ontogenetic Taxon Specific Morphospace: Pairwise Comparisons

		Juvenile	Adolescent	Adult
Gorilla	**Infant**	0.158	0.130	0.421
	Juvenile	1	0.943	0.303
	Adolescent	0.943	1	0.259
	Adult	0.303	0.259	1
Homo		Juvenile	Adolescent	Adult
	Infant	0.915	0.638	0.204
	Juvenile	1	0.743	0.290
	Adolescent	0.743	1	0.492
	Adult	0.290	0.492	1
Hylobates		Juvenile	Adolescent	Adult
	Infant	0.141	0.142	**0.012**
	Juvenile	1	0.884	0.581
	Adolescent	0.884	1	0.414
	Adult	0.581	0.414	1
Pan		Juvenile	Adolescent	Adult
	Infant	0.216	0.172	0.067
	Juvenile	1	0.842	0.599
	Adolescent	0.842	1	0.790
	Adult	0.599	0.790	1
Pongo		Juvenile	Adolescent	Adult
	Infant	0.734	0.871	0.568
	Juvenile	1	0.590	0.905
	Adolescent	0.590	1	0.313
	Adult	0.905	0.313	1

Table 1.10. Ontogenetic Taxon Specific Morphospace: Contributions to Morphological Disparity

Genus	Age	Contribution to Disparity
Gorilla	Infant	13.26%
	Juvenile	12.84%
	Adolescent	9.57%
	Adult	64.33%
Homo	Infant	16.66%
	Juvenile	13.55%
	Adolescent	14.35%
	Adult	55.44%
Hylobates	Infant	26.38%
	Juvenile	14.83%
	Adolescent	21.84%
	Adult	36.95%
Pan	Infant	19.04%
	Juvenile	23.60%
	Adolescent	18.49%
	Adult	38.87%
Pongo	Infant	9.99%
	Juvenile	9.15%
	Adolescent	16.65%
	Adult	64.21%

Table 1.11. Ontogenetic Taxon Specific Morphospace: Intra-group Variance

Genus	Age	Raw Variance	Partial Variance
Gorilla	Infant	0.0055	0.00067
	Juvenile	0.0041	0.00065
	Adolescent	0.0040	0.00049
	Adult	0.0049	0.00326
Homo	Infant	0.0023	0.00055
	Juvenile	0.0024	0.00045
	Adolescent	0.0027	0.00047
	Adult	0.0032	0.00183
Hylobates	Infant	0.0042	0.00090
	Juvenile	0.0030	0.00051
	Adolescent	0.0032	0.00075
	Adult	0.0027	0.00127
Pan	Infant	0.0038	0.00063
	Juvenile	0.0032	0.00078
	Adolescent	0.0031	0.00061
	Adult	0.0029	0.00128
Pongo	Infant	0.0040	0.00048
	Juvenile	0.0046	0.00044
	Adolescent	0.0038	0.00079
	Adult	0.0047	0.00306

Table 1.12. Contribution of Fossil Hominins to Overall Morphological Disparity

	Complete	Nearly Complete	Fragmentary
Au. afarensis	0.118%	0.533%	0.516%
Au. africanus	0.144%	0.186%	0.903%
Au. sediba	0.153%	0.234%	0.310%
H. naledi	NA	0.448%	0.584%

Table 1.13. Complete Fossil Sample: Pairwise Comparisons

	Au. afarensis	*Au. africanus*	*Au. sediba*	*Gorilla*	*Homo*	*Hylobates*	*Pan*
Au. afarensis	1.000	0.993	0.984	0.090	0.881	0.113	0.979
Au. africanus	0.993	1.000	0.991	0.085	0.869	0.110	0.971
Au. sediba	0.984	0.991	1.000	0.084	0.863	0.108	0.964
Gorilla	0.090	0.085	0.084	1.000	**0.000**	0.451	**0.000**
Homo	0.881	0.869	0.863	**0.000**	1.000	**0.000**	0.498
Hylobates	0.113	0.110	0.108	0.451	**0.000**	1.000	**0.000**
Pan	0.979	0.971	0.964	**0.000**	0.498	**0.000**	1.000
Pongo	0.671	0.650	0.644	**0.000**	0.160	**0.000**	**0.012**

Table 1.14. Nearly Complete Fossil Sample: Pairwise Comparisons

	Au. afarensis	*Au. africanus*	*Au. sediba*	*Gorilla*	*H. naledi*	*Homo*	*Hylobates*	*Pan*
Au. afarensis	1.000	0.555	0.711	0.382	0.423	0.410	0.954	0.428
Au. africanus	0.555	1.000	0.817	0.128	0.242	0.966	0.551	0.944
Au. sediba	0.711	0.817	1.000	0.236	0.314	0.839	0.730	0.868
Gorilla	0.382	0.128	0.236	1.000	0.811	**0.000**	**0.000**	**0.000**
H. naledi	0.423	0.242	0.314	0.811	1.000	0.103	0.308	0.104
Homo	0.410	0.966	0.839	**0.000**	0.103	1.000	**0.006**	0.884
Hylobates	0.954	0.551	0.730	**0.000**	0.308	**0.006**	1.000	**0.002**
Pan	0.428	0.944	0.868	**0.000**	0.104	0.884	**0.002**	1.000
Pongo	0.941	0.476	0.663	**0.001**	0.375	**0.002**	0.575	**0.000**

Table 1.15. Fragmentary Fossil Sample: Pairwise Comparisons

	Au. afarensis	*Au. africanus*	*Au. sediba*	*Gorilla*	*H. naledi*	*Homo*	*Hylobates*	*Pan*
Au. afarensis	1.000	0.894	0.876	0.520	0.133	0.448	0.913	0.715
Au. africanus	0.894	1.000	0.964	0.552	0.128	0.254	0.958	0.529
Au. sediba	0.876	0.964	1.000	0.778	0.217	0.446	0.948	0.673
Gorilla	0.520	0.552	0.778	1.000	0.114	**0.000**	**0.019**	**0.000**
H. naledi	0.133	0.128	0.217	0.114	1.000	**0.035**	0.076	0.052
Homo	0.448	0.254	0.446	**0.000**	**0.035**	1.000	**0.001**	0.148
Hylobates	0.913	0.958	0.948	**0.019**	0.076	**0.001**	1.000	**0.025**
Pan	0.715	0.529	0.673	**0.000**	0.052	0.148	**0.025**	1.000
Pongo	0.773	0.868	0.968	0.150	0.090	**0.000**	0.453	**0.005**

2. Identifying Developmental Patterns in Bone Strength via Cross-sectional Geometry

Introduction

Testing hypotheses of locomotor adaptation in the fossil hominin upper limb is heavily influenced by our ability to reasonably reconstruct the functional anatomy of the shoulder in extant apes. Our limitations in this regard may be in part due to the omission of the clavicle in many discussions of primate morphological adaptation. Furthermore, existing interspecific comparative research on the clavicle in primates is limited to only a handful of unique analyses restricted to external shape (Schultz, 1937; Ashton and Oxnard, 1964; Corruccini and Ciochon, 1976; Voisin, 2006a; Larson, 2013; Barros, 2014; Roach and Richmond, 2015; Squyres and DeLeon, 2015; Melillo, 2016; Melillo et al., 2019; Laudicina and Cartmill, 2023) and would benefit from an expanded methodological scope. Although external morphology undeniably plays a role in the function of a joint or limb, the impact of phylogenetic relatedness and anatomical constraints can limit our ability to interpret mechanical loading from it alone (Ruff and Runestad, 1992; Lieberman et al., 2001). This is clearly reflected in the results of Chapter 1 of this research as the lack of developmentally plasticity traits provides little clarity into locomotor adaptation in great apes and fossil hominins. Alternatively, the investigation of internal bone morphology may better identify functionally significant features. Internal bone organization is highly related to the structural integrity of the element itself during use (Spadaro et al., 1994; Ito et al., 2002; Augat and Schorlemmer, 2006) and is highly responsive to mechanical loading throughout life (Ruff et al., 2006). Moreover, analyses of internal bone architecture have been shown to offer new insight into the form-function relationship in other study systems (Kivell, 2016).

An increasingly popular way to study signals of locomotor adaptation in internal bone structure is through the comparison of long bone cortical cross-sectional geometry (CSG) (e.g., Demes et al., 1991; Habib and Ruff, 2008; Simons et al., 2011; Kilbourne and Hutchinson, 2019; Parsi-Pour and Kilbourne, 2020). Briefly, CSG, as applied to bony elements, is a measure of the distribution of cortical mass about the neutral axis of a long bone and is informative about the strength and rigidity of a bone under bending and torsional loads. The measurement of CSG at defined levels along the long bone diaphysis (e.g., at 50% bone length) has often been recruited to assess the strength and rigidity of limb bones in relation to locomotion and ecomorphology (Ruff and Hayes, 1983; Ruff and Runestad, 1992; Ruff, 2009; Parsi-Pour and Kilbourne, 2020), the onset of bipedality during ontogeny in anatomically modern human populations (Ruff, 2003), and to support the presence of facultative bipedality in *Orrorin tugenensis* (Pickford et al., 2002). Recent advancements in CSG have allowed for the automated calculation of geometry across the whole diaphysis by creating cross-sections at equally spaced intervals along defined lengths of the diaphysis (Kilbourne and Hutchinson, 2019; Parsi-Pour and Kilbourne, 2020; Profico et al., 2021; Cosnefroy et al., 2022). Moreover, ontogenetic studies of CSG have highlighted the utility of a developmental framework for identifying functionally relevant aspects of bony morphology (Burgess et al., 2016; Ruff et al., 2018; Swan et al., 2020; but also see Cosnefroy et al., 2022). Quantifying relative strength in the forelimb versus hindlimb in *Gorilla beringei* through ontogeny reveals a dramatic shift in interlimb strength proportions where the hindlimb becomes stronger relative to the forelimb at around two years old (Ruff et al., 2018), reflecting the transition to a predominant reliance on terrestrial substrates and is consistent with observations by Doran (1997). The cortical geometry of the femur in humans has been shown to reorganize between birth and 7 months to facilitate early load bearing behaviors like crawling, and then continues to remodel

through childhood reflecting the changes in loading associated with an increasing dependence on bipedality (Swan et al., 2020). Finally, interspecific analyses of CSG through ontogeny have been used to relate known postural shifts in locomotor behavior, or a lack thereof, to the bending rigidity of the femur in baboons and vervets (Burgess et al., 2016). These methodological expansions have provided a more complete understanding of the bending regime and torsion experienced across an element, and thus may be a powerful tool for testing hypotheses of locomotor adaptation in hominoids and the role of the clavicle.

In primates, the clavicle is the only bony articulation between the thorax and upper limb (Ljunggren, 1979; Harrington et al., 1993). Compared to the soft tissue surrounding it, the clavicle has the highest Young's modulus (Gordon, 2009), making it the stiffest structure to transfer loads between the substrate and body of the locomoting animal. Therefore, as a structurally fundamental strut (Mivart and Huxley, 1867; Schultz, 1930; Howell, 1937; Ljunggren, 1979; Barros, 2014) contributing to the large ranges of motion available at the shoulder (Chan, 2008; Levangie and Norkin, 2011), the ape clavicle is likely to be frequently subjected to strong bending and torsional forces during upper limb use. The clavicle is also one of the first to ossify in-utero (Ogata and Uhthoff, 1990) and last to fuse its epiphysis in modern humans, still growing into young-adulthood (Black and Scheuer, 1996), suggesting it may adapt to the loading incurred during a longer timeframe compared to the earlier-fusing limb bones. In most primates, the clavicle serves as an attachment site for three muscles that are crucial for upper limb flexion and abduction during locomotion: the clavicular head of the pectoralis major m. along its sternal ventral surface, the anterior deltoid m. (clavicular head of the deltoid m.) on the cranioventral surface of the lateral third of the bone, and the cranial trapezius m. along the craniodorsal surface of the same region (Figure 2.1; Swindler and Wood, 1973; although see Diogo and Wood, 2011 for variation within

anthropoids). For these reasons, understanding the cortical geometry of the clavicle in extant hominoids through ontogeny may further our ability to identify adaptations related to arboreality in the fossil hominin shoulder.

To investigate the aforementioned issues, I will test the following four hypotheses: (1) *Homo* will have the lowest relative cortical area across the clavicle reflecting the release of the upper limb from locomotor obligations and/or recently evolved skeletal gracility (Lieberman, 1996; Ruff, 2006; Chirchir et al., 2015; Ryan and Shaw, 2015); (2) *Hylobates* will have one of the most eccentric clavicular cross-section through the diaphysis to resist the stereotypic unidirectional bending habitually imposed by brachiation (Gittins, 1983) which is assumed to highly load the clavicle, and *Pongo* will have the most circular diaphysis as a result of their highly variable use of arboreal locomotor and postural behaviors and therefore may require bending resistance in multiple directions (Sugardjito and Hooff, 1986; Thorpe and Crompton, 2005, 2006); (3) cortical cross-sectional geometry will be developmentally plastic in *Pan* and *Gorilla* alongside their shift from arboreality to terrestriality (Doran, 1992, 1993, 1997; Sarringhaus et al., 2014), similar to what has been observed in the scapula (Green and Alemseged, 212); and (4) aspects of cortical geometry indicative of arboreal behavior will be present in *Australopithecus*, supporting the importance of continued arboreality in the genus (Jungers, 1982; Jungers and Stern, 1983; Stem and Susman, 1983; Stern, 2000; Green and Alemseged, 2012; Kappelman et al., 2016; Ruff et al., 2016; Stamos and Alemseged, 2023).

Materials and Methods

Sample:

The same ontogenetic sample of 326 extant, wild-origin hominoids analyzed in Chapter 1 was used here (*Homo sapiens*, N = 37; *Gorilla gorilla*, N = 53; *Gorilla beringei*, N =22; *Pan troglodytes*, N = 85; *Pongo abelii*, N = 15; *Pongo pygmaeus*, N = 40; *Hylobates lar*, N = 68; and *Hylobates concolor*, N = 6; Table 2.1; Appendix). Again, to facilitate comparison amongst individuals of similar developmental stage, dental development was used to divide the ontogenetic sample into four age bins: infants (no permanent molars erupted), juveniles (M1 erupted), adolescents (M1 and M2 erupted), and adults (M3 erupted) (Smith et al., 1994). The extant ape sample includes specimens housed in the American Museum of Natural History (AMNH), Cleveland Museum of Natural History (CMNH), Field Museum of Natural History (FMNH), Harvard Museum of Comparative Zoology (MCZ), Max Planck Institute for Evolutionary Anthropology (MPI), and Smithsonian Institution (USNM, formerly National Museum of Natural History). The modern *H. sapiens* sample is sourced from the Hammond Todd Collection at the CMNH and includes post-industrial individuals of known age and sex. Non-pathological right clavicles, free from evidence of drill holes from display were preferentially sampled. Left clavicles were occasionally sampled when the right one was missing or damaged but were mirrored prior to analysis. Fossil hominin specimens (N = 8) included in the analyses represent *Australopithecus afarensis* (DIK-1-1, KSD-VP-1/1f), *Australopithecus africanus* (StW 431g, StW 573f, StW 582), *Australopithecus sediba* (UW 88-38, -142), and *Homo naledi* (UW 101 258, UW 101 1229; Table 2.2). Prior to analyses, the two fragments from *Au. sediba* (U.W. 88-38 and -142, from the same individual) were refitted to form one complete clavicle.

Microcomputed tomographic scans (μCT) of the extant individuals were generated at the University of Chicago using a Phoenix|x-ray Nanotom and v|tome|x combination (RRID:SCR_024763), Center for Nanoscale Systems at Harvard University using an HMXST Micro-CT x-ray imaging system, and Max Planck Institute for Evolutionary Anthropology using a diondo d3. Due to the variation in specimen size and density, voltage ranged from 70 – 110 kV, current ranged from 150 – 320 μA, and resolution ranged from 27.38 – 89.20 μm for the extant sample. Copper filters ranging from 0.2 – 0.5 mm were variably used when scanning clavicles larger than 130 mm. DIK-1-1 was scanned on the ID17 beamline at the European Synchrotron Radiation Facility (ESRF) in Grenoble, France, at a resolution of 30.30 μm. Scans of KSD-VP-1/1f were generated at Penn State University using a GE v|tome|x at a resolution of approximately 62.0 μm. All other fossil specimens were scanned at the University of the Witwatersrand, Johannesburg using a Nikon Metrology XTH 225/320 LC micro-CT system.

Model volumes, measurements of cortical geometry, and analyses:

Specimens were manually segmented (*Avizo Lite 2020.2*, Visualizations Sciences Group, 2017) to define the endosteal and periosteal surfaces of the bones. Following segmentation, the defined endosteal and periosteal surfaces were exported as STLs and oriented into standardized positions (*Geomagic DesignX*, oqton, 2023). The aligned volumes were then imported into the R package *morphomap* (Profico et al., 2021) to perform the cross-sectional geometry calculations (Figure 2.2). Twenty equally spaced cross-sections were defined between 10% and 80% of total bone length for each specimen. The 10% boundary was chosen because the sternal epiphysis of the clavicle variably exhibits deep concavities, especially prevalent in *Pan*, that would affect the calculation of cortical geometry between 0 – 10% of bone length. 80% bone length was defined as

the lateral extent for calculations because after this point, the cross-sectional geometry of all hominoid clavicles becomes constrained by the physiological need for articulation with the flat and wide acromion of the scapula, therefore the geometry in this region was assumed to be relatively uninformative. Next, a landmark configuration was created for each slice, with twenty-five points describing the periosteal surface and twenty-five describing the endosteal surface. From this landmark configuration, measures of cortical cross-sectional geometry (Table 2.3) were taken. The measurements used in this study include the proportion of cortical area in a cross section (CA), second moments of area relative to the craniocaudal (I_X) and dorsoventral (I_Y) axes, second moments of area about maximum and minimum principal axes (I_{MAX} and I_{MIN}, respectively), polar moment of inertia (J), and polar section modulus (Z_{pol}) (Figure 2.3).

The proportion of cortical area (CA) in a given section is generally assumed to reflect the strength of the bone under axial compression and/or tension (Ruff and Hayes, 1983; Ruff and Runestad, 1992; Ruff et al., 1993, 2013; Trinkaus and Ruff, 2012) with the clavicle oriented orthogonally to suspensory and quadrupedal substrate reaction forces, it is unlikely that axial compression is the largest acting force and cortical area may better reflect strength under shear stress. Second moment of area of a cross section (I) estimates how well a beam will resist bending based on the distribution of its mass about its neutral axis (Ruff, 2003). Taking the ratio of I about principal axes (I_{MAX}/I_{MIN}) provides a measure of relative cross-sectional eccentricity (Jungers and Minns, 1979), while the ratio about anatomical axes (I_X/I_Y) provides insight into the orientation of the eccentricity (Swan et al., 2020). Although both ratios are used to gain insight into the circularity of a cross-section, they do not always reflect the same shape (Carlson, 2005). Here I measure the two ratios to understand the amount of variation in bending direction in the loading regime through I_{MAX}/I_{MIN} and the anatomical plane the clavicle is bending in to withstand the imposed loading via

I_X/I_Y. The polar moment of inertia (J) is a measure of how far away the cortical material is distributed relative to the centroid of the cross-section and is proportional to bending and torsional rigidity (Burr et al., 1989; Ruff, 2003). The polar section modulus (Z_{pol}) is the ratio between the polar moment of inertia and the distance to the outermost point on the cross-section from its centroid and is a measure of bending and torsional strength (Ruff, 2003; Profico et al., 2021). Although Bredt's formula for thin-walled sections, K, has also been used to compare torsional strength in mandibles (Daegling, 2007) and has been suggested to be a more accurate measure than J to compare torsional rigidity in long bones that depart from axial symmetry (Daegling, 2002), Z_{pol} and J are measured for this analysis because they are the standard for comparisons of limb bone cross-sectional geometry and are therefore more easily interpretable within the existing literature on limb bone cortical structure. Here, rigidity reflects the ability of the bone to minimize bending and deformation while strength focuses on the ability of the element to withstand loads without failure or breakage. Although cortical area and second moment of area have been shown to scale with body mass and bone length (Trinkaus and Ruff, 1999; Ruff, 2000), converting these measures into ratios, as is done here, helps to mitigate the influence of body mass for interspecific comparison. However, it is important to note that this approach does not fully account for the effects of bone length on overall bending strength and rigidity (Trinkaus and Ruff, 2012). The latter effect is captured by the polar moment of inertia and polar section modulus, which are both scaled to account for allometry by dividing the raw values by specimen bone length. Bone length was defined as the distance from the sternal articular surface to the lateral extent of the acromial end and was measured predominantly with digital calipers, but an osteometric board was used when clavicles were over 160 mm long.

For each measurement of interest, values at approximately 32%, 51%, and 73% of total bone length (slices 7, 12, and 18 respectively) were extracted from the entire dataset for statistical comparison. Interspecific and intraspecific differences were tested for using R 4.3.2 (R Core Team, 2023). Levene's tests were used to assess for significant differences in homogeneity of variance between groups and Shapiro-Wilk tests were used to identify datasets that deviated from a normal distribution. Fifty-four of the defined groups showed differences in homogeneity of variance and ninety-seven had non-normal distributions (Tables 2.4-2.7), so further differences between groups were investigated with non-parametric Kruskal-Wallis tests and post-hoc Dunn's tests with Bonferroni correction. For the datasets that did not reject the null hypotheses of the Levene's and Shapiro-Wilk tests, differences between groups were tested for using ANOVA and pairwise post-hoc Tukey's HSD tests (Tables 2.8-2.17). Significance was determined at $p = 0.05$ for all analyses

Results

Extant Hominoids:

Relative Cortical Area

Relative cortical area is a measure of the ratio of the cortical area in a cross-section to the total area of that section; the closer the value is to 1, the more area the cortical bone occupies in a given cross-section. Through ontogeny, the great ape taxa have the highest relative cortical area as juveniles and adolescents, with infants and adults exhibiting a lower relative cortical area mid-diaphysis (Figure 2.4 and 2.10). The difference between the sub-adult and adult relative cortical area is most pronounced in *Gorilla* with adults having a significantly lower cortical area than adolescents and juveniles (Tables 2.8 and 2.9). As predicted, *Homo* has a low cortical area across the clavicle in comparison with the other apes, matching the gracility noted in other skeletal

elements (Lieberman, 1996; Ruff, 2006; Chirchir et al., 2015; Ryan and Shaw, 2015). *Homo*, beginning as a juvenile, has significantly lower cortical area than *Pan* throughout ontogeny. However, adult *Pongo* has the lowest relative cortical area of the study sample, significantly different from *Pan*, *Gorilla*, and *Hylobates*. Notably, the ape taxa do not have a shared pattern of cortical area distribution across the clavicle; *Pan* and *Hylobates* have a relatively consistent cortical area while *Pongo*, *Gorilla*, and *Homo* have a parabolic distribution with the highest relative cortical area at approximately 50% bone length.

Principal Second Moment of Area (I_{MAX}/I_{MIN})

Second moment of area about principal axes is a measure of relative cross-sectional eccentricity. A ratio of 1 indicates a perfectly circular cross-section and the further the ratio deviates from one, the more eccentric or oblong the cross-section. All apes, except *Pongo* and *Gorilla*, demonstrate significant changes in cross-sectional eccentricity through ontogeny (Figure 2.5 and 2.11; Tables 2.10 and 2.11). During all age stages, *Pongo* has low I_{MAX}/I_{MIN} values indicating a relatively circular diaphyseal cross-section across the clavicle. *Gorilla* has a similar distribution of cross-sectional eccentricity through ontogeny, with sustained high values midshaft between approximately 35 – 63% of bone length. Adult *Pan* shares this peak in cross-sectional eccentricity with *Gorilla* juveniles and adolescents. This is significantly different from what is seen in *Pan* juveniles and infants in comparison. *Hylobates* also has a gradual establishment of cross-sectional eccentricity through ontogeny, starting relatively circular as infants and by adulthood they have one of the least circular diaphyses. *Hylobates* infants are significantly different from the adults and adolescents across the element. *Homo* infants are unique in starting with a peak in eccentricity between approximately 20 – 50% of bone length; they are significantly

different from adults in this region. *Homo* juveniles and adolescents have a cross-sectional eccentricity intermediate between infants and adults with the sternal end becoming gradually more circular and eccentricity increasing laterally across the bone.

Second Moment of Area about Anatomical Axes (I_X/I_Y)

Second moment of area about anatomical axes offers insight into which anatomical plane the eccentricity identified by measuring I_{MAX}/I_{MIN} occurs. Here, an I_X/I_Y value greater than 1 indicates more bone is distributed along the craniocaudal plane and a value less than 1 represents more bone along the dorsoventral plane in each cross-section (Figure 2.6 and 2.12). The orientation of eccentricity represented by I_X/I_Y is supported by the theta values, measuring the deviation of the axis of the maximum area moment of inertia from the anatomical x-axis (Figure 2.9). In the ape clavicle, this ratio captures entirely different trends in cortical morphology than I_{MAX}/I_{MIN}. Notably, the distribution of cortical bone about the craniocaudal and dorsoventral axes appears relatively stable in the clavicle through ontogeny. Where differences exist between the intraspecific age bins, they are relatively small. One exception to this trend is seen in *Hylobates*, where infants are significantly different from adults at 32% and 73% bone length (Tables 2.12 and 2.13). The other exception can be seen in *Pan* adults that differ significantly from the juveniles at 73% bone length. *Homo* adults also differ slightly from the younger individuals by having a relatively more even distribution of cortical bone about the craniocaudal and dorsoventral axes in the sternal portion of the bone; the infants, juveniles, and adolescents have a more craniocaudally oriented cortical distribution. Looking at this ratio interspecifically, none of the taxa sampled have identical trends across the clavicle. Even apes that shared similar patterns of cortical eccentricity as measured by I_{MAX}/I_{MIN}, like *Pan* and *Gorilla*, have significant differences between the

anatomical orientation of that eccentricity. *Gorilla* shows a unique increase in craniocaudal cortical distribution in the sternal third of the bone while *Pan* has a predominantly dorsoventrally oriented cortical distribution in that region. The ratio in *Homo* indicates that cross-sectional eccentricity becomes gradually more dorsoventrally oriented moving laterally across the clavicle. Cortical bone is also distributed predominantly dorsoventrally in *Hylobates* and *Pongo*, but both show a peak in craniocaudal distribution similar to that seen in *Gorilla* except on the lateral end of the element.

Polar Moment of Inertia (J) and Polar Section Modulus (Z_{pol})

Even after adjusting for body mass via bone length as a proxy, both J and Z appear to be highly related to body mass (Figures 2.7 and 2.8, 2.13 and 2.14). Given that Z_{pol} is calculated using J (Ruff, 2003; Profico et al., 2021), similar trends are seen inter- and intraspecifically and thus are reported here together. As the smallest ape in the sample, *Hylobates* has one of the lowest J and Z_{pol} values through ontogeny (Tables 2.14-2.17) Additionally, significant differences in J and Z_{pol} amongst ape taxa increase through ontogeny, with *Hylobates* as the main outlier during early sub-adulthood and more differences between the apes emerging as adults. As adults, *Gorilla* has a significantly higher J and Z_{pol} than *Pan* and *Pongo*, *Homo* has a higher J and Z_{pol} than *Pan,* and *Hylobates* has a lower J and Z_{pol} than *Homo, Pan,* and *Pongo.* The effects of increasing body mass on J and Z_{pol} during development can further been seen as all apes show significant differences in both J and Z_{pol} between adults and the youngest two age categories.

Fossil Hominins:

No significant differences emerge between fossil and extant taxa (Tables 2.9, 2.11, 2.13, 2.15, and 2.17) in part due to the small fossil sample size and therefore weak statistical power

(Table 2.18). Additionally, consideration should be given to the variation in cortical geometry measured in the extant apes and how that variation would likely exist in the extinct hominins as well. Given that most fossil hominins are represented here by a few individuals, the interpretation of the morphology presented here assumes these individuals are representative of the genus. Nevertheless, it is important to acknowledge the inherent limitations associated with such interpretations.

Looking at the general similarities between the fossil hominins and extant apes, several small trends emerge (Figure 2.4-2.14). *H. naledi* has a relatively high cortical area compared to *Homo* and *Gorilla*, more like *Pan* and *Hylobates*. The australopithecines, on the other hand, show a lower relative cortical area with some regions of the bone showing significantly lower cortical area than *Pan* and *Hylobates*. Regarding I_{MAX}/I_{MIN}, all fossil hominins except adult *Au. afarensis* (KSD-VP-1/1f) have trends that could easily fit within the range of variation of any extant ape. *Au. afarensis* in contrast shows a unique, large peak in cross-sectional eccentricity approximately at midshaft. *Au. afarensis* is also different from the other fossil hominins in its second moment of area about anatomical axes (I_X/I_Y); it has an extremely dorsoventrally oriented cortical cross-sectional geometry. *Au. africanus* and *Au. sediba* show trends similar to *Homo* and *Gorilla*, showing a variable peak in craniocaudal eccentricity in the sternal third of the diaphysis. *Au. africanus* also shows more variation in I_X/I_Y between the sampled individuals than *Au. afarensis* which has a nearly identical ratio between the adult and infant individual. Like the extant apes, the fossil hominins show very similar trends in J and Z_{pol}. The values across the clavicle in all fossil taxa are within the range of *Homo, Pongo,* and *Pan.* None approach the magnitude of J or Z_{pol} seen in adult *Gorilla*. Any significant differences indicate that the fossil hominins have significantly

higher J and/or Z_{pol} than *Hylobates*, again like the significant differences that emerged amongst the extant apes.

Discussion

Interspecific Signals of Locomotor Adaptation in Cortical Geometry

The results presented here demonstrate that hominoid taxa can be differentiated based on cortical bone distributions in the clavicle and some of the cortical distribution patterns identified are likely reflecting locomotor adaptation. In line with predictions, we see highly eccentric diaphyseal cross-sections in more locomotor-specialized taxa such as *Hylobates*, which show one of the highest degrees of eccentricity of all the hominoid taxa between 32-73% of total bone length. A high degree of shaft eccentricity suggests that the bone is strongest against unidirectional bending forces, matching both the stereotyped bending forces imposed by brachiation in *Hylobates* and the high frequency with which they perform this behavior (approximately 74% of locomotor behavior, Gittins, 1983).

Humans, also show high levels of eccentricity throughout the diaphysis, except in having a relatively circular cross-section medially between 10-30% bone length before showing a consistent increase in eccentricity laterally that peaks at the expansion of the acromial end. The circular cross-sectional shape medially combined with a relatively circular sternal articular surface suggests that bending is most variable in modern humans around the sternoclavicular joint and becomes increasingly predictable and unidirectional towards the acromial end of the bone. The distribution of cortical bone about anatomical axes in *Homo* supports the trend of increasing eccentricity, showing that the diaphysis is relatively evenly distributed at the medial end and becomes increasingly dorsoventrally eccentric moving laterally towards the acromial end. The

patterns together suggest that the modern human clavicle is subjected to loading that primarily causes strong dorsoventrally directed bending forces and those forces may be larger in magnitude and/or imposed more habitually on the lateral portion of the bone. The reinforcement against dorsoventral bending is contrary to our expectation of predominantly craniocaudal bending forces imposed given the pendular nature of the arms during locomotion and the clavicle's role in supporting the shoulder. Yet, increased resistance in the dorsoventral plane aligns with hypotheses of morphological adaptation for throwing that emphasize the importance of external rotation at the glenohumeral joint (Churchill and Trinkaus, 1990; Roach et al., 2012, 2013), and may potentially also reflect the internal rotation used in tool manufacturing and object manipulation.

Pan and *Gorilla* develop their stereotyped locomotor regime through ontogeny, with knuckle-walking comprising approximately 90% of all locomotor activity as adults (Doran, 1992, 1993, 1997; Sarringhaus et al., 2014). The shared peak in cross-sectional eccentricity seen medially in *Pan* and *Gorilla* cannot be attributed to external morphology since they differ in their pronouncement of the medial curvatures (Figure 2.15), therefore the development of this feature likely reflects locomotor adaptation. Because the peak in eccentricity is stronger in *Gorilla* adolescents than adults, its decrease may reflect a decline in habitual use of the arboreal environment at a large body mass. Interestingly, the similarities become complicated when the anatomical plane of the eccentricity is considered. In *Pan*, the increase in cross-sectional eccentricity is occurring predominantly in the dorsoventral plane, while in *Gorilla* the increase is occurring in the craniocaudal plane. This difference in the orientation of eccentricity may be related to one or a combination of factors, likely also related to differences in body mass, such as ontogenetic scaling (Inouye, 1992), kinematic differences between knuckle-walking in *Pan* versus *Gorilla* (Inouye, 1994; Kivell and Schmitt, 2009), and the higher frequency of arboreality

exhibited by chimpanzees into adulthood (Inouye, 1992, 1994; Sarmiento, 1994; Doran, 1997). Another interesting trend in *Pan* and *Gorilla* is that the patterns of cross-sectional eccentricity diverge at approximately mid-diaphysis, with *Gorilla* continuing to become increasingly eccentric towards the acromial end and *Pan* showing an increase in circularity at about 62% bone length before increasing cross-sectional eccentricity again to allow for acromioclavicular joint articulation. The sharp decline in cross-sectional eccentricity seen in *Pan* is interesting because it occurs in the region of the lateral curvature and is like the eccentricity values seen in *Pongo*, the taxon with the lowest degree of diaphyseal eccentricity. This pattern suggests *Pan* experiences more multidirectional bending forces in this region compared with the rest of the clavicle, and the similarity with *Pongo* may mean that this pattern of cortical reinforcement is necessary in this region for larger-bodied climbing taxa. I predict that the reason we don't see a similar trend towards a circular cross-section in the lateral region in *Gorilla* is because they have reduced arboreal and climbing behaviors compared to *Pan*, even if only by a little (Doran, 1997). However, because of the known variability in use of arboreal substrates by individual *Gorilla* and *Pan* species and between males and females, the differences in cortical geometry in these genera warrant further investigation and may lend insight into how subtle changes in arboreal frequency is reflected in internal cortical morphology.

Compared with the other apes, *Pongo* shows the lowest degree of cross-sectional eccentricity across ontogeny and *Hylobates* shows the highest. Interestingly, despite having opposite degrees of eccentricity, *Pongo* and *Hylobates* do share similarities in their distribution of cortical bone about anatomical axes. Both show a relative increase in craniocaudally oriented eccentricity around 65% bone length, just medial to the attachment of the coracoclavicular ligaments and where sometimes, as has been noted in *Hylobates* and modern humans, a synovial

joint can form (Haramati et al., 1994; Voisin, 2006a). This peak in eccentricity may then be present to provide resistance against the potential craniocaudal bending forces occurring during suspension, as the portion of the clavicle medial to the coracoclavicular ligaments and acromioclavicular joint capsule bends under the demands of suspending the individual's entire body mass from a single limb. The results from I_{MAX}/I_{MIN} and I_X/I_Y together suggest that highly suspensory locomotor regimes, regardless of how multi-positional or stereotyped the behaviors are, create high magnitudes of and/or habitually impose craniocaudal bending stress concentrated around two thirds bone length that must be resisted by cortical bone.

Relative cortical area appears to have a less direct relationship with locomotor behavior than the ratio of second moment of area. *Pan* and *Hylobates* have a similar relative cortical area both in term of magnitude and distribution of cortical area across the clavicle. They both have relatively high cortical areas compared with the other ape taxa and sustain that high value across the entire clavicle. This contrasts with the parabolic distribution of relative cortical area seen in *Gorilla, Homo,* and *Pongo* who each have their highest relative cortical area approximately mid-diaphysis. These similarities cannot be attributed to any shared external morphological features as *Gorilla* has a relatively straight diaphysis, *Pongo* has a slight curvature, and *Homo* has a pronounced curvature in this region. *Homo* and *Pongo* also have the lowest relative cortical areas of the adult sample. This matches the gracility predicted and documented in other skeletal elements from modern post-industrial human populations. However, the low cortical area is unexpected in *Pongo.* Given that *Pongo* predominantly locomotes arboreally using a wide variety of postures (Sugardjito and Hooff, 1986; Cant, 1987; Thorpe and Crompton, 2005, 2006), this low relative cortical area may suggest that their clavicles are built to withstand torsion and bending forces, and pure axial tensile and/or compressive forces are less prevalent. Although this cannot be the case

for all suspensory taxa as *Hylobates* have a high relative cortical area. It is also possible that *Pongo* has a low cortical area to increase clavicular bending strength and rigidity. By having relatively thinner cortical bone further from the centroid given its larger body mass compared to *Hylobates*, *Pongo* increases its resistance to deformation and fracture. However, *Hylobates* is likely to need equivalent, if not higher, bending strength in their clavicles for ricochetal brachiation.

Comparing relative strength and rigidity amongst hominoid clavicles, the trends appear to predominantly reflect differences in body mass despite both J and Z_{pol} values being scaled by bone length. *Gorilla* and *Homo* have some the highest strength and rigidity values, with adult *Gorilla* showing the maximum values for both variables across the clavicle. *Pan* and *Pongo* have very similar distributions of J across the clavicle and an almost identical Z_{pol} distribution. The similarities between *Pan* and *Pongo* are interesting given the opposite trends seen in relative cortical area. While the relative cortical area provides an indication of how much cortical bone is in each cross-section, J measures how far away that cortical bone is distributed relative to the centroid of the cross-section. *Pan* has a lot of cortical mass placed close to the centroid and *Pongo* has relatively less cortical mass placed much further from the centroid. This means that relative to their body size, *Pongo* uses less cortical material to produce the same amount of bone strength and rigidity compared to *Pan*. It is possible that *Pan* required a higher relative cortical area because overall, their locomotor regime loads the clavicle more heavily in axial compression and/or shear compared to *Pongo*. The biomechanical significance of this combination requires further consideration as it is similar to the cortical area, J, and Z_{pol} trends measured in *H. naledi* (see below).

Ontogenetic Plasticity of Extant Ape Cortical Geometry

The results indicate that cortical distribution changes through ontogeny, reflecting the shifting locomotor behaviors of the taxa under investigation. Although differences amongst apes are greater than the intraspecific differences across ontogeny, the discernable changes in cortical geometry seen in apes as they alter their primary locomotor behavior during ontogeny support the relationship between form and function in the internal cortical structure of the clavicle.

Clear changes in absolute eccentricity through ontogeny can be seen in *Pan*, *Homo*, and *Gorilla*. Notably, these are also the taxa we know to shift their locomotor regime substantially as they age and increase in body mass. In *Pan*, diaphyseal shape starts out relatively circular in infants and is consistent across the element. Eccentricity then increases across the entire diaphysis in juveniles and adolescents, gradually establishing the peak in cross-sectional eccentricity in the medial half of the element that is most predominantly seen in the adults. This incremental increase in diaphyseal eccentricity closely matches the timing of increased use of terrestrial quadrupedalism by *Pan* through ontogeny, with their adult locomotor regime being achieved sometime between first and second permanent molar eruption (Doran, 1992, 1993, 1997; Smith et al., 1994; Sarringhaus et al., 2014). Overall, the patterns of cortical distribution in *Pan* through ontogeny reflect performance of a variety of locomotor behaviors in juveniles and infants that impose multidirectional bending on the clavicle, and their behavior transitions to become less varied with more adult-like locomotor frequencies around adolescence. *Gorilla* also shows a stepwise increase in cross-sectional eccentricity in the medial half of the bone, but unlike *Pan*, *Gorilla* infants start out with a degree of eccentricity in the diaphysis and the magnitude of the eccentricity in that region is lower in adults than in juveniles and adolescents. Interestingly, because the degree of eccentricity decreases between adolescence and adulthood, it suggests a lessening of habitual

unidirectional bending which is in contrast to observational accounts of *Gorilla* locomotion that report an increase in knuckle walking and decrease in arboreality through ontogeny with adults performing terrestrial quadrupedalism approximately 96% of the time (Doran, 1997). However, in *Gorilla*, the differences in cross-sectional geometry among the age groups are not statistically significant. This may, in part, be attributable to the composition of the sample. *Gorilla* becomes predominantly terrestrial by the time they are two years old (Doran, 1997), but their first molars do not emerge until around age three and a half (Smith et al., 1994). This implies that the sample of *Gorilla* infants in this analysis includes individuals before and after this initial transition in substrate preference. Consequently, the heterogenous morphology within this group in combination with the underrepresentation of the youngest individuals may not be sufficiently distinct to yield statistically significant differences. Despite this limitation, the results in combination with behavioral observations support my hypothesis that rather than reflecting the increase in terrestrial quadrupedalism in *Pan* and *Gorilla* through ontogeny, the peak in diaphyseal eccentricity in the medial half of the bone may be more closely linked to the demands of arboreality and vertical climbing with a large body mass.

Homo sapiens shows nearly the opposite trend in cross-sectional eccentricity to *Pan* and *Gorilla*. Modern humans in the youngest age category have increased eccentricity in the medial half of the diaphysis, like the peak seen in *Pan* adults and *Gorilla* juveniles and adolescents. Interestingly, human infants also have a decrease in cross-sectional eccentricity at about 60% bone length making them most like adult *Pan* in that region of the clavicle. *Homo* juveniles and adolescents have cortical distributions that are intermediate between the infants and adults: the medial eccentricity gradually decreases until the sternal 30% of the bone is nearly circular, while the rest of the diaphysis shifts to have steadily increased eccentricity from approximately 30%

bone length through to the lateral end. This gradual transition to the adult distribution from a different pattern of sternal cross-sectional eccentricity in infants may reflect the unloading of the limb in locomotion after the child stops crawling. There is a large amount of variation in *Homo* infants, but this is likely in part due to the scale of the age categories used here and the large range of behaviors human children perform between birth and age six (e.g., be carried, crawl, climb, run, and become obligate bipeds). Overall, the distribution of cortical bone in the human clavicle through ontogeny suggests an increase in multidirectional bending forces in the sternal half of the element and an increase in dorsoventral bending in the acromial half through life.

Pongo, unlike any other apes sampled here, maintains a relatively circular diaphysis throughout ontogeny. This suggests that resistance against multidirectional bending in the clavicle is beneficial during all life-stages. Although orangutan locomotor and postural behavior data is limited, their known locomotor regime is often described as variable and non-stereotypic, usually involving the use of all four limbs in different combinations of arboreal postures (Thorpe and Crompton, 2006). This aligns closely with observations of low cross-sectional eccentricity. The non-stereotypic nature of their behavior in combination with observations suggesting no changes in locomotor regime through ontogeny (Sugardjito and Hooff, 1986; Thorpe and Crompton, 2005, 2006) may further explain the variation seen in the distribution of cortical bone about anatomical axes through ontogeny when this ratio is remarkably stable in the other ape taxa. On the other hand, *Hylobates* are known to maintain a relatively stereotyped locomotor regime through ontogeny, with brachiation as their dominant locomotor behavior (Gittins, 1983; Granatosky, 2018). Despite this, there is notable developmental plasticity in cross-sectional eccentricity. The younger *Hylobates* do show the same pattern of eccentricity as the older ones, with eccentricity relatively stable through the sternal half and becoming increasingly eccentric laterally, but the

adolescents and adults have a more eccentric cross-section from about 10 – 65% bone length. This variation may reflect the potential for increased use of ricochetal brachiation in older gibbons, which may create higher magnitude bending forces when locomoting than other types of suspensory behavior, and/or the increased bending loads imposed by brachiating with a larger body mass.

In contrast to the variation in absolute diaphyseal eccentricity noted in most taxa, the distribution of cortical bone about anatomical axes is relatively stable through ontogeny. *Gorilla* and *Pan* show negligible change through ontogeny, with overlap of all age categories across the diaphysis. *Homo* shows some minor variation medially, with infants having a more craniocaudal distribution of cortical bone, adults showing a more symmetrical distribution, and juveniles and adolescents falling intermediate between the two. This trend in *Homo,* paired with the absolute eccentricity of the cross-section, supports the presence of stereotyped craniocaudal bending of the clavicle medially in young individuals that is gradually lessened through ontogeny. *Hylobates* shows some variation through ontogeny, with adults having the strongest degree of craniocaudal eccentricity around two thirds bone length. Another ape that shows variation in anatomical distribution of cortical eccentricity is *Pongo,* with both infants and adolescents having different distributions than the adults and juveniles, which are alike. Infants show much greater craniocaudal eccentricity medially than the three older age categories. Adolescents have a pattern of distribution similar to adults and juveniles but are more craniocaudally eccentric across the entire element compared with the more evenly distributed cross-sections of the other individuals. This variation may again be attributable to the high variation in locomotor behaviors and postures used by *Pongo*.

The results presented here indicate a contrast between the relatively stable distribution of cortical eccentricity about anatomical axes throughout ontogeny and the shifting magnitudes of

absolute diaphyseal eccentricity. Thus, I argue that relative cross-sectional shape about anatomical axes is present from birth and represents environmental adaptation occurring on an evolutionary scale. That initial shape is then either accentuated through increased eccentricity in response to unidirectional bending or is diminished and cross-sectional shape becomes more circular in response to multidirectional bending, producing the trends in absolute eccentricity measured with I_{MAX}/I_{MIN}. Moreover, the ratios I_X/I_Y and I_{MAX}/I_{MIN} do not quantify the same patterns of cortical distribution in a long bone and should not be conflated in studies of form and function (Figure 2.16).

Again, compared with the other measured aspects of cross-sectional geometry, relative cortical area does not have a readily apparent link with ontogenetic stage nor locomotor behavior across all ape taxa. *Homo* and *Pan* show similar trends through ontogeny with juveniles and adolescents having higher relative cortical area, and adults and infants have similarly low cortical areas. Interestingly, *Pan* and *Homo* infants have a slightly greater cortical area than adults around the region of the primary site of ossification in the human clavicle (Ogata and Uhthoff, 1990). This is similar to results reported by Cosnefroy and colleagues (2022) in the newborn olive baboon femur. *Gorilla* sub-adults, including infants, all show the same distribution of increased cortical area relative to the adults and share the placement of peak cortical area with *Homo* and *Pan* at about 60% bone length. The greatly reduced cortical area in adult *Gorilla* relative to the sub-adults may be related to maintaining the safety factor of the clavicle; given the allometric scaling of safety factor (Biewener, 1982), larger animals can reduce bone stress by increasing the bone's diameter relative to the length (Hayes and Gerhart, 1985). In contrast to the African great apes, *Hylobates* and *Pongo* do not show any consistent trends in relative cortical area through ontogeny. In *Pongo*, this may be attributable to their variable, non-stereotypic locomotor regime through ontogeny

creating similar, but not identical, structural demands between the age categories. However, for *Hylobates*, it is less clear why the relative cortical area appears to decrease, increase, and then decrease again through ontogeny. Unlike *Pan*, *Gorilla*, and *Homo*, neither *Pongo* nor *Hylobates* have their greatest cortical area near 60% bone length; *Pongo* has its highest relative cortical area between 40 – 50% bone length whereas *Hylobates* has an approximately equal cortical area across the element. This may reflect the potential for the primary center of ossification to be in a slightly different location in the Asian apes.

In relation to clavicular growth, despite the fact that the medial endochondral ossification center contributes more to axial bone growth than the lateral center (Ogata and Uhthoff, 1990), we do not observe any trends indicating a lateral shift in cortical geometry across the element over ontogeny. This suggests two main possibilities: either the dominance of the medial contribution to the clavicular length is most significant during fetal and/or immediate postnatal development, a period not covered by the present sample, or that external factors have a greater influence on the cortical geometry of the clavicle than the ongoing growth at the secondary ossification centers. Additionally, it is likely that the generally higher cortical area in sub-adults does not reflect the variation in locomotor demands during that life stage, but rather the process of bone deposition in a growing long bone. Finally, J and Z_{pol} increase through ontogeny in all hominoids, supporting a general trend of clavicular development in which the cortex is remodeled to be placed further from the neutral axis to increase rigidity and strength as the bone grows and body mass increases.

Signals of Locomotor Adaptation in Fossil Hominins

When comparing the cortical geometry of the fossil hominins to the extant apes, interesting similarities emerge. In the ratio of second moment of area about anatomical axes, *Au. africanus*

and *Au. sediba* have distributions most similar to *Gorilla*. They have a variable increase in craniocaudal eccentricity in the sternal third to half of the bone and a dorsoventrally expanded cross-section through the acromial end. Separating the two South African *Australopithecus* species from one another is how far the craniocaudal eccentricity spreads medially; in *Au. africanus*, the craniocaudal orientation of the cross-section is highly localized around 20% of bone length, while in *Au. sediba* the craniocaudally eccentric shape is seen to a relatively even degree throughout the sternal half of the clavicle. While this does not conclusively imply that the two South African australopiths engaged in knuckle walking, it does suggest that the bending strains occurring in the medial aspect of the diaphysis were similar amongst *Au. africanus, Au. sediba*, and modern *Gorilla*. Moreover, these similarities between *Au. africanus* and *Au. sediba* may reflect the influence of environmental factors on the use of the upper limb, or, if the taxa are demonstrated to be closely phylogenetically related, these similarities could also be attributable to genetic drift. *H. naledi,* on the other hand, has a cortical distribution about anatomical axes like *Pan*. The relatively constant dorsoventral orientation of the cross-sectional eccentricity across the first 60% of bone length could fit within the range of variation seen in adult *Pan* and *Pongo*. *H. naledi* also shows a small increase in craniocaudal cortical geometry on the lateral end of the element very similar to *Hylobates*. This cortical distribution towards the acromial end has been interpreted in extant apes to reflect the increase in craniocaudal bending in that region imposed by forelimb suspension. A similar increase in craniocaudal eccentricity can be seen in *Au. afarensis*. This is especially interesting as *Au. afarensis* has a uniquely low I_X/I_Y ratio, maintained through the entire clavicle, compared to the fossil and extant taxa. Also notable, the same cortical distribution is seen in both the adult and infant *Au. afarensis* individuals, suggesting that the stability of this measure of cortical cross-sectional shape through ontogeny extends to fossil hominins as well. Trends in I_X/I_Y

predominantly support some level of arboreality in *Au. afarensis* and *H. naledi* in line with existing hypotheses (Melillo, 2016; Feuerriegel et al., 2017; Stamos and Alemseged, 2023), and similar mechanical loading of the clavicle between *Au. africanus* and *Au. sediba*, although the exact nature of that loading is still unclear.

Regarding the principal second moment of area, or the relative eccentricity of the cortical cross-sections, the South African hominins (*Au. africanus, Au. sediba,* and *H. naledi*) show individual cortical distributions that could fit within the range of any of the great apes. The small fluctuations in cross-sectional eccentricity are not diagnostic of locomotor trends given the interspecific variation expected in the fossil taxa. Again, *Au. afarensis* is distinct from the other fossil hominins in having a much higher degree of cross-sectional eccentricity with values outside the range of variation seen in the extant apes. The cortical distribution seen in the juvenile (DIK-1-1) is similar in overall trends to the other fossil hominins, but these small fluctuations in cross-sectional shape are happening at a higher average magnitude of eccentricity. The adult (KSD-VP-1/1f), on the other hand, shows a very strong trend of increased cross-sectional eccentricity in the middle third of the diaphysis. The location along the bone of this trend is similar to the increases in eccentricity measured in *Pan* and *Gorilla* through ontogeny, but again is happening at a higher average eccentricity. This ontogenetic acquisition of the increased I_{MAX}/I_{MIN} values mid-diaphysis in *Au. afarensis* supports hypotheses of continued reliance on arboreal behaviors into adulthood.

Similarities between the fossil and extant taxa are unclear when looking at the relative proportions of cortical area in each cross-section. All fossil hominins fall within the range of variation of the extant apes. *H. naledi* appears to have the highest relative cortical area of the fossil hominins, and comparatively the cortical distribution is consistent across the diaphysis as seen in

Pan and *Hylobates*. The other fossil hominins have a roughly parabolic relative cortical area across the clavicle, similar to *Gorilla, Pongo*, and *Homo* .

The pattern of bending strength and rigidity across the fossil clavicles is consistent with expectations, as J and Z_{pol} appear to be related to body mass, so in this context the distribution of these values along the diaphysis is more relevant than the magnitude of the values. Most fossil hominin taxa show distributions of J and Z_{pol} unlike anything measures in the extant apes, with the only excepting being *Au. sediba* which has a distribution of both variables very similar to *Pan* adults. *Au. afarensis* and *Au. africanus* adults both have sigmoidal distributions of cortical strength and rigidity, but the trends are in contrast to one another – *Au. afarensis* has increased bending strength medially and less laterally, while *Au. africanus* shows increase bending strength laterally and decreased strength medially. This implies that these individuals subjected their clavicles to opposite mechanical demands, a trend not necessarily reflected in the other measures of cortical geometry. Moreover, despite the similarities between *Au. africanus* and *Au. sediba* in cortical cross-sectional shape as measured by I_{MAX}/I_{MIN} and I_X/I_Y, the difference in J and Z_{pol} suggests that these hominins were not interacting with their environments in an identical manner. The distribution of bending strength and rigidity in *H. naledi* is interestingly very similar to the one hypothesized *Au. africanus* sub-adult, StW 582. The increased strength and rigidity in the lateral half of the clavicle of *H. naledi* may be the result of increased craniocaudal bending in this region as is hypothesized based on a corresponding increase in I_X/I_Y. However, this does not explain the pattern of J and Z_{pol} in StW 582, since it shows a decrease in I_X/I_Y in the same region of the diaphysis. Ultimately, the inclusion of J and Z_{pol} has strengthened the interpretations of the other aspects of clavicular cross-sectional geometry, underscoring the considerable variation in upper limb usage hypothesized among fossil hominins.

Significance

This study provides the first comparative study of the cortical distribution in the hominoid clavicle, is the first to quantify the cortical distribution in the fossil hominin clavicle, and is one of the first multi-taxon studies of cross-sectional geometry through ontogeny in primates. The examination of cortical distribution and cross-sectional eccentricity in the clavicle amongst hominoid taxa through ontogeny reveals patterns of internal morphology that shed light on how locomotor adaptations are reflected in bone structure. For instance, the pronounced eccentricity in the diaphysis of *Hylobates* aligns with their brachiating lifestyle and stereotypic locomotor regime, emphasizing resistance against unidirectional bending forces. Moreover, the shifts in cortical morphology through ontogeny identified in this analysis underscore both the dynamic relationship between form and function and the ability for the clavicle to respond to such changes in environmental stimuli despite its position far from direct contact with the substrate. Taxa known to shift their dominant locomotor behavior during ontogeny, such as *Pan* and *Homo*, show corresponding changes in cross-sectional eccentricity, while taxa with stable locomotor regimes through life, like *Pongo*, show no significant changes in diaphyseal eccentricity between age categories. After adding fossil hominins into the analysis, the quantification of internal cortical geometry reveals similarities between the hominins and modern apes that could not have been gained from analyses of external morphology alone. *Au. afarensis* and *H. naledi* are similar in some aspects of cortical geometry that are also shared with the highly suspensory *Hylobates* and *Pongo*, supporting continued arboreality in these species. *Au. africanus* and *Au. sediba*, on the other hand, have a cortical geometry most similar to *Gorilla*, stressing the likelihood that the nature and extent of arboreal behaviors were just as variable among fossil hominins as they are among extant apes. These newly identified similarities and differences contribute to our understanding of

the complex relationship between form, function, and ontogeny in the hominoid upper limb, ultimately enhancing our knowledge of ape evolution. Although the cortical signals of morphological adaptation in the hominin fossil record are equivocal, this analysis provides strong support for the use of cortical cross-sectional geometry for identifying osteological correlates of locomotor behavior in the early hominin clavicle.

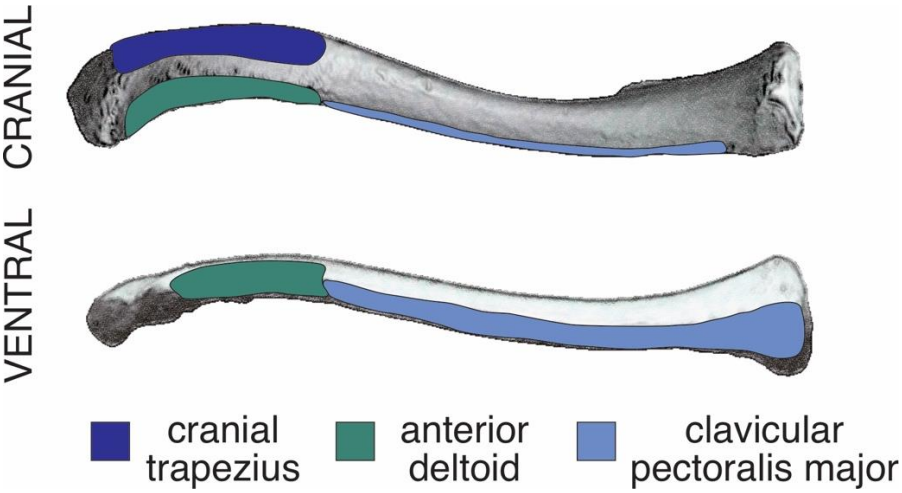

Figure 2.1. Origins sites of the cranial trapezius, anterior deltoid, and clavicular pectoralis major muscles on a modern *Homo sapiens* clavicle.

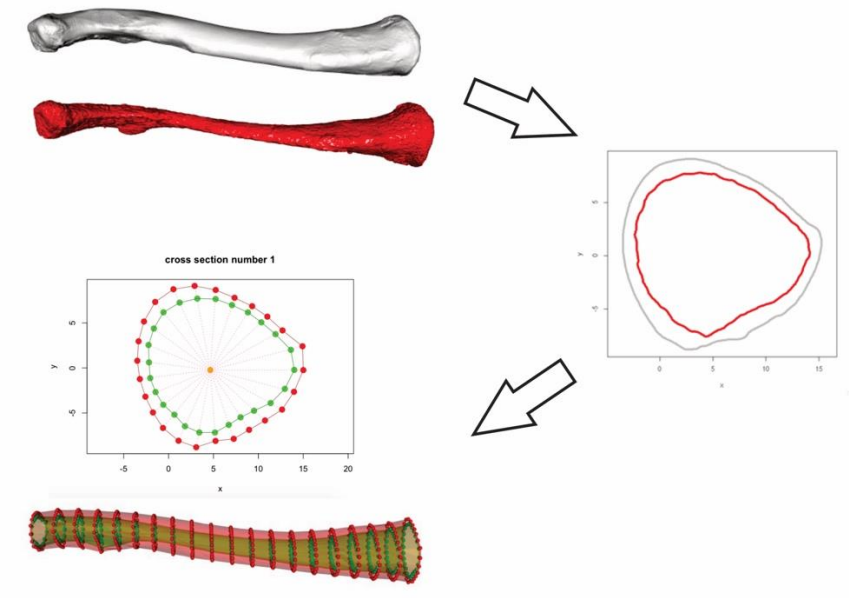

Figure 2.2. Morphomap workflow: imported volumes representing the periosteal and endosteal surfaces of the clavicle; example cross-section showing the periosteal and endosteal surfaces; example landmark configuration used to quantify the cross-sectional geometry.

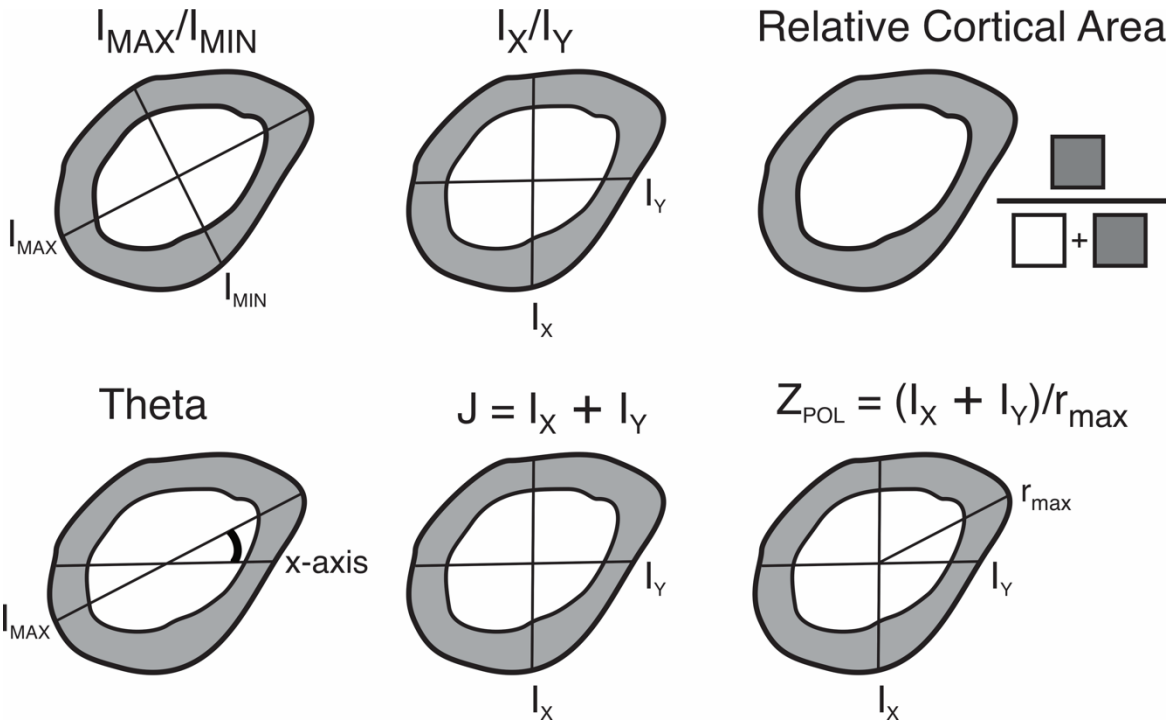

Figure 2.3. Cross-sectional variables of interest.

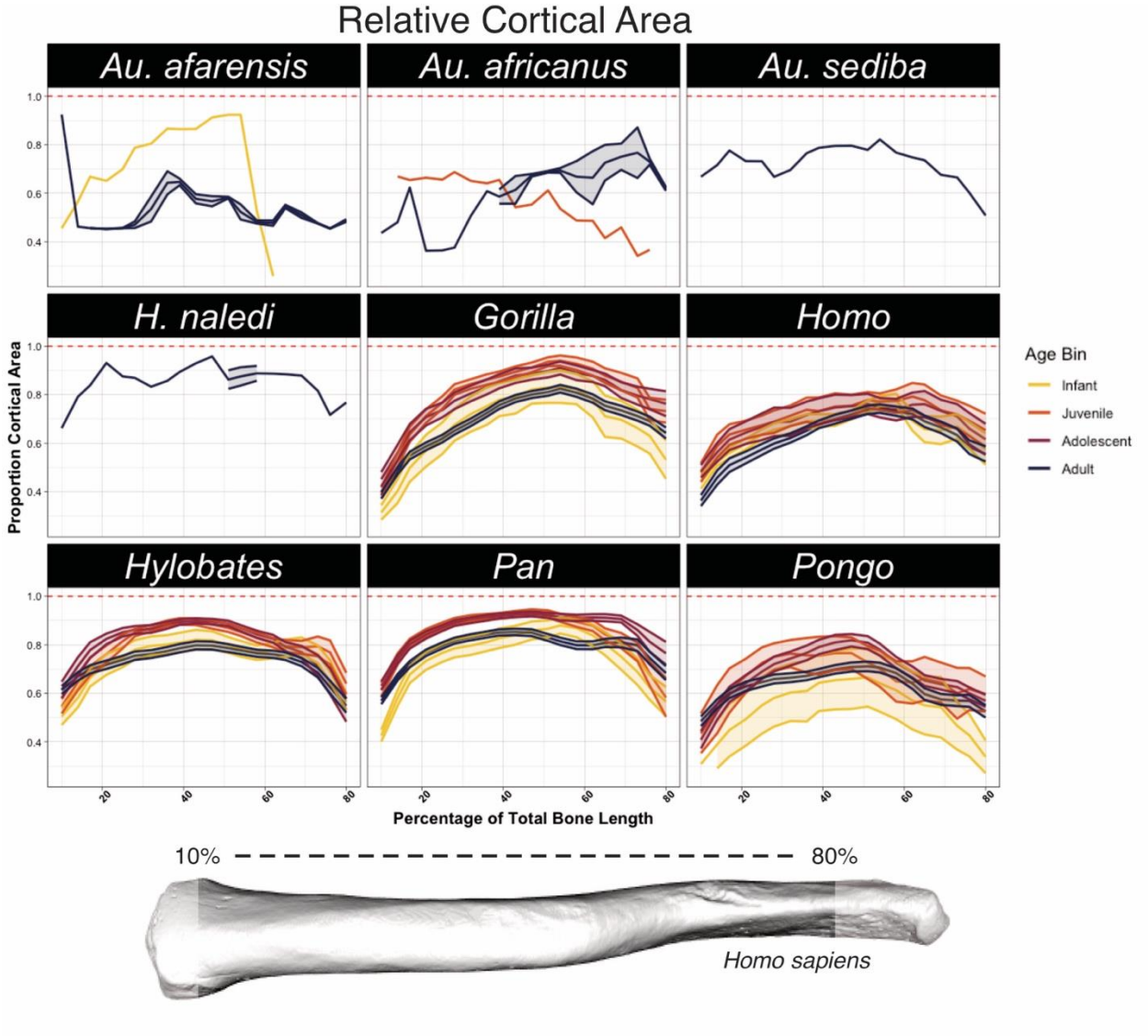

Figure 2.4. Relative cortical area through ontogeny, divided by genus.

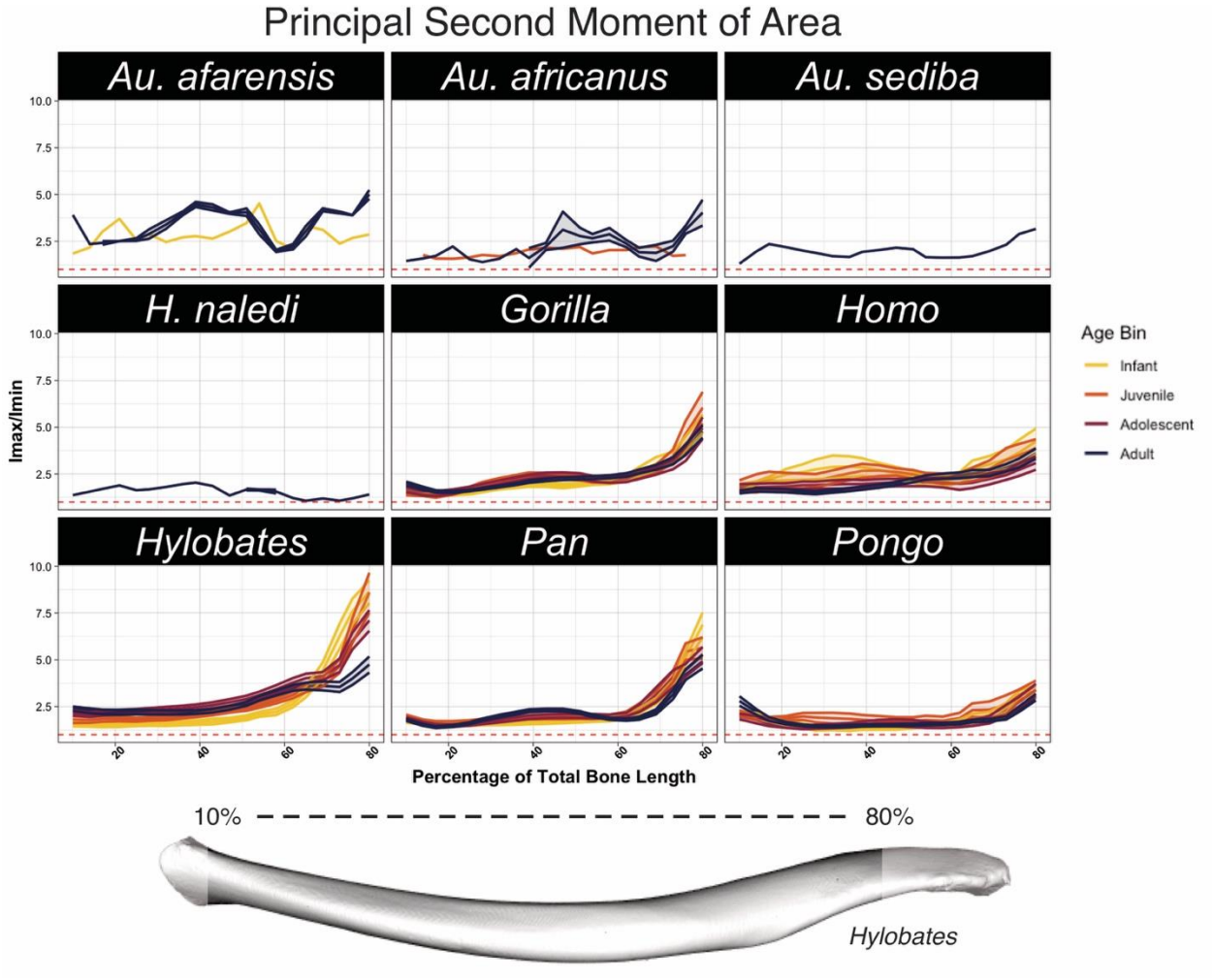

Figure 2.5. Second moment of area through ontogeny, divided by genus.

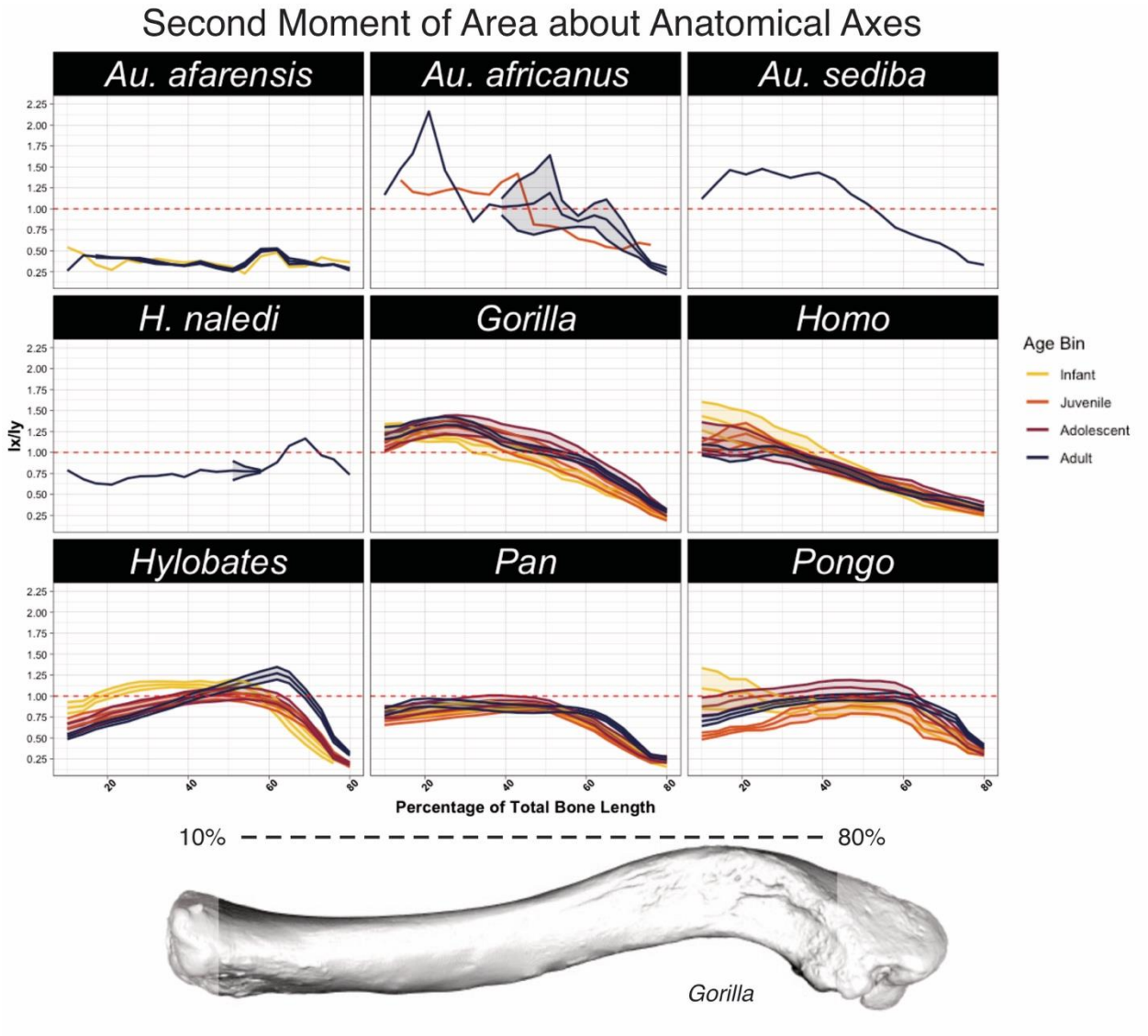

Figure 2.6. Second moment of area about anatomical axes through ontogeny, divided by genus.

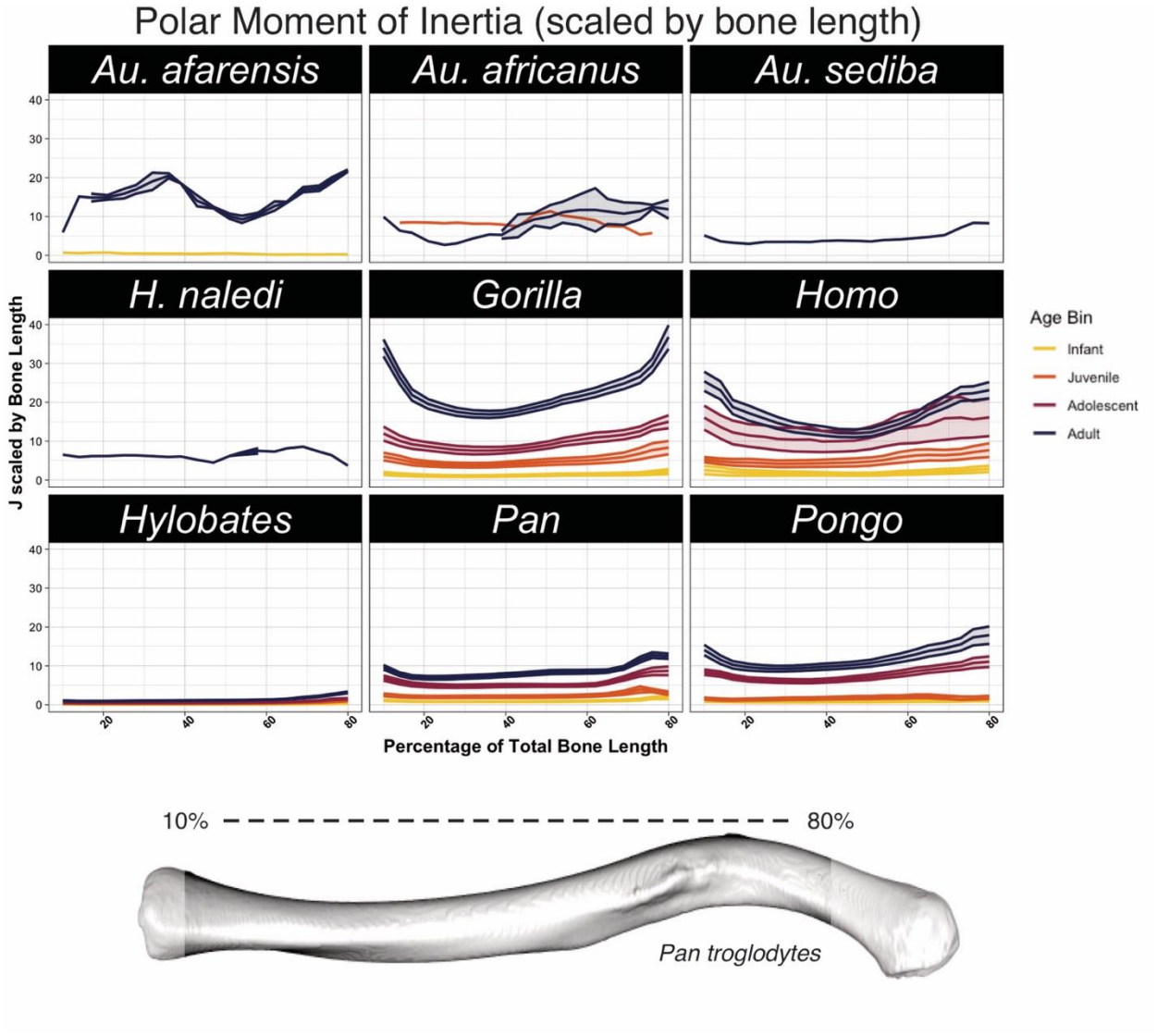

Figure 2.7. Polar moment of inertia through ontogeny, divided by genus.

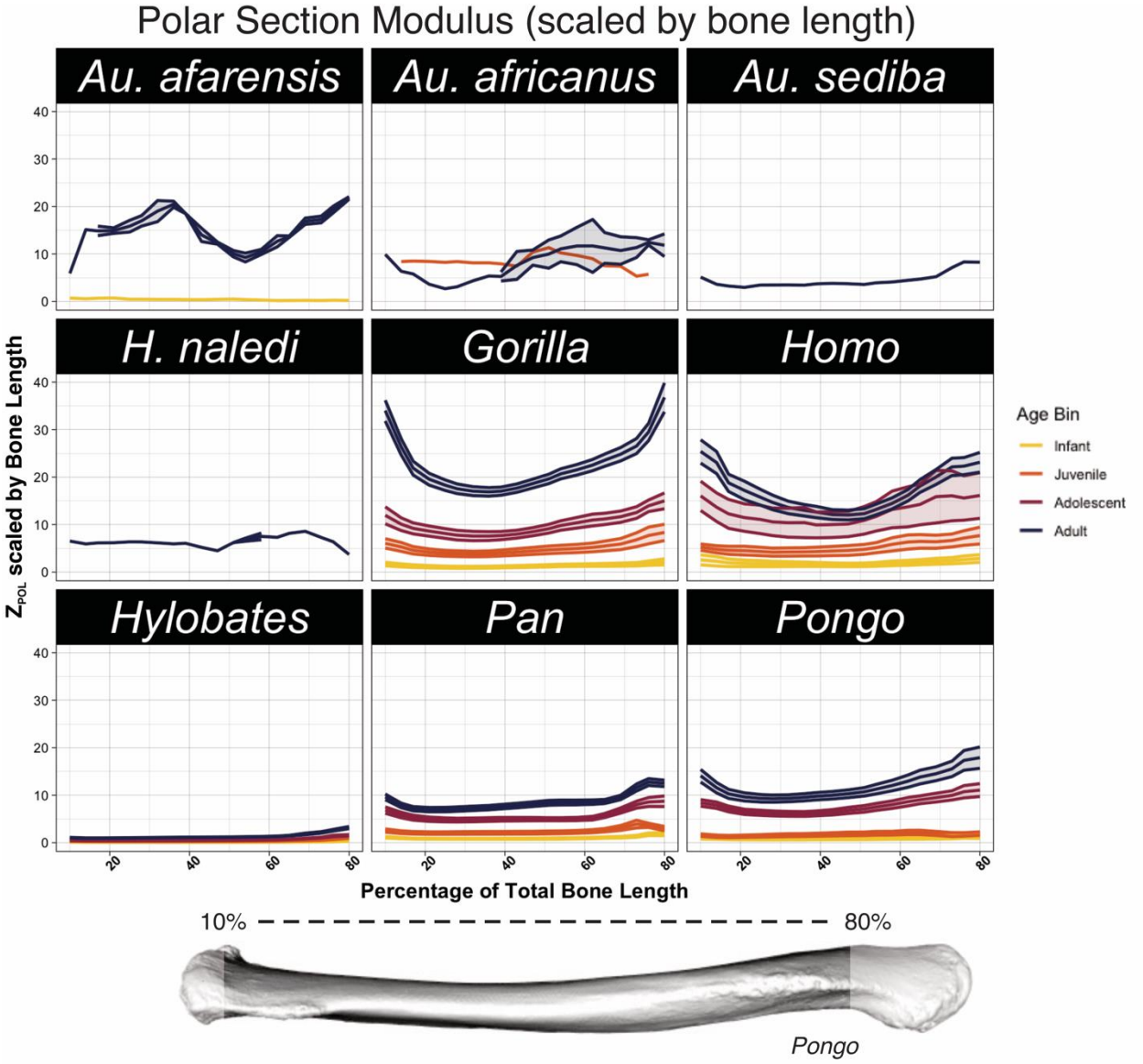

Figure 2.8. Polar section modulus through ontogeny, divided by genus.

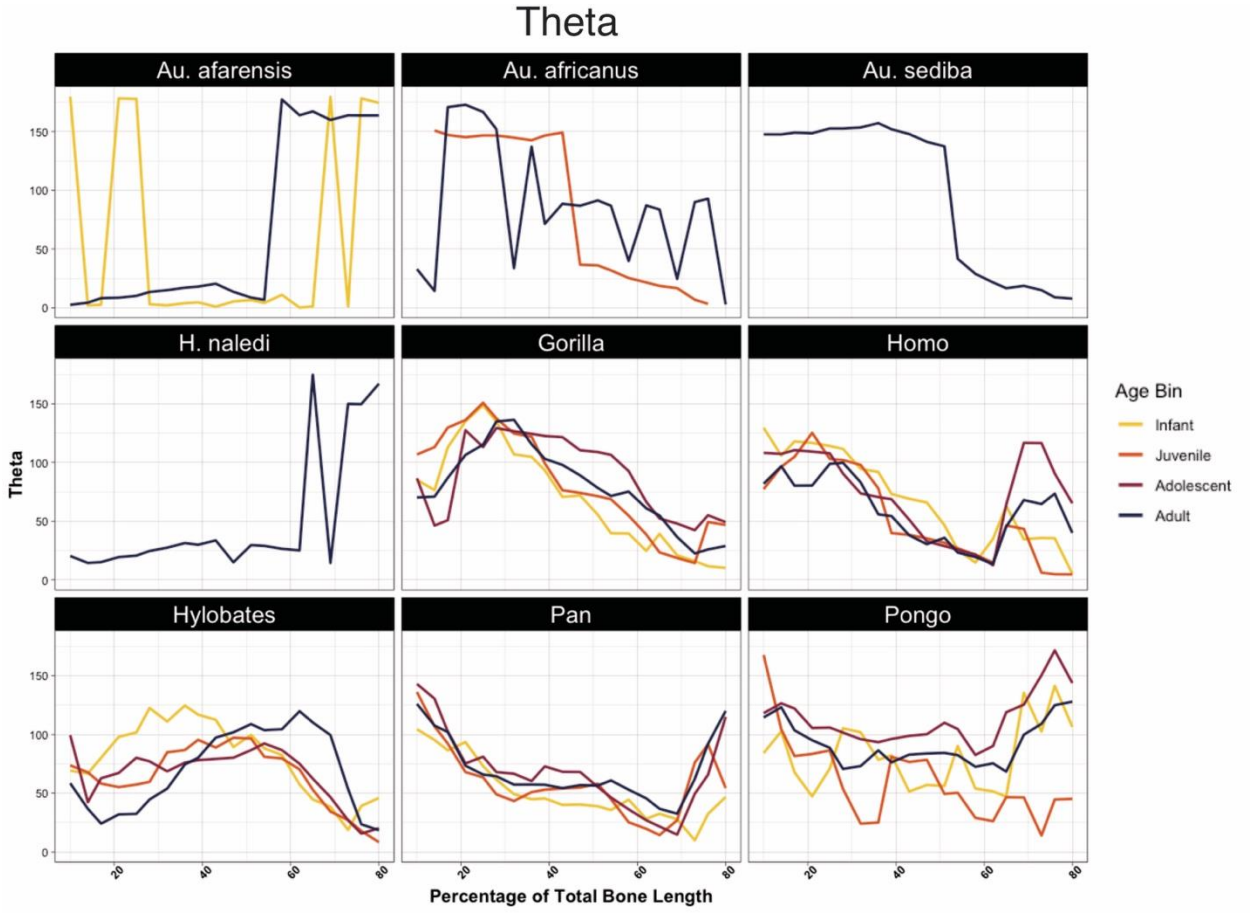

Figure 2.9. Theta through ontogeny, divided by genus.

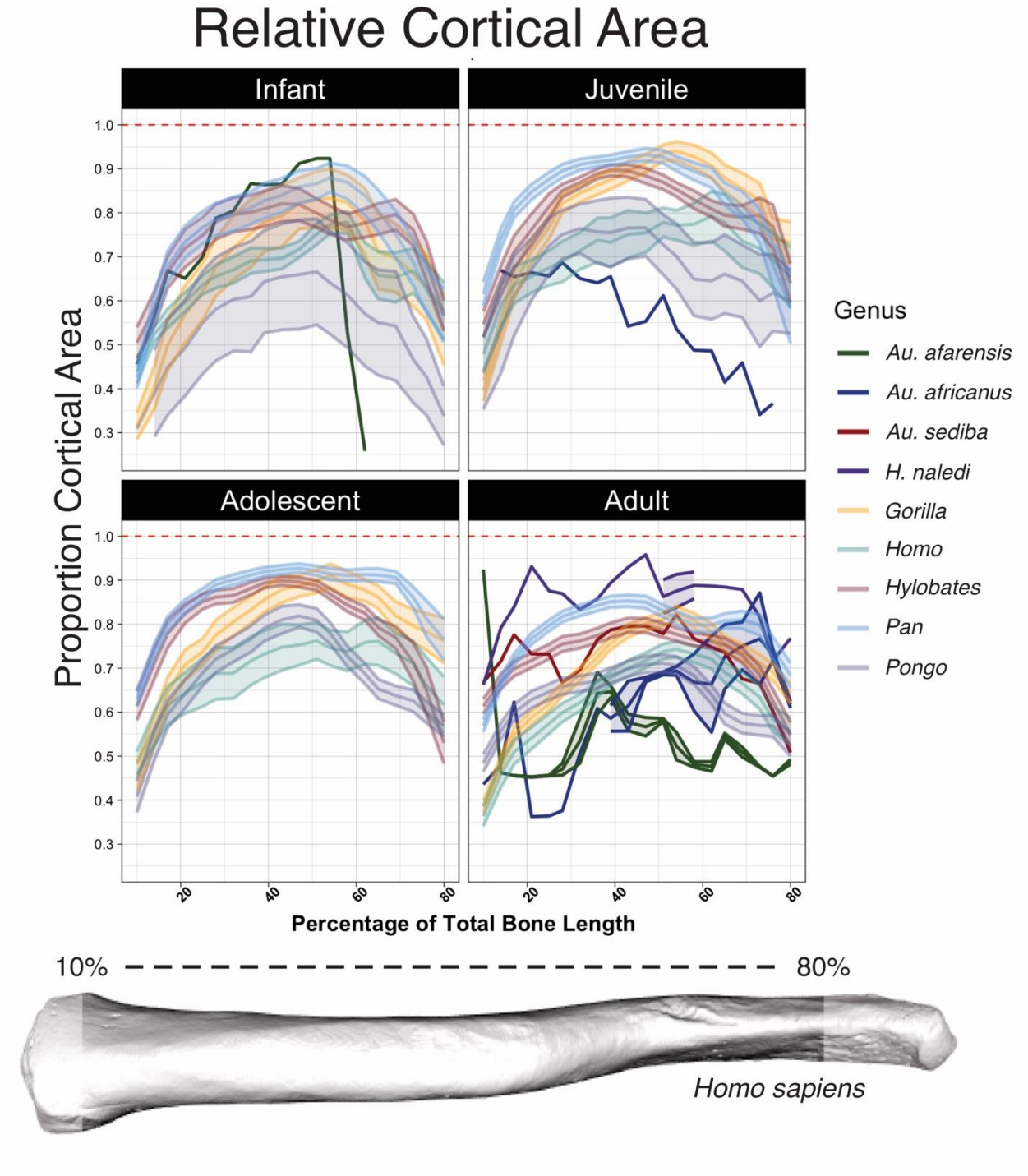

Figure 2.10. Relative cortical area through ontogeny, divided by age bin.

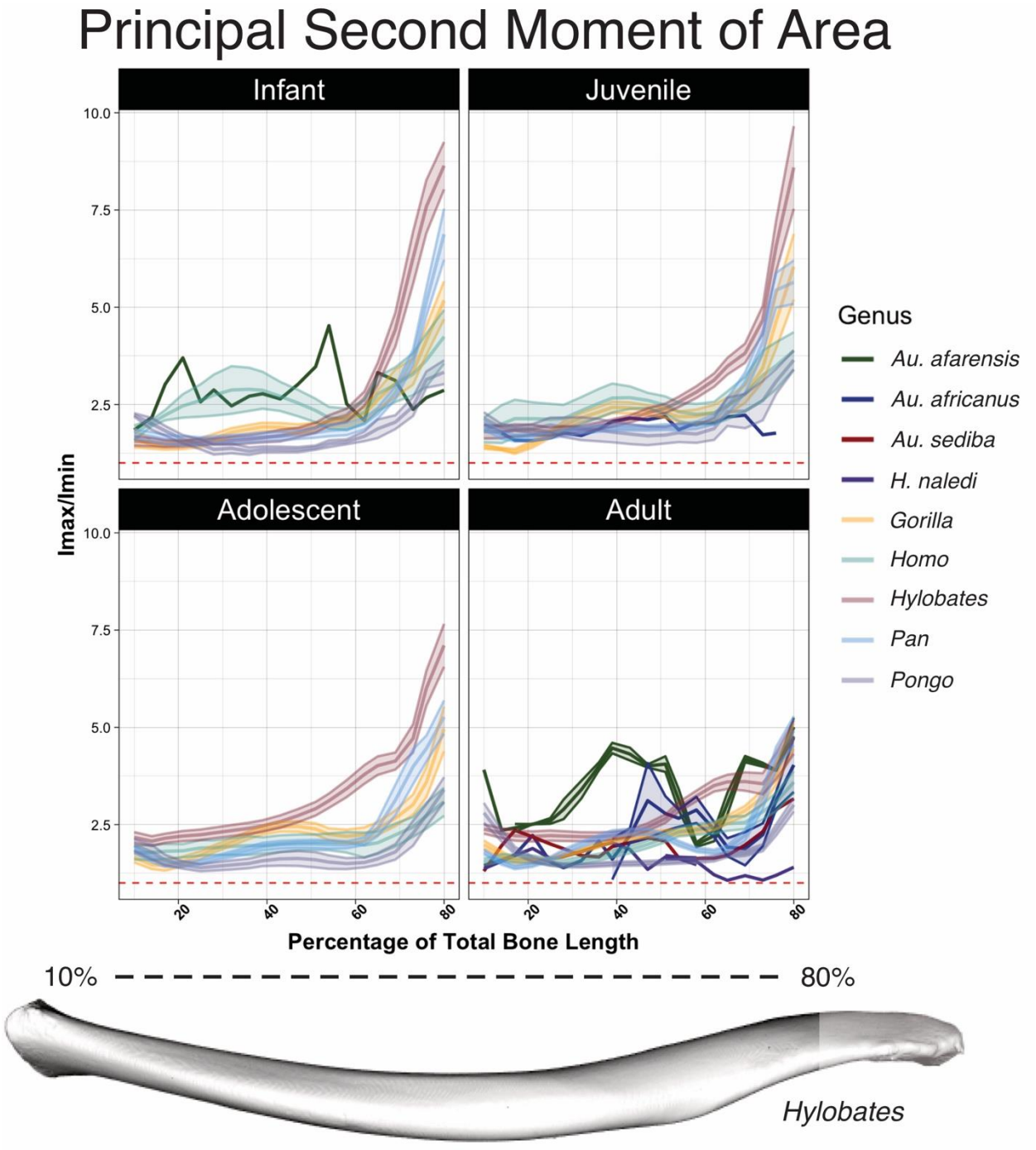

Figure 2.11. Principal second moment of area through ontogeny, divided by age bin.

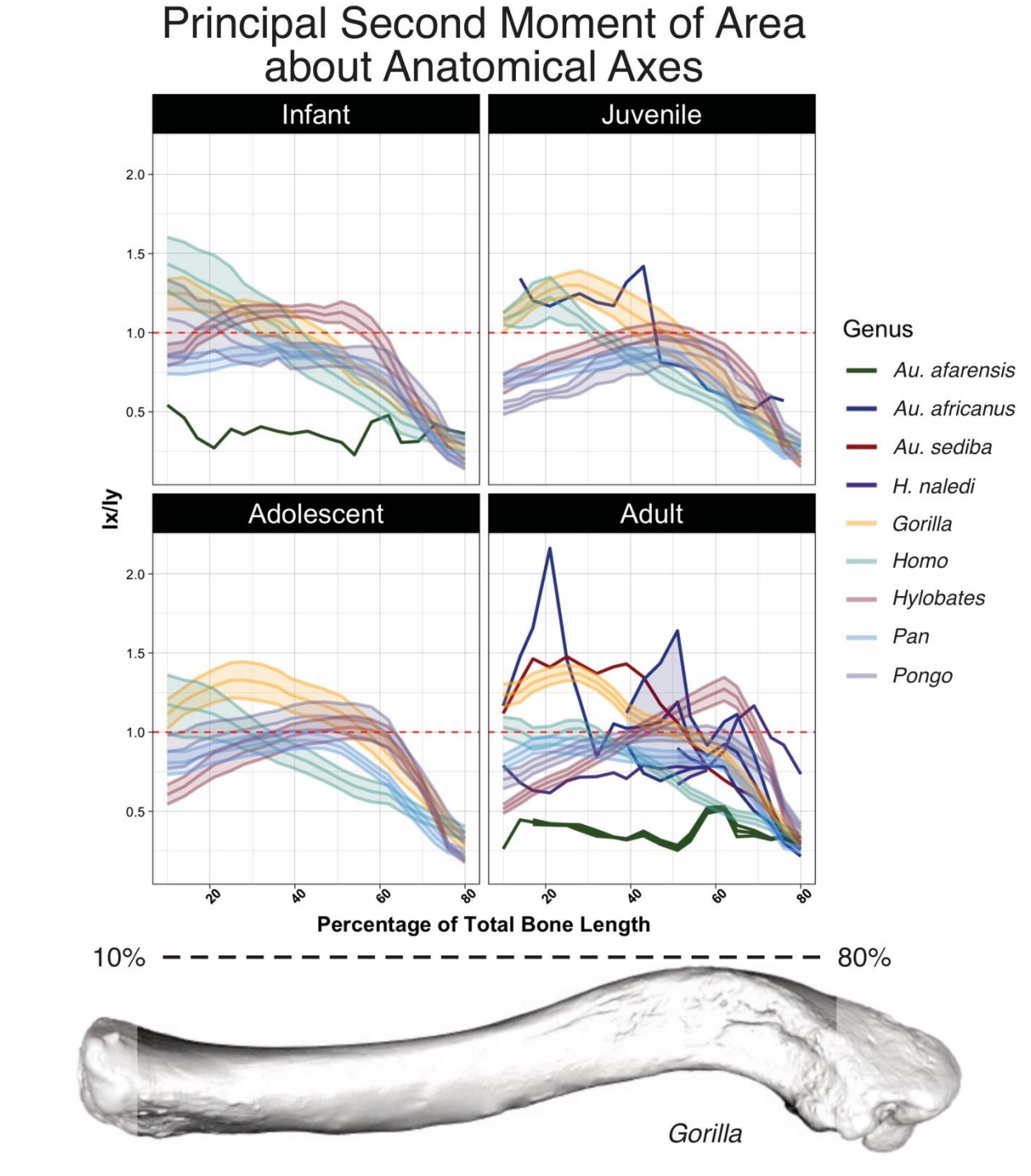

Figure 2.12. Principal second moment of area about anatomical axes through ontogeny, divided by age bin.

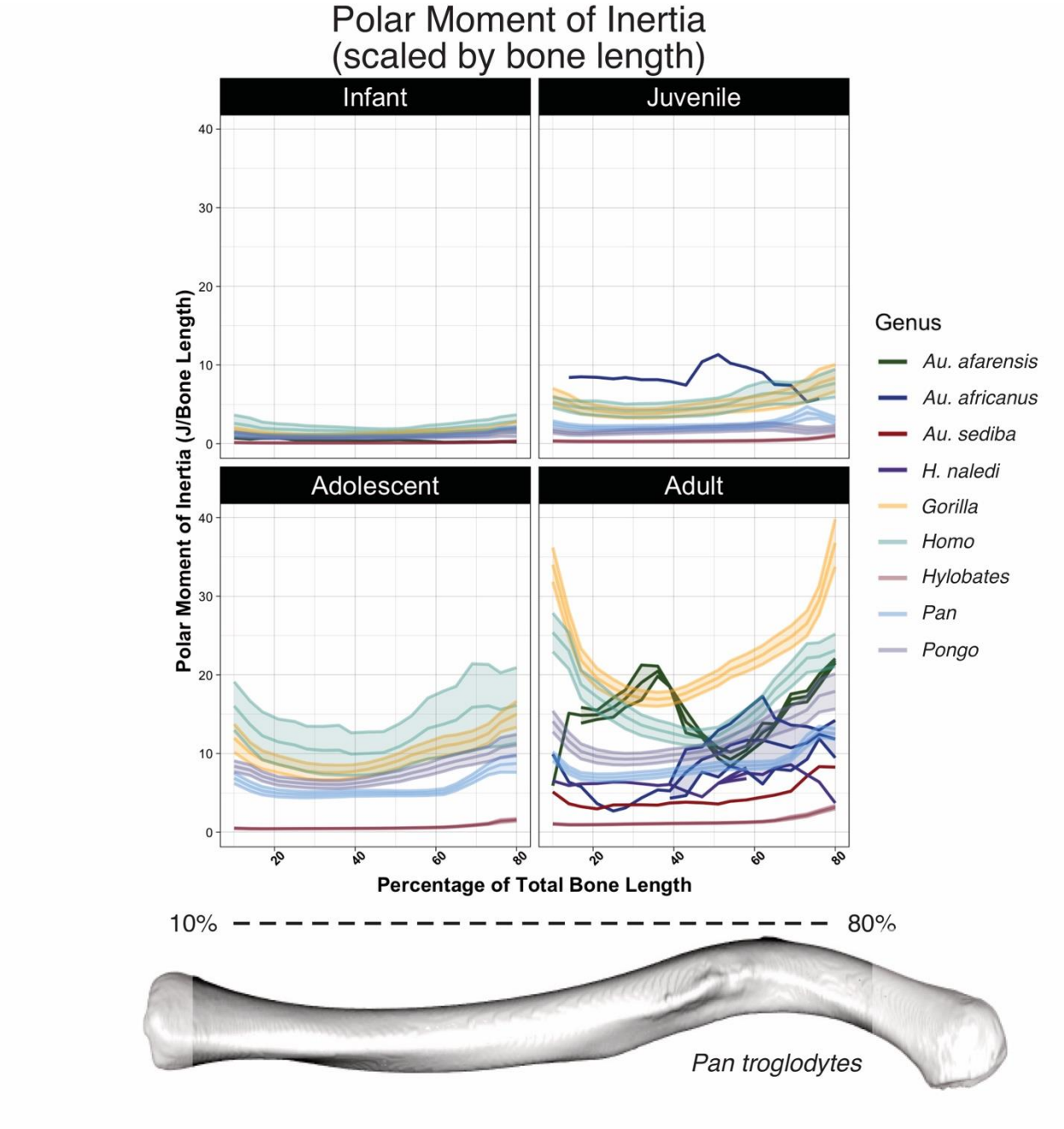

Figure 2.13. Polar moment of inertia through ontogeny, divided by age bin.

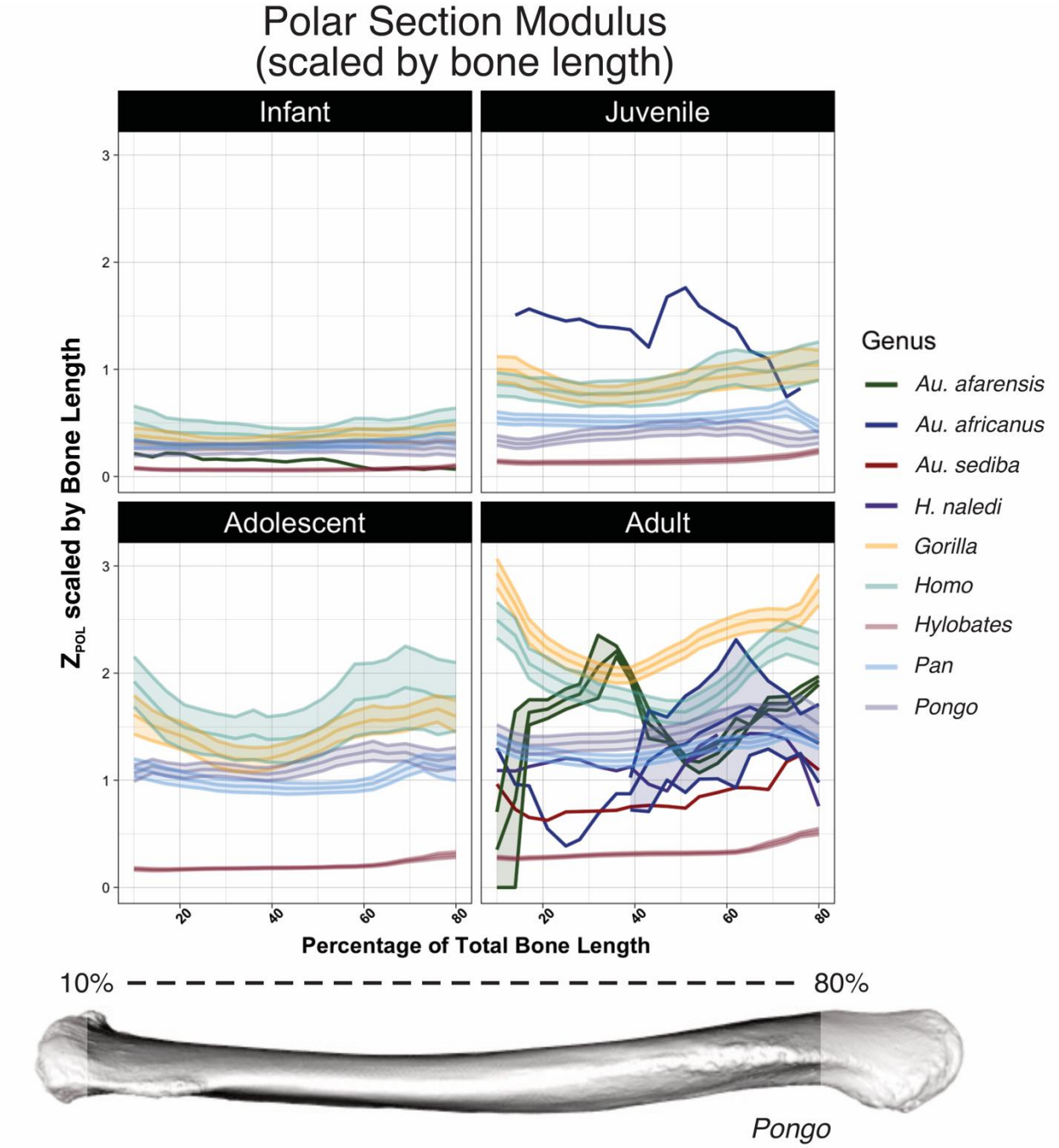

Figure 2.14. Polar section modulus through ontogeny, divided by age bin.

Figure 2.15. External shape variation in the extant hominoid clavicle. The clavicles are viewed from ventral on the left and cranial on the right. The lateral end is always on the left, and medial end on the right.

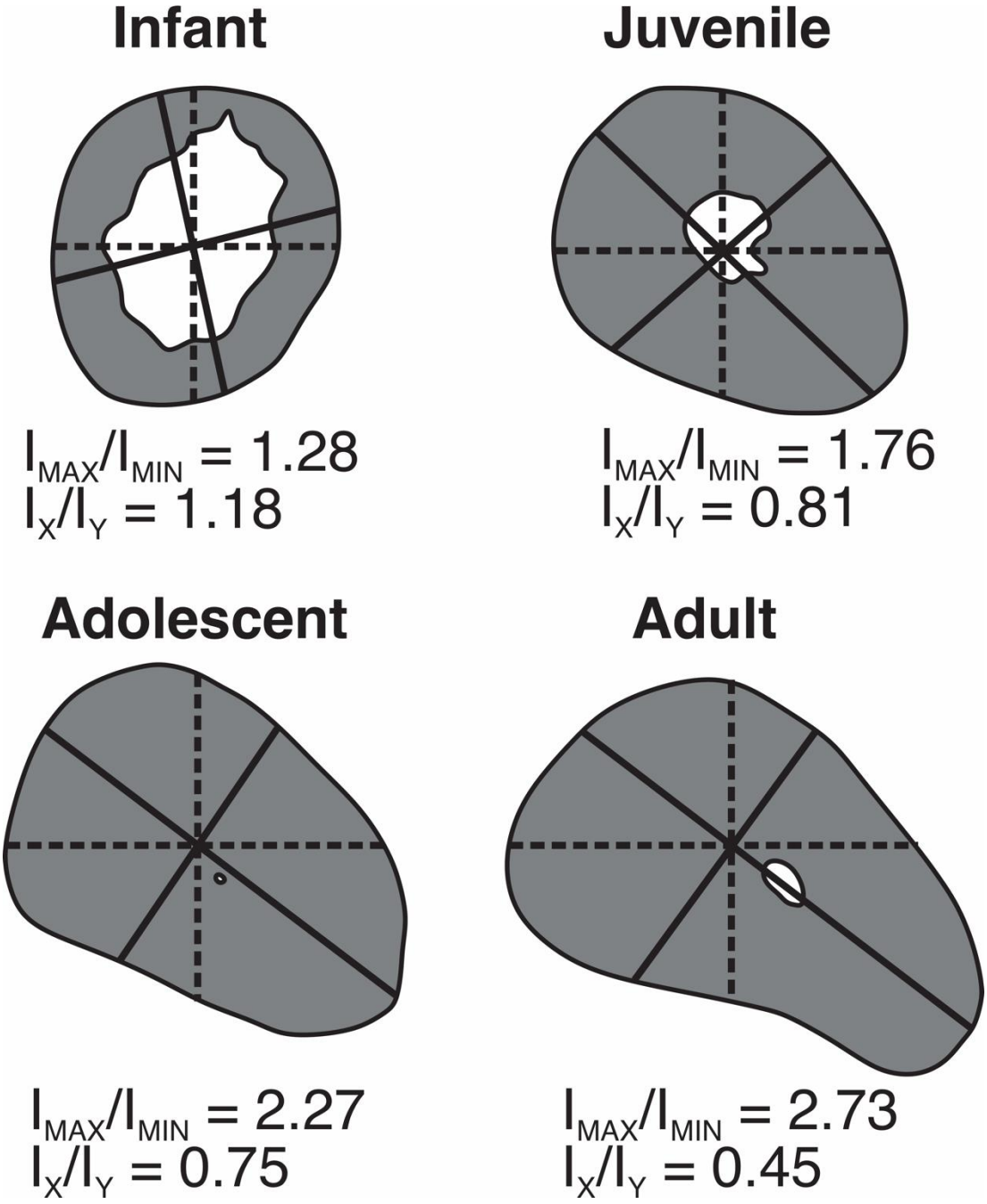

Figure 2.16. Example of absolute cross-sectional eccentricity changing through ontogeny, but the cortical distribution about anatomical axes remains relatively stable. Cross-sections above from *Pan troglodytes*.

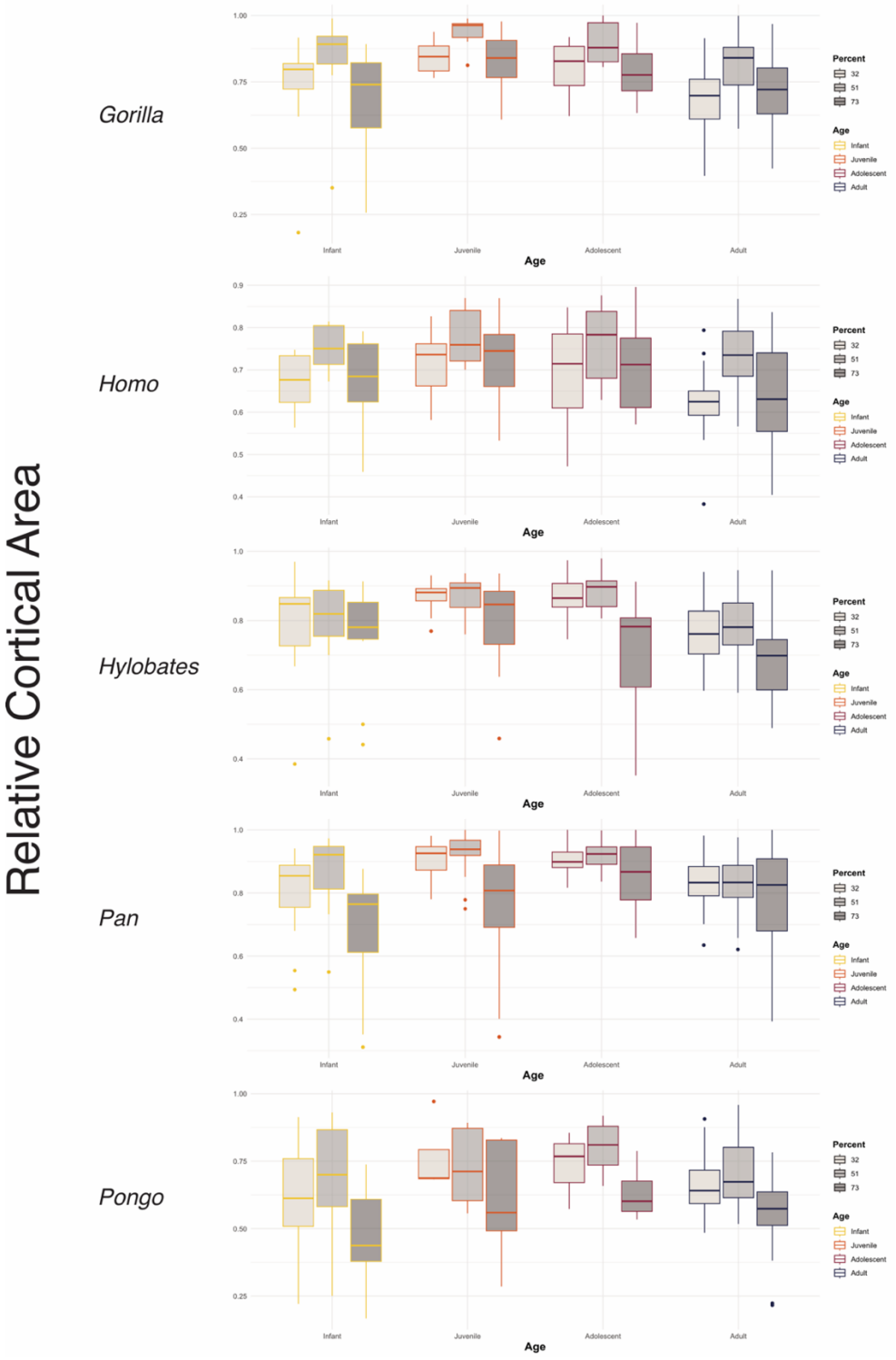

Figure 2.17. Relative cortical area at 32, 51, and 73% bone length, by age bin.

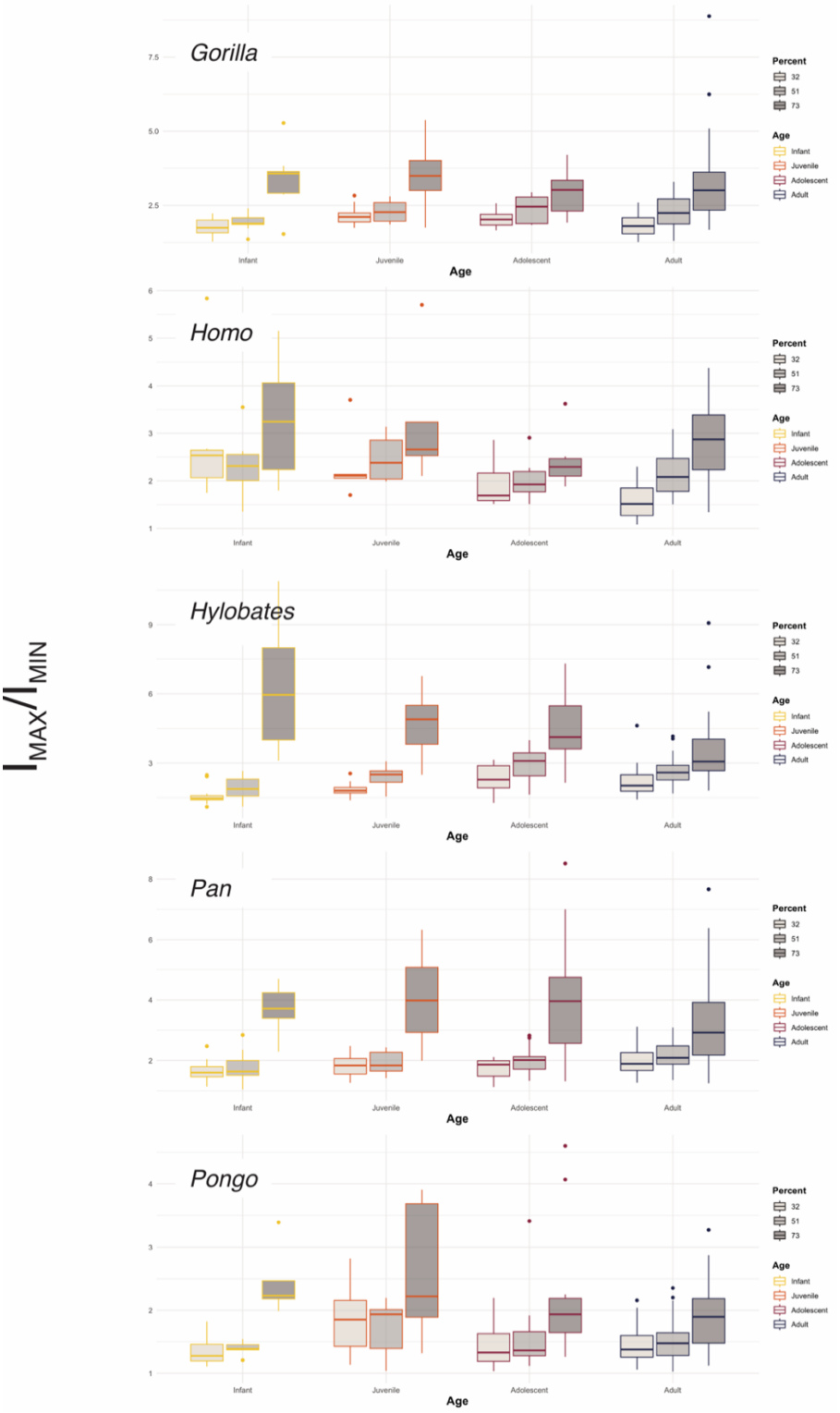

Figure 2.18. Principal second moment of area at 32, 51, and 73% bone length, by age bin.

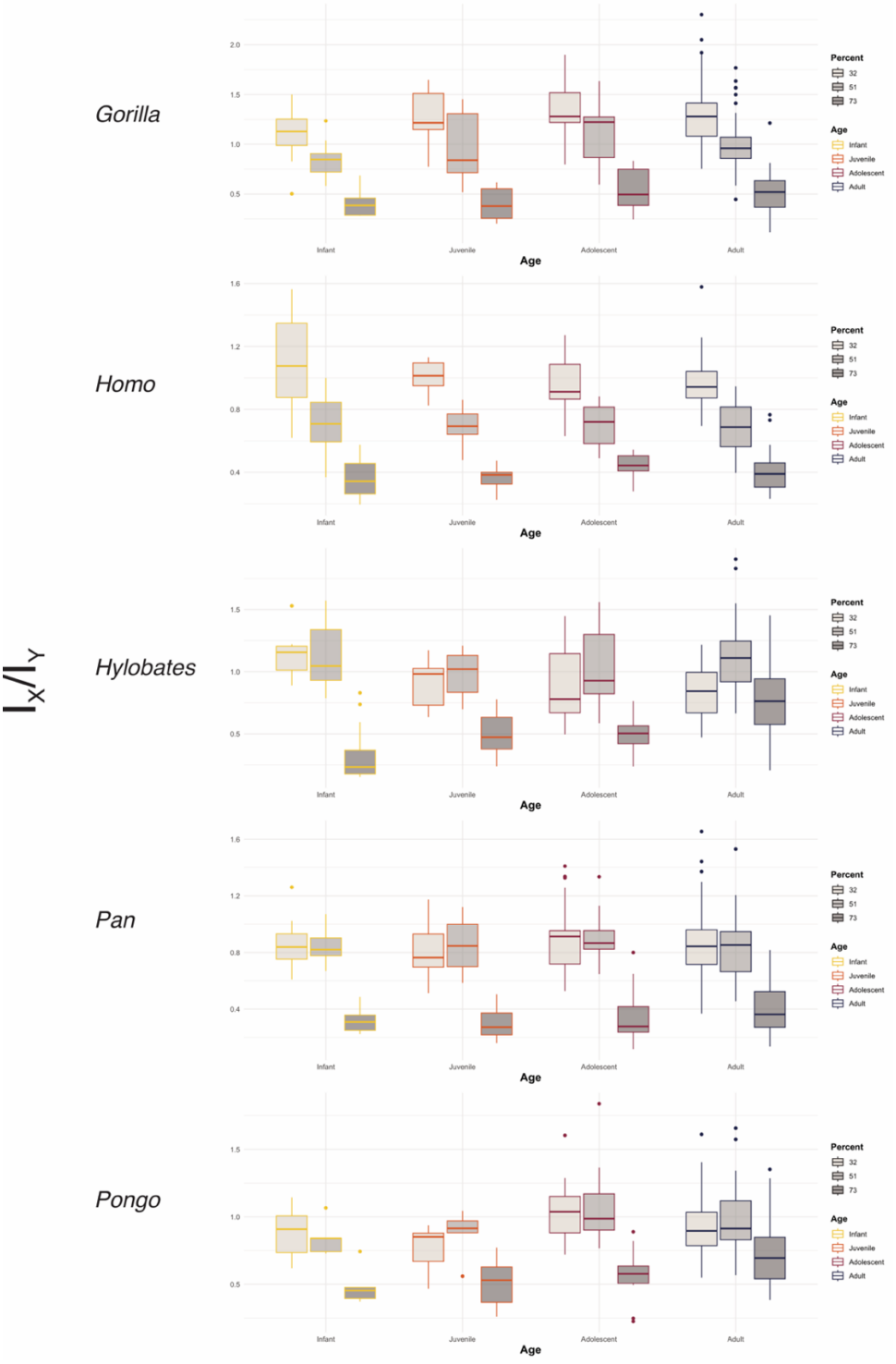

Figure 2.19. Second moment of area about anatomical axes at 32, 51, and 73% bone length, by age bin.

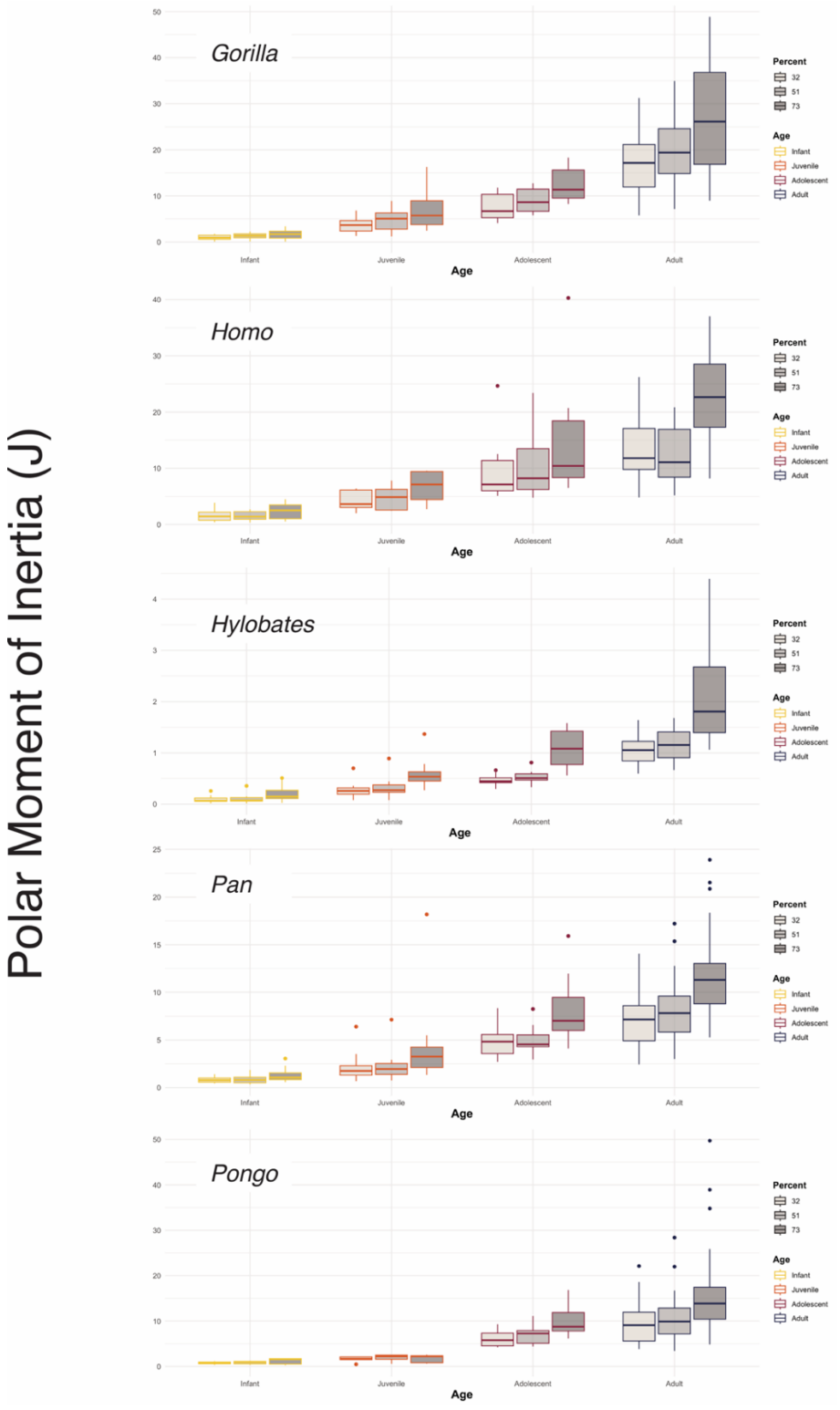

Figure 2.20. Polar moment of inertia at 32, 51, and 73% bone length, by age bin.

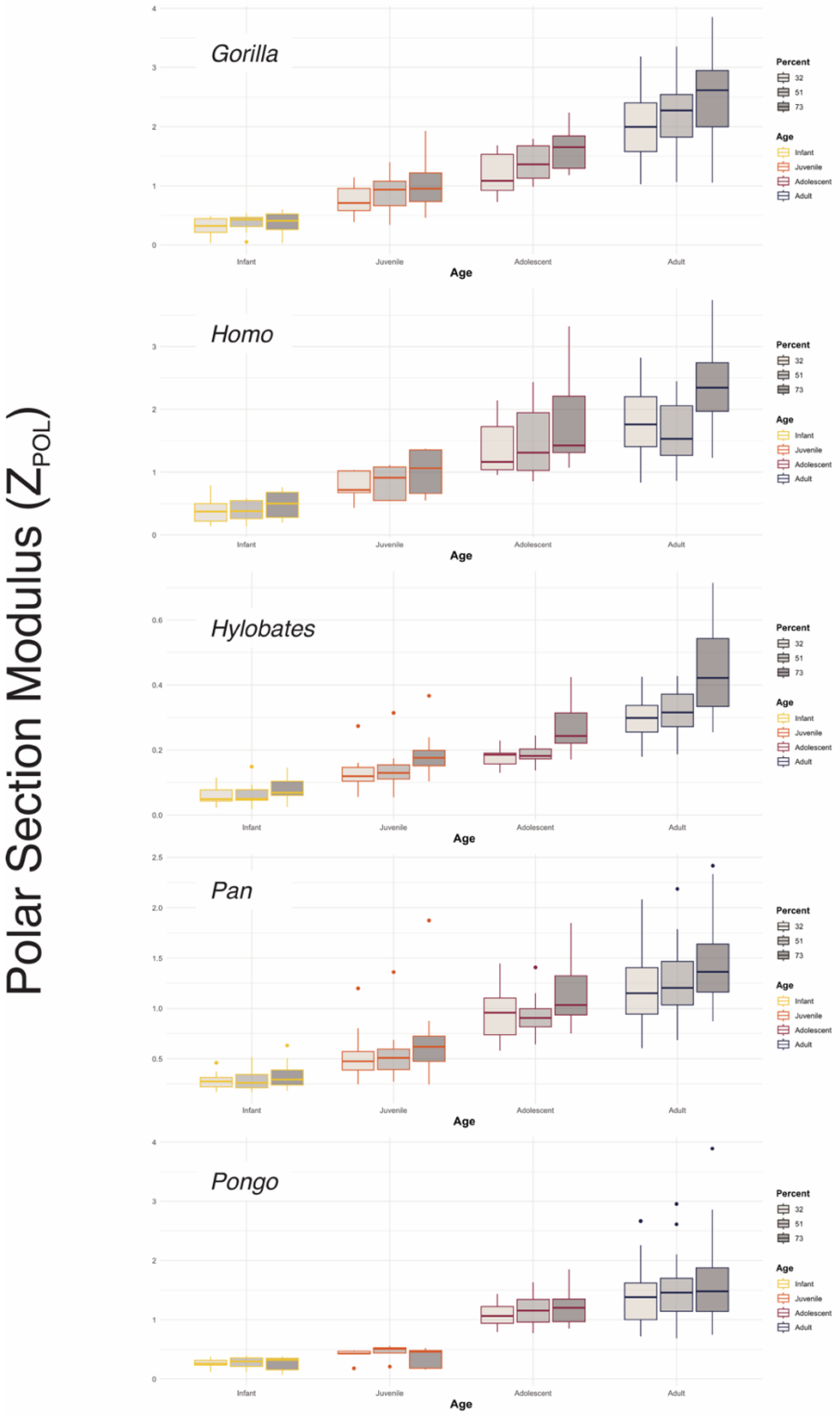

Figure 2.21. Polar section modulus at 32, 51, and 73% bone length, by age bin.

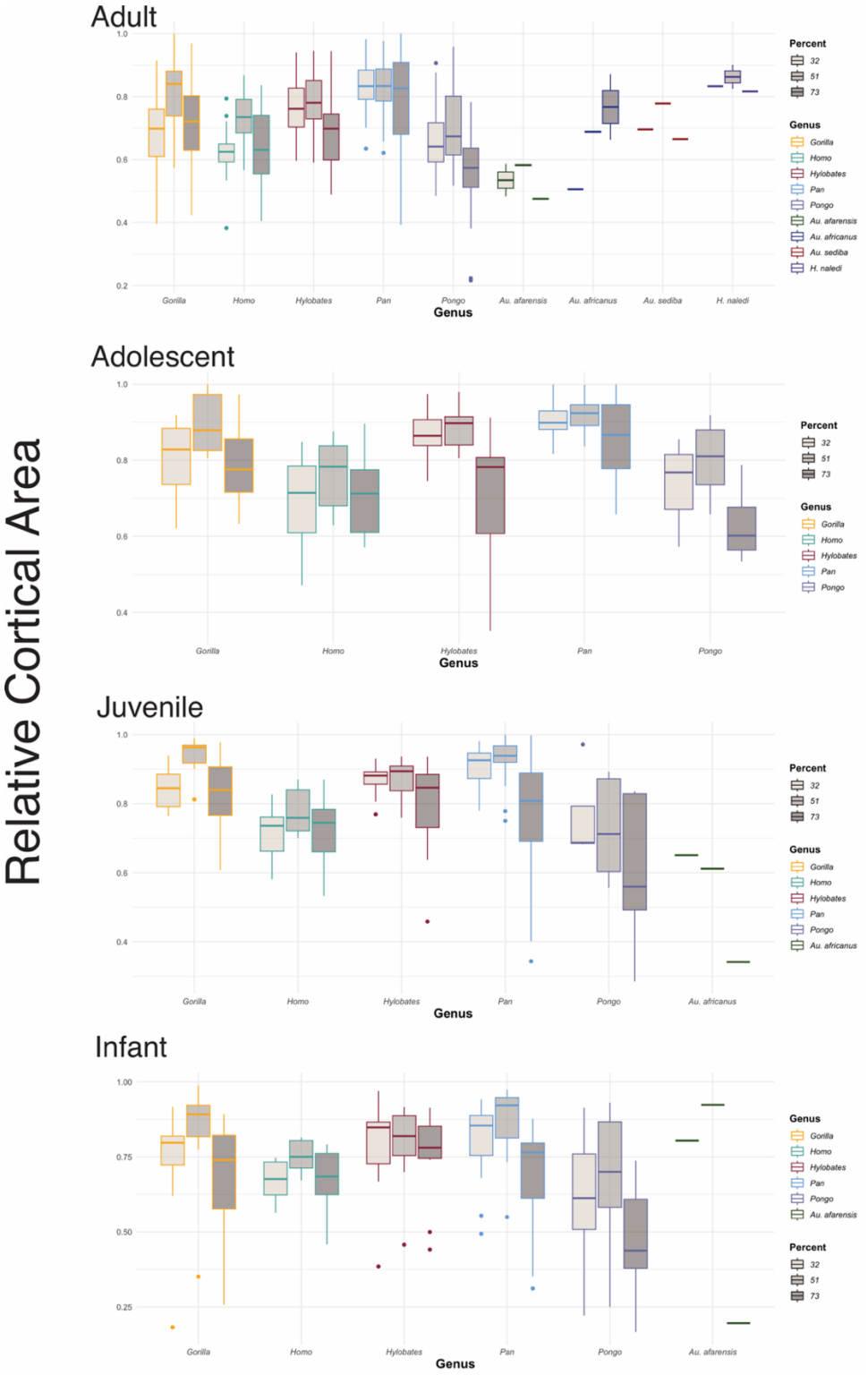

Figure 2.22. Relative cortical area at 32, 51, and 73% bone length, by genus.

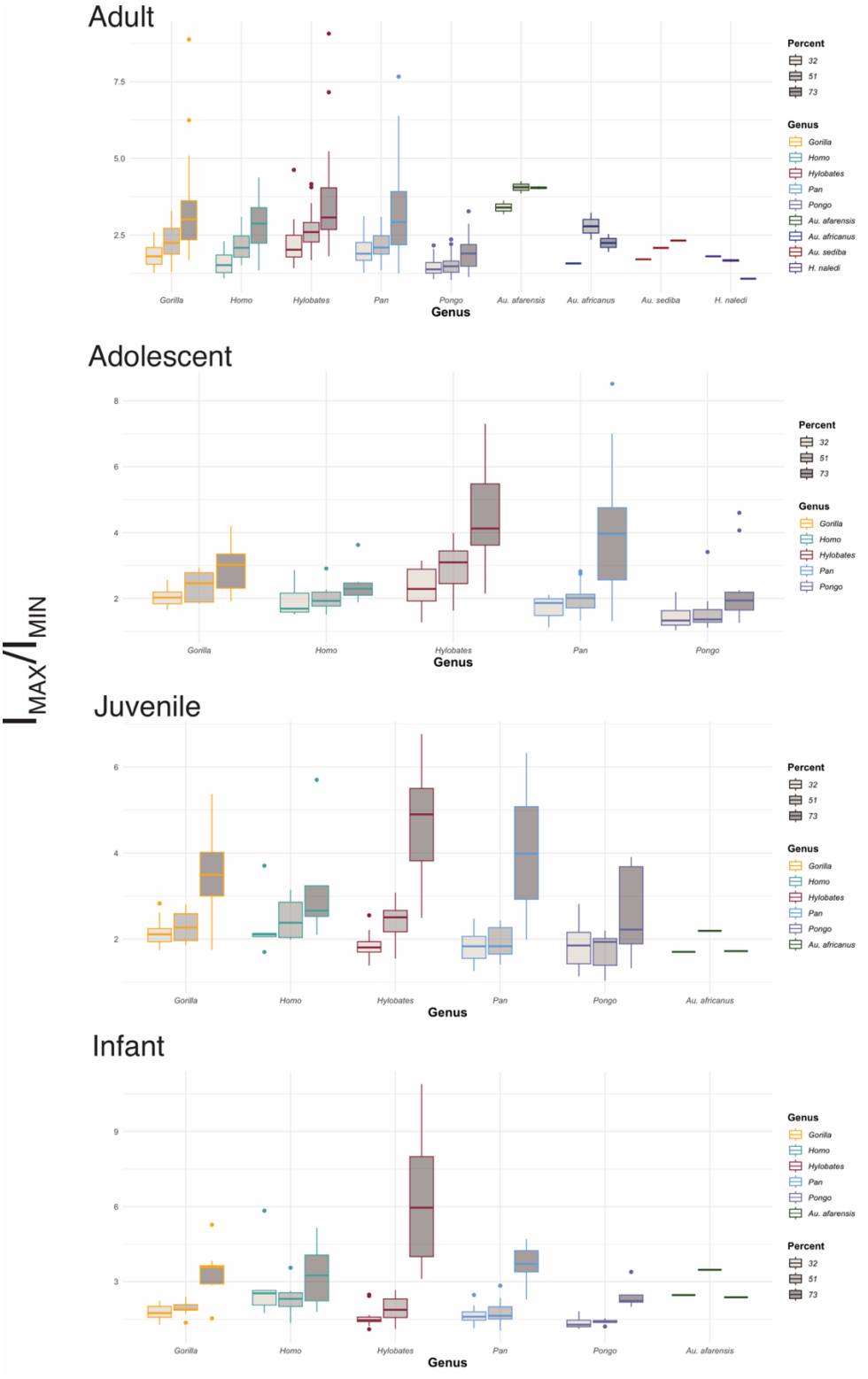

Figure 2.23. Principal second moment of area at 32, 51, and 73% bone length, by genus.

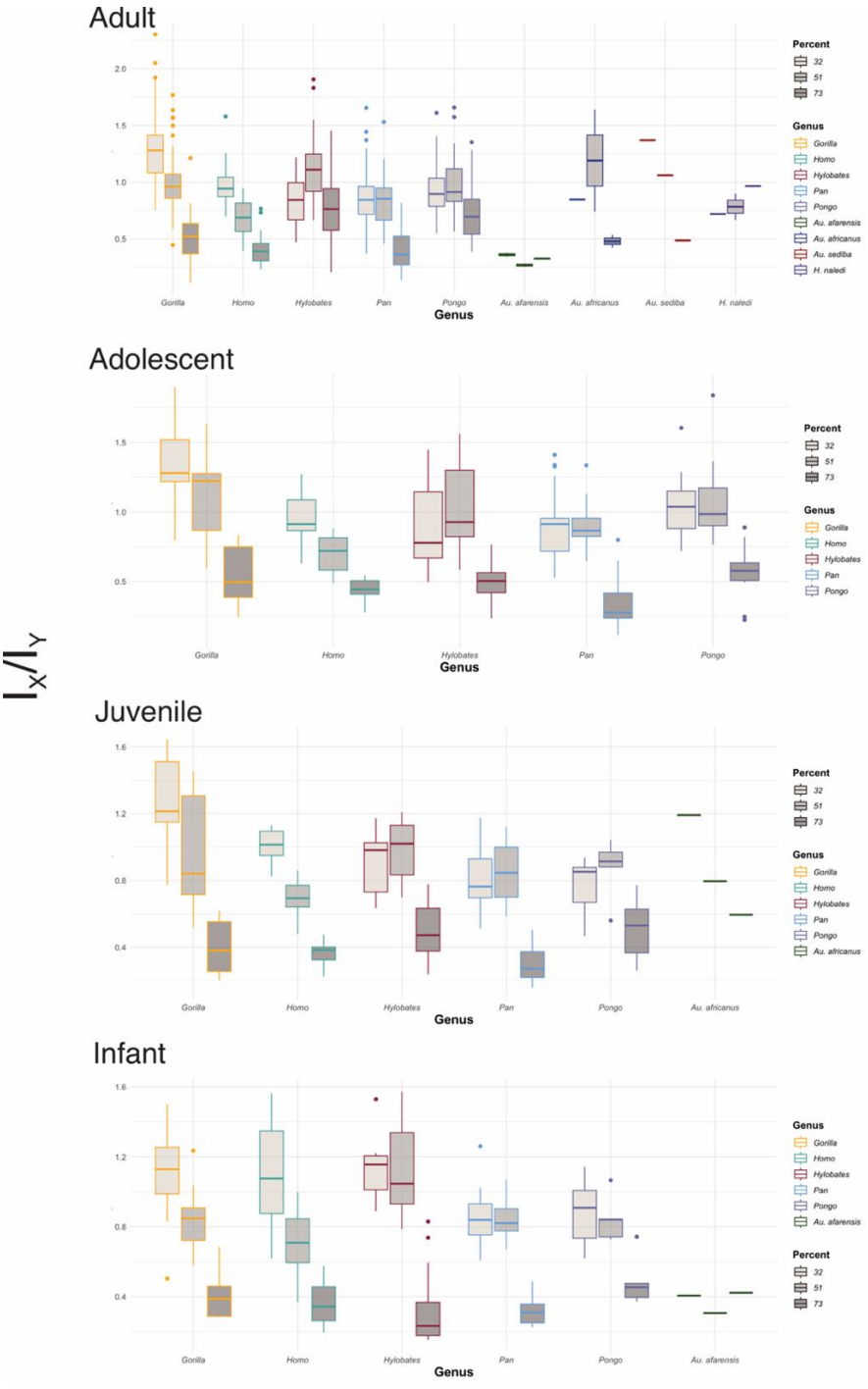

Figure 2.24. Second moment of area about anatomical axes at 32, 51, and 73% bone length, by genus.

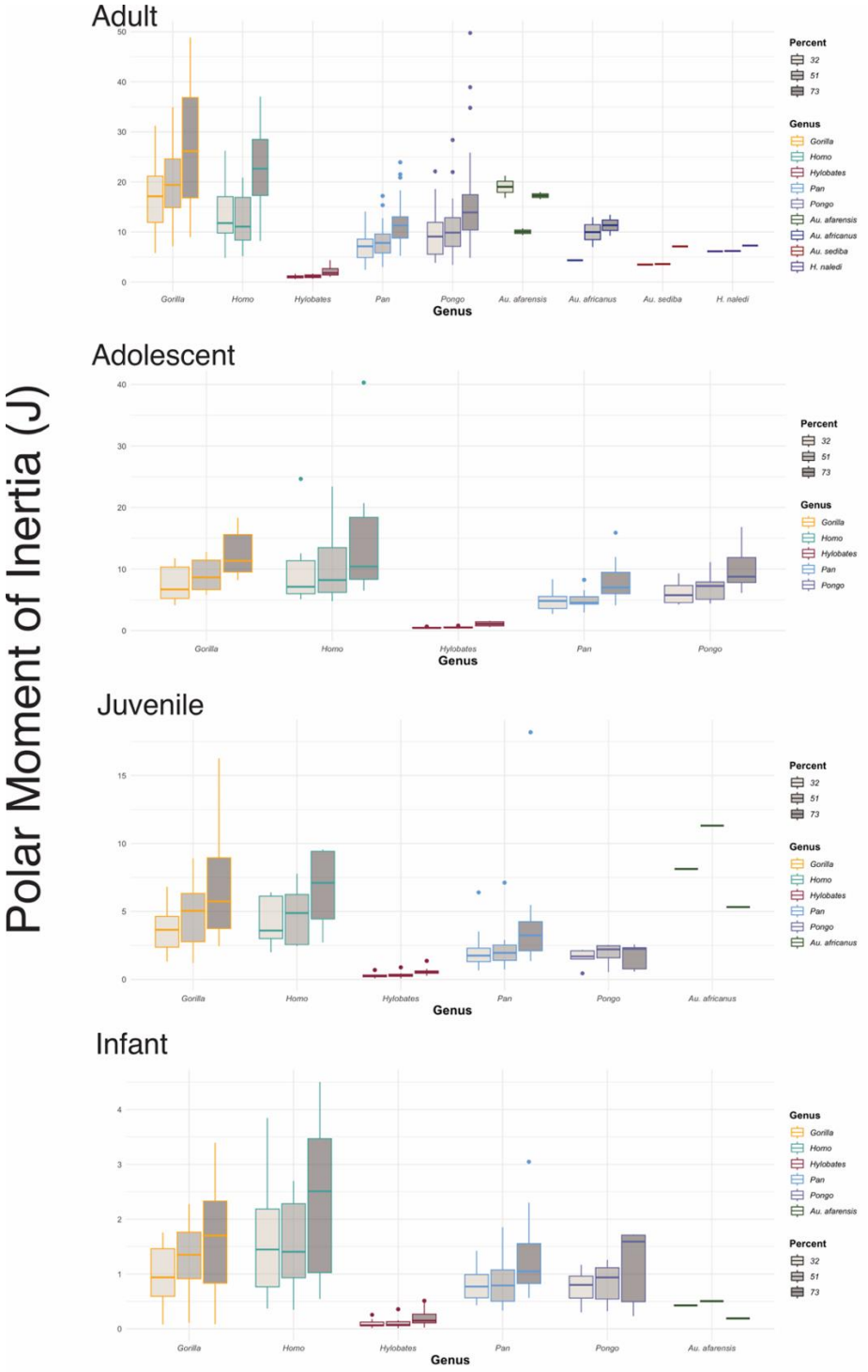

Figure 2.25. Polar moment of inertia at 32, 51, and 73% bone length, by genus.

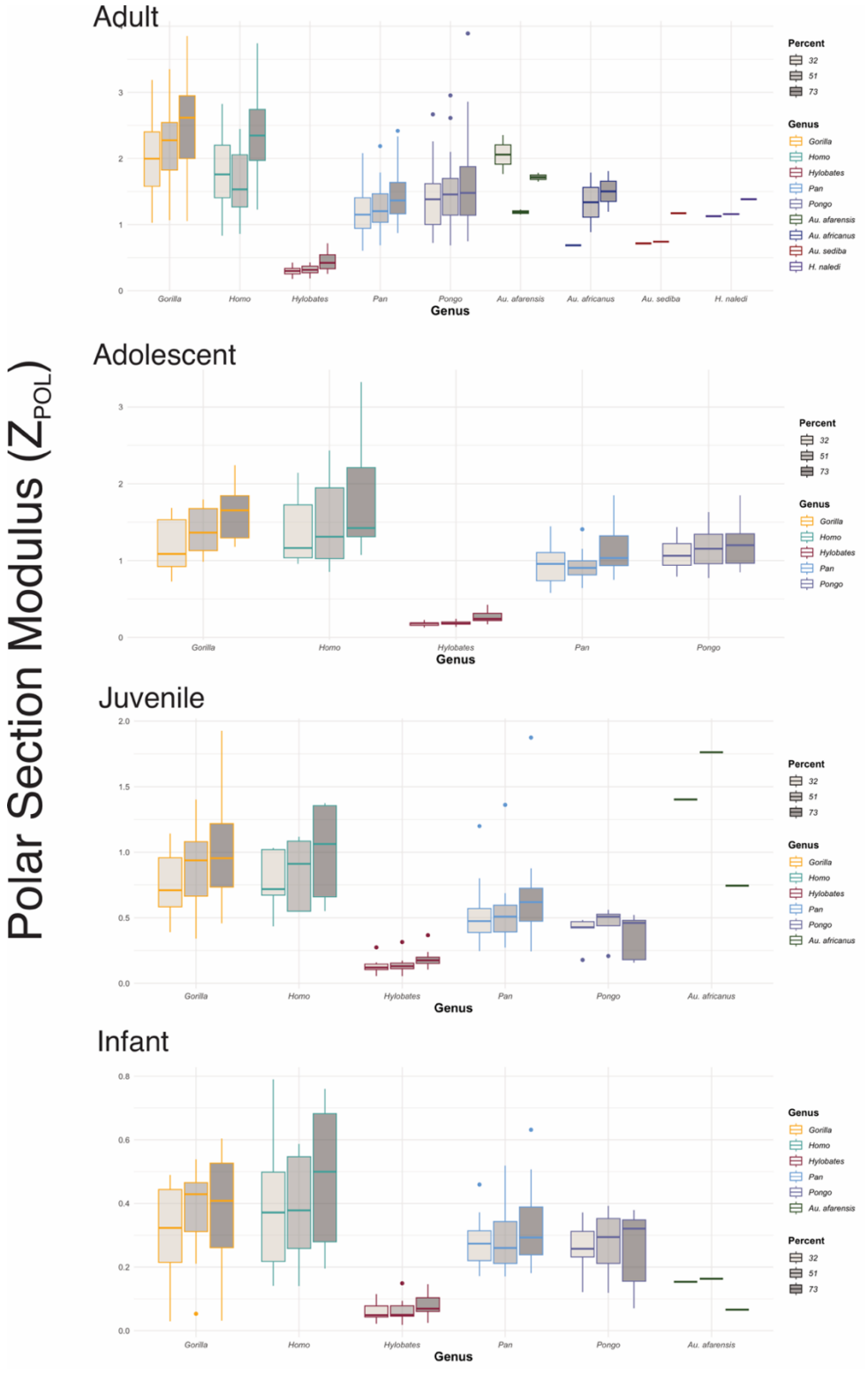

Figure 2.26. Polar section modulus at 32, 51, and 73% bone length, by genus.

Table 2.1. Extant sample

Genus	Age	N
Gorilla	Infant	9
	Juvenile	9
	Adolescent	9
	Adult	48
Homo	Infant	6
	Juvenile	5
	Adolescent	6
	Adult	20
Hylobates	Infant	14
	Juvenile	12
	Adolescent	17
	Adult	31
Pan	Infant	13
	Juvenile	20
	Adolescent	17
	Adult	35
Pongo	Infant	5
	Juvenile	5
	Adolescent	11
	Adult	34

Table 2.2. Fossil sample

Genus	Individual	Est. Age	Description	Reference
Au. afarensis	DIK-1-1	Infant	Complete left and right clavicles	Alemseged et al. (2006)
	KSD-VP-1/1f	Adult	Nearly complete left clavicle, missing the epiphyseal extremities	Haile-Selassie et al. (2010)
Au. africanus	StW 431g	Adult	Lateral half of a right clavicle missing the acromial extremity	Toussaint et al. (2003)
	StW 573f	Adult	Entire right clavicle	Carlson et al. (2021)
	StW 582	Juvenile	Lateral fragment containing both the medial and lateral curvatures, and conoid tubercle	Zipfel, Ward, and Richmond (2020)
Au. sediba	UW 88-38	Adult	Two fragments representing an entire right clavicle	Churchill et al. (2013)
H. naledi	UW 101-258	Adult	Lateral fragment containing both the medial and lateral curvatures, and conoid tubercle	Feuerriegel et al. (2016)
	UW 101-1229	Adult	Midshaft and sternal metaphysis section composed of three refitted fragments	Feuerriegel et al. (2016)

Table 2.3. Cross-sectional Geometry Variables of Interest

Variable	Abbreviation	Equation	Definition	Significance
Second Moment of Area about Anatomical Axes	I_X/I_Y	$I_x = \int y^2 dA$ $I_y = \int x^2 dA$	The sum of squares of the distances y (or x) from the x axis (or y axis) of all of the picture elements (*dA*).	A measure of relative cross-sectional eccentricity, provides insight into what anatomical planes the eccentricity is occurring in.
Principal Second Moment of Area	I_{MAX}/I_{MIN}	$I_{max} = \frac{1}{2}(I_x + I_y) + \frac{1}{2}\sqrt{(I_y - I_x)^2 + (4I_{xy})^2}$ $I_{min} = \frac{1}{2}(I_x + I_y) - \frac{1}{2}\sqrt{(I_y - I_x)^2 + (4I_{xy})^2}$	Calculated as I_x and I_y but with respect to the principal axis and the axis perpendicular to it, respectively.	A measure of relative cross-sectional eccentricity, describes the magnitude of the eccentricity.
Relative Cortical Area	CA	$A = \int delta^2 \quad = \int dA$	*delta* represents the discretized picture elements defining the cortical area.	Proportion of cortical area to the total area of the section. Is generally assumed to reflect the strength of the bone under compression
Polar Moment of Inertia	J	$J = \int (x^2 + y^2) dA = \int x^2 dA + \int y^2 dA = I_x + I_y$	The sum of the products obtained by multiplying each area of the picture elements, *dA* by the square of the distances x and y from the axes.	A measure of how far away the cortical material is distributed relative to the centroid of the cross-section; proportional to bending and torsional rigidity.
Polar Section Modulus	Z	$Z_{pol} = \frac{\int r^2 dA}{r_{max}}$	Calculated as the ratio between the polar moment of inertia and the maximum distance to the outermost fiber of the section from its centroid where r is the distance from the centroid to *dA*.	Ratio between the polar moment of inertia (J) and the distance to the outermost point on the cross-section from its centroid; a measure of bending and torsional strength
Theta	θ	$\theta = \frac{1}{2}\tan^{-1}\frac{2I_{xy}}{I_y - I_x}$	The angle between the principal axis and the x axis.	Provides insight into what anatomical planes the eccentricity is occurring in.

Table 2.4. Levene's Test, by genus.

Genus	Bone Length	I_X/I_Y	I_{MAX}/I_{MIN}	CA	J	Z
Gorilla	32%	> 0.05	> 0.05	> 0.05	**< 0.0001**	**0.0053**
	51%	> 0.05	**0.0445**	> 0.05	**< 0.0001**	**0.0084**
	73%	> 0.05	> 0.05	> 0.05	**< 0.0001**	**0.0029**
Homo	32%	> 0.05	> 0.05	> 0.05	> 0.05	> 0.05
	51%	> 0.05	> 0.05	> 0.05	> 0.05	> 0.05
	73%	> 0.05	> 0.05	> 0.05	> 0.05	> 0.05
Hylobates	32%	**0.0388**	> 0.05	> 0.05	**< 0.0001**	**0.0095**
	51%	> 0.05	> 0.05	**0.0399**	**< 0.0001**	**0.0027**
	73%	**0.0408**	**0.0064**	> 0.05	**< 0.0001**	**0.0001**
Pan	32%	> 0.05	> 0.05	> 0.05	**< 0.0001**	**0.0018**
	51%	> 0.05	> 0.05	> 0.05	**0.0003**	**0.0062**
	73%	> 0.05	> 0.05	> 0.05	**0.0344**	> 0.05
Pongo	32%	> 0.05	> 0.05	> 0.05	**0.0018**	**0.0017**
	51%	> 0.05	> 0.05	> 0.05	**0.0207**	**0.0472**
	73%	> 0.05	> 0.05	> 0.05	> 0.05	> 0.05

Table 2.5. Levene's Test, by age.

Genus	Bone Length	I_X/I_Y	I_{MAX}/I_{MIN}	CA	J	Z
Adult	32%	> 0.05	**0.0309**	> 0.05	**< 0.0001**	**< 0.0001**
	51%	> 0.05	**0.0303**	> 0.05	**< 0.0001**	**< 0.0001**
	73%	**0.0107**	> 0.05	> 0.05	**< 0.0001**	**< 0.0001**
Adolescent	32%	> 0.05	> 0.05	**0.0100**	**0.0011**	**0.0001**
	51%	> 0.05	> 0.05	**0.0032**	**0.0001**	**0.0000**
	73%	> 0.05	> 0.05	> 0.05	**0.0024**	**0.0064**
Juvenile	32%	> 0.05	> 0.05	> 0.05	**0.0134**	> 0.05
	51%	> 0.05	> 0.05	**0.0491**	**0.0034**	**0.0451**
	73%	> 0.05	> 0.05	> 0.05	> 0.05	> 0.05
Infant	32%	> 0.05	> 0.05	> 0.05	**0.0000**	**0.0006**
	51%	> 0.05	> 0.05	> 0.05	**0.0001**	**0.0068**
	73%	> 0.05	**< 0.0001**	> 0.05	**0.0001**	**0.0022**

Table 2.6. Shapiro Wilk's Test, by genus.

Genus	Bone Length	I_X/I_Y	I_{MAX}/I_{MIN}	CA	J	Z
Gorilla	32%	> 0.05	> 0.05	**0.0014**	**0.0112**	> 0.05
	51%	**0.0247**	> 0.05	**0.0001**	**0.0341**	> 0.05
	73%	**0.0208**	**< 0.0001**	**0.0387**	**0.0033**	> 0.05
Homo	32%	**0.0448**	**< 0.0001**	> 0.05	**0.0211**	> 0.05
	51%	> 0.05	> 0.05	> 0.05	> 0.05	> 0.05
	73%	> 0.05	> 0.05	> 0.05	> 0.05	> 0.05
Hylobates	32%	> 0.05	**0.0001**	**0.0003**	**0.0009**	> 0.05
	51%	> 0.05	> 0.05	**0.0001**	**0.0007**	**0.0265**
	73%	**0.0032**	**< 0.0001**	**0.0062**	**< 0.0001**	**0.0174**
Pan	32%	**0.0013**	> 0.05	**< 0.0001**	**0.0002**	**0.0137**
	51%	> 0.05	> 0.05	**< 0.0001**	**0.0002**	**0.0284**
	73%	**0.0000**	**0.0046**	**< 0.0001**	**0.0002**	**0.0455**
Pongo	32%	**0.0189**	**< 0.0001**	> 0.05	**0.0220**	> 0.05
	51%	**0.0007**	**< 0.0001**	**0.0236**	**0.0035**	> 0.05
	73%	**0.0179**	**< 0.0001**	**0.0113**	**0.0000**	**0.0207**

Table 2.7. Shapiro Wilk's Test, by age.

Genus	Bone Length	I_X/I_Y	I_{MAX}/I_{MIN}	CA	J	Z
Adult	32%	**< 0.0001**	**< 0.0001**	> 0.05	**< 0.0001**	**0.0009**
	51%	**0.0001**	**0.0005**	**0.0146**	**< 0.0001**	**0.0005**
	73%	**< 0.0001**	**< 0.0001**	> 0.05	**< 0.0001**	**0.0006**
Adolescent	32%	> 0.05	**0.0380**	**0.0006**	**< 0.0001**	**0.0013**
	51%	**0.0132**	**0.0110**	**0.0020**	**< 0.0001**	**0.0020**
	73%	> 0.05	**0.0015**	> 0.05	**< 0.0001**	**0.0018**
Juvenile	32%	**0.0386**	**0.0021**	**0.0059**	**< 0.0001**	**0.0079**
	51%	> 0.05	> 0.05	**0.0000**	**< 0.0001**	**0.0007**
	73%	**0.0145**	> 0.05	**0.0007**	**< 0.0001**	**0.0001**
Infant	32%	> 0.05	**< 0.0001**	**< 0.0001**	**< 0.0001**	**0.0045**
	51%	> 0.05	**0.0087**	**< 0.0001**	**0.0005**	**0.0070**
	73%	**0.0036**	**< 0.0001**	**0.0001**	**0.0001**	**0.0021**

Table 2.8. Intraspecific pairwise comparisons of relative cortical area (CA) through ontogeny. All three slice levels for *Homo* and the 32% slice level of *Pongo* were investigated using a parametric Tukey's HSD test. In all other regions statistical differences were tested for with a non-parametric Dunn's tests with Bonferroni correction.

Genus	Age	32% Bone Length			51% Bone Length			73% Bone Length		
Gorilla		**Adult**	**Infant**	**Juvenile**	**Adult**	**Infant**	**Juvenile**	**Adult**	**Infant**	**Juvenile**
	Adolescent	0.0099	1	1	0.0886	1	1	0.2670	0.5400	1
	Adult	-	0.2220	0.0004	-	0.5750	0.0018	-	1	0.0792
	Infant	-	-	0.3360	-	-	0.3070	-	-	0.2450
Homo	**Adolescent**	0.4500	0.9870	0.9730	0.9130	0.9960	0.9870	0.5320	0.9310	1
	Adult	-	0.7010	0.2420	-	0.9820	0.7430	-	0.9270	0.5140
	Infant	-	-	0.2960	-	-	0.9460	-	-	0.9060
Hylobates	**Adolescent**	0.0008	0.2930	1	0.0005	0.0408	1	0.3110	1	0.7280
	Adult	-	0.3610	0.0022	-	1	0.0311	-	0.0875	0.0184
	Infant	-	-	0.2960	-	-	0.3360	-	-	1
Pan	**Adolescent**	0.0048	0.0311	1	0.0018	0.9410	1	0.3760	0.0181	0.2970
	Adult	-	1	0.0004	-	0.1420	< 0.0001	-	0.2570	1
	Infant	-	-	0.0070	-	-	0.2980	-	-	0.5690
Pongo	**Adolescent**	0.2830	0.1790	0.9900	0.0687	0.4630	0.6460	0.8450	0.3340	1
	Adult	-	0.7410	0.3610	-	1	1	-	0.9310	1
	Infant	-	-	0.1950	-	-	1	-	-	1

Table 2.9. Interspecific pairwise comparisons of relative cortical area (CA) through ontogeny. The 32% and 73% slice levels for adults and 73% slice level for adolescents were investigated using a parametric Tukey's HSD test. In all other regions statistical differences were tested for with a non-parametric Dunn's tests with Bonferroni correction.

Infant						
	32% Bone Length					
		Gorilla	***Homo***	***Hylobates***	***Pan***	***Pongo***
	Au. afarensis	1	1	1	1	1
	Gorilla	-	1	1	1	1
	Homo	-	-	0.1200	0.1210	1
	Hylobates	-	-	-	1	0.5460
	Pan	-	-	-	-	0.5390
	51% Bone Length					
		Gorilla	***Homo***	***Hylobates***	***Pan***	***Pongo***
	Au. afarensis	1	0.7370	1	1	1
	Gorilla	-	0.3270	1	1	0.8230
	Homo	-	-	1	0.0836	1
	Hylobates	-	-	-	0.4700	1
	Pan	-	-	-	-	0.2990
	73% Bone Length					
		Gorilla	***Homo***	***Hylobates***	***Pan***	***Pongo***
	Au. afarensis	0.9340	1	0.3360	0.7310	1
	Gorilla	-	1	1	1	0.5370
	Homo	-	-	1	1	1
	Hylobates	-	-	-	1	0.0375
	Pan	-	-	-	-	0.2670
Juvenile	***32% Bone Length***					
		Gorilla	***Homo***	***Hylobates***	***Pan***	***Pongo***
	Au. africanus	1	1	0.8030	0.2060	1
	Gorilla	-	0.4480	1	0.2310	1
	Homo	-	-	0.0915	0.0009	1
	Hylobates	-	-	-	0.8280	1
	Pan	-	-	-	-	0.0482

Table 2.9. Continued

	51% Bone Length					
		Gorilla	**Homo**	**Hylobates**	**Pan**	**Pongo**
	Au. africanus	0.2770	1	1	0.2950	1
	Gorilla	-	0.0127	0.1630	1	0.0108
	Homo	-	-	1	0.0066	1
	Hylobates	-	-	-	0.0856	1
	Pan	-	-	-	-	0.0055
	73% Bone Length					
		Gorilla	***Homo***	***Hylobates***	***Pan***	***Pongo***
	Au. africanus	0.4670	1	0.5560	0.7440	1
	Gorilla	-	1	1	1	0.3540
	Homo	-	-	1	1	1
	Hylobates	-	-	-	1	0.4510
	Pan	-	-	-	-	0.7230
Adolescent	***32% Bone Length***					
		Gorilla	***Homo***	***Hylobates***	***Pan***	***Pongo***
	Gorilla	-	0.0694	0.4064	0.0507	0.4574
	Homo	-	-	0.0003	< 0.0001	0.6900
	Hylobates	-	-	-	0.7127	0.0030
	Pan	-	-	-	-	0.0001
	51% Bone Length					
		Gorilla	***Homo***	***Hylobates***	***Pan***	***Pongo***
	Gorilla	-	0.0031	0.9970	0.9153	0.0382
	Homo	-	-	0.0021	0.0001	0.6539
	Hylobates	-	-	-	0.6143	0.0288
	Pan	-	-	-	-	0.0006
	73% Bone Length					
		Gorilla	*Homo*	*Hylobates*	*Pan*	*Pongo*
	Gorilla	-	0.7186	0.5324	0.7412	0.0370
	Homo	-	-	1	0.1172	0.6926

Table 2.9. Continued

	Hylobates	-	-	-	**0.0129**	**0.4072**		
	Pan	-	-	-	-	0.0002		
Adult	***32% Bone Length***							
		Au. africanus	***Au. sediba***	***Gorilla***	***H. naledi***	***Homo***	***Hylobates***	***Pan***	***Pongo***
	Au. afarensis	1	0.9070	0.4180	0.2220	0.9510	0.0378	0.0012	0.6460
	Au. africanus	-	0.8970	0.6420	0.2860	0.9600	0.1860	0.0280	0.7900
	Au. sediba	-	-	1	0.9840	0.9980	0.9990	0.9000	1
	Gorilla	-	-	-	0.8480	0.2260	0.0229	< 0.0001	0.9830
	H. naledi	-	-	-	-	0.4450	0.9980	1	0.7260
	Homo	-	-	-	-	-	< 0.0001	< 0.0001	0.8180
	Hylobates	-	-	-	-	-	-	0.0874	0.0022
	Pan	-	-	-	-	-	-	-	< 0.0001
	51% Bone Length								
		Au. africanus	***Au. sediba***	***Gorilla***	***H. naledi***	***Homo***	***Hylobates***	***Pan***	***Pongo***
	Au. afarensis	1	1	0.1420	0.2590	1	0.3960	0.0650	1
	Au. africanus	-	1	1	1	1	1	0.8450	1
	Au. sediba	-	-	1	1	1	1	1	1
	Gorilla	-	-	-	1	0.1080	1	1	0.0019
	H. naledi	-	-	-	-	1	1	1	0.9810
	Homo	-	-	-	-	-	1	0.0162	1
	Hylobates	-	-	-	-	-	-	1	0.2190
	Pan	-	-	-	-	-	-	-	0.0002
	73% Bone Length								
		Au. africanus	*Au. sediba*	*Gorilla*	*H. naledi*	*Homo*	*Hylobates*	*Pan*	*Pongo*
	Au. afarensis	0.3590	0.9530	0.2100	0.4240	0.7650	0.3800	0.0183	0.9840
	Au. africanus	-	0.9990	1	1	0.8930	0.9940	1	0.4610
	Au. sediba	-	-	1	0.9950	1	1	0.9830	0.9980

Table 2.9. Continued

Gorilla	**-**	**-**	**-**	**0.9960**	**0.3450**	**0.9920**	**0.0664**	**0.0001**
H. naledi	-	-	-	-	0.8980	0.9840	1	0.6120
Homo	-	-	-	-	-	0.8950	0.0003	0.6980
Hylobates	-	-	-	-	-	-	0.0123	0.0109
Pan	-	-	-	-	-	-	-	< 0.0001

Table 2.10. Intraspecific pairwise comparisons of the ratio of principal second moment of area (I_{MAX}/I_{MIN}) through ontogeny. The 32% slice level of *Gorilla*, 51% and 73% of *Homo,* 51% of *Hylobates,* and the 32% and 51% slice levels of *Pan* were investigated using a parametric Tukey's HSD test. In all other regions statistical differences were tested for with a non-parametric Dunn's tests with Bonferroni correction.

Genus	Age	32% Bone Length			51% Bone Length			73% Bone Length		
Gorilla		**Adult**	**Infant**	**Juvenile**	**Adult**	**Infant**	**Juvenile**	**Adult**	**Infant**	**Juvenile**
	Adolescent	0.3080	0.3650	0.9120	1	0.1670	1	1	1	1
	Adult	-	0.9820	0.0535	-	0.2000	1	-	1	0.7890
	Infant	-	-	0.1080	-	-	0.3660	-	-	1
Homo	**Adolescent**	0.5640	0.4270	1	0.9700	0.7630	0.5380	0.8440	0.4880	0.5630
	Adult	-	0.0051	0.0691	-	0.8700	0.6190	-	0.7750	0.8430
	Infant	-	-	1	-	-	0.9750	-	-	1
Hylobates	**Adolescent**	0.9620	0.0001	0.1150	0.4860	0.0001	0.1150	0.0186	0.4510	1
	Adult	-	0.0005	0.4690	-	0.0011	0.5960	-	0.0001	0.0389
	Infant	-	-	0.1950	-	-	0.1520	-	-	0.6100
Pan	**Adolescent**	0.1180	0.8490	0.8720	0.4470	0.4750	0.9400	0.1130	1	1
	Adult	-	0.0200	0.4520	-	0.0186	0.1190	-	0.1820	0.0181
	Infant	-	-	0.4180	-	-	0.7700	-	-	1
Pongo	**Adolescent**	1	1	0.5200	1	1	0.8610	1	0.4870	1
	Adult	-	1	0.4830	-	1	1	-	0.1130	0.5580
	Infant	-	-	0.3860	-	-	0.6860	-	-	1

Table 2.11. Interspecific pairwise comparisons of the ratio of principal second moment of area (I_{MAX}/I_{MIN}) through ontogeny. The 51% and 73% slice levels for juveniles were investigated using a parametric Tukey's HSD test. In all other regions statistical differences were tested for with a non-parametric Dunn's tests with Bonferroni correction.

Infant

	32% Bone Length				
	Gorilla	***Homo***	***Hylobates***	***Pan***	***Pongo***
Au. afarensis	1	1	0.8440	1	0.4140
Gorilla	-	0.5130	0.8260	1	0.3080
Homo	-	-	0.0057	0.0404	0.0039
Hylobates	-	-	-	1	1
Pan	-	-	-	-	1
	51% Bone Length				
	Gorilla	***Homo***	***Hylobates***	***Pan***	***Pongo***
Au. afarensis	1	1	1	0.5980	0.1070
Gorilla	-	1	1	1	0.1620
Homo	-	-	1	0.6590	0.0357
Hylobates	-	-	-	1	0.2100
Pan	-	-	-	-	0.7460
	73% Bone Length				
	Gorilla	***Homo***	***Hylobates***	***Pan***	***Pongo***
Au. afarensis	1	1	0.3130	1	1
Gorilla	-	1	0.0140	1	1
Homo	-	-	0.0678	1	1
Hylobates	-	-	-	0.1040	0.0004
Pan	-	-	-	-	0.2070

Juvenile

	32% Bone Length				
	Gorilla	***Homo***	***Hylobates***	***Pan***	***Pongo***
Au. africanus	1	1	1	1	1
Gorilla	-	1	0.4350	0.2350	1
Homo	-	-	0.8730	0.6290	1
Hylobates	-	-	-	1	1
Pan	-	-	-	-	1

Table 2.11. Continued

			51% Bone Length			
		Gorilla	***Homo***	***Hylobates***	***Pan***	***Pongo***
	Au. africanus	1	0.9840	0.9950	0.9840	0.8750
	Gorilla	-	0.9440	0.9830	0.2190	0.1200
	Homo	-	-	0.9990	0.0681	0.0382
	Hylobates	-	-	-	0.0194	0.0227
	Pan	-	-	-	-	0.8970
			73% Bone Length			
		Gorilla	***Homo***	***Hylobates***	***Pan***	***Pongo***
	Au. africanus	0.7930	0.8820	0.2470	0.4620	0.9880
	Gorilla	-	1	0.2640	0.7900	0.8440
	Homo	-	-	0.3050	0.7590	0.9670
	Hylobates	-	-	-	0.8240	0.0416
	Pan	-	-	-	-	0.1950
Adolescent			***32% Bone Length***			
		Gorilla	***Homo***	***Hylobates***	***Pan***	***Pongo***
	Gorilla	-	0.9880	0.5037	0.4071	0.0343
	Homo	-	-	0.3125	0.8615	0.2261
	Hylobates	-	-	-	0.0015	< 0.0001
	Pan	-	-	-	-	0.5197
			51% Bone Length			
		Gorilla	***Homo***	***Hylobates***	***Pan***	***Pongo***
	Gorilla	-	0.7977	0.2027	0.4980	0.0289
	Homo	-	-	0.0225	0.9999	0.5479
	Hylobates	-	-	-	0.0003	< 0.0001
	Pan	-	-	-	-	0.3775
			73% Bone Length			
		Gorilla	*Homo*	*Hylobates*	*Pan*	*Pongo*
	Gorilla	-	0.9376	0.0372	0.4530	0.7712
	Homo	-	-	0.0104	0.1550	0.9994

Table 2.11. Continued

	Hylobates	-	-	-	**0.5612**	**0.0004**		
	Pan	-	-	-	-	0.0216		
Adult	***32% Bone Length***							
		Au. africanus	***Au. sediba***	***Gorilla***	***H. naledi***	***Homo***	***Hylobates***	***Pan***	***Pongo***
	Au. afarensis	1	1	0.4850	1	0.0546	1	1	0.0078
	Au. africanus	-	1	1	1	1	1	1	1
	Au. sediba	-	-	1	1	1	1	1	1
	Gorilla	-	-	-	1	0.4270	0.3470	1	0.0003
	H. naledi	-	-	-	-	1	1	1	1
	Homo	-	-	-	-	-	0.0013	0.0274	1
	Hylobates	-	-	-	-	-	-	1	< 0.0001
	Pan	-	-	-	-	-	-	-	< 0.0001
	51% Bone Length								
		Au. africanus	***Au. sediba***	***Gorilla***	***H. naledi***	***Homo***	***Hylobates***	***Pan***	***Pongo***
	Au. afarensis	1	1	0.6930	0.1560	0.4120	1	0.4820	0.0020
	Au. africanus	-	1	1	1	1	1	1	0.0733
	Au. sediba	-	-	1	1	1	1	1	1
	Gorilla	-	-	-	1	1	0.3440	1	< 0.0001
	H. naledi	-	-	-	-	1	0.3950	1	1
	Homo	-	-	-	-	-	0.1890	1	0.0012
	Hylobates	-	-	-	-	-	-	0.1390	< 0.0001
	Pan	-	-	-	-	-	-	-	< 0.0001
	73% Bone Length								
		Au. africanus	***Au. sediba***	***Gorilla***	***H. naledi***	***Homo***	***Hylobates***	***Pan***	***Pongo***
	Au. afarensis	1	1	1	0.2960	1	1	1	0.0452
	Au. africanus	-	1	1	1	1	1	1	1
	Au. sediba	-	-	1	1	1	1	1	1
	Gorilla	-	-	-	0.9050	1	1	1	< 0.0001
	H. naledi	-	-	-	-	1	0.5220	1	1

Table 2.11. Continued

Homo	**-**	**-**	**-**	**-**	**-**	**1**	**1**	**0.0046**
Hylobates	-	-	-	-	-	-	1	< 0.0001
Pan	-	-	-	-	-	-	-	0.0001

Table 2.12. Intraspecific pairwise comparisons of the ratio of second moment of area about anatomical axes (I_X/I_Y) through ontogeny. The 32% slice level of *Gorilla*, 51% and 73% of *Homo,* 51% of *Hylobates,* and the 51% slice level of *Pan* were investigated using a parametric Tukey's HSD test. In all other regions statistical differences were tested for with a non-parametric Dunn's tests with Bonferroni correction.

Genus	Age	32% Bone Length			51% Bone Length			73% Bone Length		
Gorilla		**Adult**	**Infant**	**Juvenile**	**Adult**	**Infant**	**Juvenile**	**Adult**	**Infant**	**Juvenile**
	Adolescent	1	0.4480	0.9790	0.9830	0.1050	0.4510	1	0.4330	0.4150
	Adult	-	0.2180	0.9530	-	0.2360	1	-	0.4250	0.4020
	Infant	-	-	0.6940	-	-	1	-	-	1
Homo	**Adolescent**	1	1	1	0.9970	1	1	0.9780	0.7790	0.7870
	Adult	-	1	1	-	0.9920	1	-	0.8630	0.8710
	Infant	-	-	1	-	-	0.9990	-	-	1
Hylobates	**Adolescent**	1	0.0156	1	0.6020	0.7280	0.9880	0.0057	0.2710	1
	Adult	-	0.0003	0.9770	-	1	0.4670	-	< 0.0001	0.0279
	Infant	-	-	0.0601	-	-	0.5920	-	-	0.2740
Pan	**Adolescent**	1	1	0.4600	0.6740	0.8250	0.7660	0.2710	1	1
	Adult	-	1	0.7280	-	1	1	-	0.8630	0.0383
	Infant	-	-	1	-	-	1	-	-	0.9660
Pongo	**Adolescent**	0.6420	0.8110	0.1280	0.7970	0.1530	0.7310	0.3510	0.9220	1
	Adult	-	1	0.4990	-	0.4910	1	-	0.0670	0.2610
	Infant	-	-	1	-	-	1	-	-	1

Table 2.13. Interspecific pairwise comparisons of the ratio of second moment of area about anatomical axes (I_X/I_Y) through ontogeny. The 32% and 73% slice levels for adolescents, 51% slice for juveniles, and 32% and 51% slice levels for infants were investigated using a parametric Tukey's HSD test. In all other regions statistical differences were tested for with a non-parametric Dunn's tests with Bonferroni correction.

Infant	***32% Bone Length***				
	Gorilla	***Homo***	***Hylobates***	***Pan***	***Pongo***
Au. afarensis	0.0634	0.0699	0.0358	0.3850	0.3970
Gorilla	-	1	0.9980	0.2030	0.5680
Homo	-	-	0.9990	0.3010	0.6200
Hylobates	-	-	-	0.0358	0.2890
Pan	-	-	-	-	1
	51% Bone Length				
	Gorilla	***Homo***	***Hylobates***	***Pan***	***Pongo***
Au. afarensis	0.1310	0.4400	0.0032	0.1160	0.1570
Gorilla	-	0.7810	0.0180	1	1
Homo	-	-	0.0011	0.7110	0.8580
Hylobates	-	-	-	0.0073	0.0842
Pan	-	-	-	-	1
	73% Bone Length				
	Gorilla	***Homo***	***Hylobates***	***Pan***	***Pongo***
Au. afarensis	1	1	1	1	1
Gorilla	-	1	0.5260	1	1
Homo	-	-	1	1	1
Hylobates	-	-	-	1	0.0908
Pan	-	-	-	-	0.3260
Juvenile	***32% Bone Length***				
	Gorilla	***Homo***	***Hylobates***	***Pan***	***Pongo***
Au. africanus	1	1	1	0.5430	0.4900
Gorilla	-	1	0.1190	0.0007	0.0135
Homo	-	-	1	0.5940	0.7130
Hylobates	-	-	-	1	1

Table 2.13. Continued

	Pan	-	-	-	-	**1**
	51% Bone Length					
		Gorilla	***Homo***	***Hylobates***	***Pan***	***Pongo***
	Au. africanus	0.9840	0.9970	0.9410	1	0.9990
	Gorilla	-	0.2630	0.9940	0.8450	0.9910
	Homo	-	-	0.0854	0.6690	0.7250
	Hylobates	-	-	-	0.3830	0.8870
	Pan	-	-	-	-	1
	73% Bone Length					
		Gorilla	***Homo***	***Hylobates***	***Pan***	***Pongo***
	Au. africanus	1	1	1	0.5780	1
	Gorilla	-	1	1	0.7220	1
	Homo	-	-	1	1	1
	Hylobates	-	-	-	0.0093	1
	Pan	-	-	-	-	0.1040
Adolescent	***32% Bone Length***					
		Gorilla	***Homo***	***Hylobates***	***Pan***	***Pongo***
	Gorilla	-	0.1367	0.0088	0.0155	0.2192
	Homo	-	-	0.9960	0.9997	0.9779
	Hylobates	-	-	-	0.9993	0.7468
	Pan	-	-	-	-	0.8560
	51% Bone Length					
		Gorilla	***Homo***	***Hylobates***	***Pan***	***Pongo***
	Gorilla	-	0.0247	0.8991	0.2607	0.9980
	Homo	-	-	0.0732	0.4648	0.0370
	Hylobates	-	-	-	0.6415	0.9760
	Pan	-	-	-	-	0.3753
	73% Bone Length					
		Gorilla	***Homo***	***Hylobates***	***Pan***	***Pongo***
	Gorilla	-	0.7628	0.8950	0.0403	0.9995

Table 2.13. Continued

	Homo	-		-		**0.9843**	**0.7435**	**0.6221**
	Hylobates	-		-		-	0.1282	0.7472
	Pan	-		-		-	-	0.0125
Adult	***32% Bone Length***							
		Au. africanus	***Au. sediba***	***Gorilla***	***H. naledi***	***Homo***	***Hylobates***	***Pan***	***Pongo***
	Au. afarensis	1	0.3120	0.0050	1	0.3920	1	1	0.8540
	Au. africanus	-	1	1	1	1	1	1	1
	Au. sediba	-	-	1	1	1	1	1	1
	Gorilla	-	-	-	0.6060	0.0093	< 0.0001	< 0.0001	< 0.0001
	H. naledi	-	-	-	-	1	1	1	1
	Homo	-	-	-	-	-	0.9910	1	1
	Hylobates	-	-	-	-	-	-	1	1
	Pan	-	-	-	-	-	-	-	1
	51% Bone Length								
		Au. africanus	***Au. sediba***	***Gorilla***	***H. naledi***	***Homo***	***Hylobates***	***Pan***	***Pongo***
	Au. afarensis	0.7390	0.7470	0.1300	1	1	0.0264	1	0.1850
	Au. africanus	-	1	1	1	1	1	1	1
	Au. sediba	-	-	1	1	1	1	1	1
	Gorilla	-	-	-	1	0.0001	1	0.1570	1
	H. naledi	-	-	-	-	1	1	1	1
	Homo	-	-	-	-	-	< 0.0001	0.3730	0.0007
	Hylobates	-	-	-	-	-	-	0.0016	1
	Pan	-	-	-	-	-	-	-	0.5980
	73% Bone Length								
		Au. africanus	***Au. sediba***	***Gorilla***	***H. naledi***	***Homo***	***Hylobates***	***Pan***	***Pongo***
	Au. afarensis	1	1	1	0.7850	1	0.3090	1	0.4050
	Au. africanus	-	1	1	1	1	1	1	1
	Au. sediba	-	-	1	1	1	1	1	1
	Gorilla	-	-	-	1	1	0.0034	0.5570	0.0087

Table 2.13. Continued

H. naledi	**-**	**-**	**-**	**-**	**0.8040**	**1**	**0.7370**	**1**
Homo	-	-	-	-	-	0.0001	1	0.0002
Hylobates	-	-	-	-	-	-	< 0.0001	1
Pan	-	-	-	-	-	-	-	< 0.0001

Table 2.14. Intraspecific pairwise comparisons of the polar moment of inertia (J) through ontogeny. The 51% and 73% slice levels of *Homo* were investigated using a parametric Tukey's HSD test. In all other regions statistical differences were tested for with a non-parametric Dunn's tests with Bonferroni correction.

Genus	Age	32% Bone Length			51% Bone Length			73% Bone Length		
Gorilla		**Adult**	**Infant**	**Juvenile**	**Adult**	**Infant**	**Juvenile**	**Adult**	**Infant**	**Juvenile**
	Adolescent	0.0050	0.1430	0.8980	0.0040	0.1630	0.8530	0.0095	0.1080	0.9280
	Adult	-	< 0.0001	< 0.0001	-	< 0.0001	< 0.0001	-	< 0.0001	0.0001
	Infant	-	-	1	-	-	1	-	-	0.8380
Homo	**Adolescent**	0.7700	0.0365	0.3550	0.9160	0.0070	0.1490	0.3830	0.0297	0.2390
	Adult	-	0.0001	0.0096	-	0.0001	0.0137	-	0.0001	0.0029
	Infant	-	-	1	-	-	0.6560	-	-	0.8200
Hylobates	**Adolescent**	0.0003	0.0032	0.4800	0.0004	0.0033	0.4340	0.0074	0.0006	0.1800
	Adult	-	< 0.0001	< 0.0001	-	< 0.0001	< 0.0001	-	< 0.0001	< 0.0001
	Infant	-	-	0.2910	-	-	0.3320	-	-	0.3330
Pan	**Adolescent**	0.1270	< 0.0001	0.0086	0.0143	0.0002	0.0242	0.0927	0.0001	0.0174
	Adult	-	< 0.0001	< 0.0001	-	< 0.0001	< 0.0001	-	< 0.0001	< 0.0001
	Infant	-	-	0.2080	-	-	0.2940	-	-	0.1800
Pongo	**Adolescent**	0.1390	0.0477	0.1310	0.1970	0.0364	0.1160	0.1790	0.0469	0.1030
	Adult	-	0.0001	0.0006	-	0.0001	0.0008	-	0.0001	0.0005
	Infant	-	-	1	-	-	1	-	-	1

Table 2.15. Interspecific pairwise comparisons of the polar moment of inertia (J) through ontogeny. All statistical differences were tested for with a non-parametric Dunn's tests with Bonferroni correction.

Infant

32% Bone Length					
	Gorilla	***Homo***	***Hylobates***	***Pan***	***Pongo***
Au. afarensis	1	1	1	1	1
Gorilla	-	1	0.0003	1	1
Homo	-	-	0.0001	1	1
Hylobates	-	-	-	0.0003	0.0307
Pan	-	-	-	-	1
51% Bone Length					
	Gorilla	***Homo***	***Hylobates***	***Pan***	***Pongo***
Au. afarensis	1	1	1	1	1
Gorilla	-	1	< 0.0001	1	1
Homo	-	-	0.0003	1	1
Hylobates	-	-	-	0.0012	0.0387
Pan	-	-	-	-	1
73% Bone Length					
	Gorilla	***Homo***	***Hylobates***	***Pan***	***Pongo***
Au. afarensis	0.6116	0.1973	1	0.7908	0.9133
Gorilla	-	0.5749	0.0046	0.9695	0.9078
Homo	-	-	0.0001	0.1659	0.1892
Hylobates	-	-	-	0.0162	0.3134
Pan	-	-	-	-	0.9977

Juvenile

32% Bone Length					
	Gorilla	***Homo***	***Hylobates***	***Pan***	***Pongo***
Au. africanus	1	1	0.0304	0.8770	0.7050
Gorilla	-	1	< 0.0001	0.2660	0.4100
Homo	-	-	0.0001	0.4920	0.5210
Hylobates	-	-	-	0.0011	0.2230
Pan	-	-	-	-	1

Table 2.15. Continued

	51% Bone Length					
		Gorilla	***Homo***	***Hylobates***	***Pan***	***Pongo***
	Au. africanus	1	1	0.0304	0.8490	0.8590
	Gorilla	-	1	< 0.0001	0.2630	0.6600
	Homo	-	-	0.0001	0.4850	0.7770
	Hylobates	-	-	-	0.0013	0.1330
	Pan	-	-	-	-	1
	73% Bone Length					
		Gorilla	***Homo***	***Hylobates***	***Pan***	***Pongo***
	Au. africanus	1	1	0.2010	1	1
	Gorilla	-	1	< 0.0001	0.6270	0.0599
	Homo	-	-	0.0002	0.9680	0.1100
	Hylobates	-	-	-	0.0003	1
	Pan	-	-	-	-	0.8720
Adolescent	***32% Bone Length***					
		Gorilla	***Homo***	***Hylobates***	***Pan***	***Pongo***
	Gorilla	-	1	< 0.0001	0.3240	1
	Homo	-	-	< 0.0001	0.2040	1
	Hylobates	-	-	-	0.0008	< 0.0001
	Pan	-	-	-	-	1
	51% Bone Length					
		Gorilla	***Homo***	***Hylobates***	***Pan***	***Pongo***
	Gorilla	-	1	< 0.0001	0.0277	1
	Homo	-	-	< 0.0001	0.1490	1
	Hylobates	-	-	-	0.0032	< 0.0001
	Pan	-	-	-	-	0.5060
	73% Bone Length					
		Gorilla	***Homo***	***Hylobates***	***Pan***	***Pongo***
	Gorilla	-	1	< 0.0001	0.1780	1
	Homo	-	-	0.0001	0.7940	1

Table 2.15. Continued

	Hylobates	-	-	-	**0.0004**	**0.0001**		
	Pan	-	-	-	-	1		
Adult	***32% Bone Length***							
		Au. africanus	***Au. sediba***	***Gorilla***	***H. naledi***	***Homo***	***Hylobates***	***Pan***	***Pongo***
	Au. afarensis	0.2040	0.1450	1	0.3710	0.8170	< 0.0001	0.0173	0.1050
	Au. africanus	-	1	0.8590	1	1	1	1	1
	Au. sediba	-	-	0.6820	1	1	1	1	1
	Gorilla	-	-	-	1	1	< 0.0001	< 0.0001	0.0006
	H. naledi	-	-	-	-	1	1	1	1
	Homo	-	-	-	-	-	< 0.0001	0.0162	0.6320
	Hylobates	-	-	-	-	-	-	0.0001	< 0.0001
	Pan	-	-	-	-	-	-	-	1
	51% Bone Length								
		Au. africanus	***Au. sediba***	***Gorilla***	***H. naledi***	***Homo***	***Hylobates***	***Pan***	***Pongo***
	Au. afarensis	1	0.9740	0.1370	0.9970	0.9990	0.2240	1	1
	Au. africanus	-	1	1	1	1	0.7760	1	1
	Au. sediba	-	-	0.5390	1	1	1	1	1
	Gorilla	-	-	-	0.1900	0.0811	< 0.0001	< 0.0001	0.0001
	H. naledi	-	-	-	-	1	1	1	1
	Homo	-	-	-	-	-	< 0.0001	0.4800	1
	Hylobates	-	-	-	-	-	-	0.0001	< 0.0001
	Pan	-	-	-	-	-	-	-	1
	73% Bone Length								
		Au. africanus	***Au. sediba***	***Gorilla***	***H. naledi***	***Homo***	***Hylobates***	***Pan***	***Pongo***
	Au. afarensis	0.9980	0.9820	0.8020	0.9840	0.9960	0.2030	0.9880	1
	Au. africanus	-	1	1	1	1	1	1	1
	Au. sediba	-	-	1	1	1	1	1	1
	Gorilla	-	-	-	1	1	< 0.0001	< 0.0001	0.0019
	H. naledi	-	-	-	-	1	1	1	1

Table 2.15. Continued

Homo	**-**	**-**	**-**	**-**	**-**	**< 0.0001**	**0.0058**	**0.3560**
Hylobates	-	-	-	-	-	-	0.0001	< 0.0001
Pan	-	-	-	-	-	-	-	1

Table 2.16. Intraspecific pairwise comparisons of the polar section modulus (Z_{pol}) through ontogeny. All three slice levels of *Homo* were investigated using a parametric Tukey's HSD test. In all other regions statistical differences were tested for with a non-parametric Dunn's tests with Bonferroni correction.

Genus	Age	32% Bone Length			51% Bone Length			73% Bone Length		
Gorilla		**Adult**	**Infant**	**Juvenile**	**Adult**	**Infant**	**Juvenile**	**Adult**	**Infant**	**Juvenile**
	Adolescent	0.0079	0.1140	0.8240	0.0085	0.1200	0.7960	0.0207	0.0734	0.7030
	Adult	-	< 0.0001	< 0.0001	-	< 0.0001	< 0.0001	-	< 0.0001	0.0001
	Infant	-	-	0.9750	-	-	1	-	-	0.8680
Homo	**Adolescent**	0.2940	0.0046	0.1570	0.9150	0.0009	0.0978	0.3490	0.0044	0.1540
	Adult	-	< 0.0001	0.0008	-	< 0.0001	0.0070	-	< 0.0001	0.0011
	Infant	-	-	0.5500	-	-	0.3590	-	-	0.5420
Hylobates	**Adolescent**	0.0005	0.0031	0.5120	0.0006	0.0032	0.5250	0.0063	0.0006	0.3420
	Adult	-	< 0.0001	< 0.0001	-	< 0.0001	< 0.0001	-	< 0.0001	< 0.0001
	Infant	-	-	0.2710	-	-	0.2640	-	-	0.1800
Pan	**Adolescent**	0.3320	< 0.0001	0.0049	0.0445	0.0001	0.0158	0.2300	< 0.0001	0.0055
	Adult	-	< 0.0001	< 0.0001	-	< 0.0001	< 0.0001	-	< 0.0001	< 0.0001
	Infant	-	-	0.2130	-	-	0.2760	-	-	0.2650
Pongo	**Adolescent**	0.4590	0.0218	0.0658	0.3890	0.0247	0.0735	0.3130	0.0329	0.0747
	Adult	-	0.0001	0.0009	-	0.0001	0.0008	-	0.0002	0.0006
	Infant	-	-	1	-	-	1	-	-	1

Table 2.17. Interspecific pairwise comparisons of the polar section modulus (Z_{pol}) through ontogeny. All statistical differences were tested for with a non-parametric Dunn's tests with Bonferroni correction.

Infant	***32% Bone Length***					
		Gorilla	***Homo***	***Hylobates***	***Pan***	***Pongo***
	Au. afarensis	1	1	1	1	1
	Gorilla	-	1	0.0008	1	1
	Homo	-	-	0.0006	1	1
	Hylobates	-	-	-	0.0003	0.0392
	Pan	-	-	-	-	1
	51% Bone Length					
		Gorilla	***Homo***	***Hylobates***	***Pan***	***Pongo***
	Au. afarensis	1	1	1	1	1
	Gorilla	-	1	0.0001	1	1
	Homo	-	-	0.0005	1	1
	Hylobates	-	-	-	0.0007	0.0434
	Pan	-	-	-	-	1
	73% Bone Length					
		Gorilla	***Homo***	***Hylobates***	***Pan***	***Pongo***
	Au. afarensis	0.9200	0.4810	1	1	1
	Gorilla	-	1	0.0018	1	1
	Homo	-	-	0.0005	1	1
	Hylobates	-	-	-	0.0009	0.2590
	Pan	-	-	-	-	1
Juvenile	***32% Bone Length***					
		Gorilla	***Homo***	***Hylobates***	***Pan***	***Pongo***
	Au. africanus	1	1	0.0309	0.9770	0.5890
	Gorilla	-	1	< 0.0001	0.4980	0.3450
	Homo	-	-	0.0002	0.7840	0.4530
	Hylobates	-	-	-	0.0006	0.3500
	Pan	-	-	-	-	1
	51% Bone Length					

Table 2.17. Continued

		Gorilla	***Homo***	***Hylobates***	***Pan***	***Pongo***
	Au. africanus	1	1	0.0309	0.9170	0.7230
	Gorilla	-	1	< 0.0001	0.2930	0.4200
	Homo	-	-	0.0003	0.9440	0.8460
	Hylobates	-	-	-	0.0009	0.2150
	Pan	-	-	-	-	1
	73% Bone Length					
		Gorilla	***Homo***	***Hylobates***	***Pan***	***Pongo***
	Au. africanus	1	1	0.2700	1	1
	Gorilla	-	1	< 0.0001	0.4870	0.0273
	Homo	-	-	0.0004	1	0.0818
	Hylobates	-	-	-	0.0007	1
	Pan	-	-	-	< 0.0001	0.5860
Adolescent	***32% Bone Length***					
		Gorilla	***Homo***	***Hylobates***	***Pan***	***Pongo***
	Gorilla	-	1	< 0.0001	1	1
	Homo	-	-	< 0.0001	0.4400	1
	Hylobates	-	-	-	0.0002	< 0.0001
	Pan	-	-	-	-	1
	51% Bone Length					
		Gorilla	***Homo***	***Hylobates***	***Pan***	***Pongo***
	Gorilla	-	1	< 0.0001	0.0714	1
	Homo	-	-	< 0.0001	0.3060	1
	Hylobates	-	-	-	0.0017	< 0.0001
	Pan	-	-	-	-	0.6120
	73% Bone Length					
		Gorilla	***Homo***	***Hylobates***	***Pan***	***Pongo***
	Gorilla	-	1	< 0.0001	0.2200	0.4230
	Homo	-	-	< 0.0001	0.6250	0.9230
	Hylobates	-	-	-	0.0002	0.0006

Table 2.17. Continued

	Pan	-	-	-	-	**1**		
Adult	***32% Bone Length***							
		Au. africanus	***Au. sediba***	***Gorilla***	***H. naledi***	***Homo***	***Hylobates***	***Pan***	***Pongo***
	Au. afarensis	1	1	1	1	1	0.0151	1	1
	Au. africanus	-	1	0.9940	1	1	1	1	1
	Au. sediba	-	-	1	1	1	1	1	1
	Gorilla	-	-	-	1	1	< 0.0001	< 0.0001	0.0014
	H. naledi	-	-	-	-	1	1	1	1
	Homo	-	-	-	-	-	< 0.0001	0.0322	0.5660
	Hylobates	-	-	-	-	-	-	0.0001	< 0.0001
	Pan	-	--	-	-	-	-	-	1
	51% Bone Length								
		Au. africanus	***Au. sediba***	***Gorilla***	***H. naledi***	***Homo***	***Hylobates***	***Pan***	***Pongo***
	Au. afarensis	1	1	0.9350	1	1	1	1	1
	Au. africanus	-	1	1	1	1	1	1	1
	Au. sediba	-	-	0.7570	1	1	1	1	1
	Gorilla	-	-	-	0.7460	0.1790	< 0.0001	< 0.0001	0.0003
	H. naledi	-	-	-	-	1	1	1	1
	Homo	-	-	-	-	-	< 0.0001	0.7170	1
	Hylobates	-	-	-	-	-	-	< 0.0001	< 0.0001
	Pan	-	-	-	-	-	-	-	1
	73% Bone Length								
		Au. africanus	***Au. sediba***	***Gorilla***	***H. naledi***	***Homo***	***Hylobates***	***Pan***	***Pongo***
	Au. afarensis	1	1	1	1	1	0.5130	1	1
	Au. africanus	-	1	1	1	1	1	1	1
	Au. sediba	-	-	1	1	1	1	1	1
	Gorilla	-	-	-	1	1	< 0.0001	< 0.0001	0.0001
	H. naledi	-	-	-	-	1	1	1	1
	Homo	-	-	-	-	-	< 0.0001	0.0063	0.0471

Table 2.17. Continued

Hylobates	-	-	-	-	-	-	**< 0.0001**	**< 0.0001**
Pan	-	-	-	-	-	-	-	1

Table 2.18. Statistical power of the sample (*effect size* = 0.2, *alpha* = 0.05). *Au. sediba* was unable to be incorporated into the test as it requires N>1.

Genus	N	Power
Gorilla	75	0.96610201
Homo	37	0.69043122
Hylobates	74	0.96374573
Pan	85	0.98305359
Pongo	55	0.88050299
Au. afarensis	2	0.06218398
Au. africanus	3	0.07521930
Au. sediba	1	N/A
H. naledi	2	0.06218398

3. Potential Signals of Locomotor Behavior in the Trabecular Structure of the Clavicle

Introduction

To continue advancing our understanding of the form-function relationship in the hominoid clavicle, signals of locomotor adaptation in the trabecular structure of the element can be explored. As trabecular and cortical bone collectively contribute to the structural integrity and mechanical resilience of bone, exploring trabecular structure may allow for the identification of additional and/or corroborating signals of locomotor adaptation in the clavicle. Similar to cortical geometry, trabecular bone is thought to be more responsive to stress and strain compared to external aspects of morphology and therefore may better reflect the behaviors an animal was engaged in as opposed to the full range of possible behaviors with a given joint or element configuration (Ruff and Runestad, 1992). However, in comparison to cortical bone which remodels at a rate of about 2 - 3% per year, trabecular bone generally remodels much faster with approximately 25% turnover annually in healthy adults (Eriksen, 1986, 2010); although, the exact remodeling rate likely varies both phylogenetically (Currey et al., 2017) and through ontogeny (Pitfield et al., 2017). Due to this higher remodeling rate, trabecular bone is likely more responsive to variation in loading throughout life and therefore may better reflect function than cortical bone (Carter et al., 1989; Jacobs, 2000; Rubin et al., 2001, 2002; but see Lovejoy et al., 2003). Trabecular bone remodeling also appears to be more localized than that of cortical bone (Rubin et al., 2001, 2002; Judex et al., 2004; Barak et al., 2011; Schulte et al., 2013), potentially allowing for the identification of more nuanced signals of locomotor adaptation.

Trabecular analysis has largely focused on analyzing bone structure beneath the articular surface of specific joints, as trabecular bone generally serves to dissipate external loads across joints by transferring them towards the surrounding cortical bone (Currey, 2002; Barak et al., 2008). However, in elements such as the clavicle, where trabecular bone extends past the subarticular regions and throughout the entire length of the bone (Harrington et al., 1993), its function may differ in relation to mechanical and non-mechanical roles. For example, the trabecular network in the clavicle may serve as a location for hematopoiesis (Keaveny et al., 2001; Wang et al., 2022) into adulthood in all apes as has been demonstrated in humans (Zawin and Jaramillo, 1993). Or clavicular trabecular bone may be maintained in a strategic manner to provide increased stiffness under habitual loading. About 88% of trabecular stiffness, or the Young's modulus of trabecular bone, can be explained by trabecular bone volume fraction (BV/TV) (Stauber et al., 2006), therefore regions of the diaphysis with increased BV/TV may have adapted to increase stiffness in response to loading during locomotion.

Changes in trabecular bone fraction are produced through shifts in a combination of several constituent variables such as trabecular thickness (Tb.Th), separation (Tb.Sp), and number (Tb.N). These variables can be quantified alongside BV/TV to better understand the potential for 'optimization' of trabecular structure amongst mammals or may reveal phylogenetic trends in bone remodeling. However, these constituent variables are complex to directly interpret as they contribute to increased BV/TV in a variety of combinations depending on both the species and skeletal element under investigation (Georgiou et al., 2018; Tsegai et al., 2018; Bird et al., 2022). Moreover, these properties may be so highly correlated with BV/TV that it would be difficult to identify their specific mechanical roles (Hodgskinson and Currey, 1990; Goldstein et al., 1993). Tb.N is thought by some to be of no structural importance (Gibson, 1985, 2005), but Saparin et.

al. (2011) believe that reductions in strut number are highly relevant in areas of lower loading. They propose that reducing the number of trabeculae in a region is structurally safer than decreasing the thickness of those trabeculae. This is because if an individual strut is made too thin, it cannot effectively bear load and becomes non-functional, despite technically still being present (Skedros et al., 2012). Additionally, by reducing Tb.N instead, a bone can preferentially resorb unnecessary or structurally redundant struts, often increasing anisotropy in that region (Saparin et al., 2011; Skedros et al., 2012). This hypothesis has been supported by the *in vivo* experimental results of Biewener et al. (1996), however, the invasive nature of these studies make the results difficult to directly interpret. Tb.N has also been shown to scale with body size negatively such that larger animals have relatively fewer trabeculae than smaller animals (Doube et al., 2011; Ryan and Shaw, 2013). Tb.Th and separation are additionally strongly related to body mass with larger animals having absolutely thicker and more widely separated trabeculae, but relative to their body mass, the struts are thinner and more tightly packed than would be expected via isometric scaling (Swartz et al., 1998; Barak et al., 2011; Doube et al., 2011; Ryan and Shaw, 2013). It should be noted, however, that the specific scaling relationships amongst trabecular structural parameters and body mass varies depending on both the bony element and taxonomic group under investigation (Cotter et al., 2009; Fajardo et al., 2013; Ryan and Shaw, 2013). Despite some lingering ambiguity surrounding the functional significance of the more nuanced aspects of trabecular remodeling, the characterization of trabecular structure has been demonstrated to be informative about joint loading and posture, and thus holds promise for the exploration of locomotor adaptation in fossil hominins.

Given the patterns and distributions of trabecular structure observed in other skeletal elements amongst adult apes, I test five main hypotheses: (1) suspensory taxa (*Pongo*, *Hylobates*)

will have decreased BV/TV in the subarticular regions of the clavicle due to more assumed tensile joint loading, while more terrestrial taxa (*Pan, Gorilla*) will have higher BV/TV in these regions reflecting more compressive joint loading; (2) regions of attachment for the clavicular pectoralis major m., anterior deltoid m, and cranial trapezius m. will have higher BV/TV than areas of the diaphysis devoid of muscle and/or ligament attachment (Figure 3.2; Doube et al 2009; Pattin et al 1996); (3) Tb.Th will be lowest in the smallest non-human apes (*Hylobates, Pan*) and greatest in the larger non-human apes (*Gorilla, Pongo*), reflecting the scaling relationship reported in analyses of other skeletal elements (Doube et al., 2011; Ryan and Shaw, 2013); (4) modern *Homo sapiens* will have the lowest relative BV/TV and Tb.Th amongst the apes, reflecting the recent gracilization of the modern human skeleton noted by other researchers (Ruff, 2006; Chirchir et al., 2015; Ryan and Shaw, 2015); and (5) trabecular adaptations for arboreality will be present in all fossil hominins included in the analysis (*Au. africanus, Au. sediba,* and *H. naledi*) supporting previous descriptions of the fossil morphology as primitive and hypotheses of a continued reliance on the upper limb for locomotion (Churchill et al., 2013, 2018; Kivell et al., 2015; Feuerriegel et al., 2017, 2019).

Materials

167 adult hominoid individuals from the original ontogenetic sample (see previous chapters), were used here (*Homo sapiens,* N = 20; *Gorilla gorilla,* N = 29; *Gorilla beringei,* N = 18; *Pan troglodytes,* N = 35; *Pongo abelii,* N = 11; *Pongo pygmaeus,* N = 23; *Hylobates lar,* N = 28; and *Hylobates concolor,* N = 3; Table 3.1; Appendix). Fossil taxa included in this analysis (StW 431g, *Au. africanus*; UW 88-38 and -142, *Au. sediba*; UW 101-258 and -1229, *H. naledi;*

Table 3.2) are also a subset of the original dataset used in Chapters 1 and 2 as preservation and CT scan quality dictates inclusion of fossil material in trabecular analyses.

Methods

Segmentation and Reorientation:

First, the original 16-bit micro-CT data was segmented and aligned such that all specimens were oriented within the same anatomical coordinate system defined for clavicle alignment in Chapter 2. Preliminary segmentation was performed using the MIA-Clustering segmentation algorithm (Dunmore et al., 2018) . This algorithm, in comparison to manual segmentation, reduces the number of subjective decisions and increases reproducibility. The resulting segmented scans were first manually inspected to ensure the segmentation was completed correctly, then binarized and aligned such that the center of the sternal epiphysis was the origin of the coordinate system using *Avizo Lite 2020.2* (Visualizations Sciences Group, 2017).Aligning the scans to a standard coordinate system ensures that all specimens are in the same position for defining the regions of interest in the analysis. The binarized and aligned voxel data are shown in (Figure 3.1. A).

The voxel data was then imported into medtool (v 4.5; www.dr-pahr.at/medtool), the cortical and trabecular bone were differentiated using morphological filters following Gross et al. (2014), and the suggested equations for calculating the ideal kernel size for the morphological filters were used. First a closing filter was used to fill in any gaps in the cortex of the element. After the surface was closed, an outer (Figure 3.1. B) and inner mask (Figure 3.1. C) of the element were created, representing the periosteal and endosteal volumes of the specimens. These masks were used to create the volumetric meshes upon which the quantified trabecular parameters are interpolated (Figure 3.1. G). A cortex only mask was then created by subtracting the inner mask

from the outer mask (Figure 3.1. D), and a trabecular bone only mask was created by subtracting the cortical image from the full original image (Figure 3.1. E). The created masks were then mathematically combined such that the cortex was removed, and the air, inner medullary region, and trabecular bone in the image are assigned the grey values 0, 1 and 2, respectively (Figure 3.1. F); this defined voxel data was used to quantify the trabecular parameters of interest.

Trabecular bone quantification:

The quantification of the trabecular parameters was performed twice for each specimen: (1) across the entire clavicle, and (2) within predefined regions of interest (Figure 3.1. H). The former allows for a visualization of the parameters throughout the element, while the latter allows for a statistical comparison of mean values within each defined region. Regions of interest were defined such that the first (ROI 1) quantified the sternal subarticular area (sternal 10% of bone length), the last (ROI 22) quantified the acromial subarticular area (acromial 10% of bone length), and the intermediate 20 regions (ROI 2 – ROI 21) quantified the parameters across the diaphysis within the remaining 80% of bone length. To quantify trabecular bone volume fraction (BV/TV), thickness (Tb.Th), separation (Tb.Sp), and number (Tb.N), each defined region was partitioned using a 2.5 mm square grid. A sphere with a 5 mm diameter is then fit to each node in the grid, creating multiple overlapping spheres, and the parameters are quantified within each sphere. 'medtool 4.5' calculates the parameters of interest as follows: BV/TV is calculated as the ratio of 'BV' or bone volume (all voxels with a '2' grey value) over 'TV' or total volume (all voxels with a '1' and '2' grey value); Tb.Th and Tb.Sp were calculated using the sphere fitting method of Hildebrand and Ruesegger (1997); Tb.N was calculated as 1 divided by the sum of Tb.Th and separation (1/(Tb.Th + Tb.Sp)). BV/TV was further standardized by dividing the original values

by the mean BV/TV for each individual specimen, resulting in the relative trabecular bone volume fraction (rBV/TV).

Comparative Analyses

To qualitatively compare the distributions of the parameters across the clavicle, values calculated for those parameters at each node in the grid during the whole bone analysis were projected onto the nodes of the 3D mesh (Figure 3.1. I). The interpolation of these values and projection onto the 3D mesh were visualized in *Paraview 5.11.0* (Ahrens et al., 2005). To better understand the regional variation in trabecular bone structure, this visualization was performed and described for the specimen with BV/TV values in each ROI closest to the genus average (*Gorilla*, AMNH M 167336; *Homo*, CMNH HTH 0315; *Hylobates*, MCZ M 41455; *Pan*, AMNH M 174860; *Pongo*, USNM M 143596).

Statistical comparison of the structural parameters was conducted in R using the mean rBV/TV, Tb.Th, Tb.Sp, and Tb.N values for each of the 22 defined ROIs. Levene's tests were used to assess for significant differences in homogeneity of variance between groups, and Shapiro-Wilk tests were used to identify datasets that deviated from a normal distribution. Fifty-six of the defined groups showed differences in homogeneity of variance (Table 3.3), and ninety-four had non-normal distributions (Table 3.4), so further differences between groups were investigated with non-parametric Kruskal-Wallis tests and post-hoc Dunn's tests with Bonferroni correction. For the datasets that did not reject the null hypotheses of the Levene's and Shapiro-Wilk tests, differences between groups were tested for using ANOVA and pairwise post-hoc Tukey's HSD tests. Significance was determined at $p = 0.05$ for all analyses.

Results

Extant Hominoids:

Relative trabecular bone volume fraction (rBV/TV):

Even after scaling the BV/TV values by individual specimen means, significant differences exist among hominoid taxa (Figure 3.3. A; Figures 3.12 – 3.14; Table 3.7). *Homo* has a higher rBV/TV in the sternal half of the diaphysis than *Pan, Gorilla,* and *Pongo. Hylobates,* on the other hand, has a lower rBV/TV than all the great apes between 41 – 75% bone length. *Pan* and *Gorilla* rBV/TV distributions mostly overlap, except for around 86 – 91% bone length where rBV/TV in *Pan* decreases to a magnitude more similar to *Homo*. Within the same region, rBV/TV in *Gorilla* is more similar to *Pongo.* All great apes share a general trend in distributions where around 60 – 70% bone length rBV/TV increases. *Hylobates* shows a different distribution across the clavicle where rBV/TV is highest within the epiphyses and there are low values maintained across the diaphysis.

To better understand the regional variation in trabecular bone structure, the distribution of rBV/TV from the specimen representing the individual with BV/TV values in each ROI closest to the genus mean is described. *Gorilla* shows the highest values on the cranial surface of the lateral curvature and small areas of high rBV/TV along the cranio-dorsal surface of the lateral curvature and acromial end (Figure 3.4). *Gorilla* (AMNH M 167336) also has notably low values mid-diaphysis. In the articular subarticular regions, the sternal region has high rBV/TV directly in the center of the sternal epiphysis and low values surrounding it. Acromially, *Gorilla* has a relatively even spread of rBV/TV throughout the region. *Pan* (AMNH M 174860) also has high rBV/TV around the lateral curvature (Figure 3.5), but it stretches more medially into the diaphysis than is seen in *Gorilla*. In contrast to *Gorilla*, *Pan* has high rBV/TV across the acromial and sternal

subarticular regions. Additionally, in the sternal end of the clavicle, *Pan* has particularly high rBV/TV around the region of attachment of the sternocleidomastoid m. In the subarticular regions, acromially *Pan* has high rBV/TV across the entire area and sternally it shows the opposite trend to *Gorilla* by having high rBV/TV everywhere except the center of the subarticular region. This may be, in part, due to the pitting that is especially common in this area in *Pan* (see sternal subarticular region in Figure 3.5).

Homo (CMNH HTH 0315) shows the highest rBV/TV values along the ventral margin in the region of attachment for the clavicular head of the pectoralis major m. which then spreads cranially around the lateral curvature, near where the anterior deltoid m. originates (Figure 3.6). In the region of attachment for the cranial trapezius m., *Homo* has slightly elevated rBV/TV, but it is lower than the other noted regions. On the inferior side of the clavicle in the region of the lateral curvature, *Homo* has high rBV/TV on the ventral half while the dorsal half has a far lower trabecular bone volume fraction. This split pattern is more similar to *Gorilla* as opposed to *Pan* and *Pongo*. Additionally, very low rBV/TV is seen in the dorsal aspect of the diaphysis. In the subarticular regions, *Homo* has high rBV/TV across the sternal area, with values being the highest on the edges – particularly in the ventroinferior and dorsocranial region. Acromially, there is a similar pattern of high rBV/TV across the whole region but there are particularly high concentrations on the dorsoventral edges.

Pongo (USNM M 143596) has a much more sporadic distribution of increased and decreased rBV/TV across the element in comparison with the other great apes (Figure 3.7). There are clusters of high values around the lateral curvature spreading medially into the diaphysis, similar to *Pan*, but the high concentration of rBV/TV are found more on the ventral and dorsal sides as opposed to the cranial side of the clavicle. Also similar to *Pan*, *Pongo* has a region of high

rBV/TV on the cranial aspect of the sternal end where the sternocleidomastoid attaches. Unlike *Pan, Pongo* has quite low rBV/TV in the dorsal aspect of the medial diaphysis, similar to *Homo.* In the sternal subarticular region, *Pongo* has high rBV/TV around the edges of the area, except for the middle of the craniocaudal edges, with relatively low values in the center of the region. Unlike *Pan,* a small amount of pitting has been observed in *Pongo*, so this may be a more meaningful signal than in *Pan*. Acromially, the distribution of rBV/TV is high compared to other regions of the clavicle, but again the concentrations of high values are seemingly random across the subarticular region.

Finally, the only lesser ape in the sample with a much lower average body mass than the other apes (Fleagle, 2013), *Hylobates* (MCZ M 41455), has a unique rBV/TV distribution across the clavicle (Figure 3.8). There is only high rBV/TV in the epiphyseal regions with little to no trabecular bone in the diaphysis. Sternally, *Hylobates* has especially high rBV/TV on the dorsoinferior aspect of the epiphysis and subarticular surface. In the acromial end of the clavicle, cranially there is a concentration of high rBV/TV just medial to the articular surface, but the high values do not appear to continue onto the subarticular surface proper. On the inferior side of the acromial region there are higher rBV/TV values than seen cranially and the concentrations appear to be where the coracoclavicular ligaments and acromioclavicular ligaments attach.

Trabecular thickness, separation, and number (Tb.Th, Tb.Sp, Tb.N):

Known to scale with body mass (Doube et al., 2011; Ryan and Shaw, 2013), Tb.Th is highest in *Gorilla* and lowest in *Hylobates* (Figure 3.3. D; Figures 3.15 – 3.17; Table 3.9). The relationship between Tb.Th and bone length as a proxy for body mass is significant for the entire dataset ($p < 0.0001$, $R^2 = 0.37$) but loses that significant relationship once *Hylobates* is omitted

(Figure 3.25, Table 3.6. *Pan* and *Pongo* have trabeculae that are slightly thinner than in *Gorilla*, while *Homo* has a Tb.Th equivalent to *Gorilla* medially, but after approximately 50% bone length, the thickness is more similar to *Pan* and *Pongo*. In contrast to the great apes, *Hylobates* has a low Tb.Th in the sternal half of the bone that then sharply increases at around 75% of bone length. The other apes show a more gradual increase in Tb.Th between 50 – 90% of bone length. The trends in Tb.Th across the clavicle do not mirror those seen in rBV/TV nor Tb.N, discussed below.

In the ape clavicle, Tb.N does not strongly scale allometrically (Figure 3.25, Table 3.6), but it does show a weak positive correlation amongst all apes (p = 0.03, R^2 = 0.02) and a weak negative correlation within just the great apes (p = 0.0005, R^2 = 0.08). *Pan* and *Pongo* show higher values than *Gorilla* and *Homo* (Figure 3.3. B; Figures 3.18 – 3.20; Table 3.8) who, on average, have larger body masses (Fleagle, 2013). *Homo* has significantly less trabeculae per area unit than *Pan* between 55 – 100% bone length and *Pongo* between 64 – 91% bone length. Like rBV/TV, the great apes follow a similar trend where Tb.N begins increasing around mid-bone and peaks at approximately 75% bone length. *Hylobates* is distinct from the great apes again by only having increased Tb.N in the epiphyseal regions of the clavicle. Looking at the distribution of Tb.N in the mean species representatives, all apes have more trabeculae per unit area in the epiphyses than in the diaphysis, even in regions of the diaphysis that show high trabecular bone volume fraction. *Gorilla* and *Pan* have a high Tb.N in both the sternal and acromial subarticular regions with some continuation into epiphysis. *Hylobates* also has more trabeculae in its epiphyses, but unlike *Gorilla* and *Pan*, the trend does not extend past the subarticular area. In *Homo*, again there are more trabeculae in the articular ends of the clavicle, but acromially there is a higher Tb.N in the inferior aspect of the region. *Pongo* is unique compared to the other apes. It has a high Tb.N in the sternal subarticular region, but not the acromial region. Unlike other apes, *Pongo* has sporadic small

regions of increased Tb.N around the lateral curvature in the diaphysis, especially on the inferior side.

Tb.Sp also displays a weak allometric relationship (Figure 3.25, Table 3.6). There is a moderate negative relationship between separation and bone length within the entire dataset ($p < 0.0001$, $R^2 = 0.13$), but that relationship turns to slightly positive when just looking at the great apes ($p = 0.03$, $R^2 = 0.03$). Like the other trabecular parameters, there appears to be a great ape trend and a *Hylobates* trend in the amount of Tb.Sp across the clavicle (Figure 3.3. C; Figures 3.21 – 3.23; Table 3.10). All great apes have increased separation sternally. It then decreases around 60 – 75% bone length to its minimum diaphyseal value, increases again around 85 – 90% bone length, then decreases again in the acromial epiphysis. Amongst the great apes, *Gorilla* and *Homo* have the highest separation sternally, and *Homo* has the highest separation acromially with *Gorilla* falling in with the other apes in this region. *Homo* has significantly higher separation than *Pan* between 59 and 82% bone length, and *Pongo* from 64% to the end of the element with minor departures from significant in one or two defined regions. *Hylobates*, on the other hand, have high Tb.Sp along the entire diaphysis, showing decreased separation in only the epiphyseal regions.

Fossil Hominins:

Australopithecus africanus (StW 431g):

Overall, *Au. africanus* shows an African ape-like trabecular structure (Figure 3.9), however, most unique *Homo* trends in trabecular bone appear in the sternal portion of the clavicle which is missing in this individual. rBV/TV shows a great ape like trend of increasing between 60 – 70% estimated bone length, and more specifically show the *Pan*-like trend of a minor decrease in rBV/TV after that initial increase, before increasing again in the acromial epiphysis. Moreover,

the region of high rBV/TV on the cranioventral aspect of the lateral curvature extends medially into the diaphysis, and is very similar to the pattern in *Pan*. There are also clusters of high rBV/TV along the craniodorsal margin of the lateral curvature where the cranial trapezius m. attaches in an extant ape. Tb.Sp is also relatively ape-like by having an increase in separation around 75 – 80% of estimated bone length before decreasing in the acromial epiphysis. Within this region, the increased separation is within the caudal aspect of the diaphysis just medial to the lateral inflection. Tb.Th also shows an extant ape-like pattern in being highest along the ventral margin of the lateral inflection, spreading along both the cranial and caudal surfaces.

Australopithecus sediba (UW 88-38, UW 88-142):

In comparison to the other fossil hominins, *Au. sediba* has a unique trabecular structure (Figure 3.10). In the lateral third of the element, *Au. sediba* is relatively similar to the extant apes, but the trabecular structure in the medial half of the element has a notably high rBV/TV produced through the combination of decreased Tb.Sp, increased Tb.N, and increased Tb.Th. Interestingly, the increased rBV/TV medially is not located in the ventral aspect of the diaphysis like in *Homo*, it is dorsal. In the lateral portion of the bone, *Au. sediba* is similar to the other great apes in having a concentration of increased rBV/TV on the anterior side of the acromial epiphysis and along the dorsal aspect of the lateral curvature. Within the subarticular regions of the epiphyses, *Au. sediba* has high rBV/TV along the cranio- and caudoventral margins acromially and spread along the craniocaudal region of the center of the sternal subarticular surface. This region of high rBV/TV is achieved by increasing Tb.Th in the dorsal region of the diaphysis, and increasing both Tb.N and thickness along the ventral aspect. Tb.Sp is greatest within the cranial region of the medial diaphysis. Unlike the extant great apes, Tb.N is not higher in the epiphyses than the diaphyseal

region. Instead, similar to *Au. africanus*, there are regions of increased Tb.N throughout the diaphysis. In addition to the increased Tb.Th along the dorsal aspect of the medial diaphysis, contributing to the increased rBV/TV in that region, trabeculae are also relatively thicker in the sternal and acromial epiphyses than elsewhere in the diaphysis. Within the sternal and acromial epiphyses, Tb.Th is highest in the caudal region. There are also small concentrations of very high Tb.Th within the flange of the conoid tubercle.

Homo naledi (UW 101-258, UW 101-1229):

The trabecular structure of *H. naledi* is most like *Pan* and *Homo* across the clavicle, but it does have a few distinct trends that separate it from extant apes (Figure 3.11). The mean values of rBV/TV across the clavicle are most similar to *Pan*, but the distribution of increased trabecular bone volume fraction on the ventral margin of the sternal diaphysis is more similar to *Homo*. Also as in *Homo*, *H. naledi* has very low rBV/TV in the craniodorsal aspect of the mid-diaphysis. Tb.Sp is intermediate between *Pan* and *Homo*, with the pattern of separation most like *Pan* sternally and *Homo* acromially. The regions where separation is highest corresponds to areas where rBV/TV is lower. Tb.N in *H. naledi* is also similar to both *Pan* and *Homo* with regions of lower Tb.N sternally within the range of *Homo* and regions of higher Tb.N acromially in the range of *Pan*. Tb.Th is the parameter in which *H. naledi* deviates the most from the other extant and fossil individuals. *H. naledi* has an absolutely high Tb.Th in the sternal majority of the clavicle. The high thickness values in this region are driven by concentrations of thick trabeculae along the ventral aspect of the diaphysis.

Discussion

Trabecular structure in the extant ape clavicle:

Amongst the apes, trabecular structure across the clavicle does appears to separate the taxa. The most obvious distinction is between the great apes (*Pan, Pongo, Gorilla,* and *Homo*) and lesser apes (*Hylobates*). *Hylobates* is unique in having a parabolic distribution of Tb.N and separation, producing a distribution of rBV/TV that is very low in the diaphysis and increases towards the epiphyses. Even though they share common trends in trabecular structure, the great apes can also be differentiated from one another by more closely looking at the distribution of rBV/TV, Tb.N, separation, and thickness across the clavicle.

Recent humans differ from the other great apes in having increased rBV/TV in the region of attachment of the clavicular pectoralis major. *Homo* even has high BV/TV in this region compared to the other apes before scaling the values for relative comparison (Figure 3.3. E). In modern humans, the clavicular pectoralis major acts to flex the arm up to 90° and is involved in both arm adduction and medial rotation, movements that are assumed common in object manipulation by humans. Laterally, *Homo* has comparable rBV/TV to the other great apes with increased trabecular bone volume fraction in the region of attachment of the anterior deltoid. The concentration of high rBV/TV is more cranially oriented in the non-human great apes, reflecting the more anterior attachment site of the muscle in modern humans (Swindler and Wood, 1973; Larson, 2007; Diogo and Wood, 2012). In modern humans, the anterior deltoid acts to flex and internally rotate the arm, again supporting its habitual recruitment during the manipulation of objects. Similar raw bone volume fraction among all great apes in the medial clavicle contrasts with previous research suggesting a recent gracilization of the modern human skeleton, including the trabecular structure (Ruff, 2006; Chirchir et al., 2015; Ryan and Shaw, 2015). However,

modern humans do have lower raw BV/TV than *Pongo, Pan,* and *Gorilla* in the lateral half of the clavicle. Based on EMG data for the anterior deltoid in chimpanzees, Larson and Stern (1986, 1987) suggest that the muscle serves to elevate the arm during the swing phase of climbing and arm swinging, and controls the retraction of the forelimb during knuckle-walking. The increased trabecular bone volume fraction in this region in non-human apes may therefore be present in response to the habitual action of the anterior deltoid during varied locomotor behaviors. *Pongo* and *Homo* also show increased rBV/TV on the dorsocranial aspect of the lateral curvature and acromial diaphysis, in the region of attachment for the cranial trapezius muscle. The cranial trapezius is highly active in chimpanzees during both pendular and non-pendular arm swinging, potentially related to scapular retraction during the stance phase and head stabilization during swing phase (Larson et al., 1991). Its recruitment during arboreal behaviors would support the possible signal of habitual use in *Pongo*, but its significance in *Homo* is less straight forward. In modern humans, the cranial trapezius primarily acts to support our shoulder girdle against the forces of gravity and elevate the scapula. The trabecular distribution patterns suggest that our more descended and dorsally placed shoulder configuration may require constant action of the cranial trapezius to maintain, which then might ultimately be contributing to the increased trabecular bone volume fraction underlying the enthesis.

The distribution of rBV/TV across the sternal subarticular region provides insight into the range of motion habitually used at the sternoclavicular joint but not, surprisingly, the orientation of the clavicle relative to the manubrium. *Homo* has high trabecular bone volume fraction across the whole region, but it is especially high on the dorsoventral margins. This pattern suggests an emphasis on clavicular protraction, retraction, and habitual compressive loading. It also supports the use of the clavicle in the dorsoventral plane as is suggested by the increased dorsoventral

distribution of cortical bone found in modern humans in Chapter 2. *Pongo* also has relatively high rBV/TV in the sternal epiphysis, but in contrast to humans, the concentrations of increased trabecular volume are found along all margins of the region but not in the center. This may reflect the use of the joint in more varied postures and under tensile loads, reducing axial compression in the element, in contrast to *Homo*. Notably, *Gorilla* does not have increased rBV/TV along any of the margins of the sternal subarticular region. Instead, it has high trabecular bone volume fraction in the center of the sternal subarticular area that spreads slightly ventrally, likely reflecting stereotypic compressive loading of the joint during knuckle-walking and the habitual use of few other behaviors. The acromial subarticular area has a relatively consistent distribution of trabecular bone volume fraction in most apes. Given the relatively small range of motion available in the acromioclavicular joint (Levangie and Norkin, 2011), the lack of a clear trabecular signal here is unsurprising. *Homo* uniquely has increased rBV/TV in the dorsoventral margins of the acromial subarticular region, again supporting an emphasis on clavicular, and thus scapular protraction and retraction (Levangie and Norkin, 2011).

Comparing trends in Tb.Th, separation, and number alongside overall trabecular bone volume fraction lends further insight into the loading environment across the clavicle. In regions of muscle attachment, increased trabecular bone volume fraction is produced through the combination of increased Tb.N and thickness, and reduced separation. However, increased trabecular bone volume fraction in subarticular regions is produced through increased Tb.N and decreased separation. This suggests a different remodeling response to the often compressive loading across a joint surface and the tensile pull from muscle contraction.

Combining the patterning of trabecular bone volume fraction across the diaphysis and within the subarticular epiphysis, signatures of locomotor behaviors can be identified. *Pongo* uses

a large range of motion at the sternoclavicular joint to facilitate scapular movement during a varied suite of arboreal behaviors requiring both arm flexion via the anterior deltoid and head stabilization via the cranial trapezius. *Gorilla* loads the sternoclavicular joint predominantly with invariable compression during knuckle walking which involves control over forelimb retraction via the anterior deltoid. *Pan* falls somewhere in between *Pongo* and *Gorilla*, reflecting its use of both arboreal and terrestrial behaviors. Lastly, *Homo* predominantly uses the forelimb in the dorsoventral plane, habitually recruiting the clavicular pectoralis major during arm flexion, adduction, and medial rotation.

Interpreting the trabecular structure in fossil hominins:

Overall, the fossil hominin taxa have trabecular structures within the distributions seen in extant apes. *Au. africanus* has high rBV/TV in the region of the cranial trapezius and anterior deltoid that spreads ventrally as in *Homo*. Also, like *Homo* and unlike *Pongo*, the increased trabecular bone volume fraction is not seen in the inferior aspect of the diaphysis in this region. However, as in *Pongo*, the increased trabecular bone volume fraction seen in the cranioventral aspect of the diaphysis appears to continue medially into the diaphysis. It is also possible that this 'medial continuation' is actually a lateral continuation of increased trabecular bone volume fraction underlying the clavicular pectoralis major enthesis, but because the specimen is missing the sternal diaphysis, the former hypothesis takes precedent.

Au. sediba is the only fossil taxon in this analysis with the articular ends intact, allowing for the comparison with extant apes. The trabecular bone volume fraction in the sternal subarticular region is most similar to *Gorilla*, with high rBV/TV in the center of the region but not along the margins. This suggests that the sternoclavicular joint may have been loaded primarily in

compression with a minimal variation in the range of motion used. The trabecular bone in the acromial subarticular area is most similar to *Homo* but does show some notable differences. While *Homo* has relatively high trabecular bone volume fraction across the area with especially high concentrations along the dorsoventral margins, *Au. sediba* has high rBV/TV within the margins and has very low trabecular bone volume fraction in the center of the subarticular region, suggesting the scapula may have often been protracted but not necessarily retracted as habitually or as forcefully. Previously, high maximum ranges of motion for scapular protraction have been correlated with increased climbing ability in extant hominoids (Isler, 2005).

On the inferior aspect of the acromial epiphysis, there is an area with especially high rBV/TV underlying a region that has highly rugose external morphology and likely representing where the coracoclavicular ligaments attach to the clavicle in this individual. This concentration of high trabecular bone volume fraction also suggests the retention of climbing ability, or similar behavior, as this region is demonstrated to be under high tensile stress during simulated vertical climbing from the results of the FEA in Chapter 4. Further supporting the use of habitual climbing by *Au. sediba* is the trend of increased cortical eccentricity in the medial diaphysis which is also shared by adult *Pan* and adolescent *Gorilla* who climb with a large body mass. Along the diaphysis, *Au. sediba* has the highest trabecular bone volume fraction in the region of attachment of the cranial trapezius like *Homo* and *Pongo*, but there is notably not increased rBV/TV in the region of the anterior deltoid. The inferior aspect of this region also does not show a decrease in trabecular bone volume fraction like in *Homo*. Overall, the distribution of trabecular volume in the lateral curvature of *Au. sediba* suggests the cranial trapezius muscle may have been used to stabilize the head, similar to the extant great apes. However, it does not support the recruitment of the anterior deltoid in a manner similar to *Homo*, *Pan*, or *Gorilla*. Further distinguishing *Au. sediba*

from modern humans, there is no sign of increased use of the clavicular pectoralis major. Ultimately, the trabecular structure of the clavicle supports initial interpretations of *Au. sediba* upper limb morphology that suggested a heavy reliance on climbing and potentially suspensory behaviors (Churchill et al., 2013, 2018) and does not support modern human like use of the shoulder by *Au. sediba*.

Lastly, *H. naledi* shows a trabecular structure most similar to modern *Homo* across the two clavicles. Both individuals have higher trabecular bone volume fraction in the ventral aspect of the medial diaphysis, a feature characteristic of modern *Homo*, and lower volume dorsally as seen in *Homo* and *Pongo*. This may suggest human-like use of the clavicular pectoralis major by *H. naledi*, potentially during behaviors involving the manipulation and/or modification of objects, as has been hypothesized based on the thumb and wrist morphology (Kivell et al., 2015) and stands in contrast to initial interpretations of its shoulder morphology (Feuerriegel et al., 2017, 2019). In the lateral diaphysis, *H. naledi* has high rBV/TV in the cranial, ventral, and caudal areas, but it does not extend dorsally nor medially into the diaphysis. This potentially supports the habitual use of the cranial trapezius and anterior deltoid, but the distribution does not well align *H. naledi* with any extant ape. One *H. naledi* individual has a portion of the sternal metaphysis preserved, and while the entire subarticular area has relatively high trabecular bone volume fraction, it is highest within the ventrocaudal region. Similar to the mosaic of features described in the hand (Kivell et al., 2015; Bowland et al., 2021), the combination of the trabecular structure in the lateral curvature, medial diaphysis, and sternal metaphysis suggests *H. naledi* may have been manipulating objects in a similar manner and frequency to modern humans, while other aspects of upper limb use may have been more similar to arboreal apes.

Significance

Ultimately, this analysis provides proof that the trabecular bone structure in the hominoid clavicle is functionally informative. Additionally, this is the first study to directly investigate the trabecular bone distribution patterns in relation to muscle insertion and use in a comparative sample. In extant apes, increased trabecular bone volume fraction underlies muscles commonly recruited during locomotion, supporting hypotheses of a lower strain threshold for bone deposition in regions under tension in comparison to compression (Pattin et al., 1996; Doube et al., 2009; Bird et al., 2022) and lending insight into muscle use in fossil hominins. *Au. africanus* and *H. naledi* both have increased trabecular bone volume fraction in the lateral region of the diaphysis, supporting an arboreal component of their locomotor behavior, but in *H. naledi* this arboreal signal is coupled with a trabecular structure in the medial diaphysis suggestive of modern human like arm use during object manipulation. The trabecular structure of *Au. sediba* supports habitual climbing involving relatively stereotyped movement at the acromioclavicular joint and does not support modern human like use of the upper limb. Some of the locomotor signals identified here are further supported by the cross-sectional geometry of the clavicle presented in Chapter 2, but others, like the overall distribution of trabecular structure in *Au. sediba* remain unexplained by the extant taxa. Despite the remaining ambiguities, the newly identified similarities and differences in trabecular structure amongst extant hominoids and fossil hominins adds more nuance to our understanding of the form-function relationship in the evolving ape shoulder and supports the analysis of trabecular structure to identify osteological correlates of locomotion in the clavicle.

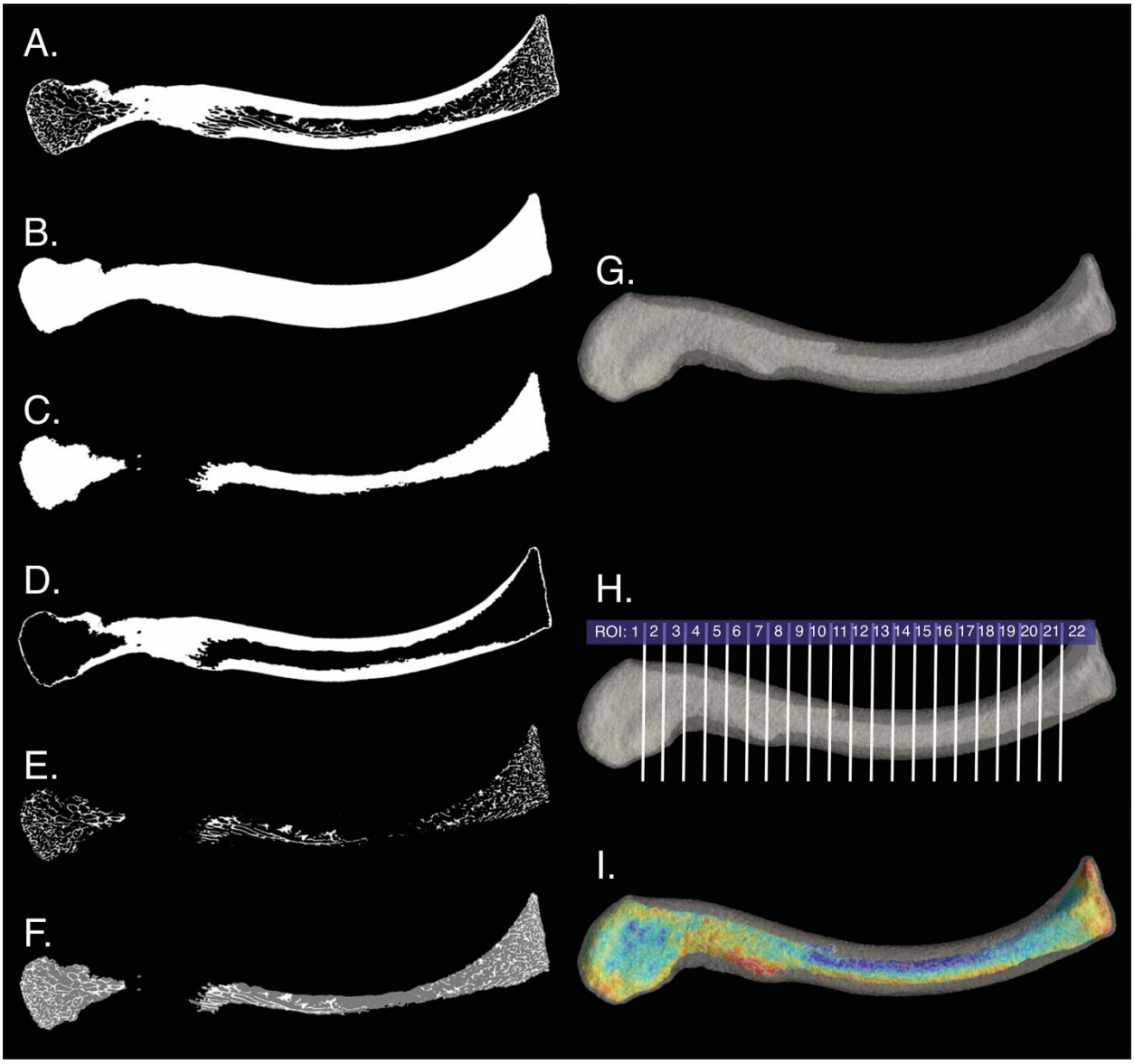

Figure 3.1. 'medtool 4.5' image processing workflow: A. binarized and aligned image; B. outer mask; C. inner mask; D. cortex only mask; E. trabeculae only mask; F. 'three grey-value' image; G. 3D finite element meshes created from the outer and inner masks representing the periosteal and endosteal surfaces; H. 22 ROIs as defined on a modern human clavicle; I. BV/TV values interpolated onto the inner 3D mesh.

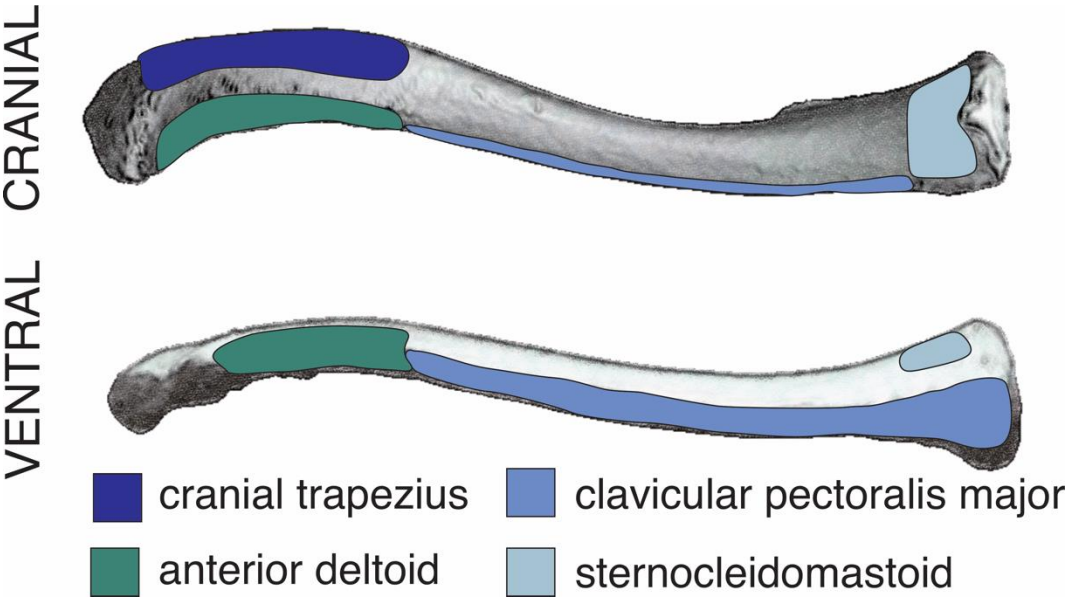

Figure 3.2. Origins sites of the cranial trapezius, anterior deltoid, and clavicular pectoralis major muscles on a modern Homo sapiens clavicle.

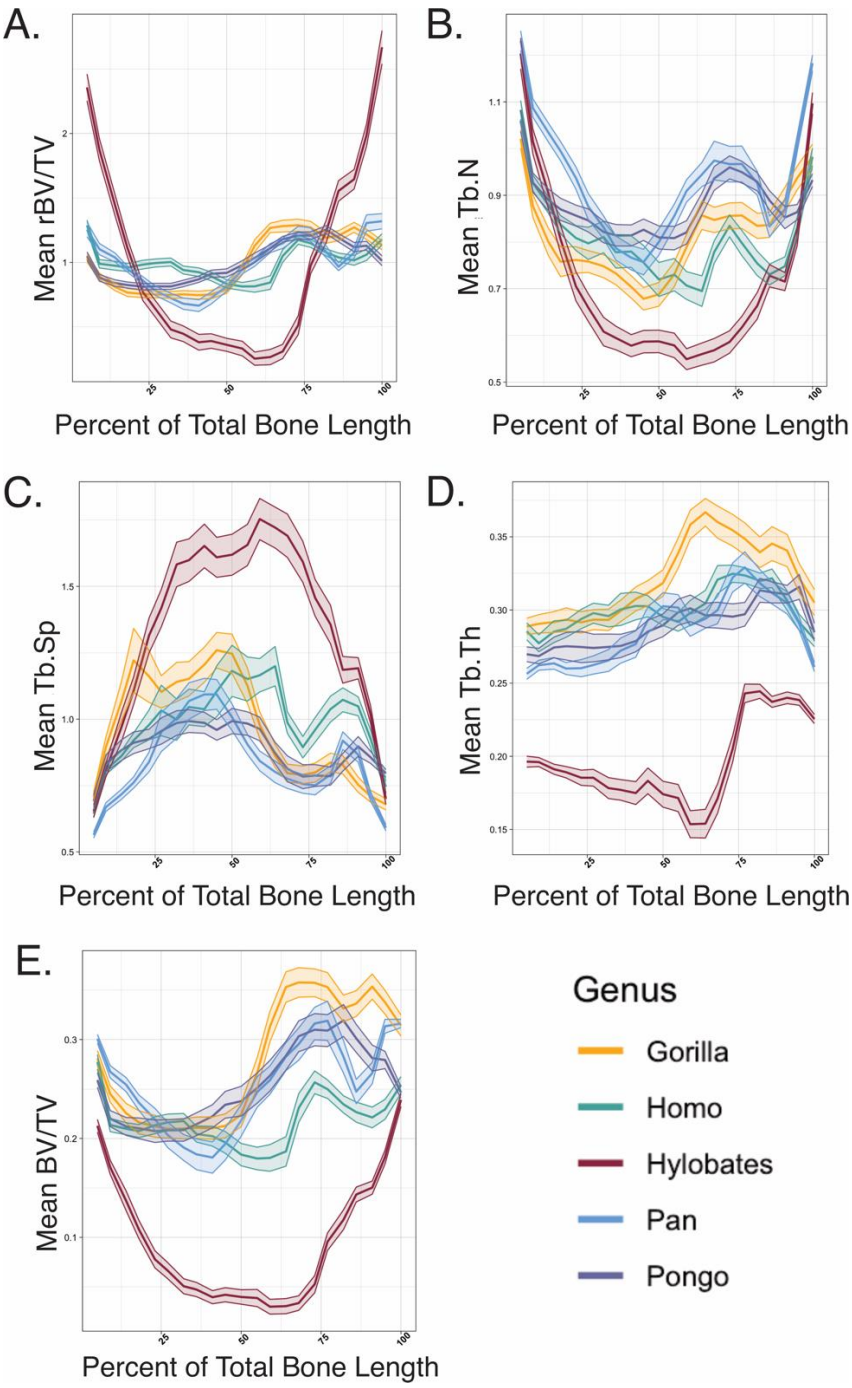

Figure 3.3. Mean trabecular structure parameters for the extant apes within the ROIs: A. mean relative BV/TV (rBV/TV) amongst genera; B. mean trabecular number (Tb.N) amongst genera; C. mean trabecular separation (Tb.Sp) amongst genera; D. trabecular thickness (Tb.Th) amongst genera; E. unscaled, raw BV/TV amongst genera.

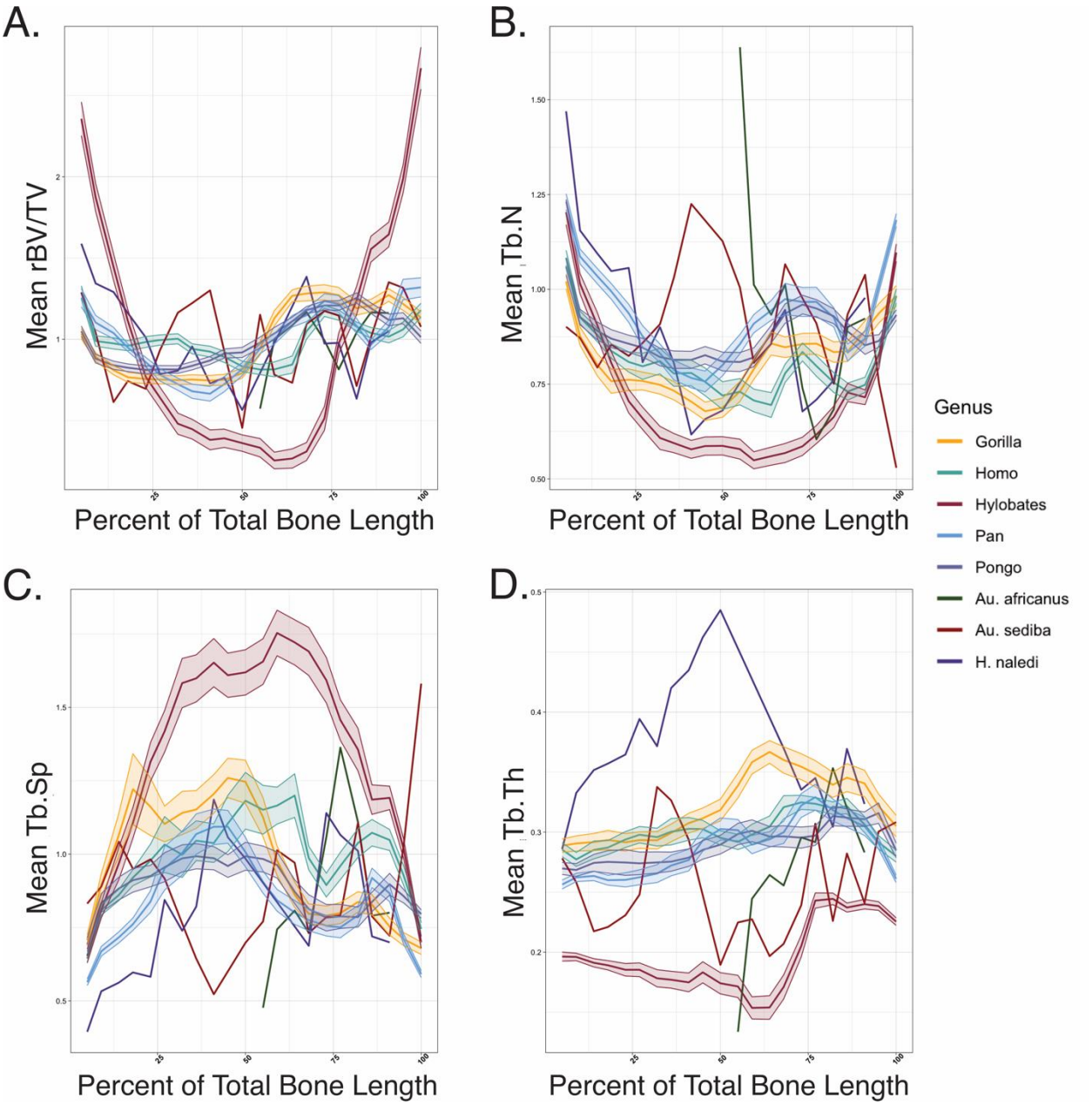

Figure 3.4. Mean trabecular structure parameters for the entire dataset within the ROIs: A. mean relative BV/TV (rBV/TV) amongst genera; B. mean trabecular number (Tb.N) amongst genera; C. mean trabecular separation (Tb.Sp) amongst genera; D. trabecular thickness (Tb.Th) amongst genera.

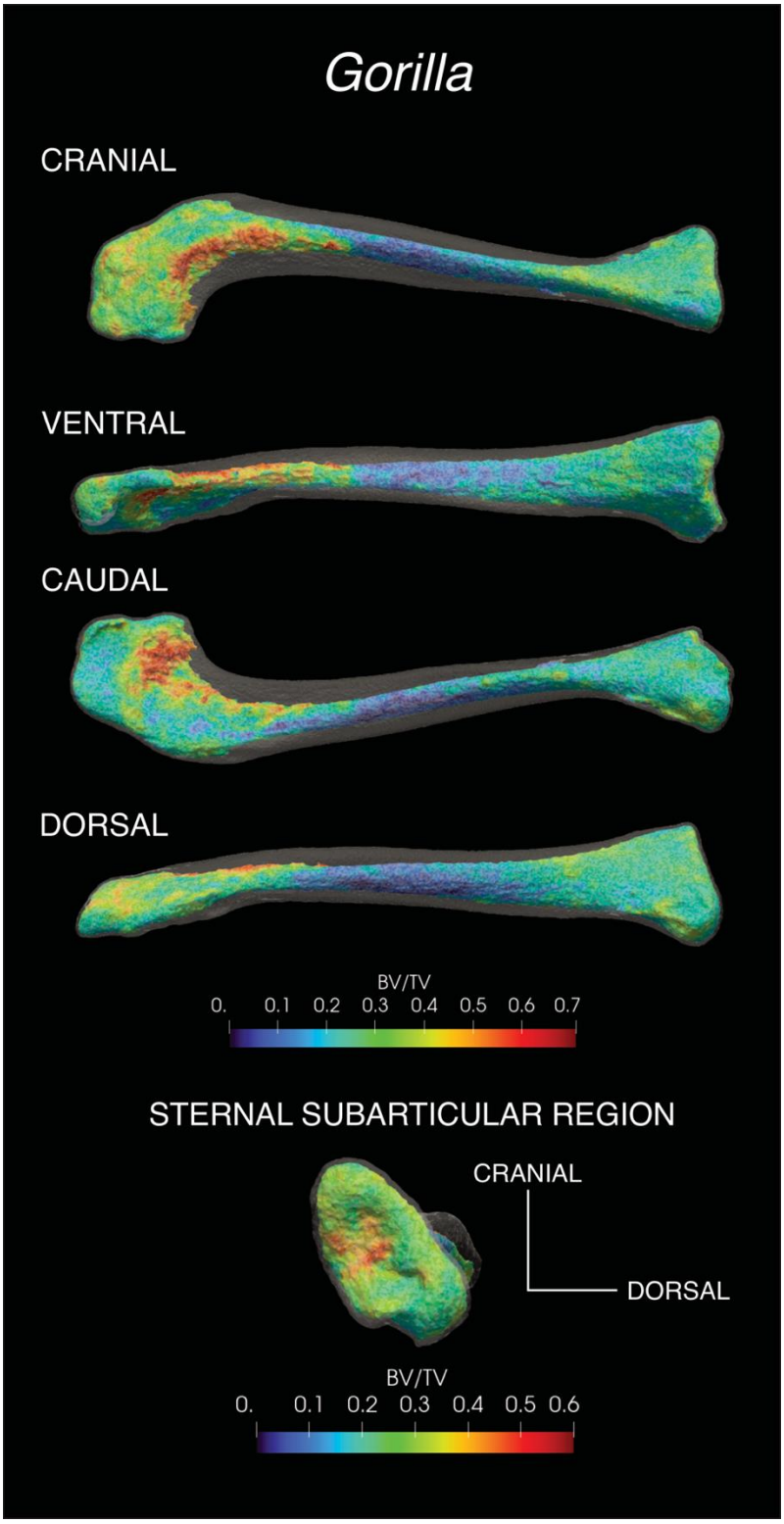

Figure 3.5. BV/TV in *Gorilla*, represented by the mean individual AMNH M 167336.

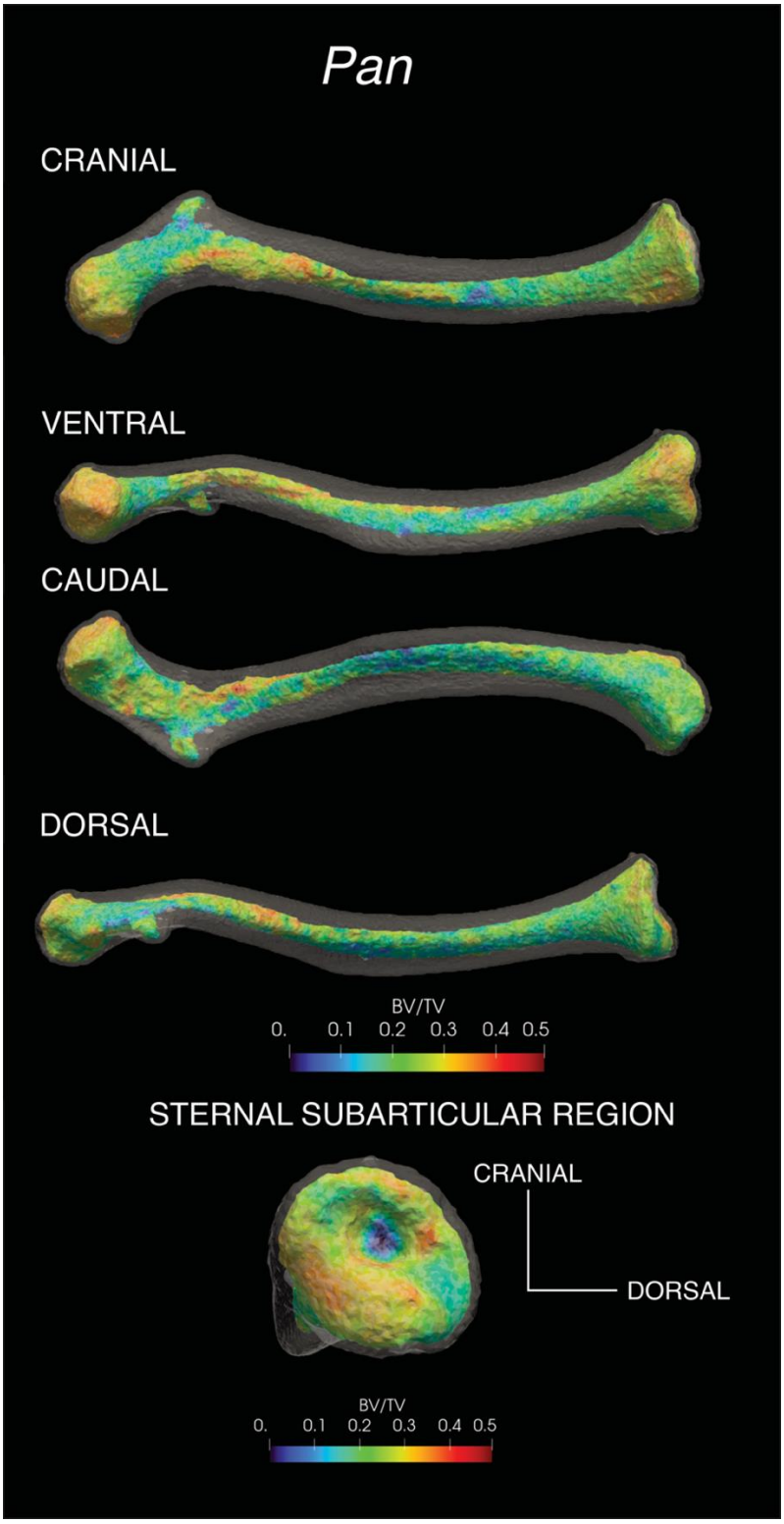

Figure 3.6. BV/TV in *Pan troglodytes*, represented by the mean individual AMNH M 174860.

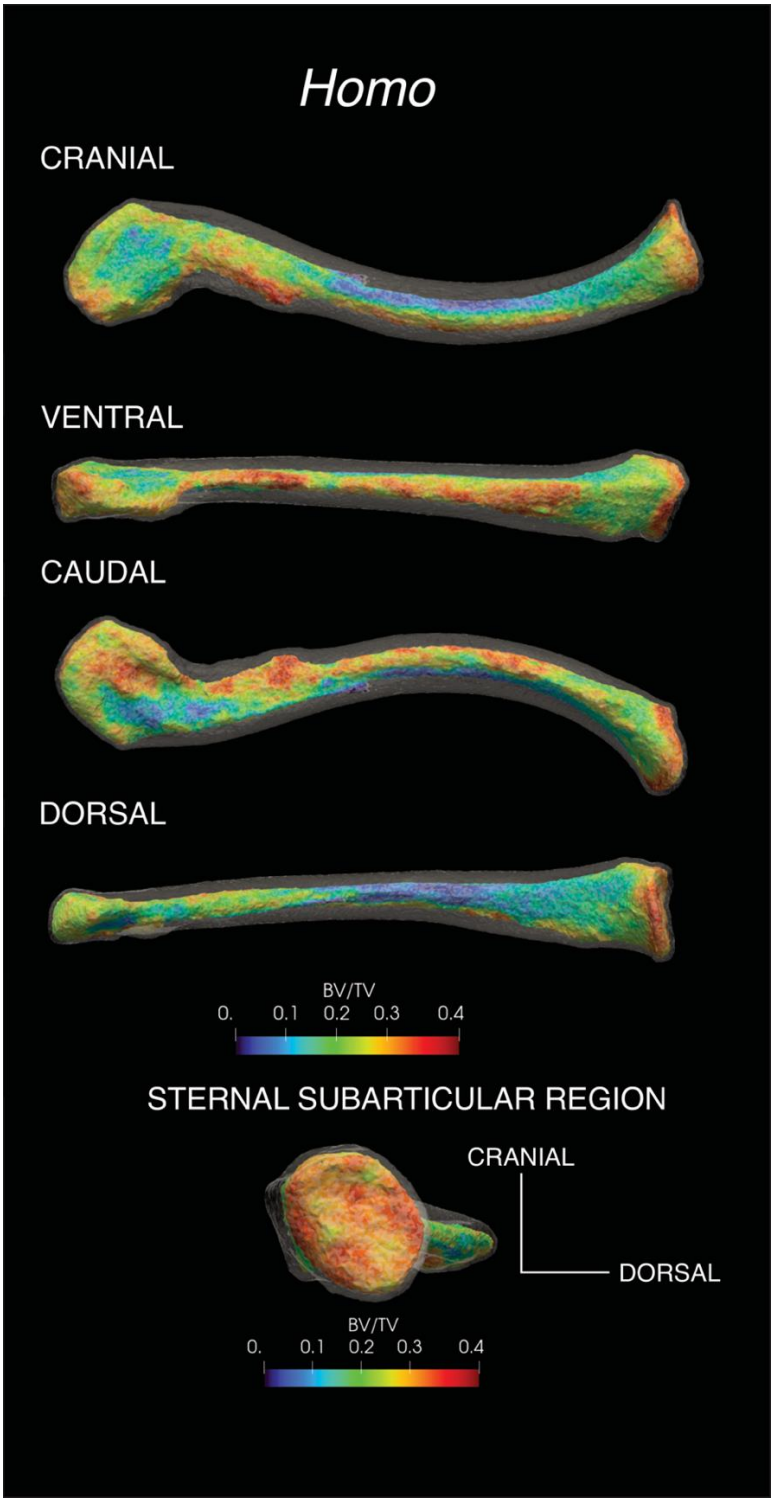

Figure 3.7. BV/TV in modern *Homo sapiens*, represented by the mean individual CMNH HTH 0315.

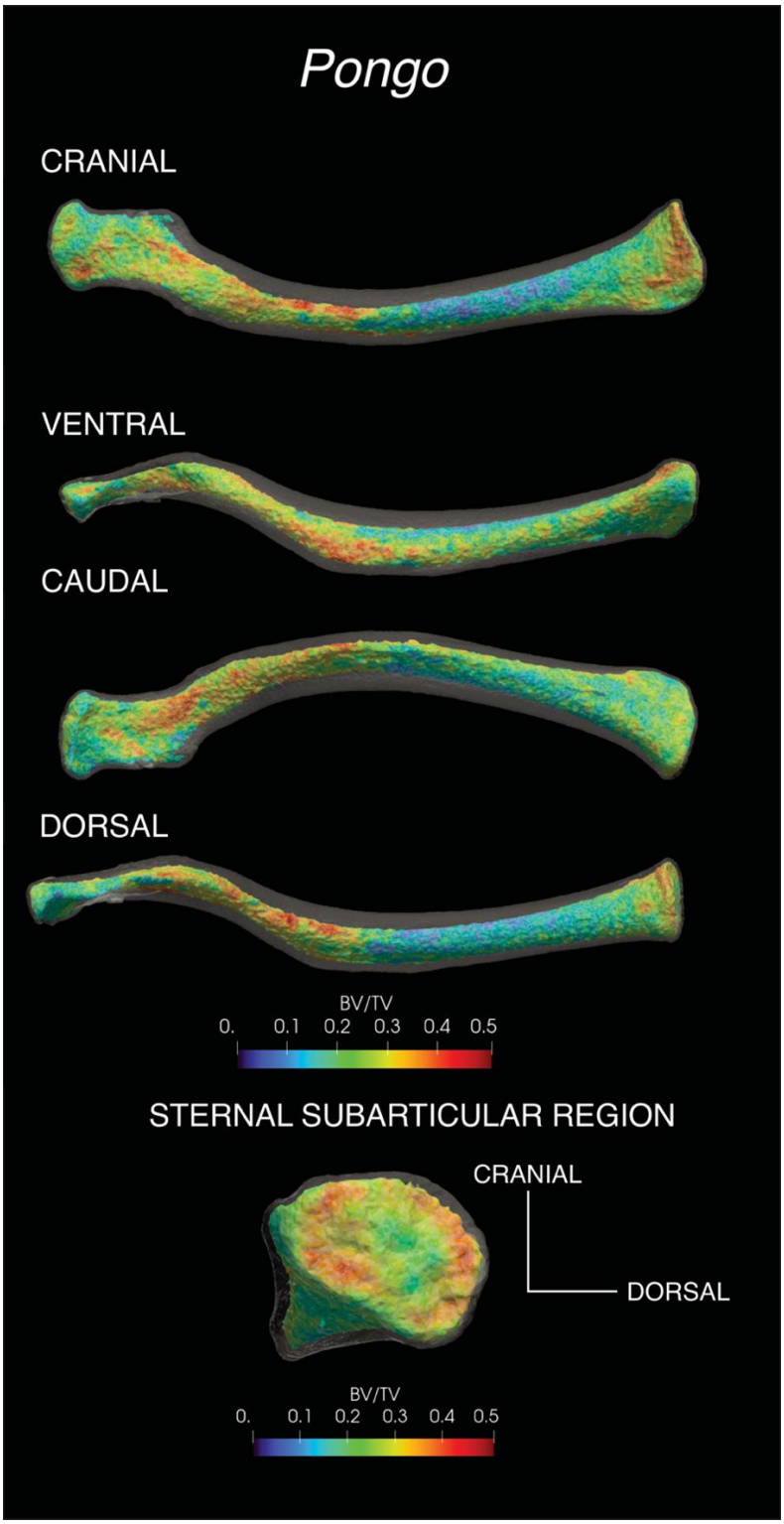

Figure 3.8. BV/TV in *Pongo*, represented by the mean individual USNM M 143596.

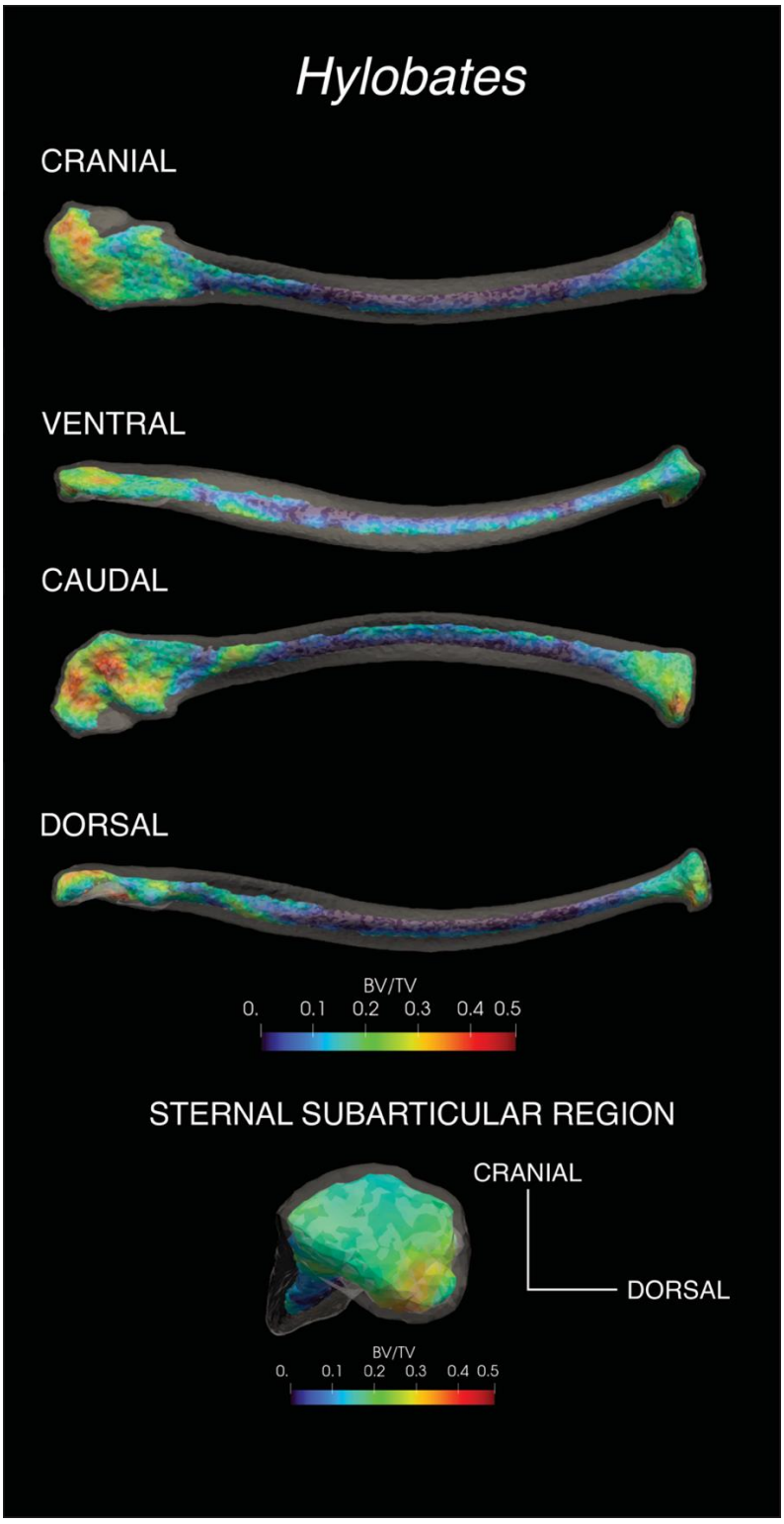

Figure 3.9. BV/TV in *Hylobates*, represented by the mean individual MCZ M 41455.

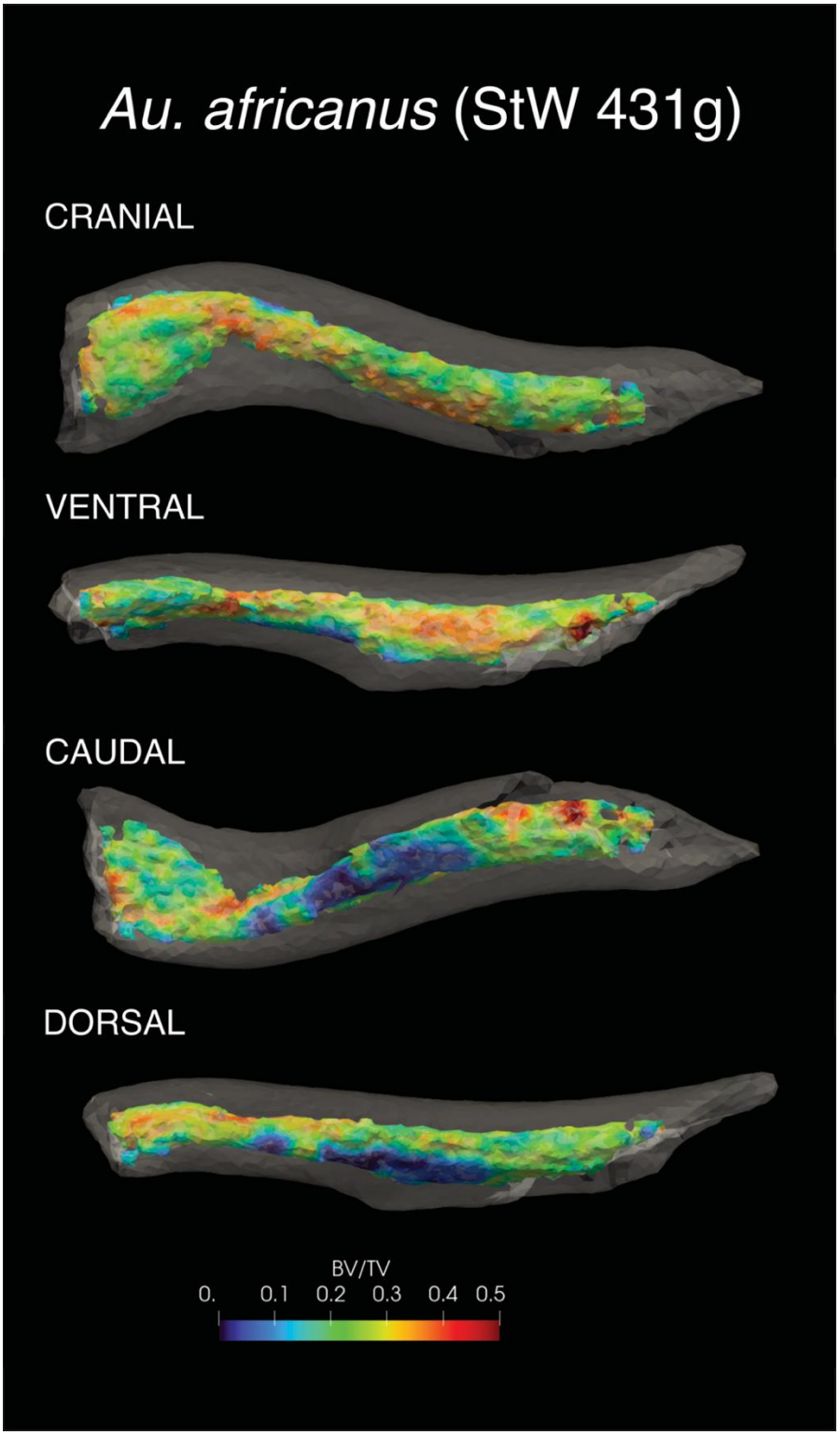

Figure 3.10. BV/TV in *Au. africanus* as represented by StW 431g.

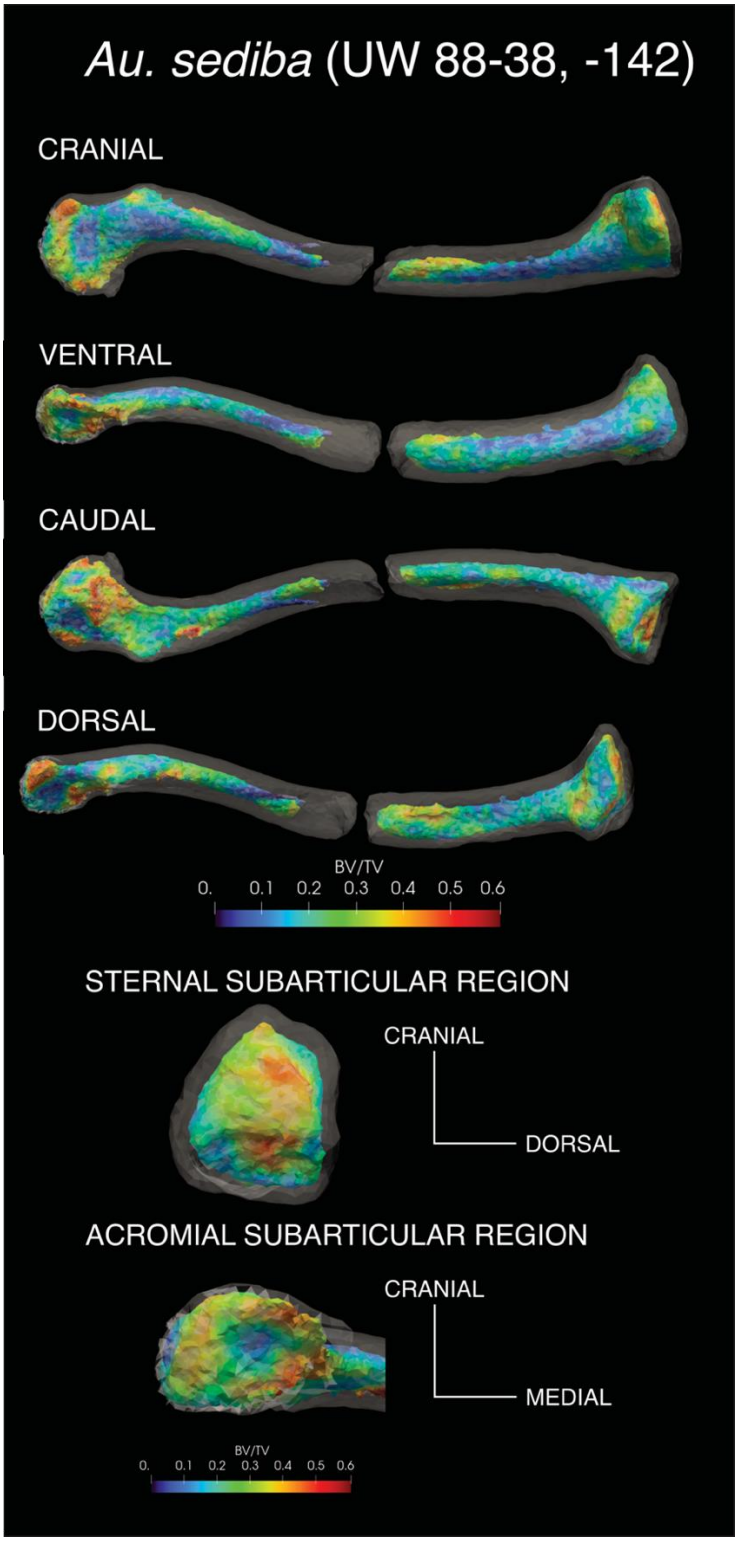

Figure 3.11. BV/TV in *Au. sediba* as represented by UW 88-38 and UW 88-142.

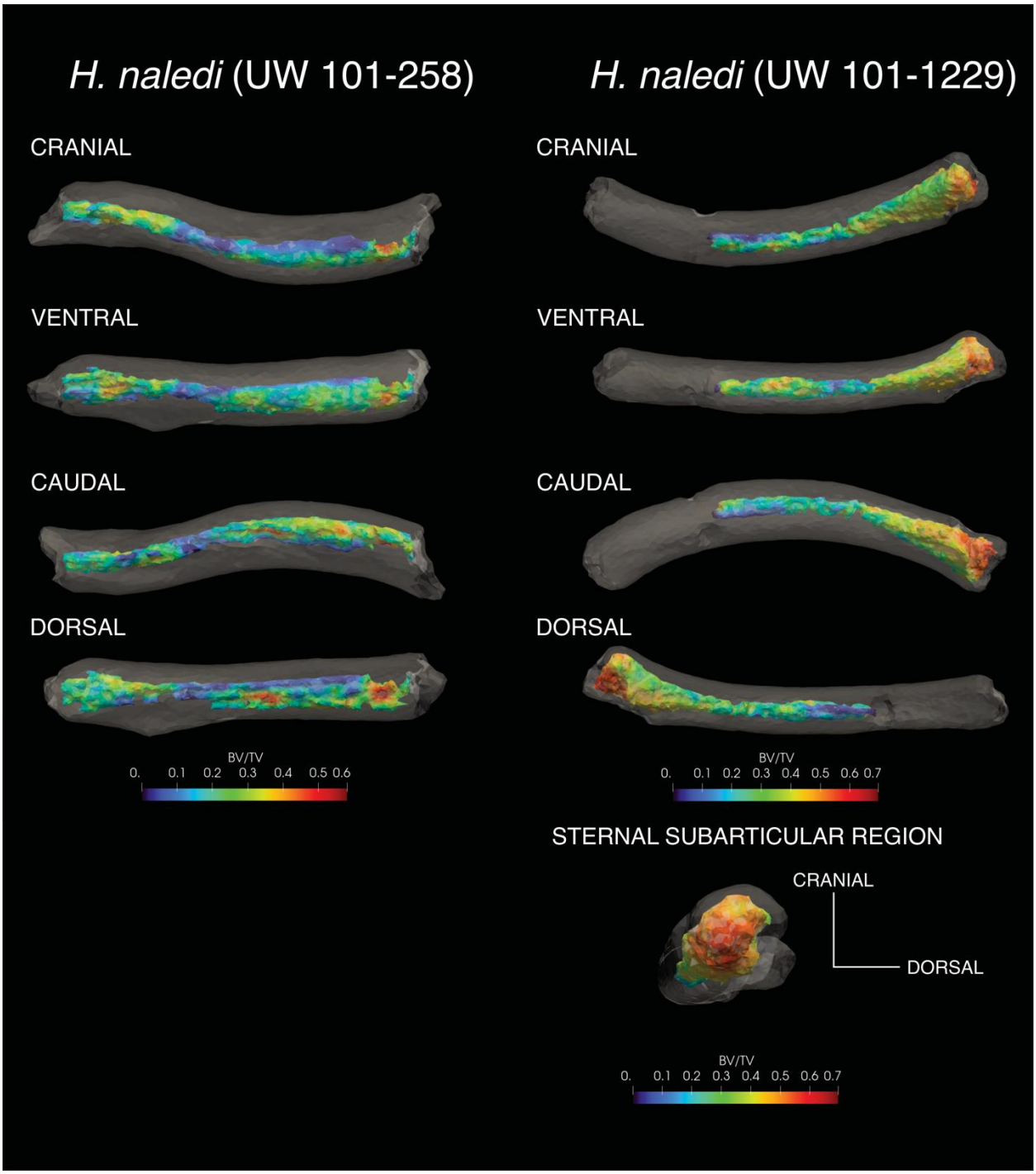

Figure 3.12. BV/TV in *H. naledi* as represented by UW 101-258 (left) and UW 101-1229 (right).

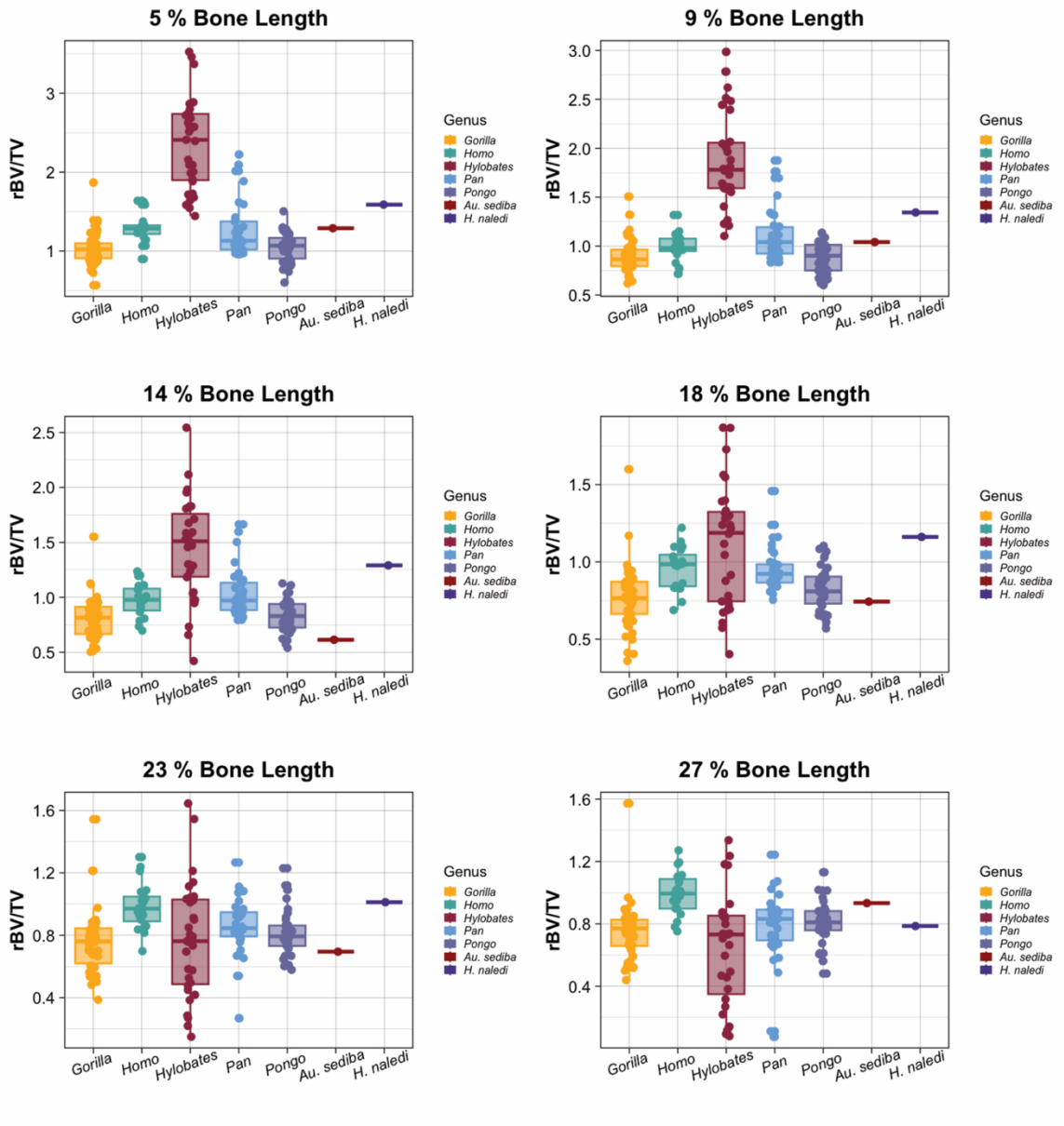

Figure 3.13. Mean rBV/TV values in the first 6 ROIs representing 0 - 27% bone length.

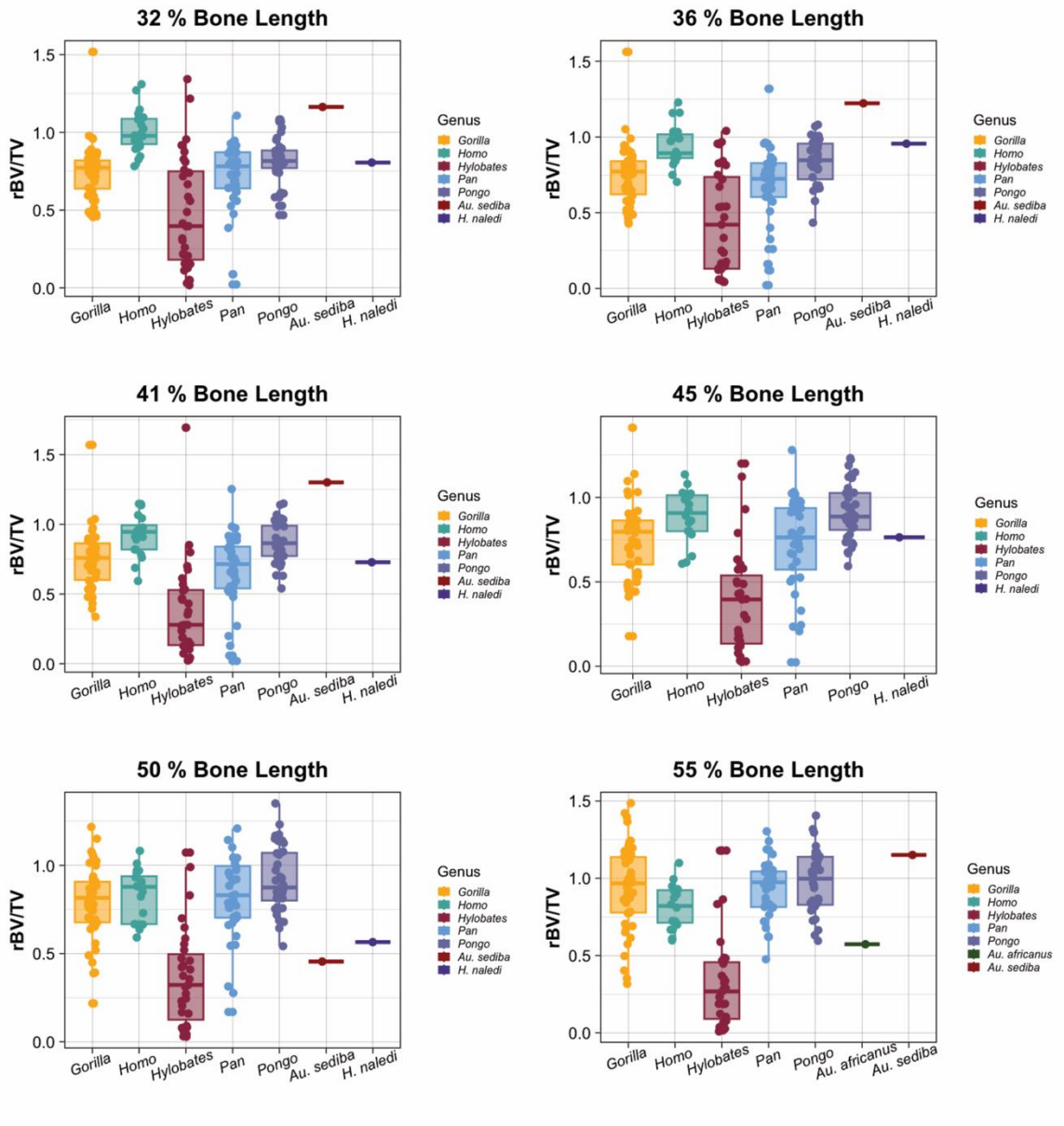

Figure 3.14. Mean rBV/TV values in the next 6 ROIs representing 32 - 55% bone length.

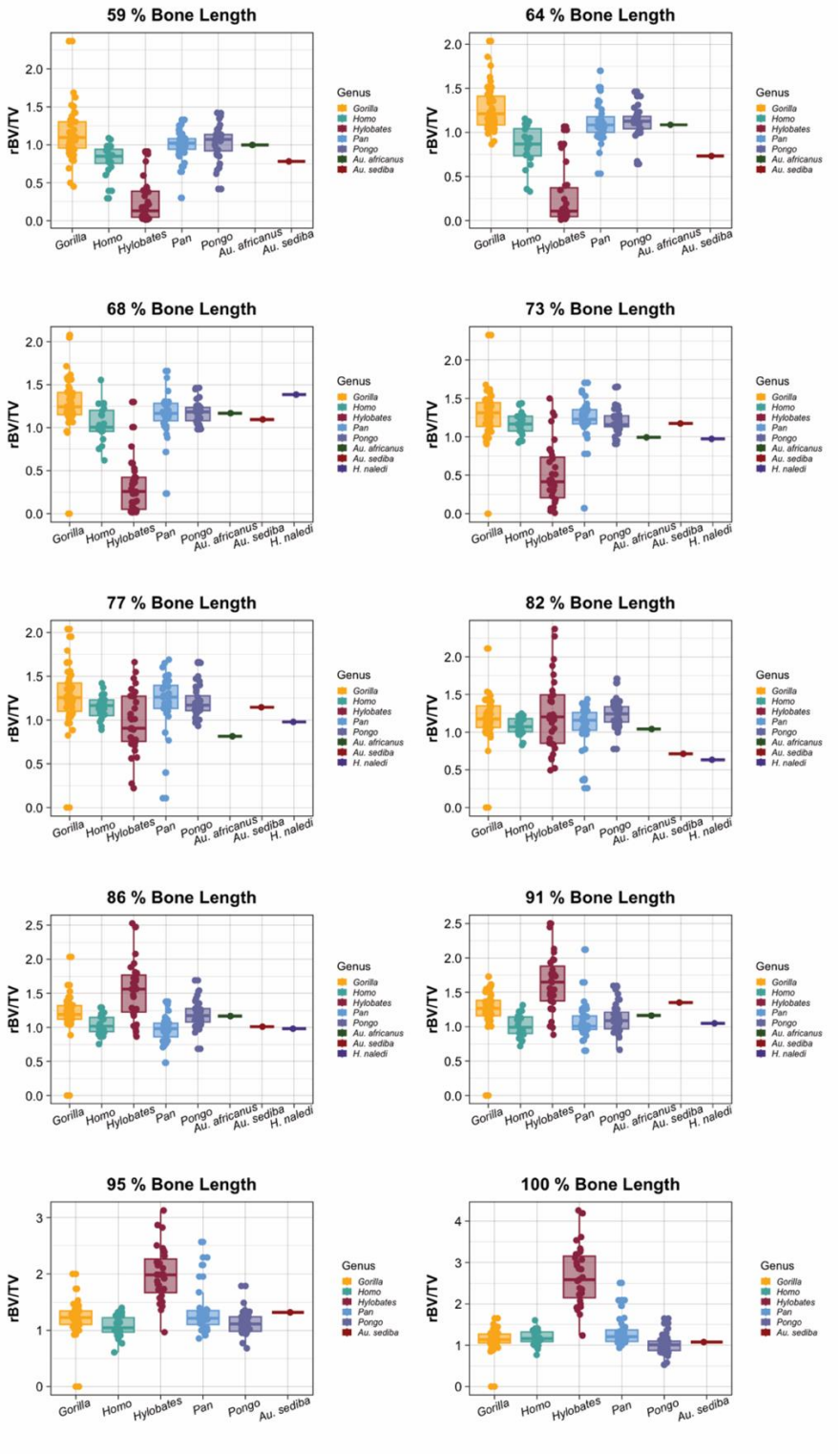

Figure 3.15. Mean rBV/TV values in the final 8 ROIs representing 59 - 100% bone length.

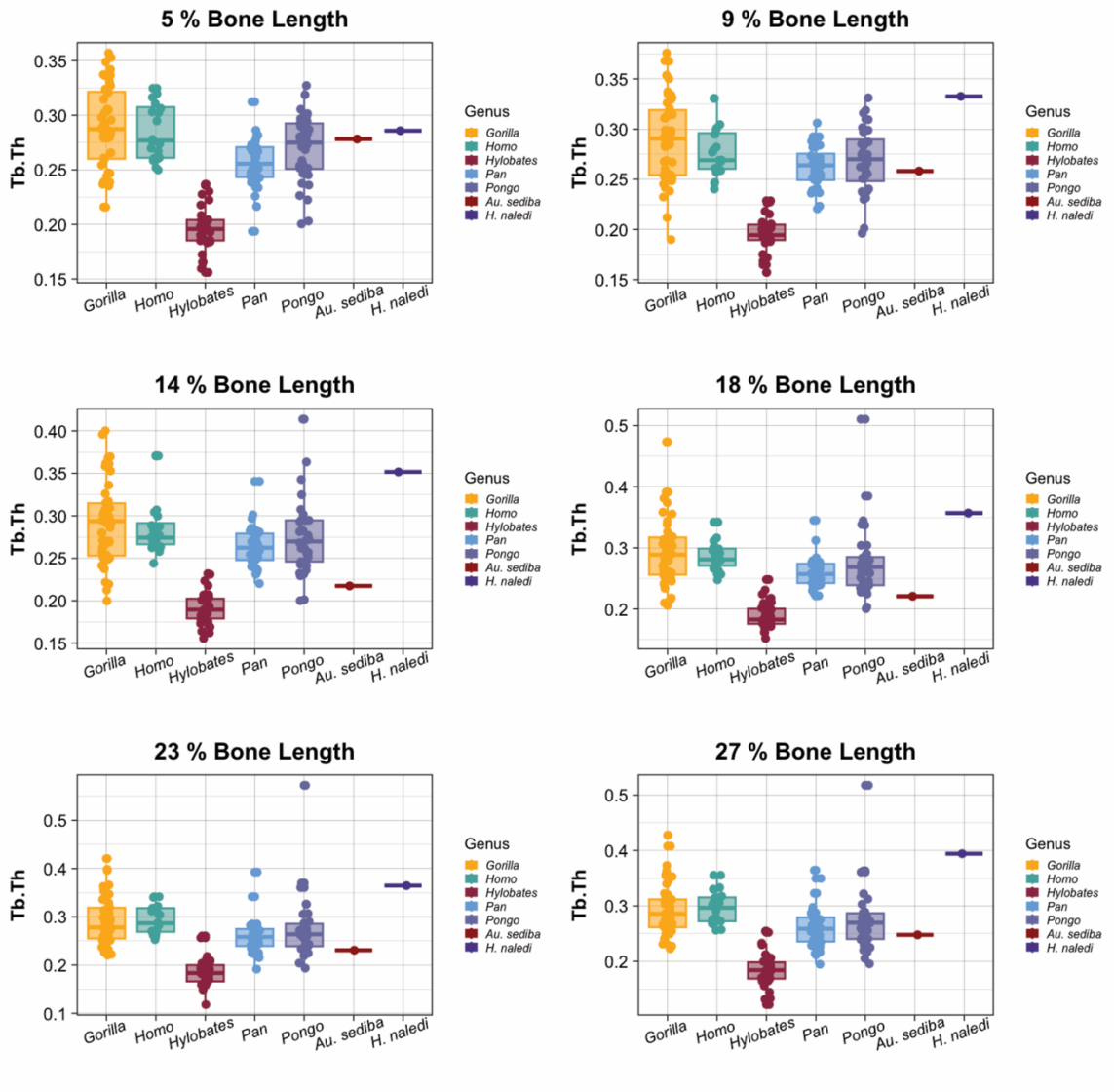

Figure 3.16. Mean Tb.Th values in the first 6 ROIs representing 0 - 27% bone length.

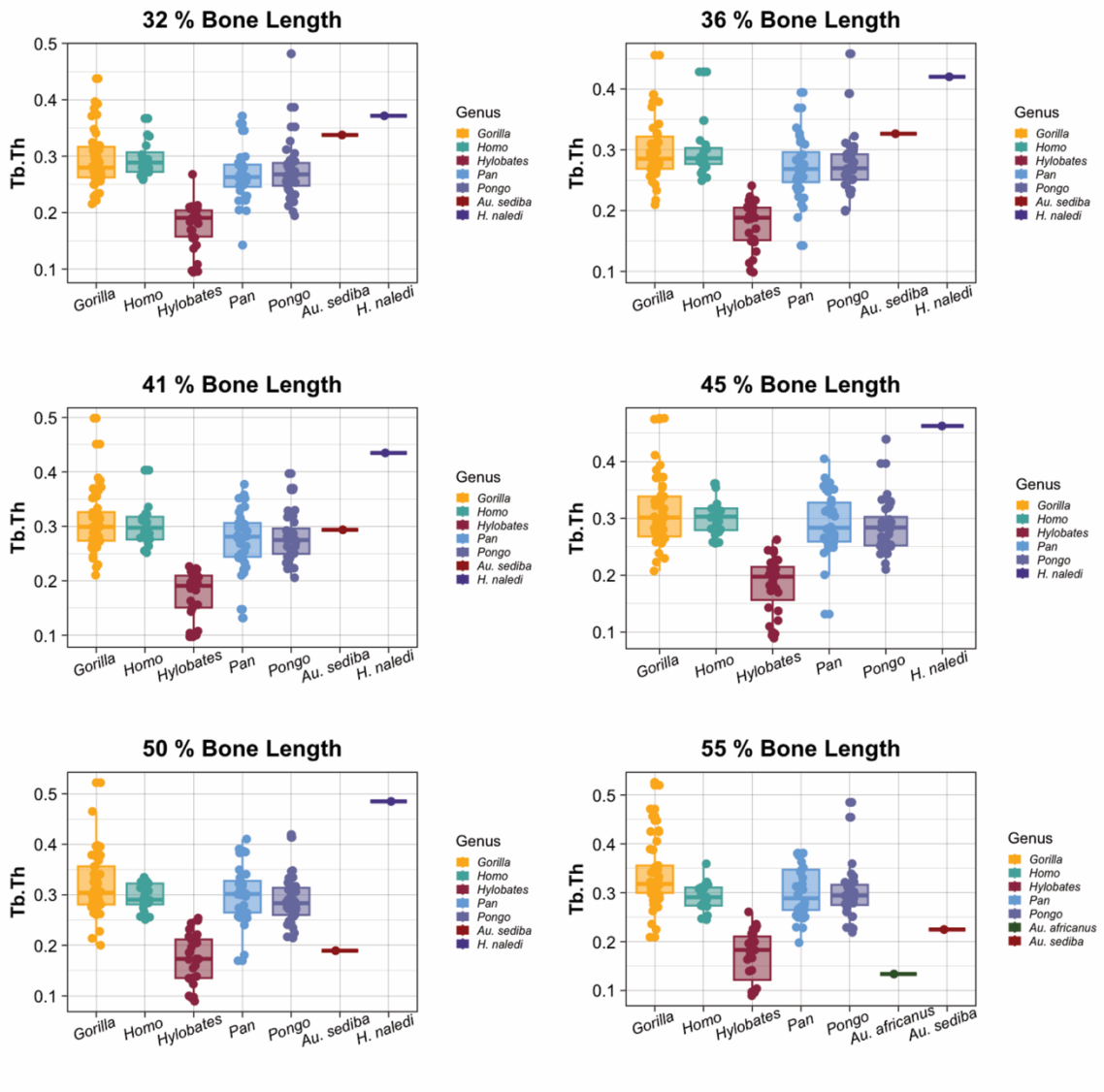

Figure 3.17. Mean Tb.Th values in the next 6 ROIs representing 32 - 55% bone length.

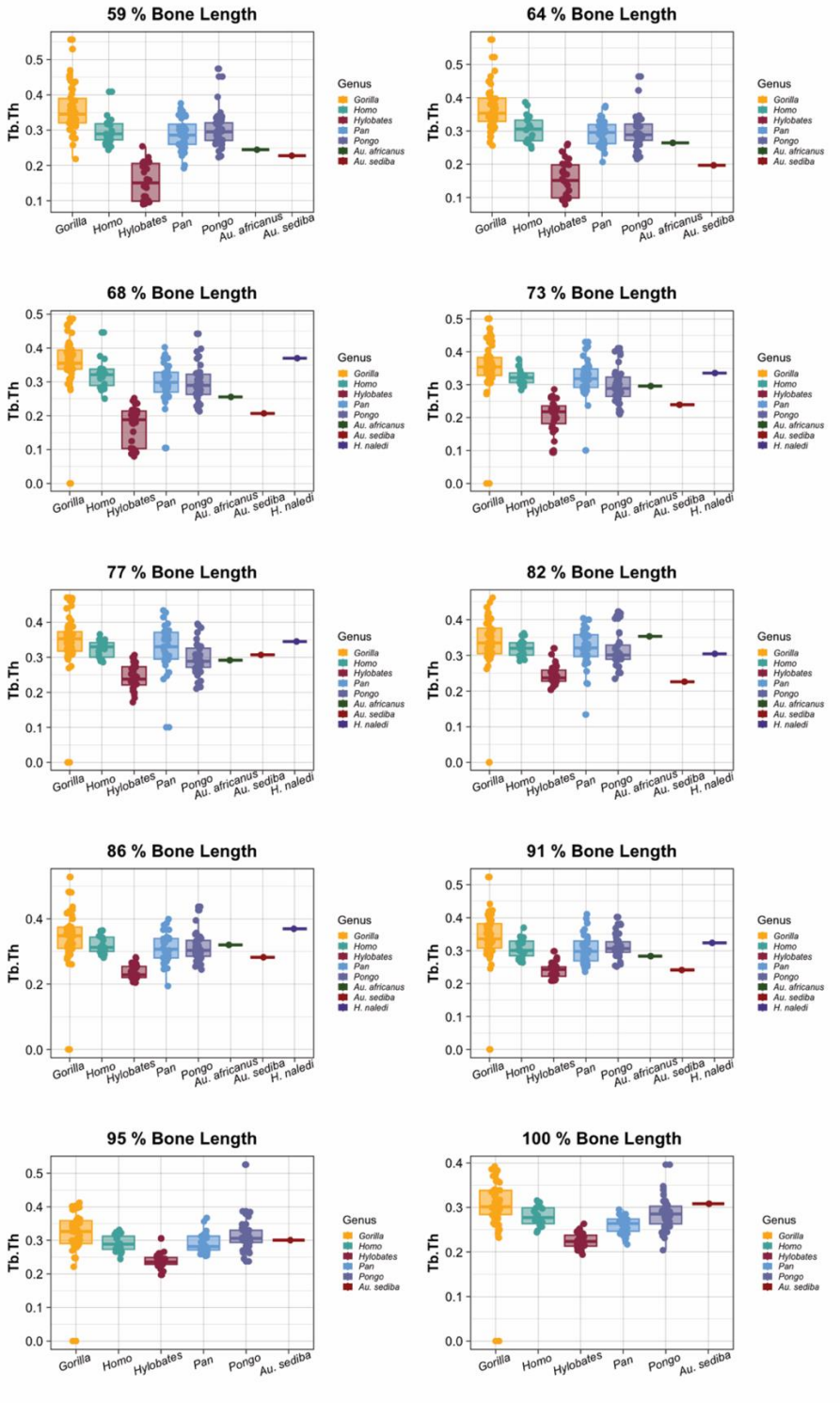

Figure 3.18. Mean Tb.Th values in the final 8 ROIs representing 59 - 100% bone length.

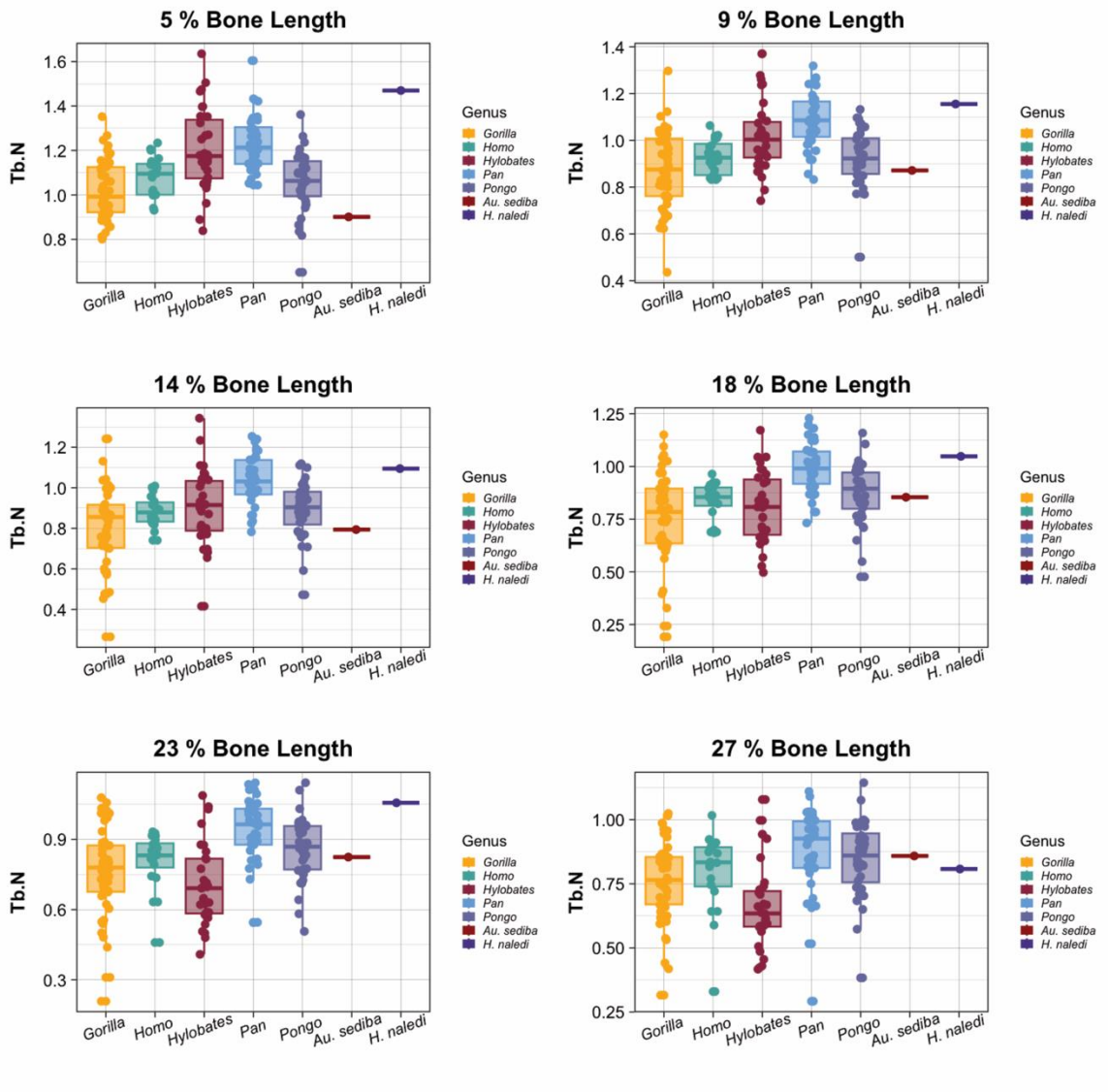

Figure 3.19. Mean Tb.N values in the first 6 ROIs representing 0 - 27% bone length.

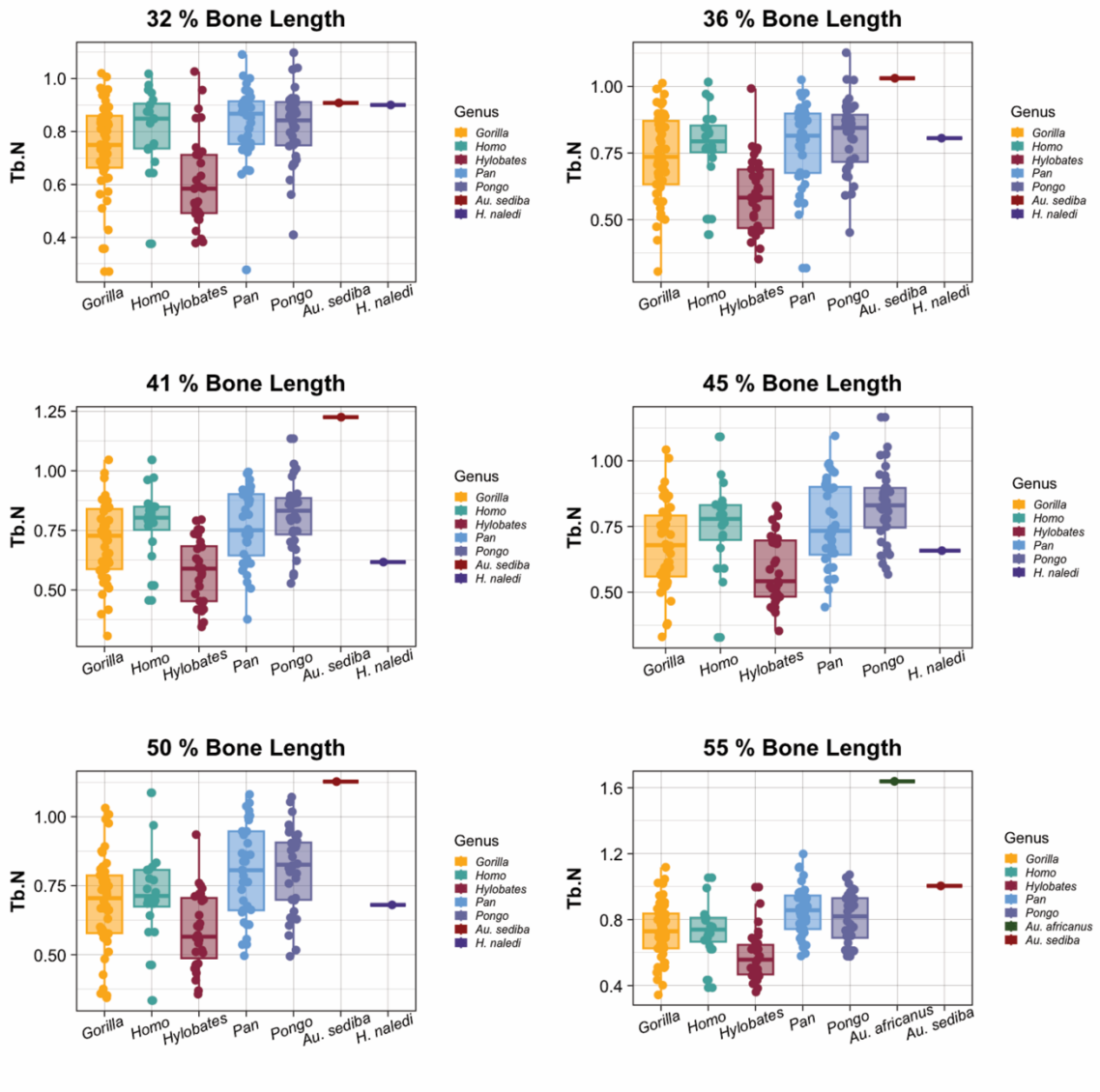

Figure 3.20. Mean Tb.N values in the next 6 ROIs representing 32 - 55% bone length.

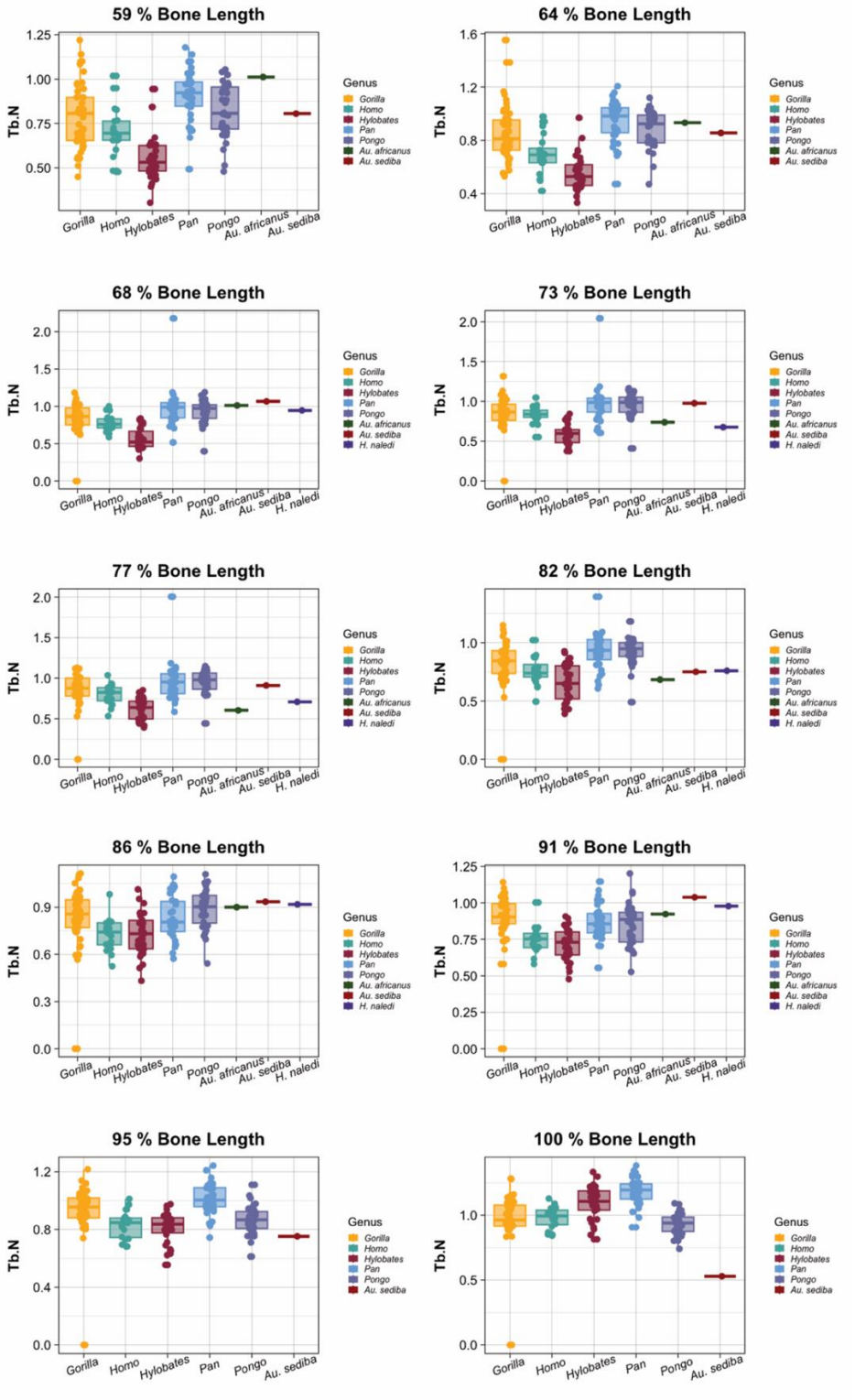

Figure 3.21. Mean Tb.N values in the final 8 ROIs representing 59 - 100% bone length.

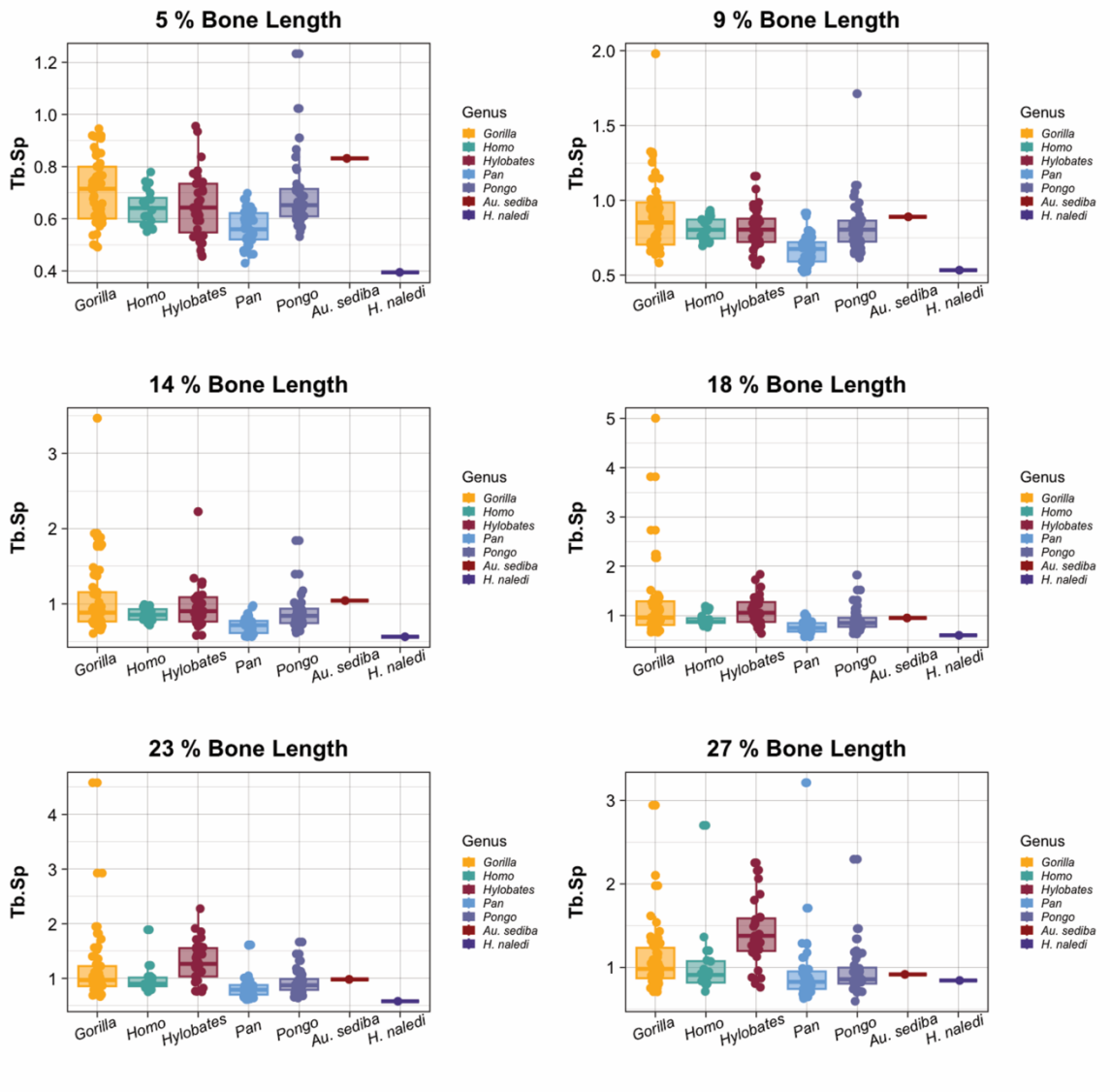

Figure 3.22. Mean Tb.Sp values in the first 6 ROIs representing 0 - 27% bone length.

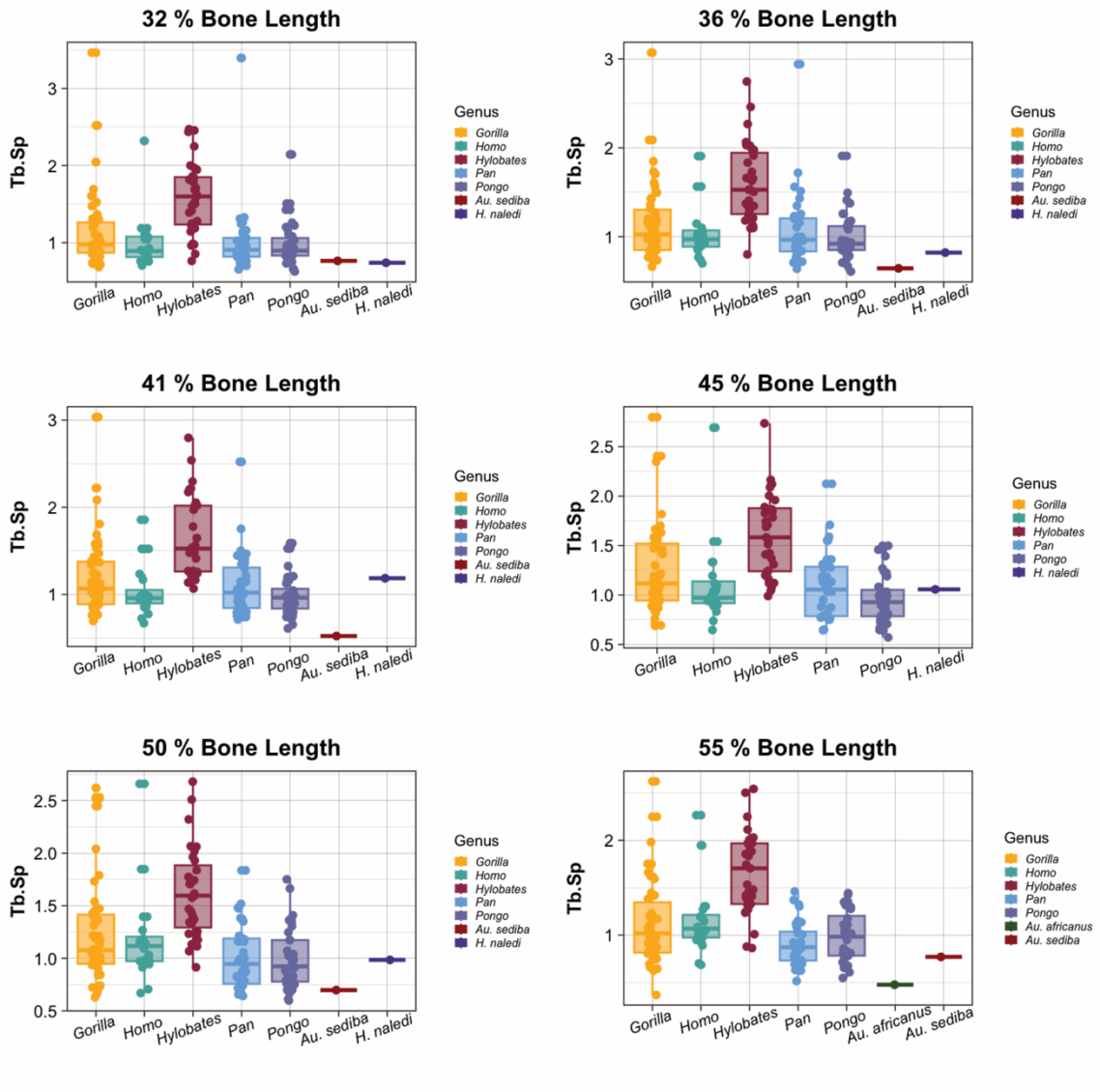

Figure 3.23. Mean Tb.Sp values in the next 6 ROIs representing 32 - 55% bone length.

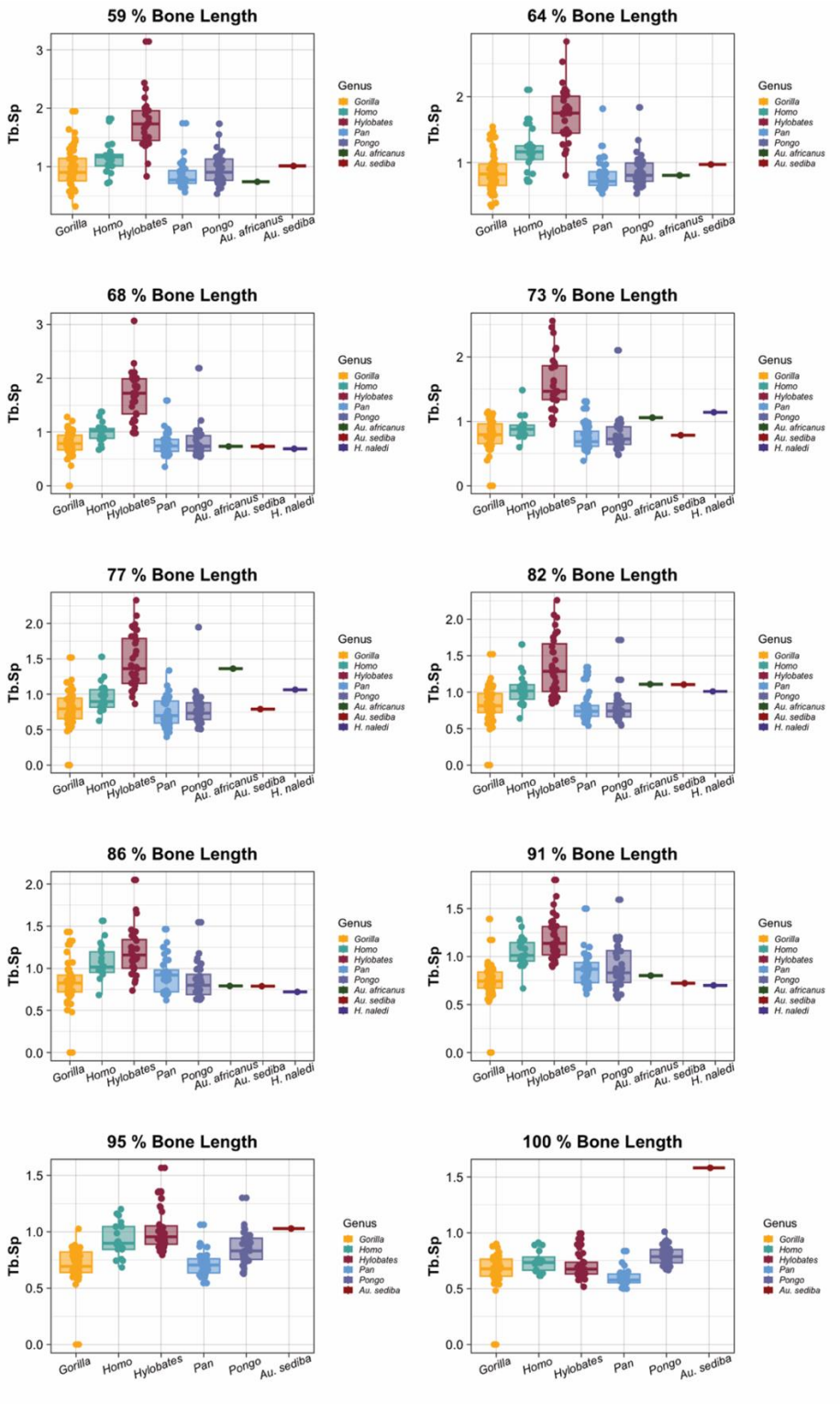

Figure 3.24. Mean Tb.Sp values in the final 8 ROIs representing 59 - 100% bone length.

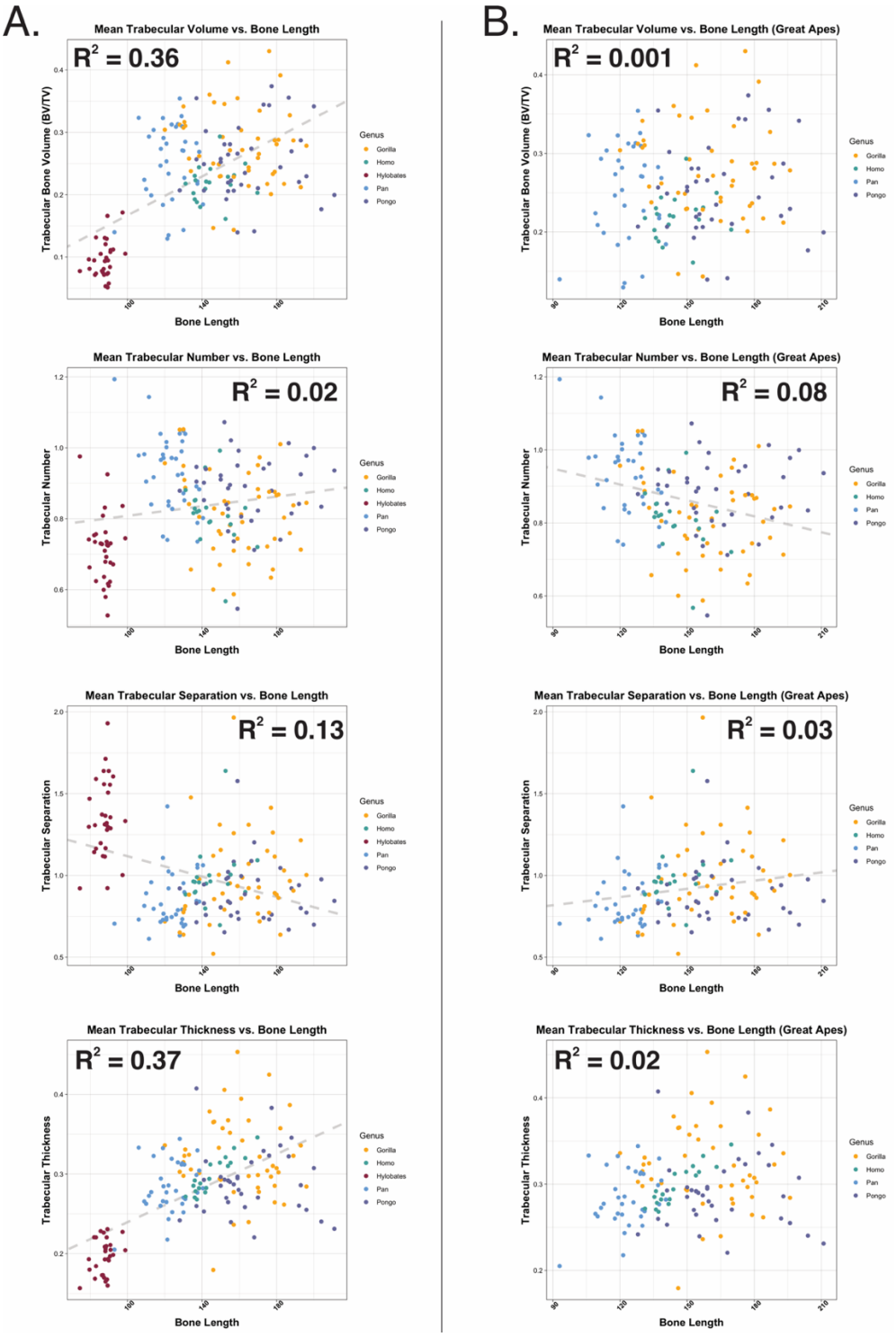

Figure 3.25. Linear regressions of mean trabecular parameters against bone length as a proxy for body mass to test for allometric relationships in the dataset. A. Analysis performed on entire dataset; B. Analysis performed on great apes.

Table 3.1. Extant adult hominoid sample.

Genus	N
Gorilla	48
Homo	20
Hylobates	31
Pan	35
Pongo	34

Table 3.2. Fossil sample.

Genus	Individual	Est. Age	Description	Reference
Au. africanus	StW 431g	Adult	Lateral half of a right clavicle missing the acromial extremity	Toussaint et al. (2003)
Au. sediba	UW 88-38, -142	Adult	Two fragments representing an entire right clavicle	Churchill et al. (2013)
H. naledi	UW 101-258	Adult	Lateral fragment containing both the medial and lateral curvatures, and conoid tubercle	Feuerriegel et al. (2016)
	UW 101-1229	Adult	Midshaft and sternal metaphysis section composed of three refitted fragments	Feuerriegel et al. (2016)

Table 3.3. Levene's test for homogeneity of variance. Significant p-values are bolded.

Levene's Test

% bone length	BV/TV	Tb.N	Tb.Th	Tb.Sp	rBV/TV
5	**0.0225600**	0.1084000	**0.0035390**	**0.0153300**	**< 0.00001**
9	0.0556900	**0.0330500**	**0.0000146**	**0.0034000**	**0.0000005**
14	**0.0121300**	**0.0133200**	**0.0002269**	**0.0058320**	**0.0000006**
18	**0.0387200**	**0.0029190**	**0.0013410**	**0.0074280**	**< 0.00001**
23	0.2433000	0.1505000	0.1765000	0.0818000	**0.0000031**
27	0.1377000	0.8503000	0.4036000	0.7600000	**0.0000295**
32	**0.0213800**	0.5591000	0.6507000	0.2255000	**0.0000023**
36	**0.0028440**	0.4627000	0.7510000	0.1507000	**0.0000025**
41	**0.0000324**	0.3507000	0.5699000	0.0862000	**0.0123200**
45	**0.0000897**	0.3490000	0.2662000	0.0606200	**0.0088820**
50	**0.0001030**	0.3195000	0.0880300	0.2568000	0.0783900
55	**0.0023550**	0.3768000	0.1055000	**0.0159500**	0.0702700
59	**0.0088810**	0.0550400	0.1718000	**0.0442900**	0.2848000
64	**0.0035300**	0.2612000	0.1439000	**0.0197000**	0.1595000
68	**0.0036480**	0.7020000	0.6107000	**0.0011160**	0.1410000
73	**0.0246900**	0.6708000	0.3770000	**0.0015430**	**0.0072050**
77	**0.0143600**	0.4481000	0.0647800	**0.0030620**	**0.0213900**
82	0.0557300	0.1959000	**0.0217400**	**0.0000696**	**0.0000786**
86	**0.0433000**	0.4951000	**0.0046930**	0.4682000	**0.0000369**
91	0.0725300	0.3848000	**0.0052430**	0.3298000	**0.0035380**
95	0.0743400	0.7413000	**0.0014880**	0.3583000	**0.0018070**
100	**0.0073930**	0.2340000	**0.0021880**	0.0786600	**< 0.00001**

Table 3.4. Shapiro Wilk's test to identify deviation from a normal distribution. Significant p-values are bolded.

Shapiro Wilk's

% bone length	BV/TV	Tb.N	Tb.Th	Tb.Sp	rBV/TV
5	**0.0012510**	0.1772000	0.0998300	**0.0000081**	**< 0.00001**
9	0.6324000	0.3064000	0.1708000	**< 0.00001**	**< 0.00001**
14	0.5550000	**0.0072980**	**0.0120000**	**< 0.00001**	**< 0.00001**
18	**0.0306800**	**0.0010050**	**0.0000141**	**< 0.00001**	**0.0000003**
23	**0.0015970**	**0.0074070**	**0.0000078**	**< 0.00001**	**0.0008698**
27	**0.0027630**	**0.0027760**	**0.0037150**	**< 0.00001**	**0.0000013**
32	**0.0028940**	**0.0001474**	**0.0051860**	**< 0.00001**	**0.0000013**
36	**0.0061340**	**0.0125000**	**0.0025840**	**< 0.00001**	**0.0000006**
41	**0.0015870**	0.3269000	**0.0172300**	**< 0.00001**	**0.0000330**
45	**0.0160100**	0.5955000	**0.0083280**	**< 0.00001**	**0.0000720**
50	**0.0122900**	0.3016000	**0.0049530**	**< 0.00001**	**0.0000100**
55	**0.0033600**	**0.0044530**	**0.0009806**	**< 0.00001**	**0.0000037**
59	**0.0003299**	**0.0459900**	**0.0006289**	**< 0.00001**	**< 0.00001**
64	**0.0006884**	**0.0262500**	**0.0004813**	**< 0.00001**	**< 0.00001**
68	**0.0000452**	**< 0.00001**	**0.0007714**	**< 0.00001**	**< 0.00001**
73	**0.0000693**	**0.0000002**	**0.0012570**	**< 0.00001**	**< 0.00001**
77	**0.0457100**	**0.0000002**	**0.0005250**	**< 0.00001**	**0.0000073**
82	0.0772200	**0.0001132**	**0.0000525**	**< 0.00001**	**0.0000002**
86	0.3609000	**0.0000207**	**0.0000368**	**0.0000059**	**< 0.00001**
91	0.2195000	**0.0000233**	**0.0000079**	**0.0000515**	**< 0.00001**
95	0.5593000	**< 0.00001**	**0.0000002**	**0.0000025**	**< 0.00001**
100	**0.0016350**	**< 0.00001**	**0.0000001**	**< 0.00001**	**< 0.00001**

Table 3.5. Test for intraspecific differences within each ROI. Because all tests were significant, a bolded p-value indicates a parametric AOV was run. All other comparisons were tested for using a non-parametric Kruskall-Wallis test.

Test for Interspecific Differences (parametric AOV, non-parametric Kruskall-Wallis)

% bone length	BV/TV	Tb.N	Tb.Th	Tb.Sp	rBV/TV
5	**< 0.00001**	**< 0.00001**	< 0.00001	0.0000012	< 0.00001
9	**< 0.00001**	< 0.00001	< 0.00001	0.0000007	< 0.00001
14	< 0.00001	0.0000005	< 0.00001	0.0000007	< 0.00001
18	< 0.00001	0.0000003	< 0.00001	0.0000003	0.0000003
23	< 0.00001	0.0000004	< 0.00001	< 0.00001	0.0000602
27	< 0.00001	0.0000032	< 0.00001	0.0000002	0.0000052
32	< 0.00001	0.0000029	< 0.00001	0.0000001	< 0.00001
36	< 0.00001	**0.0000003**	< 0.00001	0.0000001	< 0.00001
41	< 0.00001	**< 0.00001**	< 0.00001	< 0.00001	< 0.00001
45	< 0.00001	**0.0000001**	< 0.00001	< 0.00001	< 0.00001
50	< 0.00001	**0.0000001**	< 0.00001	< 0.00001	< 0.00001
55	< 0.00001	< 0.00001	< 0.00001	< 0.00001	< 0.00001
59	< 0.00001	< 0.00001	< 0.00001	< 0.00001	< 0.00001
64	< 0.00001	< 0.00001	< 0.00001	< 0.00001	< 0.00001
68	< 0.00001	< 0.00001	< 0.00001	< 0.00001	< 0.00001
73	< 0.00001	< 0.00001	< 0.00001	< 0.00001	< 0.00001
77	< 0.00001	< 0.00001	< 0.00001	< 0.00001	0.0022420
82	**< 0.00001**	< 0.00001	< 0.00001	< 0.00001	0.0122300
86	< 0.00001	0.0000122	< 0.00001	< 0.00001	< 0.00001
91	**< 0.00001**	< 0.00001	< 0.00001	< 0.00001	< 0.00001
95	**< 0.00001**	< 0.00001	< 0.00001	< 0.00001	< 0.00001
100	< 0.00001	< 0.00001	< 0.00001	< 0.00001	< 0.00001

Table 3.6. Linear regressions of mean trabecular parameters against bone length as a proxy for body mass to test for allometric relationships in the dataset. Significant p-values are bolded.

	All Apes			Great Apes		
	F-statistic	**Adjusted R^2**	***p*-value**	**F-statistic**	**Adjusted R^2**	***p*-value**
BV/TV	94.64	0.362	**< 0.0001**	1.15	0.001	0.29
Tb.Th	97.84	0.370	**< 0.0001**	3.64	0.019	0.06
Tb.N	5.15	0.025	**0.025**	12.89	0.081	**0.0005**
Tb.Sp	25.92	0.131	**< 0.0001**	4.76	0.027	**0.03**

Table 3.7. Intraspecific pairwise comparisons of relative trabecular bone volume (rBV/TV) amongst extant apes and fossil hominins. All statistical differences were tested for with a non-parametric Dunn's tests with Bonferroni correction. Significant p-values are bolded.

% Bone Length	**Intraspecific Pairwise Comparisons (non-parametric Dunn's tests with Bonferroni correction)**						
		Gorilla	***H. naledi***	***Homo***	***Hylobates***	***Pan***	***Pongo***
5%	***Au. sediba***	1	1	1	1	1	1
	Gorilla	-	1	**0.0012040**	**< 0.00001**	**0.0400131**	1
	H. naledi	-	-	1	1	1	1
	Homo	-	-	-	**0.0046175**	1	**0.0153380**
	Hylobates	-	-	-	-	**0.0000001**	**< 0.00001**
	Pan	-	-	-	-	-	0.3625375
		Gorilla	***H. naledi***	***Homo***	***Hylobates***	***Pan***	***Pongo***
9%	***Au. sediba***	1	1	1	1	1	1
	Gorilla	-	0.9861228	0.3943855	**< 0.00001**	**0.0021256**	1
	H. naledi	-	-	1	1	1	1
	Homo	-	-	-	**0.0000080**	1	0.7080335
	Hylobates	-	-	-	-	**0.0000291**	**< 0.00001**
	Pan	-	-	-	-	-	**0.0098362**
		Gorilla	***H. naledi***	***Homo***	***Hylobates***	***Pan***	***Pongo***
14%	***Au. sediba***	1	0.5468497	0.9953939	0.1215288	0.6666936	1
	Gorilla	-	0.6803273	**0.0200291**	**< 0.00001**	**0.0000720**	1
	H. naledi	-	-	-	1	1	0.9868568
	Homo	-	-	-	**0.0307091**	1	0.1837590
	Hylobates	-	-	-	-	0.0551014	**< 0.00001**
	Pan	-	-	-	-	-	**0.0043594**

Table 3.7. Continued

		Gorilla	*H. naledi*	*Homo*	*Hylobates*	*Pan*	*Pongo*
18%	***Au. sediba***	1	1	1	1	1	1
	Gorilla	-	0.6672037	**0.0009245**	**0.0000104**	**0.0001184**	1
	H. naledi	-	-	1	1	1	1
	Homo	-	-	-	1	1	0.0612398
	Hylobates	-	-	-	-	1	**0.0050202**
	Pan	-	-	-	-	-	**0.0331741**
		Gorilla	***H. naledi***	***Homo***	***Hylobates***	***Pan***	***Pongo***
23%	***Au. sediba***	1	1	0.7899770	1	1	1
	Gorilla	-	1	**0.0000205**	1	**0.0240487**	1
	H. naledi	-	-	1	1	1	1
	Homo	-	-	-	**0.0022818**	0.3426200	**0.0054146**
	Hylobates	-	-	-	-	0.6075773	1
	Pan	-	-	-	-	-	1
		Gorilla	***H. naledi***	***Homo***	***Hylobates***	***Pan***	***Pongo***
27%	***Au. sediba***	1	1	1	1	1	1
	Gorilla	-	1	**0.0000031**	1	0.9795356	0.5334380
	H. naledi	-	-	1	1	1	1
	Homo	-	-	-	**0.0000021**	**0.0035374**	**0.0080124**
	Hylobates	-	-	-	-	0.4712674	0.2531662
	Pan	-	-	-	-	-	1
		Gorilla	***H. naledi***	***Homo***	***Hylobates***	***Pan***	***Pongo***
32%	***Au. sediba***	0.8082813	1	1	0.1952033	0.9586684	1
	Gorilla	-	1	**0.0000042**	0.0984773	1	0.4697911
	H. naledi	-	-	1	1	1	1

Table 3.7. Continued

	Homo	-	-	-	***< 0.00001***	***0.0000453***	***0.0114670***
	Hylobates	-	-	-	-	0.0583279	**0.0001905**
	Pan	-	-	-	-	-	1
		Gorilla	***H. naledi***	***Homo***	***Hylobates***	***Pan***	***Pongo***
	Au. sediba	0.9098660	1	1	0.1746659	0.6263071	1
	Gorilla	-	1	**0.0019933**	**0.0267723**	1	0.2529334
36%	***H. naledi***	-	-	1	0.5792781	1	1
	Homo	-	-	-	**< 0.00001**	**0.0002555**	0.7805543
	Hylobates	-	-	-	-	0.3422010	**0.0000096**
	Pan	-	-	-	-	-	**0.0413931**
		Gorilla	***H. naledi***	***Homo***	***Hylobates***	***Pan***	***Pongo***
	Au. sediba	1	1	1	0.0723978	0.6962256	1
	Gorilla	-	1	**0.0128937**	**0.0000498**	1	0.0741542
41%	***H. naledi***	-	-	1	1	1	1
	Homo	-	-	-	**< 0.00001**	**0.0018619**	1
	Hylobates	-	-	-	-	**0.0032710**	**< 0.00001**
	Pan	-	-	-	-	-	**0.0099202**
		H. naledi	***Homo***	***Hylobates***	***Pan***	***Pongo***	
	Gorilla	1	0.1561204	**0.0002255**	1	**0.0205115**	
	H. naledi	-	1	1	1	1	
45%	***Homo***	-	-	**0.0000002**	0.2112985	1	
	Hylobates	-	-	-	**0.0005041**	**< 0.00001**	
	Pan	-	-	-	-	**0.0384349**	
		Gorilla	***H. naledi***	***Homo***	***Hylobates***	***Pan***	***Pongo***
50%	***Au. sediba***	1	1	1	1	1	0.9564416
	Gorilla	-	1	1	**0.0000024**	1	0.3144784

Table 3.7. Continued

	H. naledi	-	-	*1*	*1*	*1*	*1*
	Homo	-	-	-	**0.0000251**	1	1
	Hylobates	-	-	-	-	**0.0000003**	**< 0.00001**
	Pan	-	-	-	-	-	1
55%		***Au. sediba***	***Gorilla***	***Homo***	***Hylobates***	***Pan***	***Pongo***
	Au. africanus	1	1	1	1	1	1
	Au. sediba	-	1	1	0.1989383	1	1
	Gorilla	-	-	0.2804827	**< 0.00001**	1	1
	Homo	-	-	-	**0.0169168**	0.3976488	0.1338704
	Hylobates	-	-	-	-	**< 0.00001**	**< 0.00001**
	Pan	-	-	-	-	-	1
59%		***Au. sediba***	***Gorilla***	***Homo***	***Hylobates***	***Pan***	***Pongo***
	Au. africanus	1	1	1	1	1	1
	Au. sediba	-	1	1	1	1	1
	Gorilla	-		**0.0005418**	**< 0.00001**	1	1
	Homo	-	-	-	**0.0400561**	0.0953513	**0.0132448**
	Hylobates	-	-	-	-	**< 0.00001**	**< 0.00001**
	Pan	-	-	-	-	-	1
64%		***Au. sediba***	***Gorilla***	***Homo***	***Hylobates***	***Pan***	***Pongo***
	Au. africanus	1	1	1	1	1	1
	Au. sediba	-	0.8182355	1	1	1	1
	Gorilla	-	-	**0.0000032**	**< 0.00001**	0.1663177	0.6020390
	Homo	-	-	-	0.1553529	**0.0292508**	**0.0071055**
	Hylobates	-	-	-	-	**< 0.00001**	**< 0.00001**

Table 3.7. Continued

	Pan	-	-	-	-	-	*1*	
68%		***Au. sediba***	***Gorilla***	***H. naledi***	***Homo***	***Hylobates***	***Pan***	***Pongo***
	Au. africanus	1	1	1	1	1	1	1
	Au. sediba	-	1	1	1	1	1	1
	Gorilla	-	-	1	**0.0131964**	**< 0.00001**	0.6519572	1
	H. naledi	-	-	-	1	0.1487214	1	1
	Homo	-	-	-	-	**0.0040605**	1	0.90405491
	Hylobates	-	-	-	-	-	**< 0.00001**	**< 0.00001**
	Pan	-	-	-	-	-	-	1
73%		***Au. sediba***	***Gorilla***	***H. naledi***	***Homo***	***Hylobates***	***Pan***	***Pongo***
	Au. africanus	1	1	1	1	1	1	1
	Au. sediba	-	1	1	1	1	1	1
	Gorilla	-	-	1	0.9430339	**< 0.00001**	1	1
	H. naledi	-	-	-	1	1	1	1
	Homo	-	-	-	-	**0.0014472**	1	1
	Hylobates	-	-	-	-	-	**< 0.00001**	**0.0000117**
	Pan	-	-	-	-	-	-	1
77%		***Au. sediba***	***Gorilla***	***H. naledi***	***Homo***	***Hylobates***	***Pan***	***Pongo***
	Au. africanus	1	1	1	1	1	1	1
	Au. sediba	-	1	1	1	1	1	1
	Gorilla	-	-	1	0.8167113	**0.0011383**	1	1
	H. naledi	-	-	-	1	1	1	1
	Homo	-	-	-	-	1	1	1
	Hylobates	-	-	-	-	-	**0.0057205**	0.19090302

Table 3.7. Continued

	Pan	-	-	-	-	-	-	*1*
82%		***Au. sediba***	***Gorilla***	***H. naledi***	***Homo***	***Hylobates***	***Pan***	***Pongo***
	Au. africanus	1	1	1	1	1	1	1
	Au. sediba	-	1	1	1	1	1	0.85492589
	Gorilla	-	-	1	0.3496384	1	1	1
	H. naledi	-	-	-	1	1	1	0.71271806
	Homo	-	-	-	-	0.5474823	1	**0.02170269**
	Hylobates	-	-	-	-	-	1	1
	Pan	-	-	-	-	-	-	0.17897233
86%		***Au. sediba***	***Gorilla***	***H. naledi***	***Homo***	***Hylobates***	***Pan***	***Pongo***
	Au. africanus	1	1	1	1	1	1	1
	Au. sediba	-	1	1	1	1	1	1
	Gorilla	-	-	1	**0.0137760**	0.1659058	**0.0000025**	1
	H. naledi	-	-	-	1	0.8470724	1	1
	Homo	-	-	-	-	**0.0000044**	1	0.12695805
	Hylobates	-	-	-	-	-	**< 0.00001**	**0.03556752**
	Pan	-	-	-	-	-	-	**0.00027141**
91%		***Au. sediba***	***Gorilla***	***H. naledi***	***Homo***	***Hylobates***	***Pan***	***Pongo***
	Au. africanus	1	1	1	1	1	1	1
	Au. sediba	-	1	1	1	1	1	1
	Gorilla	-	-	1	**0.0003425**	0.1328525	**0.0002031**	**0.01386699**
	H. naledi	-	-	-	1	1	1	1
	Homo	-	-	-	-	**< 0.00001**	1	1
	Hylobates	-	-	-	-	-	**< 0.00001**	**0.0000007**

Table 3.7. Continued

	Pan	-	-	-	-	-	*1*
95%		***Gorilla***	***Homo***	***Hylobates***	***Pan***	***Pongo***	
	Au. sediba	1	1	1	1	1	
	Gorilla	-	0.1010711	**0.0000001**	1	0.3317312	
	Homo	-	-	**< 0.00001**	0.0915515	1	
	Hylobates	-	-	-	**0.0000014**	**< 0.00001**	
	Pan	-	-	-	-	0.2977782	
100%		***Gorilla***	***Homo***	***Hylobates***	***Pan***	***Pongo***	
	Au. sediba	1	1	0.3477791	1	1	
	Gorilla	-	1	**< 0.00001**	0.7490535	0.0741210	
	Homo	-	-	**0.0000011**	1	0.0968162	
	Hylobates	-	-	-	**0.0000019**	**< 0.00001**	
	Pan	-	-	-	-	**0.0004974**	

Table 3.8. Intraspecific pairwise comparisons of relative trabecular number (Tb.N) amongst extant apes and fossil hominins. The 5%, 36%, 41%, 45%, and 50% bone length ROIs were investigated using a parametric Tukey's HSD test. In all other regions statistical differences were tested for with a non-parametric Dunn's tests with Bonferroni correction. Significant p-values are bolded.

% Bone Length	**Intraspecific Pairwise Comparisons (non-parametric Dunn's tests with Bonferroni correction, parametric Tukey's HSD test)**						
		Gorilla	***H. naledi***	***Homo***	***Hylobates***	***Pan***	***Pongo***
	Au. sediba	1	0.3257996	1	0.6510895	0.3362961	1
	Gorilla	-	0.2837641	1	**0.0000344**	**< 0.00001**	1
5%	***H. naledi***	-	-	0.7681713	1	1	0.5835054
	Homo	-	-	-	0.1825776	**0.0060834**	1
	Hylobates	-	-	-	-	1	**0.0138749**
	Pan	-	-	-	-	-	**0.0000662**
		Gorilla	***H. naledi***	***Homo***	***Hylobates***	***Pan***	***Pongo***
	Au. sediba	1	1	1	1	1	1
	Gorilla	-	0.6378120	1	**0.0069503**	**< 0.00001**	1
9%	***H. naledi***	-	-	1	1	1	1
	Homo	-	-	-	0.3716206	**0.0002560**	1
	Hylobates	-	-	-	-	0.2018350	0.4067916
	Pan	-	-	-	-	-	**0.0000483**
		Gorilla	***H. naledi***	***Homo***	***Hylobates***	***Pan***	***Pongo***
	Au. sediba	1	1	1	1	0.9586684	1
	Gorilla	-	0.7258516	1	0.2939298	**< 0.00001**	0.4944621
14%	***H. naledi***	-	-	1	1	1	1
	Homo	-	-	-	1	**0.0013982**	1
	Hylobates	-	-	-	-	**0.0090299**	1
	Pan	-	-	-	-	-	**0.0018101**
18%		***Gorilla***	***H. naledi***	***Homo***	***Hylobates***	***Pan***	***Pongo***

Table 3.8. Continued

Au. sediba	*1*	*1*	*1*	*1*	*1*	*1*
Gorilla	-	0.7335596	1	1	**0.0000001**	0.1487830
H. naledi	-	-	1	1	1	1
Homo	-	-	-	1	**0.0028642**	1
Hylobates	-	-	-	-	**0.0000299**	1
Pan	-	-	-	-	-	**0.0159628**

23%

Gorilla	***H. naledi***	***Homo***	***Hylobates***	***Pan***	***Pongo***
Au. sediba	1	1	1	1	1	1
Gorilla	-	0.8067587	1	1	**0.0000432**	0.2844491
H. naledi	-	-	1	0.3643343	1	1
Homo	-	-	-	0.4118707	**0.0480989**	1
Hylobates	-	-	-	-	**0.0000002**	**0.0055684**
Pan	-	-	-	-	-	0.2491815

27%

Gorilla	***H. naledi***	***Homo***	***Hylobates***	***Pan***	***Pongo***
Au. sediba	1	1	1	1	1	1
Gorilla	-	1	1	0.1454453	**0.0063059**	0.2068519
H. naledi	-	-	1	1	1	1
Homo	-	-	-	**0.0405368**	0.7265923	1
Hylobates	-	-	-	-	**0.0000005**	**0.0000894**
Pan	-	-	-	-	-	1

32%

Gorilla	***H. naledi***	***Homo***	***Hylobates***	***Pan***	***Pongo***
Au. sediba	1	1	1	0.7447231	1	1
Gorilla	-	1	1	**0.0136765**	0.2144182	0.6065786
H. naledi	-	-	1	0.9230167	1	1
Homo	-	-	-	**0.0009494**	1	1
Hylobates	-	-	-	-	**0.0000027**	**0.0000191**

Table 3.8. Continued

	Pan	-	-	-	-	-	*1*
36%		***Gorilla***	***H. naledi***	***Homo***	***Hylobates***	***Pan***	***Pongo***
	Au. sediba	0.8494911	1	1	0.1160955	1	1
	Gorilla	-	1	1	**0.0045852**	1	0.3736029
	H. naledi	-	-	1	1	1	1
	Homo	-	-	-	**0.0018516**	1	1
	Hylobates	-	-	-	-	**0.0000185**	**0.0000016**
	Pan	-	-	-	-	-	1
41%		***Gorilla***	***H. naledi***	***Homo***	***Hylobates***	***Pan***	***Pongo***
	Au. sediba	0.6717730	0.8549118	1	0.1133565	1	1
	Gorilla	-	1	0.9428405	**0.0211263**	0.7878659	**0.0264710**
	H. naledi	-	-	1	1	1	1
	Homo	-	-	-	**0.0004596**	1	1
	Hylobates	-	-	-	-	**0.0000575**	**0.0000001**
	Pan	-	-	-	-	-	1
45%		***H. naledi***	***Homo***	***Hylobates***	***Pan***	***Pongo***	
	Gorilla	0.9999943	0.4123792	0.1086820	0.1975636	**0.0003576**	
	H. naledi	-	0.9891118	0.9974323	0.9879775	0.8873312	
	Homo	-	-	**0.0022773**	1	0.5694331	
	Hylobates	-	-	-	**0.0001567**	**< 0.00001**	
	Pan	-	-	-	-	0.3953011	
50%		***Gorilla***	***H. naledi***	***Homo***	***Hylobates***	***Pan***	***Pongo***
	Au. sediba	0.0968734	0.4273252	0.1663503	**0.0175005**	0.4012417	0.4383683
	Gorilla	-	1	0.9891854	0.0982806	**0.0293525**	**0.0128092**
	H. naledi	-	-	0.9999829	0.9973818	0.9896151	0.9845147
	Homo	-	-	-	0.0616604	0.5421476	0.4026483

Table 3.8. Continued

	Hylobates	-	-	-	-	***0.0000035***	***0.0000011***
	Pan	-	-	-	-	-	0.9999777
55%		***Au. sediba***	***Gorilla***	***Homo***	***Hylobates***	***Pan***	***Pongo***
	Au. africanus	1	0.7812303	0.8122855	0.0982794	1	1
	Au. sediba	-	1	1	0.2134158	1	1
	Gorilla	-	-	1	**0.0033280**	**0.0373196**	0.8047706
	Homo	-	-	-	**0.0397817**	0.1976225	1
	Hylobates	-	-	-	-	**< 0.00001**	**0.0000053**
	Pan	-	-	-	-	-	1
59%		***Au. sediba***	***Gorilla***	***Homo***	***Hylobates***	***Pan***	***Pongo***
	Au. africanus	1	1	0.9791376	0.1394567	1	1
	Au. sediba	-	1	1	1	1	1
	Gorilla	-	-	1	**0.0000019**	**0.0251417**	1
	Homo	-	-	-	0.0580127	**0.0009301**	0.2249883
	Hylobates	-	-	-	-	**< 0.00001**	**< 0.00001**
	Pan	-	-	-	-	-	0.5809606
64%		***Au. sediba***	***Gorilla***	***Homo***	***Hylobates***	***Pan***	***Pongo***
	Au. africanus	1	1	1	0.9043817	1	1
	Au. sediba	-	1	1	1	1	1
	Gorilla	-	-	**0.0406208**	**0.0000001**	0.1336407	1
	Homo	-	-	-	0.5703936	**0.0000201**	**0.0046221**
	Hylobates	-	-	-	-	**< 0.00001**	**< 0.00001**
	Pan	-	-	-	-	-	1
68%		***Au. sediba***	***Gorilla***	***H. naledi***	***Homo***	***Hylobates***	***Pan***	***Pongo***

Table 3.8. Continued

	Au. africanus	*1*	*1*	*1*	*1*	*0.3667277*	*1*	*1*
	Au. sediba	-	1	1	0.9324015	0.1309485	1	1
	Gorilla	-	-	1	0.8821913	**0.0000008**	0.2302046	0.39593315
	H. naledi	-	-	-	1	1	1	1
	Homo	-	-	-	-	0.1118294	**0.0030235**	**0.00569683**
	Hylobates	-	-	-	-	-	**< 0.00001**	**< 0.00001**
	Pan	-	-	-	-	-	-	1
73%		***Au. sediba***	***Gorilla***	***H. naledi***	***Homo***	***Hylobates***	***Pan***	***Pongo***
	Au. africanus	1	1	1	1	1	1	1
	Au. sediba	-	1	1	1	0.7232419	1	1
	Gorilla	-	-	1	1	**0.0000007**	0.3135200	0.08032509
	H. naledi	-	-	-	1	1	1	1
	Homo	-	-	-	-	**0.0026583**	0.1592078	0.05010134
	Hylobates	-	-	-	-	-	**< 0.00001**	**< 0.00001**
	Pan	-	-	-	-	-	-	1
77%		***Au. sediba***	***Gorilla***	***H. naledi***	***Homo***	***Hylobates***	***Pan***	***Pongo***
	Au. africanus	1	1	1	1	1	0.9275578	0.77620835
	Au. sediba	-	1	1	1	1	1	1
	Gorilla	-	-	1	1	**0.0000011**	0.6587072	0.26686399
	H. naledi	-	-	-	1	1	1	1
	Homo	-	-	-	-	0.0520512	**0.0289887**	**0.01067967**
	Hylobates	-	-	-	-	-	**< 0.00001**	**< 0.00001**
	Pan	-	-	-	-	-	-	1
82%		***Au. sediba***	***Gorilla***	***H. naledi***	***Homo***	***Hylobates***	***Pan***	***Pongo***

Table 3.8. Continued

	Au. africanus	*1*	*1*	*1*	*1*	*1*	*1*	*1*
	Au. sediba	-	1	1	1	1	1	1
	Gorilla	-	-	1	0.3769279	**0.0006189**	0.2643010	0.07690622
	H. naledi	-	-	-	1	1	1	1
	Homo	-	-	-	-	1	**0.0008928**	**0.00019908**
	Hylobates	-	-	-	-	-	**< 0.00001**	**< 0.00001**
	Pan	-	-	-	-	-	-	1
86%		***Au. sediba***	***Gorilla***	***H. naledi***	***Homo***	***Hylobates***	***Pan***	***Pongo***
	Au. africanus	1	1	1	1	1	1	1
	Au. sediba	-	1	1	1	1	1	1
	Gorilla	-	-	1	**0.0109146**	**0.0038543**	1	1
	H. naledi	-	-	-	1	1	1	1
	Homo	-	-	-	-	1	0.0985228	**0.00033122**
	Hylobates	-	-	-	-	-	0.0622898	**0.0000626**
	Pan	-	-	-	-	-	-	0.97792646
91%		***Au. sediba***	***Gorilla***	***H. naledi***	***Homo***	***Hylobates***	***Pan***	***Pongo***
	Au. africanus	1	1	1	1	1	1	1
	Au. sediba	-	1	1	0.5015171	0.3212553	1	1
	Gorilla	-	-	1	**0.0001102**	**0.0000001**	1	1
	H. naledi	-	-	-	0.9951194	0.6712624	1	1
	Homo	-	-	-	-	1	**0.0098013**	**0.04121938**
	Hylobates	-	-	-	-	-	**0.0000904**	**0.00075719**
	Pan	-	-	-	-	-	-	1
95%		***Gorilla***	***Homo***	***Hylobates***	***Pan***	***Pongo***		

Table 3.8. Continued

	Au. sediba	*0.6290902*	*1*	*1*	*0.2304871*	*1*
	Gorilla	-	**0.0011343**	**0.0000131**	0.3486519	**0.0061085**
	Homo	-	-	1	**0.0000013**	1
	Hylobates	-	-	-	**< 0.00001**	1
	Pan	-	-	-	-	**0.0000035**
100%		***Gorilla***	***Homo***	***Hylobates***	***Pan***	***Pongo***
	Au. sediba	1	1	0.2584998	0.0551370	1
	Gorilla	-	1	**0.0115556**	**< 0.00001**	0.1886962
	Homo	-	-	**0.0243914**	**0.0000030**	1
	Hylobates	-	-	-	0.1515647	**0.0000036**
	Pan	-	-	-	-	**< 0.00001**

Table 3.9. Intraspecific pairwise comparisons of relative trabecular thickness (Tb.Th) amongst extant apes and fossil hominins. All statistical differences were tested for with a non-parametric Dunn's tests with Bonferroni correction. Significant p-values are bolded.

% Bone Length	**Intraspecific Pairwise Comparisons (non-parametric Dunn's tests with Bonferroni correction)**						
		Gorilla	***H. naledi***	***Homo***	***Hylobates***	***Pan***	***Pongo***
	Au. sediba	1	1	1	0.7899907	1	1
	Gorilla	-	1	1	**< 0.00001**	**0.0024082**	0.7449794
5%	***H. naledi***	-	-	1	0.3778311	1	1
	Homo	-	-	-	**< 0.00001**	0.0537057	1
	Hylobates	-	-	-	-	**0.0000209**	**< 0.00001**
	Pan	-	-	-	-	-	0.7996174
		Gorilla	***H. naledi***	***Homo***	***Hylobates***	***Pan***	***Pongo***
	Au. sediba	1	1	1	1	1	1
	Gorilla	-	1	1	**< 0.00001**	0.0525187	0.5505727
9%	***H. naledi***	-	-	-	**0.0409772**	1	1
	Homo	-	-	-	**< 0.00001**	1	1
	Hylobates	-	-	-	-	**0.0000003**	**< 0.00001**
	Pan	-	-	-	-	-	1
		Gorilla	***H. naledi***	***Homo***	***Hylobates***	***Pan***	***Pongo***
	Au. sediba	1	0.7317473	1	1	1	1
	Gorilla	-	1	1	**< 0.00001**	0.1543127	1
14%	***H. naledi***	-	-	1	0.0518740	1	1
	Homo	-	-	-	**< 0.00001**	0.6923493	1
	Hylobates	-	-	-	-	**0.0000002**	**< 0.00001**
	Pan	-	-	-	-	-	1
18%		**Gorilla**	**H. naledi**	**Homo**	**Hylobates**	**Pan**	**Pongo**

Table 3.9. Continued

Au. sediba	*1*	*0.7089526*	*1*	*1*	*1*	*1*
Gorilla	-	1	1	**< 0.00001**	0.0543706	0.7803632
H. naledi	-	-	1	**0.0421614**	1	1
Homo	-	-	-	**< 0.00001**	0.1091769	0.8312291
Hylobates	-	-	-	-	**0.0000011**	**< 0.00001**
Pan	-	-	-	-	-	1

23%

	Gorilla	***H. naledi***	***Homo***	***Hylobates***	***Pan***	***Pongo***
Au. sediba	1	0.9651238	1	1	1	1
Gorilla	-	1	1	**< 0.00001**	0.0917041	0.9122939
H. naledi	-	-	1	**0.0438183**	1	1
Homo	-	-	-	**< 0.00001**	**0.0449833**	0.3481609
Hylobates	-	-	-	-	**0.0000025**	**< 0.00001**
Pan	-	-	-	-	-	1

27%

	Gorilla	***H. naledi***	***Homo***	***Hylobates***	***Pan***	***Pongo***
Au. sediba	1	1	1	1	1	1
Gorilla	-	1	1	**< 0.00001**	0.0715853	0.5807865
H. naledi	-	-	1	**0.0339881**	0.9246177	1
Homo	-	-	-	**< 0.00001**	**0.0359522**	0.2269087
Hylobates	-	-	-	-	**0.0000027**	**< 0.00001**
Pan	-	-	-	-	-	1

32%

	Gorilla	***H. naledi***	***Homo***	***Hylobates***	***Pan***	***Pongo***
Au. sediba	1	1	1	0.0901510	1	1
Gorilla	-	1	1	**< 0.00001**	0.2564896	1
H. naledi	-	-	1	**0.0435528**	1	1
Homo	-	-	-	**< 0.00001**	0.1686999	0.6249880
Hylobates	-	-	-	-	**0.0000009**	**< 0.00001**

Table 3.9. Continued

	Pan	-	-	-	-	-	*1*
36%		***Gorilla***	***H. naledi***	***Homo***	***Hylobates***	***Pan***	***Pongo***
	Au. sediba	1	1	1	0.0962783	1	1
	Gorilla	-	1	1	**< 0.00001**	0.3467198	0.4972837
	H. naledi	-	-	1	**0.0340586**	1	1
	Homo	-	-	-	**< 0.00001**	0.7628872	0.9836629
	Hylobates	-	-	-	-	**0.0000001**	**0.0000001**
	Pan	-	-	-	-	-	1
41%		***Gorilla***	***H. naledi***	***Homo***	***Hylobates***	***Pan***	***Pongo***
	Au. sediba	1	1	1	0.7056205	1	1
	Gorilla	-	1	1	**< 0.00001**	0.6334731	0.3772505
	H. naledi	-	-	1	**0.0299308**	1	1
	Homo	-	-	-	**< 0.00001**	1	1
	Hylobates	-	-	-	-	**< 0.00001**	**0.0000001**
	Pan	-	-	-	-	-	1
45%		***H. naledi***	***Homo***	***Hylobates***	***Pan***	***Pongo***	
	Gorilla	1	1	**< 0.00001**	1	0.3269645	
	H. naledi	-	1	**0.0229565**	1	0.7785687	
	Homo	-	-	**< 0.00001**	1	1	
	Hylobates	-	-	-	**< 0.00001**	**0.0000002**	
	Pan	-	-	-	-	1	
50%		***Gorilla***	***H. naledi***	***Homo***	***Hylobates***	***Pan***	***Pongo***
	Au. sediba	0.7679848	0.3499167	1	1	1	1
	Gorilla	-	1	1	**< 0.00001**	1	0.5634382
	H. naledi	-	-	1	**0.0287001**	1	1
	Homo	-	-	-	**0.0000002**	1	1

Table 3.9. Continued

	Hylobates	-	-	-	-	***< 0.00001***	***0.0000001***
	Pan	-	-	-	-	-	1
55%		***Au. sediba***	***Gorilla***	***Homo***	***Hylobates***	***Pan***	***Pongo***
	Au. africanus	1	0.2778192	1	1	0.8884003	1
	Au. sediba	-	0.7886692	1	1	1	1
	Gorilla	-	-	0.2382254	**< 0.00001**	0.2739987	0.1250692
	Homo	-	-	-	**0.0000058**	1	1
	Hylobates	-	-	-	-	**< 0.00001**	**< 0.00001**
	Pan	-	-	-	-	-	1
59%		***Au. sediba***	***Gorilla***	***Homo***	***Hylobates***	***Pan***	***Pongo***
	Au. africanus	1	0.8654786	1	1	1	1
	Au. sediba	-	0.6956819	1	1	1	1
	Gorilla	-	-	**0.0242128**	**< 0.00001**	**0.0005398**	**0.0035370**
	Homo	-	-	-	**0.0000037**	1	1
	Hylobates	-	-	-	-	**0.0000002**	**< 0.00001**
	Pan	-	-	-	-	-	1
64%		***Au. sediba***	***Gorilla***	***Homo***	***Hylobates***	***Pan***	***Pongo***
	Au. africanus	1	1	1	1	1	1
	Au. sediba	-	0.2869368	1	1	1	1
	Gorilla	-	-	**0.0220482**	**< 0.00001**	**0.0000832**	**0.0001077**
	Homo	-	-	-	**0.0000014**	1	1
	Hylobates	-	-	-	-	**0.0000005**	**0.0000003**
	Pan	-	-	-	-	-	1

Table 3.9. Continued

68%		***Au. sediba***	***Gorilla***	***H. naledi***	***Homo***	***Hylobates***	***Pan***	***Pongo***
	Au. africanus	1	1	1	1	1	1	1
	Au. sediba	-	0.5030372	1	1	1	1	1
	Gorilla	-	-	1	0.2712083	**< 0.00001**	**0.0011965**	**0.00013509**
	H. naledi	-	-	-	1	0.2263978	1	1
	Homo	-	-	-	-	**0.0000003**	1	1
	Hylobates	-	-	-	-	-	**0.0000004**	**0.0000047**
	Pan	-	-	-	-	-	-	1
73%		***Au. sediba***	***Gorilla***	***H. naledi***	***Homo***	***Hylobates***	***Pan***	***Pongo***
	Au. africanus	1	1	1	1	1	1	1
	Au. sediba	-	0.9016692	1	1	1	1	1
	Gorilla	-	-	1	0.8834856	**< 0.00001**	0.2723726	**0.0000505**
	H. naledi	-	-	-	1	0.7958112	1	1
	Homo	-	-	-	-	**0.0000005**	1	0.78263843
	Hylobates	-	-	-	-	-	**< 0.00001**	**0.00027307**
	Pan	-	-	-	-	-	-	0.42235954
77%		***Au. sediba***	***Gorilla***	***H. naledi***	***Homo***	***Hylobates***	***Pan***	***Pongo***
	Au. africanus	1	1	1	1	1	1	1
	Au. sediba	-	1	1	1	1	1	1
	Gorilla	-	-	1	1	**< 0.00001**	1	**0.00021161**
	H. naledi	-	-	-	1	0.9036184	1	1
	Homo	-	-	-	-	**0.0000107**	1	0.59669456
	Hylobates	-	-	-	-	-	**< 0.00001**	**0.00701865**

Table 3.9. Continued

	Pan	-	-	-	-	-	-	*0.08162525*
82%		***Au. sediba***	***Gorilla***	***H. naledi***	***Homo***	***Hylobates***	***Pan***	***Pongo***
	Au. africanus	1	1	1	1	0.5379566	1	1
	Au. sediba	-	0.5695687	1	1	1	1	1
	Gorilla	-	-	1	1	**< 0.00001**	1	0.10176379
	H. naledi	-	-	-	1	1	1	1
	Homo	-	-	-	-	**0.0000050**	1	1
	Hylobates	-	-	-	-	-	**0.0000001**	**0.0000184**
	Pan	-	-	-	-	-	-	1
86%		***Au. sediba***	***Gorilla***	***H. naledi***	***Homo***	***Hylobates***	***Pan***	***Pongo***
	Au. africanus	1	1	1	1	1	1	1
	Au. sediba	-	1	1	1	1	1	1
	Gorilla	-	-	1	1	**< 0.00001**	0.1621641	0.08596698
	H. naledi	-	-	-	1	0.1423099	1	1
	Homo	-	-	-	-	**0.0000002**	1	1
	Hylobates	-	-	-	-	-	**0.0000002**	**0.0000005**
	Pan	-	-	-	-	-	-	1
91%		***Au. sediba***	***Gorilla***	***H. naledi***	***Homo***	***Hylobates***	***Pan***	***Pongo***
	Au. africanus	1	1	1	1	1	1	1
	Au. sediba	-	0.5630665	1	1	1	1	1
	Gorilla	-	-	1	0.4107611	**< 0.00001**	**0.0276088**	0.2682711
	H. naledi	-	-	-	1	1	1	1
	Homo	-	-	-	-	**0.0000154**	1	1
	Hylobates	-	-	-	-	-	**0.0000019**	**< 0.00001**

Table 3.9. Continued

	Pan	-	-	-	-	-	*1*
95%		***Gorilla***	***Homo***	***Hylobates***	***Pan***	***Pongo***	
	Au. sediba	1	1	0.9838108	1	1	
	Gorilla	-	0.1264320	**< 0.00001**	**0.0120387**	1	
	Homo	-	-	**0.0000903**	1	0.9076038	
	Hylobates	-	-	-	**0.0000084**	**< 0.00001**	
	Pan	-	-	-	-	0.2696047	
100%		***Gorilla***	***Homo***	***Hylobates***	***Pan***	***Pongo***	
	Au. sediba	1	1	0.1651463	1	1	
	Gorilla	-	0.2723074	**< 0.00001**	**0.0000032**	0.1965852	
	Homo	-	-	**0.0000019**	0.3225347	1	
	Hylobates	-	-	-	**0.0014334**	**< 0.00001**	
	Pan	-	-	-	-	0.0561169	

Table 3.10. Intraspecific pairwise comparisons of relative trabecular separation (Tb.Sp) amongst extant apes and fossil hominins. All statistical differences were tested for with a non-parametric Dunn's tests with Bonferroni correction. Significant p-values are bolded.

% Bone Length	**Intraspecific Pairwise Comparisons (non-parametric Dunn's tests with Bonferroni correction)**					
	Gorilla	***H. naledi***	***Homo***	***Hylobates***	***Pan***	***Pongo***
	Au. sediba	1	0.3031233	1	1	0.3414509	1
	Gorilla	-	0.3664633	1	0.8595966	**0.0000006**	1
5%	***H. naledi***	-	-	0.9591177	0.9343455	1	0.5424706
	Homo	-	-	-	1	**0.0399556**	1
	Hylobates	-	-	-	-	**0.0106910**	1
	Pan	-	-	-	-	-	**0.0000886**
	Gorilla	***H. naledi***	***Homo***	***Hylobates***	***Pan***	***Pongo***
	Au. sediba	1	0.7317473	1	1	0.8462621	1
	Gorilla	-	0.4911730	1	1	**0.0000005**	1
9%	***H. naledi***	-	-	0.6693667	0.8078160	1	0.7438965
	Homo	-	-	-	1	**0.0007707**	1
	Hylobates	-	-	-	-	**0.0004452**	1
	Pan	-	-	-	-	-	**00001129**
	Gorilla	***H. naledi***	***Homo***	***Hylobates***	***Pan***	***Pongo***
	Au. sediba	1	0.4946517	1	1	0.6038276	1
	Gorilla	-	0.4292092	1	1	**0.0000011**	1
14%	***H. naledi***	-	-	0.6664106	0.4539663	1	0.9246177
	Homo	-	-	-	1	**0.0026861**	1
	Hylobates	-	-	-	-	**0.0000182**	1
	Pan	-	-	-	-	-	**0.0034125**
18%	**Gorilla**	**H. naledi**	**Homo**	**Hylobates**	**Pan**	**Pongo**

Table 3.10. Continued

Au. sediba	*1*	*1*	*1*	*1*	*1*	*1*
Gorilla	-	0.5427167	1	1	**0.0000081**	0.4550394
H. naledi	-	-	0.8767517	0.2902742	1	1
Homo	-	-	-	1	**0.0120847**	1
Hylobates	-	-	-	-	**0.0000002**	**0.0344658**
Pan	-	-	-	-	-	0.0608838

23%

	Gorilla	***H. naledi***	***Homo***	***Hylobates***	***Pan***	***Pongo***
Au. sediba	1	1	1	1	1	1
Gorilla	-	0.6266067	1	0.0600241	**0.0009206**	0.6275168
H. naledi	-	-	0.9710898	0.1283456	1	1
Homo	-	-	-	**0.0437675**	0.1357005	1
Hylobates	-	-	-	-	**< 0.00001**	**0.0001561**
Pan	-	-	-	-	-	0.5683569

27%

	Gorilla	***H. naledi***	***Homo***	***Hylobates***	***Pan***	***Pongo***
Au. sediba	1	1	1	1	1	1
Gorilla	-	1	1	**0.0073207**	**0.0316232**	0.4435917
H. naledi	-	-	1	1	1	1
Homo	-	-	-	**0.0025862**	1	1
Hylobates	-	-	-	-	**< 0.00001**	**0.0000044**
Pan	-	-	-	-	-	1

32%

	Gorilla	***H. naledi***	***Homo***	***Hylobates***	***Pan***	***Pongo***
Au. sediba	1	1	1	0.2455599	1	1
Gorilla	-	1	1	**0.0004753**	0.7798029	1
H. naledi	-	-	1	0.1602494	1	1
Homo	-	-	-	**0.0000426**	1	1
Hylobates	-	-	-	-	**0.0000004**	**0.0000018**

Table 3.10. Continued

	Pan	-	-	-	-	-	*1*
36%		***Gorilla***	***H. naledi***	***Homo***	***Hylobates***	***Pan***	***Pongo***
	Au. sediba	1	1	1	0.0873027	1	1
	Gorilla	-	1	1	**0.0001063**	1	1
	H. naledi	-	-	1	0.2907499	1	1
	Homo	-	-	-	**0.0002508**	1	1
	Hylobates	-	-	-	-	**0.0000027**	**0.0000001**
	Pan	-	-	-	-	-	1
41%		***Gorilla***	***H. naledi***	***Homo***	***Hylobates***	***Pan***	***Pongo***
	Au. sediba	0.8384431	1	1	0.0704665	1	1
	Gorilla	-	1	1	**0.0002416**	1	0.1749621
	H. naledi	-	-	1	1	1	1
	Homo	-	-	-	**0.0000123**	1	1
	Hylobates	-	-	-	-	**0.0000016**	**< 0.00001**
	Pan	-	-	-	-	-	1
45%		***H. naledi***	***Homo***	***Hylobates***	***Pan***	***Pongo***	
	Gorilla	1	0.8819676	**0.0032387**	0.7692054	**0.0069585**	
	H. naledi	-	1	1	1	1	
	Homo	-	-	**0.0001207**	1	1	
	Hylobates	-	-	-	**0.0000107**	**< 0.00001**	
	Pan	-	-	-	-	0.8470524	
50%		***Gorilla***	***H. naledi***	***Homo***	***Hylobates***	***Pan***	***Pongo***
	Au. sediba	1	1	1	0.1633912	1	1
	Gorilla	-	1	1	**0.0016491**	0.2456676	0.1317555
	H. naledi	-	-	1	1	1	1
	Homo	-	-	-	**0.0090167**	1	0.9098939

Table 3.10. Continued

	Hylobates	-	-	-	-	***0.0000002***	***0.0000001***
	Pan	-	-	-	-	-	1
55%		***Au. sediba***	***Gorilla***	***Homo***	***Hylobates***	***Pan***	***Pongo***
	Au. africanus	1	1	0.7916751	0.0695182	1	1
	Au. sediba	-	1	1	0.3760468	1	1
	Gorilla	-	-	1	**0.0000214**	0.2229995	1
	Homo	-	-	-	**0.0114348**	0.1556001	1
	Hylobates	-	-	-	-	**< 0.00001**	**0.0000003**
	Pan	-	-	-	-	-	1
59%		***Au. sediba***	***Gorilla***	***Homo***	***Hylobates***	***Pan***	***Pongo***
	Au. africanus	1	1	1	0.2902742	1	1
	Au. sediba	-	1	1	1	1	1
	Gorilla	-	-	0.2934764	**< 0.00001**	0.4784358	1
	Homo	-	-	-	**0.0188849**	**0.0022086**	0.2969739
	Hylobates	-	-	-	-	**< 0.00001**	**< 0.00001**
	Pan	-	-	-	-	-	0.7710735
64%		***Au. sediba***	***Gorilla***	***Homo***	***Hylobates***	***Pan***	***Pongo***
	Au. africanus	1	1	1	1	1	1
	Au. sediba	-	1	1	1	1	1
	Gorilla	-	-	**0.0048251**	**< 0.00001**	1	1
	Homo	-	-	-	0.1941956	**0.0001697**	**0.0150632**
	Hylobates	-	-	-	-	**< 0.00001**	**< 0.00001**
	Pan	-	-	-	-	-	1
68%		***Au. sediba***	***Gorilla***	***H. naledi***	***Homo***	***Hylobates***	***Pan***	***Pongo***

Table 3.10. Continued

	Au. africanus	*1*	*1*	*1*	*1*	*0.8946230*	*1*	*1*
	Au. sediba	-	1	1	1	0.8181341	1	1
	Gorilla	-	-	1	0.1041527	**< 0.00001**	1	1
	H. naledi	-	-	-	1	0.4424939	1	1
	Homo	-	-	-	-	**0.0263459**	**0.0148698**	**0.03339617**
	Hylobates	-	-	-	-	-	**< 0.00001**	**< 0.00001**
	Pan	-	-	-	-	-	-	1
73%		***Au. sediba***	***Gorilla***	***H. naledi***	***Homo***	***Hylobates***	***Pan***	***Pongo***
	Au. africanus	1	1	1	1	1	1	1
	Au. sediba	-	1	1	1	1	1	1
	Gorilla	-	-	1	1	**< 0.00001**	1	1
	H. naledi	-	-	-	1	1	1	1
	Homo	-	-	-	-	**0.0005738**	0.2052540	0.40483348
	Hylobates	-	-	-	-	-	**< 0.00001**	**< 0.00001**
	Pan	-	-	-	-	-	-	1
77%		***Au. sediba***	***Gorilla***	***H. naledi***	***Homo***	***Hylobates***	***Pan***	***Pongo***
	Au. africanus	1	1	1	1	1	0.8764206	1
	Au. sediba	-	1	1	1	1	1	1
	Gorilla	-	-	1	0.2895926	**< 0.00001**	1	1
	H. naledi	-	-	-	1	1	1	1
	Homo	-	-	-	-	**0.0175778**	**0.0258122**	0.07937992
	Hylobates	-	-	-	-	-	**< 0.00001**	**< 0.00001**
	Pan	-	-	-	-	-	-	1
82%		***Au. sediba***	***Gorilla***	***H. naledi***	***Homo***	***Hylobates***	***Pan***	***Pongo***

Table 3.10. Continued

	Au. africanus	*1*	*1*	*1*	*1*	*1*	*1*	*1*
	Au. sediba	-	1	1	1	1	1	1
	Gorilla	-	-	1	0.0540137	**0.0000004**	1	1
	H. naledi	-	-	-	1	1	1	1
	Homo	-	-	-	-	1	**0.0009328**	**0.00065253**
	Hylobates	-	-	-	-	-	**< 0.00001**	**< 0.00001**
	Pan	-	-	-	-	-	-	1
86%		***Au. sediba***	***Gorilla***	***H. naledi***	***Homo***	***Hylobates***	***Pan***	***Pongo***
	Au. africanus	1	1	1	1	1	1	1
	Au. sediba	-	1	1	1	1	1	1
	Gorilla	-	-	1	**0.0006483**	**0.0000001**	1	1
	H. naledi	-	-	-	1	0.8028051	1	1
	Homo	-	-	-	-	1	0.1706324	**0.00073941**
	Hylobates	-	-	-	-	-	**0.0017691**	**0.0000003**
	Pan	-	-	-	-	-	-	0.96774715
91%		***Au. sediba***	***Gorilla***	***H. naledi***	***Homo***	***Hylobates***	***Pan***	***Pongo***
	Au. africanus	1	1	1	1	1	1	1
	Au. sediba	-	1	1	1	0.7136445	1	1
	Gorilla	-	-	1	**0.0000018**	**< 0.00001**	0.2258559	0.06892635
	H. naledi	-	-	-	1	0.4210353	1	1
	Homo	-	-	-	-	1	**0.0230213**	0.06642354
	Hylobates	-	-	-	-	-	**0.0000035**	**0.0000237**
	Pan	-	-	-	-	-	-	1
95%		***Gorilla***	***Homo***	***Hylobates***	***Pan***	***Pongo***		

Table 3.10. Continued

	Au. sediba	*0.4369047*	*1*	*1*	*0.3438009*	*1*
	Gorilla	-	**0.0000134**	**< 0.00001**	1	**0.0005535**
	Homo	-	-	1	**0.0000047**	1
	Hylobates	-	-	-	**< 0.00001**	**0.0150423**
	Pan	-	-	-	-	**0.0001920**
100%		***Gorilla***	***Homo***	***Hylobates***	***Pan***	***Pongo***
	Au. sediba	0.5896352	1	0.6392840	0.0544077	1
	Gorilla	-	0.5739044	1	**0.0001653**	**0.0004413**
	Homo	-	-	0.9041984	**0.0000027**	0.9936023
	Hylobates	-	-	-	**0.0005333**	**0.0031228**
	Pan	-	-	-	-	**< 0.00001**

Table 3.11. Intraspecific pairwise comparisons of unscaled trabecular bone volume (BV/TV) amongst extant apes and fossil hominins. The 9%, 82%, 91%, and 95% bone length ROIs were investigated using a parametric Tukey's HSD test. In all other regions statistical differences were tested for with a non-parametric Dunn's tests with Bonferroni correction. Significant p-values are bolded.

% Bone Length	**Intraspecific Pairwise Comparisons (non-parametric Dunn's tests with Bonferroni correction, parametric Tukey's HSD test)**					
		Gorilla	***H. naledi***	***Homo***	***Hylobates***	***Pan***	***Pongo***
5%	***Au. sediba***	1	1	1	1	1	1
	Gorilla	-	1	1	**0.0000001**	0.4486361	0.3196512
	H. naledi	-	-	1	0.0592347	1	0.5917149
	Homo	-	-	-	**0.0001869**	0.3960892	1
	Hylobates	-	-	-	-	**< 0.00001**	**0.0035838**
	Pan	-	-	-	-	-	**0.0007991**
		Gorilla	***H. naledi***	***Homo***	***Hylobates***	***Pan***	***Pongo***
9%	***Au. sediba***	1	1	1	1	1	1
	Gorilla	-	1	0.1385359	**0.0000001**	0.5364450	0.4307916
	H. naledi	-	-	0.4702080	0.0721191	1	0.7188544
	Homo	-	-	-	0.1691914	**0.0008670**	1
	Hylobates	-	-	-	-	**< 0.00001**	**0.0025430**
	Pan	-	-	-	-	-	**0.0017095**
		Gorilla	***H. naledi***	***Homo***	***Hylobates***	***Pan***	***Pongo***
14%	***Au. sediba***	1	0.3142857	1	1	0.4639356	1
	Gorilla	-	1	1	**0.0000008**	0.2609771	1
	H. naledi	-	-	0.8404438	0.0653280	1	0.9914280
	Homo	-	-	-	**0.0061589**	0.0649549	1
	Hylobates	-	-	-	-	**< 0.00001**	**0.0001016**
	Pan	-	-	-	-	-	**0.0499183**

Table 3.11. Continued

18%		***Gorilla***	***H. naledi***	***Homo***	***Hylobates***	***Pan***	***Pongo***
	Au. sediba	1	0.6867453	1	1	1	1
	Gorilla	-	1	1	**0.0000001**	0.5444407	1
	H. naledi	-	-	1	0.0527071	1	1
	Homo	-	-	-	**0.0000729**	0.8450388	1
	Hylobates	-	-	-	-	**< 0.00001**	**0.0000018**
	Pan	-	-	-	-	-	0.3711658
23%		***Gorilla***	***H. naledi***	***Homo***	***Hylobates***	***Pan***	***Pongo***
	Au. sediba	1	0.8549118	1	1	1	1
	Gorilla	-	1	1	**< 0.00001**	1	1
	H. naledi	-	-	1	**0.0439071**	1	1
	Homo	-	-	-	**0.0000006**	1	1
	Hylobates	-	-	-	-	**< 0.00001**	**0.0000001**
	Pan	-	-	-	-	-	1
27%		***Gorilla***	***H. naledi***	***Homo***	***Hylobates***	***Pan***	***Pongo***
	Au. sediba	1	1	1	1	1	1
	Gorilla	-	1	1	**< 0.00001**	1	1
	H. naledi	-	-	1	0.2484537	1	1
	Homo	-	-	-	**< 0.00001**	1	1
	Hylobates	-	-	-	-	**< 0.00001**	**< 0.00001**
	Pan	-	-	-	-	-	1
32%		***Gorilla***	***H. naledi***	***Homo***	***Hylobates***	***Pan***	***Pongo***
	Au. sediba	1	1	1	0.3666515	1	1
	Gorilla	-	1	1	**< 0.00001**	1	1
	H. naledi	-	-	1	0.1511407	1	1
	Homo	-	-	-	**< 0.00001**	1	1

Table 3.11. Continued

	Hylobates	-	-	-	-	***< 0.00001***	***< 0.00001***
	Pan	-	-	-	-	-	1
36%		***Gorilla***	***H. naledi***	***Homo***	***Hylobates***	***Pan***	***Pongo***
	Au. sediba	1	1	1	0.2560312	1	1
	Gorilla	-	1	1	**< 0.00001**	1	1
	H. naledi	-	-	1	0.0668719	1	1
	Homo	-	-	-	**0.0000001**	1	1
	Hylobates	-	-	-	-	**0.0000003**	**< 0.00001**
	Pan	-	-	-	-	-	1
41%		***Gorilla***	***H. naledi***	***Homo***	***Hylobates***	***Pan***	***Pongo***
	Au. sediba	1	1	1	0.1771247	1	1
	Gorilla	-	1	1	**< 0.00001**	1	1
	H. naledi	-	-	1	0.5598984	1	1
	Homo	-	-	-	**0.0000003**	1	1
	Hylobates	-	-	-	-	**0.0000003**	**< 0.00001**
	Pan	-	-	-	-	-	1
45%		***H. naledi***	***Homo***	***Hylobates***	***Pan***	***Pongo***	
	Gorilla	1	1	**< 0.00001**	1	1	
	H. naledi	-	1	0.3031604	1	1	
	Homo	-	-	**0.0000022**	1	1	
	Hylobates	-	-	-	**< 0.00001**	**< 0.00001**	
	Pan	-	-	-	-	1	
50%		***Gorilla***	***H. naledi***	***Homo***	***Hylobates***	***Pan***	***Pongo***
	Au. sediba	1	1	1	1	1	1
	Gorilla	-	1	0.8575375	**< 0.00001**	1	1
	H. naledi	-	-	1	1	1	1

Table 3.11. Continued

	Homo	-	-	-	***0.0001245***	*1*	*0.7048735*
	Hylobates	-	-	-	-	**< 0.00001**	**< 0.00001**
	Pan	-	-	-	-	-	1
55%		***Au. sediba***	***Gorilla***	***Homo***	***Hylobates***	***Pan***	***Pongo***
	Au. africanus	1	1	1	1	1	1
	Au. sediba	-	1	1	1	1	1
	Gorilla	-	-	**0.0198853**	**< 0.00001**	1	1
	Homo	-	-	-	**0.0034125**	0.1491425	0.1910982
	Hylobates	-	-	-	-	**< 0.00001**	**< 0.00001**
	Pan	-	-	-	-	-	1
59%		***Au. sediba***	***Gorilla***	***Homo***	***Hylobates***	***Pan***	***Pongo***
	Au. africanus	1	1	1	1	1	1
	Au. sediba	-	1	1	1	1	1
	Gorilla	-	-	**0.0001460**	**< 0.00001**	0.7653493	0.5097551
	Homo	-	-	-	**0.0128954**	0.0640861	0.0980763
	Hylobates	-	-	-	-	**< 0.00001**	**< 0.00001**
	Pan	-	-	-	-	-	1
64%		***Au. sediba***	***Gorilla***	***Homo***	***Hylobates***	***Pan***	***Pongo***
	Au. africanus	1	1	1	1	1	1
	Au. sediba	-	0.8275122	1	1	1	1
	Gorilla	-	-	**0.0000042**	**< 0.00001**	0.2997236	0.1460843
	Homo	-	-	-	**0.0431125**	**0.0189634**	**0.0385452**
	Hylobates	-	-	-	-	**< 0.00001**	**< 0.00001**
	Pan	-	-	-	-	-	1
68%		***Au. sediba***	***Gorilla***	***H. naledi***	***Homo***	***Hylobates***	***Pan***	***Pongo***
	Au. africanus	1	1	1	1	1	1	1

Table 3.11. Continued

	Au. sediba	*-*	*1*	*1*	*1*	*1*	*1*	*1*
	Gorilla	-	-	1	**0.0004538**	**< 0.00001**	0.3192192	0.3877679
	H. naledi	-	-	-	1	0.9537619	1	1
	Homo	-	-	-	-	**0.0067683**	0.4152209	0.3561871
	Hylobates	-	-	-	-	-	**< 0.00001**	**< 0.00001**
	Pan	-	-	-	-	-	-	1
73%		***Au. sediba***	***Gorilla***	***H. naledi***	***Homo***	***Hylobates***	***Pan***	***Pongo***
	Au. africanus	1	1	1	1	1	1	1
	Au. sediba	-	1	1	1	1	1	1
	Gorilla	-	-	1	**0.0029425**	**< 0.00001**	1	0.3891727
	H. naledi	-	-	-	1	1	1	1
	Homo	-	-	-	-	**0.0025381**	0.3438641	0.9968385
	Hylobates	-	-	-	-	-	**< 0.00001**	**< 0.00001**
	Pan	-	-	-	-	-	-	1
77%		***Au. sediba***	***Gorilla***	***H. naledi***	***Homo***	***Hylobates***	***Pan***	***Pongo***
	Au. africanus	1	1	1	1	1	1	1
	Au. sediba	-	1	1	1	1	1	1
	Gorilla	-	-	1	**0.0023703**	**< 0.00001**	1	0.5872942
	H. naledi	-	-	-	1	1	1	1
	Homo	-	-	-	-	**0.0080037**	0.1427650	0.6538155
	Hylobates	-	-	-	-	-	**< 0.00001**	**< 0.00001**
	Pan	-	-	-	-	-	-	1
82%		***Au. sediba***	***Gorilla***	***H. naledi***	***Homo***	***Hylobates***	***Pan***	***Pongo***
	Au. africanus	1	1	1	1	1	1	1
	Au. sediba	-	0.8869370	1	1	1	1	1
	Gorilla	-	-	1	**0.0005835**	**< 0.00001**	1	1

Table 3.11. Continued

	H. naledi	-	-	-	*1*	*1*	*1*	*1*
	Homo	-	-	-	-	0.0771740	0.1706324	**0.0191916**
	Hylobates	-	-	-	-	-	**< 0.00001**	**< 0.00001**
	Pan	-	-	-	-	-	-	1
86%		***Au. sediba***	***Gorilla***	***H. naledi***	***Homo***	***Hylobates***	***Pan***	***Pongo***
	Au. africanus	1	1	1	1	1	1	1
	Au. sediba	-	1	1	1	1	1	1
	Gorilla	-	-	1	**0.0000413**	**< 0.00001**	**0.0006204**	0.8035383
	H. naledi	-	-	-	1	1	1	1
	Homo	-	-	-	-	0.0645254	1	**0.0412731**
	Hylobates	-	-	-	-	-	**0.0000334**	**< 0.00001**
	Pan	-	-	-	-	-	-	0.5497481
91%		***Au. sediba***	***Gorilla***	***H. naledi***	***Homo***	***Hylobates***	***Pan***	***Pongo***
	Au. africanus	1	1	1	1	1	1	1
	Au. sediba	-	1	1	1	1	1	1
	Gorilla	-	-	1	**0.0000010**	**< 0.00001**	**0.0005269**	0.0057098
	H. naledi	-	-	-	1	1	1	1
	Homo	-	-	-	-	0.0783072	0.8267569	0.2587337
	Hylobates	-	-	-	-	-	**0.0000010**	**< 0.00001**
	Pan	-	-	-	-	-	-	1
95%		**Gorilla**	**Homo**	**Hylobates**	**Pan**	**Pongo**		
	Au. sediba	0.9918040	1	1	1	1		
	Gorilla	-	**0.0000001**	**< 0.00001**	1	**0.0013463**		
	Homo	-	-	0.4468471	**0.0000922**	0.1108556		
	Hylobates	-	-	-	**< 0.00001**	**0.0000048**		
	Pan	-	-	-	-	0.1655613		

Table 3.11. Continued

100%

	Gorilla	***Homo***	***Hylobates***	***Pan***	***Pongo***
Au. sediba	0.2326410	1	1	0.1694599	1
Gorilla	-	**0.0001295**	**< 0.00001**	1	**< 0.00001**
Homo	-	-	1	**0.0000318**	1
Hylobates	-	-	-	**< 0.00001**	1
Pan	-	-	-	-	**< 0.00001**

4. Assessing Hypotheses of Clavicular Form and Function Using Finite Element Modeling

Introduction

Over the last three chapters, I have highlighted aspects of clavicular morphology I hypothesize to be functionally informative and structurally significant. While these hypotheses are deeply rooted in our fundamental understanding of bone functional adaptation and beam mechanics, identifying morphological traits suspected to have biomechanical relevance is not the same as directly testing their mechanical behavior. Moreover, not all analyses performed have pointed unequivocally to a form-function relationship in the clavicle. The geometric morphometric analysis of shape through ontogeny (Chapter 1) revealed that there is very little developmental plasticity in external clavicular shape and nor does shape appear to reliably group all hominoids by locomotor mode, leaving the significance of the clear variation in curvature unresolved. Lastly, there is still the remaining question, as often lingers in the background of most analyses of functional morphology, of whether bony morphology better reflects osteological adaptation for the most habitually used locomotor behavior or those that impose the highest magnitudes of strain on the structure.

These areas of ambiguity all relate to understanding how the structure of the clavicle deforms under external loads and the potential functional consequences of morphological diversity. Quantifying strain, which is a measure of how much a structure is deforming under the loading conditions, is especially relevant to studies of bone functional adaptation as bone remodeling occurs in response to the strain regime across the element, whereby increased strain

typically results in bone formation and decreased strain leads to bone resorption (Figure 4.1 A.; Richmond et al., 2005; Ruff et al., 2006). Because of the relationship between sensed bone strain and its remodeling response, hypotheses relating bony morphology to patterns of strain can be tested using the finite element method (FEM) (Ross, 2005). For this reason, biological applications of the FEM have increased in use over the last few decades to evaluate the mechanical behavior of structures under varying loads (e.g., Marinescu et al., 2005; Rayfield, 2007; Berthaume et al., 2010; Porro et al., 2013; Panagiotopoulou et al., 2016, 2017, 2020; Sellers et al., 2017; Wilken et al., 2019; Cost et al., 2020; Pollock et al., 2022; Tseng et al., 2023)

FE modeling is an especially powerful tool for functional morphologists and biomechanists due its wide range of applications in testing form-function hypotheses. It can be used to investigate the functional significance of specific anatomical features like the zygomatic root (Ledogar et al., 2017), palatal thickness (Strait et al., 2007), and cortical geometry (Lieberman et al., 2004). In an evolutionary context, this allows researchers to better evaluate whether such features should be considered functional adaptations in extinct taxa (Richmond et al., 2005). The FEM can also be used to compare the mechanical performance of different morphological designs of the same element (Richmond, 1998; Ryan and van Rietbergen, 2005; Smith et al., 2015a, 2015b, 2021; Püschel and Sellers, 2016). In this way, researchers can apply the same loading conditions to a unique fossil morphology alongside a range of extant taxa to compare its strain regimes and assess which aspects of the unique morphology may be functionally relevant (Richmond et al., 2005).

This latter application of FE modeling is leveraged here to test three form-function hypotheses about the hominoid clavicle: (1) increased cortical cross-sectional eccentricity approximately mid-diaphysis in *Gorilla, Pan,* and *Au. afarensis* resists the strain regime imposed

by vertical climbing; (2) suspensory behavior subjects the lateral third of the clavicle to high magnitudes of strain that must be resisted by cortical mass distributed along the craniocaudal axis; (3) curvature develops opposite habitual bending loads to act as a pre-stressed beam that would be 'straightened' by deformation during locomotion (Milne, 2016; Henderson et al., 2017; Milne and Granatosky, 2021).

Materials and Methods

Model construction:

Four model geometries were created to test for the impact of variation in external shape and cortical geometry (Figure 4.2A). The anatomical model was created using the image data from the adult chimpanzee with the mean relative cortical area in the dataset used for the previous three chapters (AMNH M 51377). This measure was used to select the model geometry due to its minimal direct impact on biomechanical properties. By deliberately choosing a metric that is less structurally influential, the model is a more generalized representation of chimpanzee anatomy, which is beneficial for comparison with theoretical model geometries and broad interpretations of the model solutions. The cortical bone was extracted from the micro-CT data, exported as a volume, and cleaned in preparation for FE meshing. The beam model, representing a clavicle with a straight diaphysis and consistent cortical geometry, was created in *Geomagic Design X* (oqton, 2023). Two circular shapes representing the two ends of the clavicle were spaced apart according to the length of the anatomical model. The shapes were then connected and meshed to create a closed cylindrical volume. The volume had walls with a thickness of 3 mm, constituting approximately 40% of the model's cross-sectional diameter. This setup aimed to replicate the lowest percent cortical area values observed in the diaphysis of adult apes

(Chapter 2). This volume was then cleaned and exported for FE meshing. The cortical model was made by combining the external shape of the beam model with the internal geometry of the anatomical model. To fit inside the non-curved external structure, the endosteal volume from the anatomical model was straightened and scaled accordingly. Once the two volumes were merged, the model was cleaned for FE meshing. Finally, to make the curved model, the two circular shapes used to define the beam model were duplicated and offset from one another such that once connected and meshed, the volume would have a similar external curvature to the average chimpanzee clavicle. This model was also thickened to have 3 mm thick walls and cleaned for FE meshing. In all models, trabecular bone was represented by a solid volume that filled the entire medullary cavity.

Prior to analysis, all models were aligned to the same global coordinate system such that the origin is in the center of the sternal articular end. The X, Y, and Z axes correspond to specific orientations: the X-axis represents the dorsoventral direction, the Y-axis indicates the craniocaudal direction, and the Z-axis corresponds to the long axis of the clavicle. All models were assigned isotropic material properties for human cortical and trabecular bone (Table 4.1, Rusovici et al., 2013).

Applied forces:

One previously fixed and frozen male *Pan troglodytes* individual (CR-Chimp-1) was first thawed and repositioned as closely to standard anatomical position as its condition allowed, and then was CT scanned using a Vimago veterinary CT scanner to obtain skeletal information for

muscle vector orientation and dissected for muscle mass that informed the applied forces (Table 4.2).

Physiological cross-sectional area (PCSA) of the anterior deltoid, cranial trapezius, clavicular pectoralis major, and sternocleidomastoid muscles was estimated using the muscle mass information obtained from the chimpanzee dissection, conventional muscle tissue density (1.06 g/cm^3), and measures of muscle fascicle length (Table 4.2). In the final PCSA calculations, pennation angle was assumed to be zero as all reported angles from the human literature are under 30° which is within a threshold that has negligible effects on the calculations (Cost et al., 2020; Martin et al., 2020). Fascicle length for the anterior deltoid was estimated from the existing chimpanzee dissection literature (Thorpe et al., 1999; Carlson, 2006; Oishi et al., 2009; Gómez et al., 2022). The fascicle lengths of the clavicular pectoralis major and cranial trapezius muscles were estimated as an average of the available chimpanzee (Carlson, 2006) and modern human values (Kamibayashi and Richmond, 1998; Langenderfer et al., 2004). Lastly, the fascicle length for the sternocleidomastoid was estimated by comparing the available human values (Kamibayashi and Richmond, 1998) to the muscle lengths measured from my own dissection.

Muscle vector orientation was estimated using the skeletal data obtained from the CT scanned whole chimpanzee. First the humerus, scapula, clavicle, and skull were isolated from the scan (*Avizo Lite 2020.2,* Visualizations Sciences Group, 2017). The elements were then repositioned (*Geomagic DesignX*, oqton, 2023) to represent the mid-stance phase of knuckle walking, unimanual suspension, and vertical climbing based on available reported and estimated skeletal orientation (Figure 4.2.C; Hunt, 1991; Preuschoft, 2002; Preuschoft et al., 2010; MacLean, 2018; Thompson et al., 2018; Fannin et al., 2023). The attachment regions for the anterior deltoid, cranial trapezius, clavicular pectoralis major, and sternocleidomastoid muscles

were then defined on the clavicle model geometries (Figure 4.2.B) and posed elements (Figure 4.2.C) using attachments as described in the literature (Swindler and Wood, 1973; Diogo and Wood, 2011, 2012; Diogo et al., 2013) and those observed during my own dissection. Mapped muscle origins on the four models were standardized such that each defined attachment region covered the same relative surface area on each model geometry (+/- 5%). Defined muscle insertion regions on the humerus and skull were isolated and the centroids of each were calculated for the three loading scenarios (Figure 4.2.C). The centroid coordinates were then used to define the endpoint of the muscle vectors.

Applied muscle forces (Table 4.5) were estimated by first calculating PCSA to obtain the maximum possible isometric force, then scaling that maximum force by its relative activation in chimpanzees during the stance phase of the three modeled behaviors of interest (Table 4.2, Tuttle and Basmajian, 1978; Larson and Stern, 1986, 1987; Larson et al., 1991; MacLean and Dickerson, 2020). Because similar EMG data does not exist for the sternocleidomastoid, the assumption is made for all loading scenarios that the muscle is 40% active as a neck stabilizer. Muscle force was applied across the entire defined surface representing the origin on the model geometry using the computational toolkit Boneload (Davis et al., 2010). This was done for all combinations of model geometry and loading scenarios, ultimately creating twelve unique load cases.

Substrate reaction forces (SRFs; Table 4.3) were estimated for the three loading scenarios by scaling reported SRFs from bonobos (Samuel et al., 2018) by an average chimpanzee body mass calculated from three male *Pan troglodytes* individuals representing the subspecies *P.t. schweinfurthii*, *P.t. troglodytes*, and *P.t. verus* (Fleagle, 2013) because chimpanzees are on average larger than bonobos and the subspecific designation of the dissected individual was not

known. Since these SRFs represent the force transferred at the interface between the limb and the substrate, the assumption is made that only 50% of the estimated force will reach the clavicle. The other half is assumed to be transmitted across the shoulder joint by the surrounding glenohumeral musculature. SRF components were applied to a single node in the center of the lateral end of each model. Their vector orientations were assumed to be the same as those passing through the humerus – in humans, medially directed force travels from the humeral head to the glenoid of the scapula whose medial displacement is then resisted by the coracoclavicular ligaments which serve to transfer the remaining force to the clavicle (Figure 4.1 B., Levangie and Norkin, 2011).

Constraints were inspired by previous FE modeling of the clavicle in human clinical literature by Cronskär and colleagues (2015), descriptions of the range of motion available at both clavicular joints and how they contribute to overall scapular movement (Levangie and Norkin, 2011), and the regions of ligament attachment observed in my own dissection. A central node on the medial end of each model was restricted in all degrees of translation but allowed all degrees of rotation to mimic the range of motion available at the sternoclavicular joint. To constrain the lateral end of the model, two cut-off bars representing the conoid and trapezoid ligaments were created to connect the underside of the model to a solid volume, fixed in space, acting as the coracoid of the scapula. Cut-off bars were chosen to model the ligaments because they can be modeled as tension-only elements and thus are an efficient representation of ligaments predominantly loaded in axial tension. These cut-off bars were assigned the material properties of the human coracoclavicular ligament as reported by Koh and colleagues (2004).

Finite element analysis (FEA):

FE models were solved in Strand7 R3.1.3 using the 'linear static' solver. Principal and axial strain regimes were visualized for the four model geometries during each of the three loading scenarios with colors representing the strain magnitudes (Figures 4.3 – 4.5).

Results

Effects of model geometry:

Model geometry highly impacts the distribution of principal strain across the clavicle, with external shape of the model appearing to affect the resulting strain regime more than variation in internal cortical geometry (Figures 4.3 and 4.4). The beam and cortical models both have high strain across larger regions than the anatomical and curved models. The cortical model exhibits a much lower magnitude of strain in its caudal aspect compared to the beam model, and the concentration of high strain cranially does not extend as far laterally as it does in the beam model. Comparing the beam and curved models, the addition of curvature appears to alter the strain regime, localizing it more on the curved model. Depending on the applied loading condition, strain concentrates either more dorsoventrally or more craniocaudally on the curved model compared to the beam. The anatomical and curved models have relatively similar strain regimes, but the bony ridges on the anatomical model appear to localize the areas of highest strain more than the smooth surfaces of the curved model. The long axis (ZZ) strain distribution is also impacted by model geometry (Figure 4.5). Similar to what is observed in the principal strain regimes, the beam and cortical models are most like one another as are the curved and anatomical models. The cortical model appears to have lower ZZ strain on the caudal side than the beam model, again like what is seen in the principal strain distributions. In comparing the beam and curved models, the addition of curvature localizes the regions of high tensile and

compressive ZZ strain to definable surfaces of the model. Now comparing this to the anatomical model, the anatomical model again appears to localize strain – the concentration of high tensile strain does not extend as far into the lateral end of the model as is seen in the curved model.

Given that the cortical model does not reflect any known clavicular morphologies and model solutions are not realistic compared to the other two theoretical morphologies, it will not be discussed further.

Effects of loading scenario:

As in the case of the various model geometries, the loading scenario also impacts the principal strain regime of the models. First discussing the principal tensile strain regime (ε1; Figure 4.3), when applied to the beam model, the loading conditions of vertical climbing produced a concentration of moderate strain on the dorsal aspect of the medial diaphysis. Suspensory loading creates high strain across the cranial surface and slightly lower but still high strain across the corresponding caudal surface. Knuckle walking loading leads to a similar strain regime to the suspensory condition, except that from medial to lateral the cranial strain concentration migrates dorsally, and the caudal strain concentration moves ventrally beginning at about mid-diaphysis. Comparing the loading scenarios as applied to the curved model, vertical climbing produces a small concentration of moderate strain on the ventro-caudal aspect of the lateral curvature. Under suspensory conditions, high strain is observed on the cranial aspect of the diaphysis from about 10% model length medially, through the mid-point of the lateral curvature. The highest strain is in the middle of this area, and on the corresponding caudal side, there is moderately high strain mid-diaphysis. The loading of knuckle walking creates high strain on the ventral aspect again from about 10% model length medially through mid-lateral curvature. Like under suspensory conditions, small concentrations of moderate strain are on the

corresponding aspect of the diaphysis. When the same loading scenarios are applied to the anatomical model, smaller differences can be identified than in the curved model. Under vertical climbing, there is a small concentration of moderately high strain on the edge between the caudal and ventral surfaces of the lateral curvature and on the border between the cranial and dorsal surfaces of the medial diaphysis. Suspensory loading produces high tensile strain on the cranial surface of the diaphysis, with the region of highest strain ending before the lateral curvature. Moderately high strain does continue into the lateral curvature, but not at the magnitude seen mid-diaphysis and is fairly localized to the crest for the anterior deltoid. When the knuckle walking loading scenario is applied, the highest strain is seen on the cranioventral aspect in the medial half of the diaphysis. Moderately high strain continues laterally from this larger strain concentration, but only on the edge between the ventral and caudal surfaces and does not extend past the middle of the lateral curvature. Notably, amongst all model geometries, the vertical climbing scenario produces the lowest strain magnitudes. This is likely because the modeled loading scenario reflects observations of chimpanzees predominantly supporting their body mass during vertical climbing with their hindlimbs (Hanna et al., 2017).

When comparing the principal tensile strain regime to the principal compressive strain regime ($\varepsilon 3$; Figure 4.3), the beam model exhibits the most direct overlap between concentrations of high tensile and high compressive strain, indicating the presence of shear forces. In the beam model, knuckle walking and unimanual suspension imposes the most shear strain, with the forces acting along the entire length of the model. The curved and anatomical models show less overlap between the principal tensile and principal compressive strain regimes than the beam model. In the curved model, shear strains are most pronounced on the dorsal aspect of the mid-diaphysis under the loading conditions of knuckle walking and on the inferior aspect of the same region

under suspensory conditions. In the anatomical model, on the other hand, shear strains are imposed on the cranial and caudal surfaces of sternal third of the diaphysis during knuckle walking and in approximately the same region on the caudal aspect of the diaphysis during unimanual suspension.

The differences in principal strain regime amongst the loading scenarios are also reflected in the long axis (ZZ) strain regimes. In the beam model under the loading conditions of vertical climbing, there is moderate tensile strain across the entire dorsal aspect, with the highest concentration in the sternal ¼ of the model. Under suspensory loading conditions, the beam model has very high tensile strain on the cranial side and high compressive strain caudally. During knuckle walking, the beam model has the opposite ZZ strain regime with compression cranially and compression caudally, with the cranial strain concentration showing a slight dorsal twist and the caudal concentration having a slight ventral twist along the diaphysis. When the curved model is subjected to the loading conditions of vertical climbing, there is a region of tensile strain on the ventrocaudal aspect of the lateral curvature and a corresponding region of high compressive strain on the dorsocranial aspect of the curvature. Under suspensory loading, there is a high tensile strain on the cranial side of the model from about 10% model length to the middle of the lateral curvature with a corresponding region of high compressive strain on the caudal side. The loading conditions of knuckle walking produce almost the same strain regime as the suspensory conditions, except the high tensile strain is on the ventral side of the model and the high compressive strain is on the dorsal side. For the anatomical model, when loaded under the conditions of vertical climbing, the same regions highlighted in the description of principal strain are shown to be areas of high tensile ZZ strain as well, with corresponding regions of compression on the opposite side. During suspensory loading, there is high tensile strain on the

cranial aspect of the medial diaphysis, stopping just before the lateral curvature. There is also a corresponding region of high compressive strain on the caudal surface. Under knuckle walking loading conditions, there is a region of high tensile stress on the cranial side of the medial diaphysis as in suspensory loading, but here the strain concentration does not extend as far laterally. The region of highest strain only reaches the medial half of the diaphysis, but a small region of moderate tensile strain continues onto the ventral aspect of the lateral curvature. As with other areas of high tensile strain, there are corresponding regions of high compressive strain on the caudal aspect of the sternal diaphysis and on the dorsal aspect of the lateral curvature.

Discussion

In this analysis, the primary goal was to explore how different combinations of internal and external clavicular geometry affect the way the structure mechanically responds to variation in loading regimes. The model comparisons presented here offer meaningful insights into the contributions of bone curvature to mechanical function, the influence of internal bone geometry on the resulting strain regimes, and how the feedback loop between bone strain and remodeling may drive morphological change through evolution.

Although this has proven to be a useful tool to unpack the biomechanical relevance of variation in clavicular morphology, the limitations must also be recognized since many assumptions underly these models. First, the assumption that 50% of the SRF reached the clavicle was very likely an overestimate because the strain magnitudes, not explicitly discussed above due to their potentially inflated values, exceed the peak functional strain recorded in

galloping racehorses by magnitudes (Ehrlich and Lanyon, 2002). Based on work by Ratcliffe and Holt (1997) measuring the absorption of shock from the ankle to the head during human bipedality, this estimation did not seem out of the question. During a bipedal gait, approximately 60% of the SRF faced by the ankle is passed through to the knee joint and from there, about 30% of the original SRF is imposed upon the shoulder (Ratcliffe and Holt, 1997); given the distance between the wrist and the clavicle in comparison to the knee and ankle, 50% force transfer was a reasonable first assumption. Future iterations of this analysis should further investigate the manner in which force propagates through various soft tissue structures to better estimate how much force would reach the clavicle *in vivo*. However, in the context of this analysis, the inflated strain values still provide insight into the mechanical behavior of the models relative to one another.

Second, the muscle mass collected from the dissected chimpanzee, which was likely a captive individual, may not reflect the mass of the same muscles in wild chimpanzees. This in combination with the impact of the first assumption may have led to a large underprediction of muscle force acting on the clavicle and an overrepresentation of the impact of SRFs on the strain regimes. Additionally, to simplify model meshing and solving, the trabecular bone in each of the models was represented by a single volume filling the entire medullary cavity, potentially undermining the structural role of the trabecular network in force transfer during locomotion. Finally, the data informing the orientation and magnitude of the muscle vectors was estimated with less precision than is ideal for such models. The muscle vectors were scaled based on estimated percent activation during mid-stance from reported EMG data and were oriented based on estimated positioning of the humerus, scapula, and cranium during the three modeled behaviors as the actual kinematic information is not available. Moreover, EMG data for the

sternocleidomastoid muscle during the three loading scenarios does not exist, so the estimation of 40% activation was decided upon based on the assumed neck stabilization required during these modeled behaviors. The large number of assumptions that underly these modeling experiments may, in part, be contributing to the larger differences in strain regime among the model geometries and loading conditions like what is seen between the curved and anatomical models during knuckle walking.

The results from the principal strain calculations suggest that the closer the models were to the actual geometry of a chimpanzee clavicle, the more localized the strain distributions became. They also suggest that knuckle walking and suspension are larger drivers of clavicular bone remodeling, and therefore morphological evolution, as they impose much larger strain magnitudes on the models. In these two loading scenarios, the beam model is highly strained along the length of the model. Adding curvature to the simple beam localizes the strain to more definable surfaces (e.g., craniocaudal in suspension and dorsoventral in knuckle walking). The addition of curvature to the model geometry also appears to reduce the shear forces acting on the clavicle in comparison to the straight beam model. Further elaborations on the model geometry in the anatomical model both increase the localization of the high strain concentrations to bony ridges and increase the similarity in strain regimes between the knuckle walking and suspensory loading scenarios. Moreover, even though the three modeled behaviors do show variation in their strain regimes when applied to the anatomical model, no loading scenario produced strain in a unique region of the model. This differs substantially from the effect of loading scenarios on the curved model, in which the strain regimes show very little overlap. Given that *Pan* performs all three behaviors to different extents, its clavicular geometry may reflect remodeling to produce a more predictable strain regime under a variety of loading scenarios. This would allow even

fallback behaviors to be supported by a clavicular geometry equally or better mechanically suited to the strain regime of another behavior. Further, the localization of the regions of highest strain to the bony ridges on the anatomical model supports work by Wilken and colleagues (*in review*, JEB) that suggests the primary load path is on the periphery of the model geometry and prefers the shortest, stiffest route that is also furthest from the neutral axis.

Previous investigations of long bone curvature suggest that it develops in response to habitual loading such that bone is deposited on the side of the element under compressive strain, becoming the convex side of the curvature, and bone is resorbed on the side under tensile strain, becoming the concave side (Milne, 2016; Henderson et al., 2017; Milne and Granatosky, 2021). Although this process has been proposed to act on a developmental time scale (Lanyon, 1980), which contrasts with the findings of Chapter 1, it is also reasonable to assume that such a process could also act on an evolutionary scale (Swartz, 1990). Using this hypothesis to interpret the beam model principal strain solutions, a beam shaped clavicle habitually used for suspension should remodel such that the cranial surface became concave, and the caudal surface became convex – as seen in *Hylobates* (Figure 4.8). Knuckle walking, or potentially quadrupedalism generally, would then produce a clavicle with a cranially convex diaphysis and potentially a dorsally convex curvature in the lateral diaphysis. Interestingly, the strain regime on the curved model interpreted in the context of this hypothesis suggests that the sigmoidal shape characteristic of the *Pan* and *Homo* clavicle would not have developed from a beam shaped clavicle habitually loaded during knuckle walking. Moreover, when loading under the conditions of knuckle walking, the tensile stress on the ventral aspect of the diaphysis suggests this region would gradually be resorbed and the dorsal aspect loading in compressive strain would see bone deposition, ultimately remodeling this region to become straighter as is seen in *Gorilla* (Figure

4.8). With the addition of internal cortical geometry, the chimpanzee clavicle is able to alter the strain distribution such that regions of tensile strain are in the concave aspects of the curvature and regions of compressive strain are in the convex aspects, and results then confirm the hypotheses of Milne and colleagues under both knuckle walking and suspensory loading conditions. This has several important evolutionary implications. First, it does not support the sigmoidal shape of the clavicle as an adaptation for knuckle walking. Instead, it suggests the sigmoidal shape as the ancestral condition for the African great apes that was then altered during the evolutionary history of *Gorilla* in response to its strong reliance on knuckle walking leading to the straighter diaphysis of extant gorillas. If true, this adds evidence to hypotheses of the convergent evolution of knuckle walking in *Pan* and *Gorilla* (Dainton and Macho, 1999; Kivell and Schmitt, 2009; Williams, 2010), and does not support a knuckle walking *Pan-Homo* most recent common ancestor (see Richmond and Strait, 2000). Further, it supports a stronger evolutionary importance of suspension in particular as an arboreal behavior being acted upon by stabilizing selection in the early hominin shoulder.

Given the limitations of using FE modeling to explore the mechanical behavior of great ape skeletal morphology and the number of assumptions underlying the models, the model solutions leave some questions of the form-function relationship in the chimpanzee clavicle unanswered. The relationship between shear strain, diaphyseal curvature, cortical cross-sectional geometry should be further explored as results suggest that curvature reduces shear but changes in cortical geometry may increase shear during certain loading scenarios. Additionally, the drastic differences in strain regime between the curved and anatomical models under the loading conditions of knuckle walking were not expected. Although these differences are somewhat explained by the interaction between the moments acting on the models and the variation in

principal second moment of area between them, the moments acting on the models warrant further investigation to gain insight into which aspect of model geometry is most directly influencing the resulting strain regimes. Finally, if possible given restrictions on *in vivo* experiments involving great apes, efforts should be made to reduce the number of assumptions informing the analysis.

Significance

Applying FE modeling to questions of the form-function relationship in the hominoid clavicle has confirmed some hypotheses drawn from previous analyses of morphological variation, but also called others into question. These analyses have supported the importance of knuckle walking as a behavior that heavily loads the shoulder with high magnitudes of strain, thus impacting the remodeling of the clavicle, but results do not support knuckle walking as the main driver of *Pan* clavicular shape. Also, vertical climbing imposes relatively low magnitudes of strain onto the clavicle relative to the other modeled behaviors, suggesting this aspect of morphology affects ape clavicular shape less than originally hypothesized based on the interpretations of the data presented in Chapters 2 and 3. Importantly, the strain regimes modeled here support previous hypotheses that long bone curvature results from habitual locomotor strains (Milne, 2016; Henderson et al., 2017; Milne and Granatosky, 2021), but within this context, these results do not support a common knuckle walking origin for African great apes. Instead, they suggest the sigmoidal shape of the *Pan* and *Homo* clavicle may represent the primitive condition of the African great apes which was then remodeled to reduce diaphyseal curvature through evolution in *Gorilla* in response to high strains during knuckle walking. On the other hand, the convergence of the suspensory and knuckle walking locomotor regimes in the anatomical mode suggests that *Pan* mitigates the high strains imposed by knuckle walking and

its conflicting demands with suspension through the alteration of its internal cortical structure. To continue testing the biomechanical significance of clavicular morphological diversity in apes, further expansions of these analyses should seek to include other anatomically accurate models from taxa with different locomotor regimes and evolutionary histories from *Pan*, forming a better comparative context in which to interpret the morphology of fossil hominins.

Table 4.1. Applied bone and ligament material properties.

Material	Young's Modulus (MPa)	Poisson's Ratio	Citation
Trabecular bone	445	0.4	Rusovici et. al. 2013
Cortical bone	14,200	0.46	Rusovici et. al. 2013
Coracoclavicular ligament	9.5	-	Koh et. al. 2004

Table 4.2. Calculations for applied muscle force. Loading scenario abbreviations: KW = knuckle walking, SUS = unimanual suspension, VC = vertical climbing.

Muscle	Muscle Mass (g)	Fascicle Length (cm)	PCSA (cm^2)	Maximum Isometric Force (N)	Percent of Muscle Activation		Applied Force (N)
Anterior Deltoid	40	8.125	4.644	139.32	KW	25%	34.83
					SUS	100%	139.32
					VC	25%	34.83
Cranial Trapezius	61	7.419	7.757	232.71	KW	0%	0
					SUS	100%	232.71
					VC	10%	23.27
Clavicular Pectoralis Major	56	16.916	3.123	93.70	KW	0%	0
					SUS	10%	9.37
					VC	100%	93.70
Sternocleidomastoid	49	12.607	3.667	110.01	KW	40%	44
					SUS	40%	44
					VC	40%	44

Table 4.3. Substrate reaction forces applied to the beam, curved, and anatomical model geometries. X,Y, and Z coordinates are in mm and are the locations where the forces are applied to the model geometry.

Model	X	Y	Z	Loading Scenario	Fx (N)	Fy (N)	Fz (N)
anatomical	3.22	-4.81	123.48	Knuckle Walking	-244.6	244.6	0
	2.77	-4.74	123.71	Suspension	0	-497.49	0
	2.71	-4.49	123.97	Vertical Climbing	0	0	618.32
curved	3.81	-5.91	115.28	Knuckle Walking	-244.6	244.6	0
	2.98	-4.99	115.25	Suspension	0	-497.49	0
	3.77	-5.48	115.27	Vertical Climbing	0	0	618.32
beam	-0.88	-0.58	111.4	Knuckle Walking	-244.6	244.6	0
	-0.88	-0.58	111.94	Suspension	0	-497.49	0
	-0.88	-0.58	111.94	Vertical Climbing	0	0	618.32

Table 4.4. Reaction forces at the sternal constrained node of the beam, curved, and anatomical model geometries. X,Y, and Z coordinates are in mm and are the locations of the constrained sternal nodes for each model geometry.

Model	X	Y	Z	Loading Scenario	Fx (N)	Fy (N)	Fz (N)
anatomical	0.45	0.16	-3.60	Knuckle Walking	-527.84	40.06	-6618.39
	0.45	0.16	-3.60	Suspension	-141.61	-379.32	-2381.0
	0.45	0.16	-3.60	Vertical Climbing	-43.73	2.13	-1535.22
curved	1.86	0.97	-6.88	Knuckle Walking	-341.77	360.84	28.87
	1.86	0.97	-6.88	Suspension	-19.18	-600.17	-322.8
	1.86	0.97	-6.88	Vertical Climbing	9.74	34.9	-628.88
beam	-0.21	-0.89	-8.92	Knuckle Walking	233.92	318.83	288.89
	-0.21	-0.89	-8.92	Suspension	-259.03	-425.43	-482.37
	-0.21	-0.89	-8.92	Vertical Climbing	113.10	21.77	-542.66

Table 4.5. Muscle forces applied to the beam, curved, and anatomical model geometries. Origin centroid coordinates refer to the centroid of the applied force on the clavicle models, and insertion centroid coordinates indicate the position of the centroid of the insertion region on the humerus or cranium. AD = anterior deltoid; CPM = clavicular pectoralis major; CT = cranial trapezius; SCM = sternocleidomastoid; KW = knuckle walking; SUS = suspension; VC = vertical climbing.

Model	Muscle	Loading Scenario	Origin Centroid X	Origin Centroid Y	Origin Centroid Z	Total Applied Muscle Force	Insertion Centroid X	Insertion Centroid Y	Insertion Centroid Z	Dx (mm)	Dy (mm)	Dz (mm)	Fx (N)	Fy (N)	Fz (N)
anatomical	AD	KW	2.45	7.39	100.63	34.83	118.50	-13.52	120.55	116.05	-20.91	19.92	33.80	-6.09	5.80
anatomical	AD	SUS	2.45	7.39	100.63	139.32	15.98	-12.96	188.96	13.53	-20.35	88.33	20.57	-30.93	134.28
anatomical	AD	VC	2.45	7.39	100.63	34.83	90.95	-4.10	96.66	88.50	-11.49	-3.97	34.51	-4.48	-1.55
anatomical	CPM	SUS	7.87	-1.84	48.32	9.37	26.58	-20.89	154.10	18.71	-19.05	105.78	1.61	-1.64	9.09
anatomical	CPM	VC	7.87	-1.84	48.32	93.70	54.16	-4.67	102.70	46.29	-2.83	54.38	60.68	-3.71	71.29
anatomical	CT	SUS	-7.44	8.46	106	232.71	-22.46	80.13	104.80	-15.02	71.67	-1.20	-47.73	227.73	-3.83
anatomical	CT	VC	-7.44	8.46	106	23.27	-81.03	63.46	-24.31	-73.59	55.00	-130.31	-10.74	8.03	-19.02
anatomical	SCM	KW	-0.1	3.01	4.36	44.00	-78.50	74.50	19.40	-78.40	71.49	15.04	-32.19	29.35	6.18
anatomical	SCM	SUS	-0.1	3.01	4.36	44.00	-16.76	55.83	132.35	-16.66	52.82	127.99	-5.26	16.66	40.38
anatomical	SCM	VC	-0.1	3.01	4.36	44.00	-83.44	73.10	11.52	-83.34	70.09	7.16	-33.60	28.26	2.89
beam	AD	KW	6.53	2.7	91.67	34.83	118.50	-13.52	120.55	111.97	-16.22	28.88	33.40	-4.84	8.61
beam	AD	SUS	6.53	2.7	91.67	139.32	15.98	-12.96	188.96	9.45	-15.66	97.29	13.30	-22.03	136.92
beam	AD	VC	6.53	2.7	91.67	34.83	90.95	-4.10	96.66	84.42	-6.80	4.99	34.66	-2.79	2.05
beam	CPM	SUS	7.7	2.7	40.3	9.37	26.58	-20.89	154.10	18.88	-23.59	113.80	1.50	-1.88	9.06
beam	CPM	VC	7.7	2.7	40.3	93.70	54.16	-4.67	102.70	46.46	-7.37	62.40	55.70	-8.84	74.82
beam	CT	SUS	-5.2	6.11	91.38	232.71	-22.46	80.13	104.80	-17.26	74.02	13.42	-52.04	223.18	40.45
beam	CT	VC	-5.2	6.11	91.38	23.27	-81.03	63.46	-24.31	-75.83	57.35	-115.69	-11.78	8.91	-17.98

Table 4.5. Continued

beam	SCM	KW	-3.5	6.88	3	44.00	-78.50	74.50	19.40	-75.00	67.62	16.40	-32.26	29.08	7.05
beam	SCM	SUS	-3.5	6.88	3	44.00	-16.76	55.83	132.35	-13.26	48.95	129.35	-4.20	15.50	40.96
beam	SCM	VC	-3.5	6.88	3	44.00	-83.44	73.10	11.52	-79.94	66.22	8.52	-33.77	27.98	3.60
curved	AD	KW	0.84	4.79	91.92	34.83	118.50	-13.52	120.55	117.66	-18.31	28.63	33.46	-5.21	8.14
curved	AD	SUS	0.84	4.79	91.92	139.32	15.98	-12.96	188.96	15.14	-17.75	97.04	21.13	-24.77	135.46
curved	AD	VC	0.84	4.79	91.92	34.83	90.95	-4.10	96.66	90.11	-8.89	4.74	34.61	-3.41	1.82
curved	CPM	SUS	11.39	3.09	38.03	9.37	26.58	-20.89	154.10	15.19	-23.98	116.07	1.19	-1.88	9.10
curved	CPM	VC	11.39	3.09	38.03	93.70	54.16	-4.67	102.70	42.77	-7.76	64.67	51.42	-9.33	77.76
curved	CT	SUS	-9.44	8.85	92.91	232.71	-22.46	80.13	104.80	-13.02	71.28	11.89	-41.26	225.90	37.67
curved	CT	VC	-9.44	8.85	92.91	23.27	-81.03	63.46	-24.31	-71.59	54.61	-117.22	-11.27	8.60	-18.45
curved	SCM	KW	-1.06	3.85	3.68	44.00	-78.50	74.50	19.40	-77.44	70.65	15.72	-32.15	29.33	6.53
curved	SCM	SUS	-1.06	3.85	3.68	44.00	-16.76	55.83	132.35	-15.70	51.98	128.67	-4.95	16.38	40.54
curved	SCM	VC	-1.06	3.85	3.68	44.00	-83.44	73.10	11.52	-82.38	69.25	7.84	-33.59	28.24	3.20

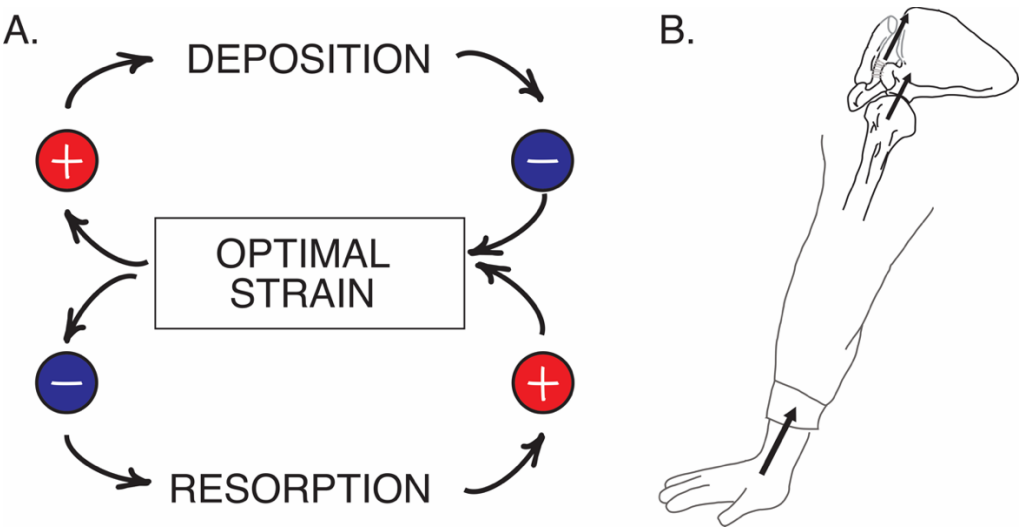

Figure 4.1. A. Feedback model of bone functional adaptation in relation to strain (Adapted from Ruff et al., 2006); B. Transfer of medial force from the substrate to humerus through to the clavicle.

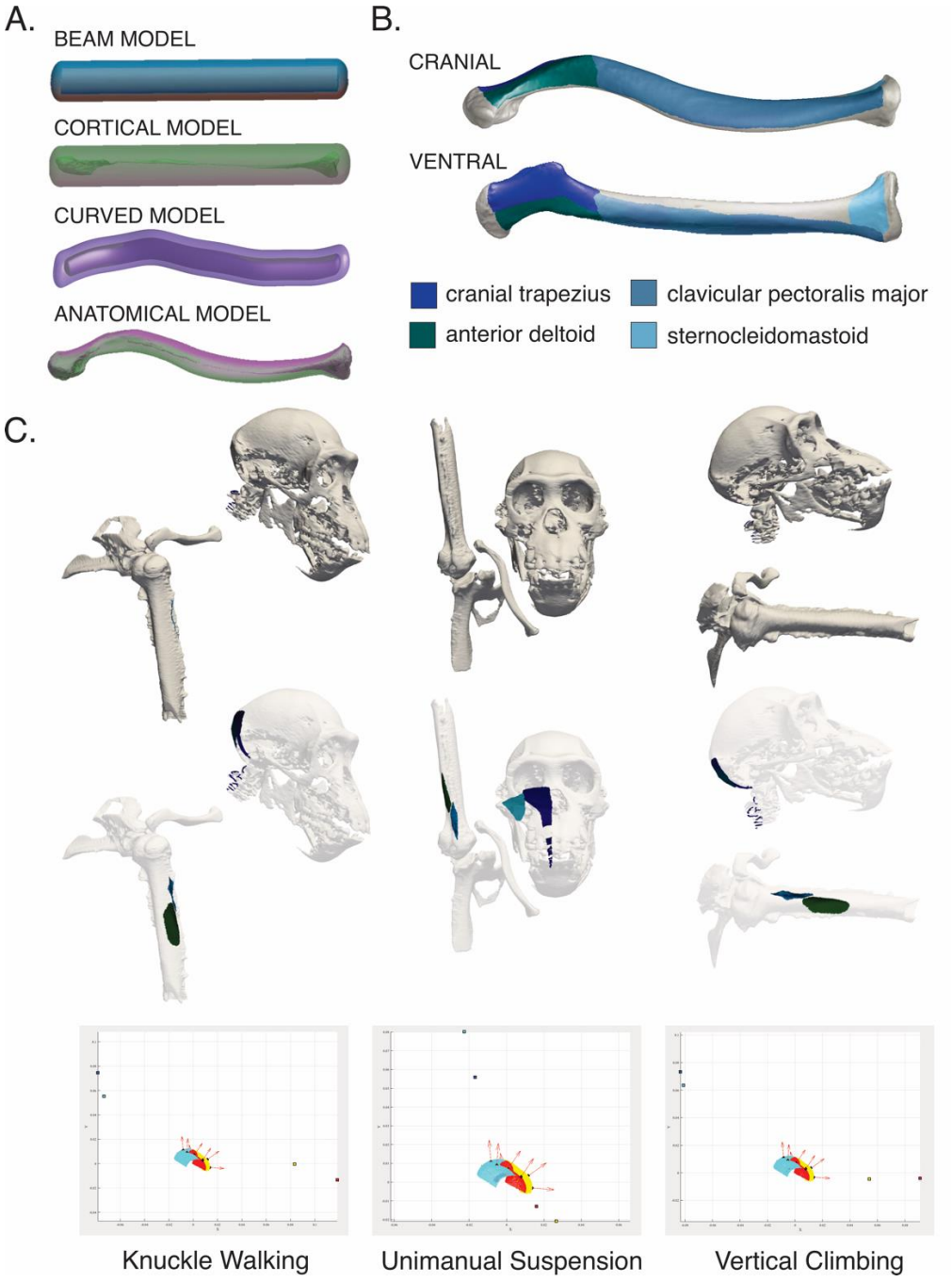

Figure 4.2. A. The four tested model geometries; B. Muscle attachment regions as mapped onto the 'anatomical' model; C. Posed models, defined muscle insertion regions, and muscle vector orientation applied for the four mapped muscles under loading conditions representing knuckle walking, unimanual suspension, and vertical climbing.

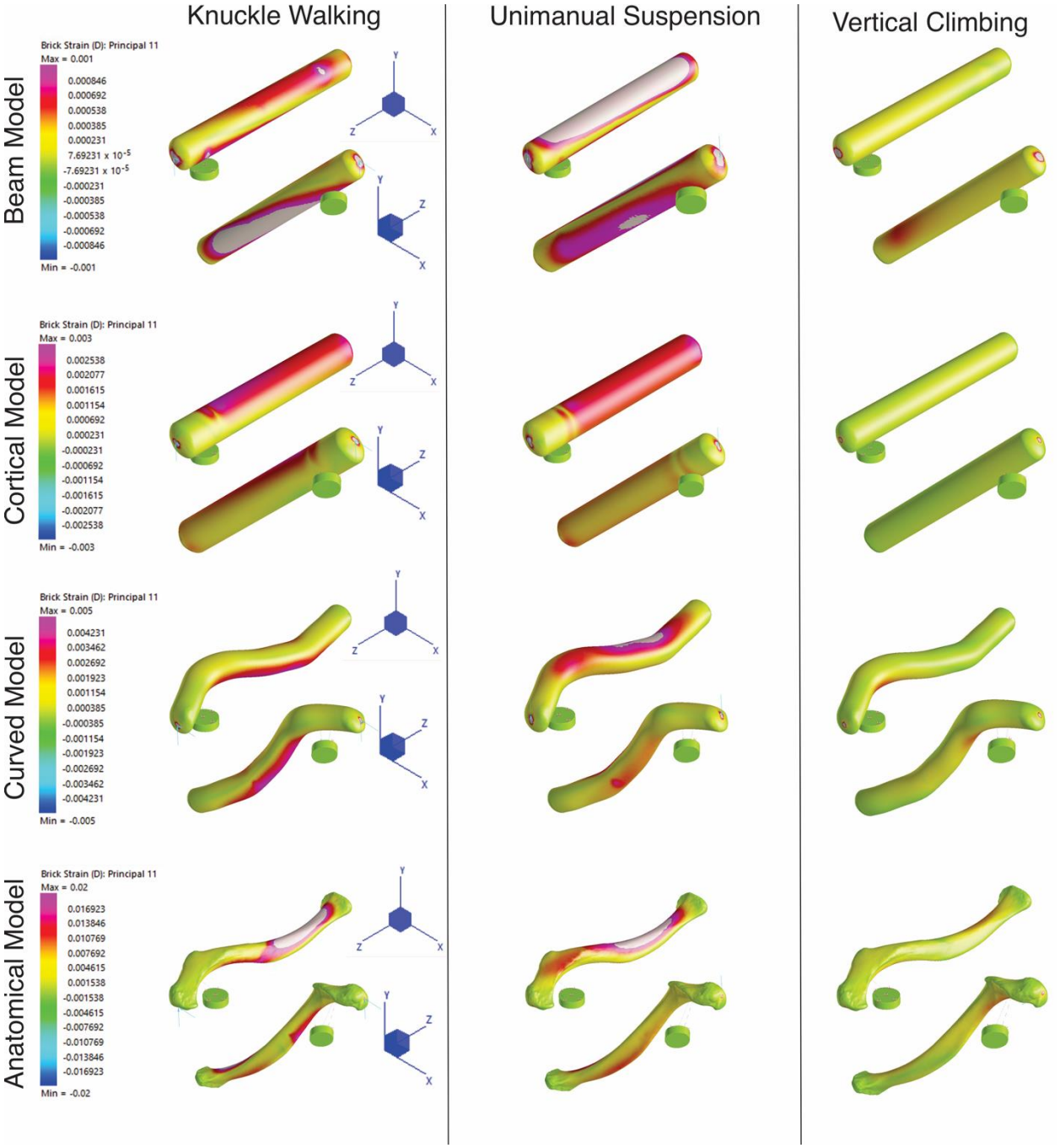

Figure 4.3. Principal tensile strain (ε1). Warmer colors represent higher tensile strain and cooler colors represent lower tensile strain. The Y axis is craniocaudal, the X axis is dorsoventral, and the Z axis is mediolateral, with the origin placed in the center of the sternal articular surface. For each visualized load case, the superior model is viewed from a cranioventral perspective, with the lateral end of the element on the left, and the medial end on the right and the inferior model is viewed from dorsocaudal with lateral on the right and medial on the left.

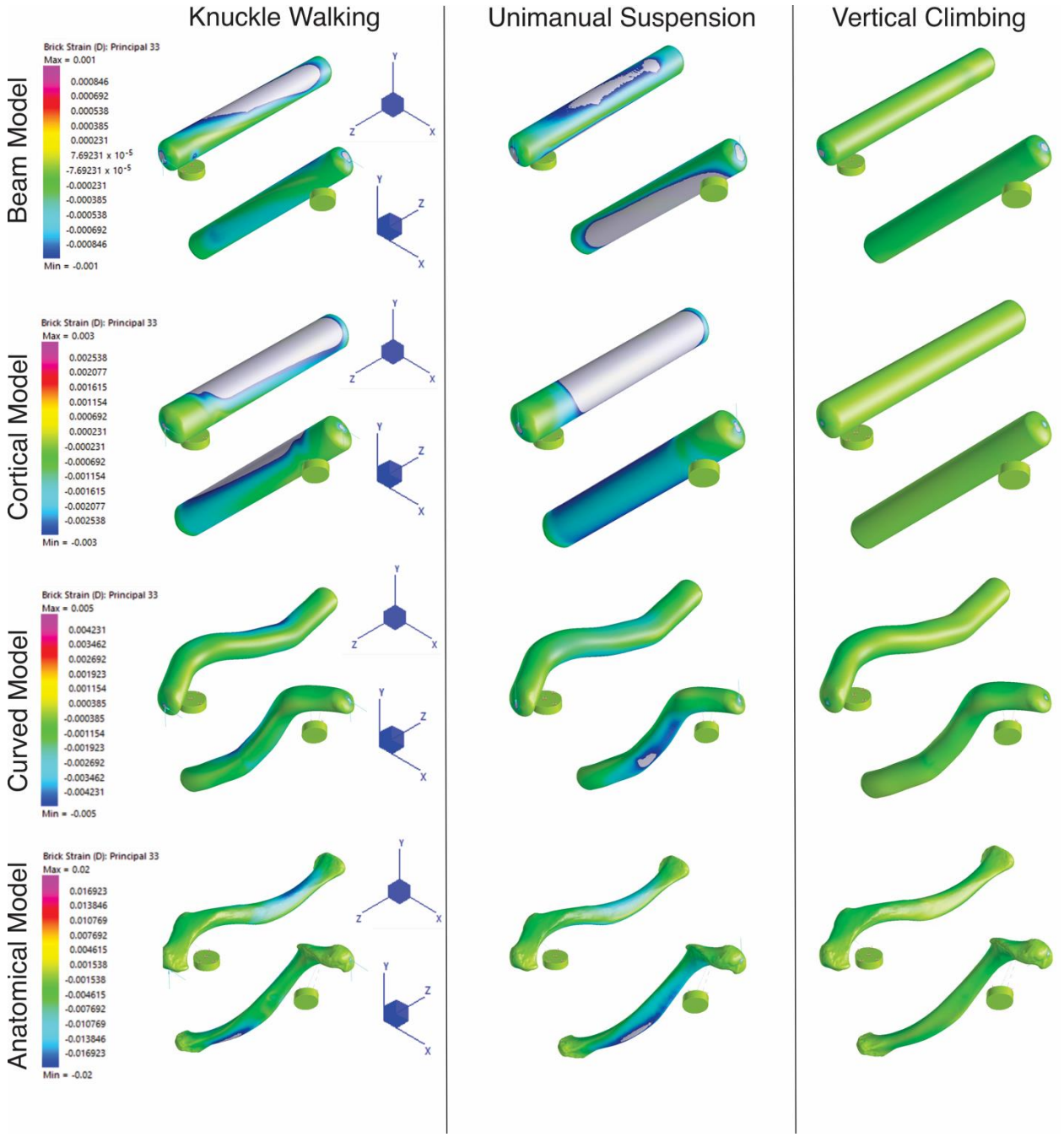

Figure 4.4. Principal compressive strain (ε3). Warmer colors represent lower compressive strain and cooler colors represent higher compressive strain. The Y axis is craniocaudal, the X axis is dorsoventral, and the Z axis is mediolateral, with the origin placed in the center of the sternal articular surface. For each visualized load case, the superior model is viewed from a cranioventral perspective, with the lateral end of the element on the left, and the medial end on the right and the inferior model is viewed from dorsocaudal with lateral on the right and medial on the left.

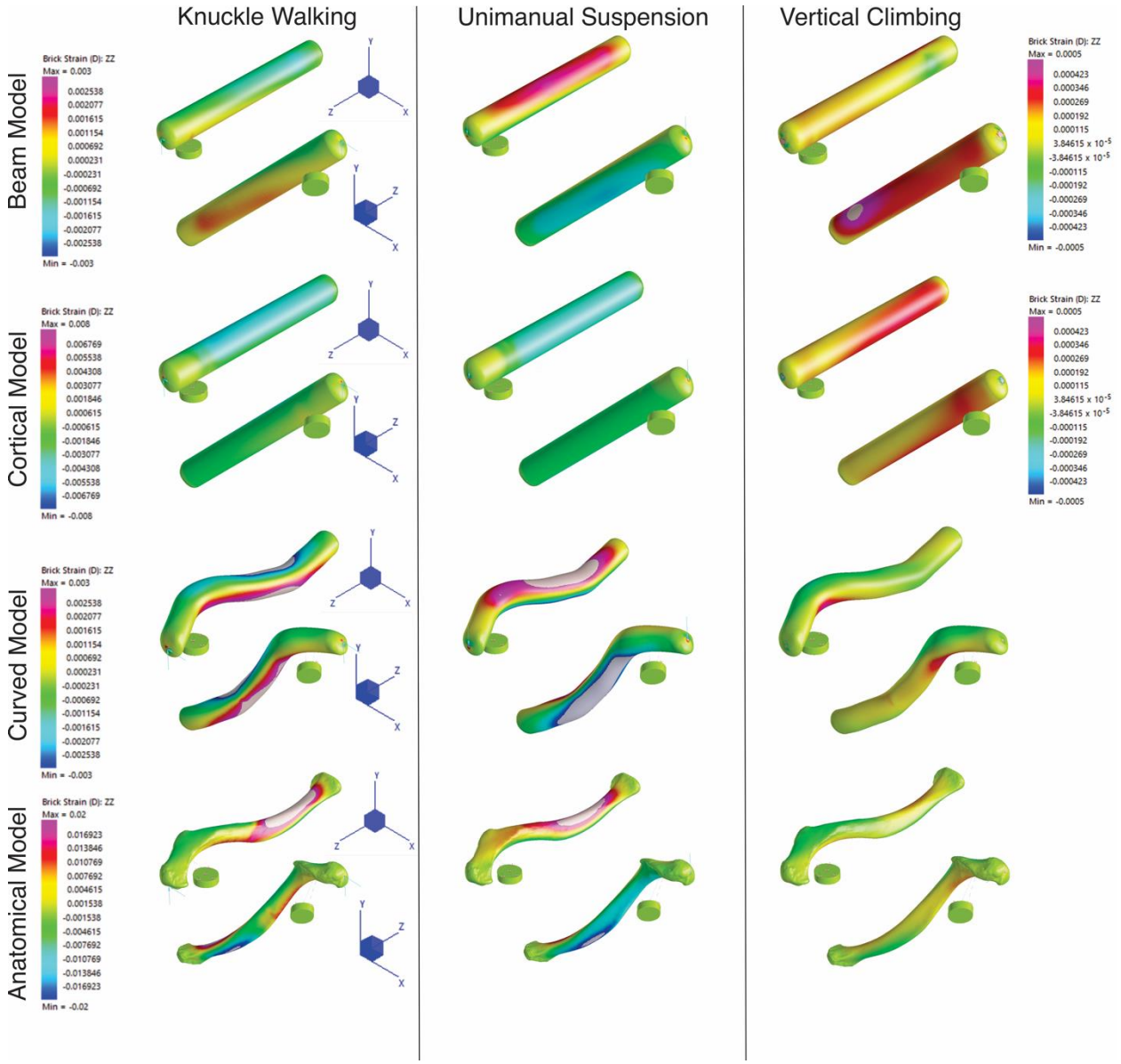

Figure 4.5. Long axis (ZZ) strain. Warmer colors represent tensile strain and cooler colors represent compressive strain. The Y axis is craniocaudal, the X axis is dorsoventral, and the Z axis is mediolateral, with the origin placed in the center of the sternal articular surface. For each visualized load case, the superior model is viewed from a cranioventral perspective, with the lateral end of the element on the left, and the medial end on the right and the inferior model is viewed from dorsocaudal with lateral on the right and medial on the left.

Figure 4.6. External shape variation in the extant hominoid clavicle. The clavicles are viewed from ventral on the left and cranial on the right. The lateral end is always on the left, and medial end on the right.

Significance

My dissertation focuses on a holistic characterization and comparison of hominoid clavicular morphology to better understand the evolution of the hominin shoulder. An ape-like shoulder persists in the hominin fossil record far past the evidence of habitual bipedality, even in hominins potentially associated with stone tool technology, leading to uncertainty and disagreement regarding how to functionally interpret the retained features. Here, I center my analyses around identifying plastic aspects of morphology both hypothesized to change through ontogeny, like clavicular curvature, and those known to remodel during life in response to mechanical forces, such as cortical cross-sectional geometry and trabecular architecture. My research endeavor aims to identify morphological features that change alongside shifts in locomotor behavior during ontogeny in living apes or those that only manifest under the loading conditions of specific behaviors like knuckle walking. Such traits can then be more concretely tied back to function to interpret the locomotor adaptations of extinct hominins. Moreover, these analyses support the utility of looking at multiple aspects of morphology in concert when trying to discern the relationship between form and function. Ultimately, the results of the four analyses combined will provide me with a robust context to interpret the presence and role or arboreality in *Australopithecus* to contribute toward addressing some of the prominent issues in paleoanthropology pertaining to locomotion.

The first chapter of this dissertation aims to address the potential for developmental plasticity in the external shape of the hominoid clavicle. Previous analyses of clavicular shape have pointed to a lack of ontogenetic change (Corrigan, 1960), but the identification of plastic traits linked to locomotion in other skeletal elements of the shoulder (Cowgill, 2007; Green and Alemseged, 2012; Barros, 2014) support the reinvestigation of shape presented here. The

primary finding is that there are no substantive changes in clavicular shape or curvature during ontogeny; sub-adult and adult extant apes exhibit approximately the same range of morphological variation. These results support previous reports on large amounts of intraspecific disparity in clavicular shape (Schultz, 1937; Ashton and Oxnard, 1964; Oxnard, 1969; Sarmiento, 1985; Berger, 1994), however, no new insight has emerged regarding the significance of this variation.

Results also importantly emphasize the similarity between modern *Pan* and *Homo* in overall clavicular shape. Despite the seemingly distinctive differences in curvature described by Voisin (2006a), both chimpanzees and modern human clavicles fall within the range of morphological variation of one another, supporting the results of Squyres and De Leon (2015). These results highlight the influence of methodology on the results, as has also been noted by Barros (2014) in their analyses of clavicular curvature. When quantifying the overall shape of the element in 3D, which allows for the consideration of diaphyseal curvature as a single datapoint, *Pan* and *Homo* greatly overlap. However, when each curvature contributing to diaphyseal shape is measured and compared independently in 2D, differences in average inferior curvature differentiates between the two taxa. This begs caution when describing the curvature of fossil hominin clavicles as *Pan*-like, or a primitive condition, as it suggests a dichotomy in shape that is not supported by many clavicular shape analyses. Instead, when looking to differentiate between *Pan*-like and *Homo*-like clavicular morphology, continued emphasis should be placed on describing localized features such as the prominence of the conoid tubercle, placement of the crest for the anterior deltoid, and shape of the acromial end as viewed cranially. Although not all of these features can be related back to upper limb function, they should be the focus of those interested in taxonomically assigning clavicular fragments to *Australopithecus* and early *Homo*.

Based on the results from Chapter 1, my second chapter began to explore the other morphological traits contributing to element structure that could be more readily tied back to the osteological remodeling occurring during an individual lifetime. Here, the results for the extant apes provide strong evidence for the presence of developmental plasticity in clavicular cross-sectional eccentricity and supports a functional link between locomotor behavior and internal bone geometry. Ontogenetic trends in *Au. afarensis* mimic those in *Pan* through adulthood and in *Gorilla* up until adolescence, thus supporting the active use of arboreality with a large adult body mass in this species. Because this increase in mid-diaphyseal eccentricity is hypothesized to result from the combination of arboreal behaviors and a large body mass, similar trends may not be seen in other fossil hominins even if they were arboreal as they have a smaller estimated body mass than *Au. afarensis* generally (Grabowski et al., 2015; Jungers et al., 2016; Garvin et al., 2017). Compared with extant apes, the estimated body mass ranges for *Au. sediba*, *Au. africanus*, and *H. naledi* suggest that higher estimates would fall within the range of variation of modern chimpanzees and orangutans, but all estimates are smaller than average modern humans and gorillas (Grabowski et al., 2015; Jungers et al., 2016; Garvin et al., 2017). In addition, KSD-VP-1/1, the representative *Au. afarensis* adult in this sample, is estimated to have been a particularly large individual based on the size of its postcranial skeleton (Haile-Selassie et al., 2010). The additional support for continued arboreality in any early hominin is important, but it is especially notable for *Au. afarensis* given the historical relevance of the species – it is often the model species to which others are compared and is therefore central to our understanding of all early hominins (Ward, 2002).

Turning to the other hominins, trends in cortical geometry that appear related to suspensory behavior in *Pongo* and *Hylobates* are also shared amongst *H. naledi* and *Au.*

afarensis. In contrast, *Au. sediba* and *Au. africanus* share traits with *Gorilla*. This does not necessarily mean that the two South African australopiths were knuckle walking, but it does suggest that they experienced considerable craniocaudal bending strain in the medial clavicle in a manner potentially similar to modern gorillas and unlike *Au. afarensis* and *H. naledi*. Further, the similarities between *Au. sediba* and *Au. africanus* may reflect the impact of the environmental context on the range of potential upper limb behaviors as at present they are both considered endemic to South Africa (Alemseged, 2023), or if the taxa are phylogenetically related (Irish et al., 2013; Alemseged, 2023), could also be reflecting genetic drift. Overall, the combination of trends in clavicular cortical cross-sectional geometry amongst the fossil hominins supports continued arboreality and implies variation in locomotor regimes. While *Australopithecus* locomotor diversity is not a novel idea, it is most commonly mentioned in the context of bipedality (Harcourt-Smith and Aiello, 2004; Hatala et al., 2023; Stamos and Alemseged, 2023); the results here suggest a similarly varied use of the upper limb during arboreal and other overhead behaviors.

Chapter 3 continues the exploration of internal bone morphology through the quantification of the trabecular structure. Previous trabecular analyses have highlighted the connection between subarticular trabecular morphology and joint orientation in frequently used postures (Barak et al., 2011; Dunmore et al., 2020), so this aspect of clavicular morphology may be able to lend insight into the position of the shoulder girdle on the thorax. Unfortunately, no such osteological correlates emerged in the sternal subarticular area of the extant taxa. Instead, in line with hypotheses for Chapter 3, the subarticular trabecular bone appears to better reflect the hypothesized range of motion commonly used at the sternoclavicular joint and the relative amount of axial force transmitted to the manubrium. The sternal subarticular trabecular bone in

Au. sediba most closely resembles *Gorilla*, suggesting the clavicle was predominantly loaded in the center of the sternal articular surface with little variation in joint orientation. This is the second developmentally plastic morphological trait that aligns the medial clavicle of *Au. sediba* with modern *Gorilla*, supporting similar regional patterns of strain on the clavicle.

The presence of trends in diaphyseal trabecular structure is unique to the clavicle. Similar whole-bone trabecular analyses of smaller long bones such as the metacarpals predominantly do not analyze the diaphysis (Griffin, 2008; Chirchir et al., 2017; Stephens et al., 2018; Dunmore et al., 2020) and those that do, have not reported any notable connection between form and function in the diaphysis (Dunmore et al., 2023). Here, there are clear concentrations of increased trabecular bone volume in regions of muscle attachment. Moreover, the extant apes differ amongst one another in a manner that suggests the increased trabecular bone volume underlying these regions is indicative of habitual muscle use. Despite the similarity in muscle attachment regions on the clavicle, this analysis interpreted alongside the context of EMG data from locomoting apes (Tuttle and Basmajian, 1978; Larson and Stern, 1986, 1987; Larson et al., 1991) suggests the diaphyseal trabecular bone is modeling in response to increased strain produced through muscle activation. The trabecular structure of *H. naledi* suggests it performed more derived behaviors, potentially related to object manipulation, than its cortical geometry was interpreted to indicate in Chapter 2. *Au. sediba* showed a combination of diaphyseal patterns in trabecular structure unlike the other fossil hominins and extant apes. It is possible that this unique structure is an artifact of taphonomic damage that was uncorrected for. Alternatively, given the small fossil hominin sample, my analysis may not be capturing the full range of trabecular variation. Thus, it is possible that *Au. sediba* does not possess unique characteristics,

but the results as interpreted in the currently available context suggest that *Au. sediba* used its upper limb in a manner at least partially unlike the other fossil hominins.

Finally, Chapter 4 allowed for the explicit testing of hypotheses related to bone strain, including predicted patterns of remodeling in response to behaviorally specific loading using Finite Element Analysis (FEA). This analysis emphasizes the importance of pushing our functional hypotheses one step further, as the inclusion of computational modeling has both supported and challenged conclusions drawn in the previous chapters. Though these analyses are ongoing and parameters are still being fine-tuned, the FEA showed that vertical climbing places relatively low magnitudes of strain on the clavicle compared to suspension and knuckle walking, suggesting that the latter two behaviors are larger drivers of clavicular bone remodeling and therefore are likely more important evolutionary selective pressures than vertical climbing. Further supporting the significance of suspension, regions identified to be under high principal strain during suspension are very similar to the regions in which cortical eccentricity is high in *Pan, Gorilla,* and *Au. afarensis*. Additionally, the sigmoidal shape characterizing the *Pan, Homo,* and fossil hominin clavicle, when interpreted in the context of the theorized feedback loop between bone remodeling and strain (Lanyon et al., 1982; Ruff et al., 2006), does not appear to be the result of knuckle walking nor appears structurally best suited for that locomotor behavior. Instead, the chimpanzee clavicle appears secondarily adapted via its cortical geometry to be equally suited to handle the strain imposed by knuckle walking and suspension. Furthermore, the knuckle walking strain regime on a sigmoidal clavicle with non-specific cortical geometry, as represented by the curved model, would eventually remodel the element to reduce diaphyseal curvature – as seen in modern *Gorilla*. These results, in combination with the morphological

features suggesting adaptation for arboreal behaviors, do not support knuckle walking as a substantial selective force acting on clavicular morphology in the hominin lineage.

Together, the results from all analyses stress the importance of continued arboreality amongst the early, habitually bipedal hominins and highlight the potential diversity in arboreal locomotor behaviors used by these taxa. This is an especially notable finding as diversity in the way bipedality is practiced is discussed at length, but there has been little to no conversation around the potential for variation in how the arboreal environment was used by hominins. No fossil individuals included show the same combined trend in cortical geometry, trabecular structure, and external shape, but the similarities and differences amongst them most likely reflect the impact of the surrounding environmental conditions on locomotor behavior. The results presented here also provide a potential explanation for why modern humans and chimpanzee clavicles are so alike despite very different uses of the upper limb and positioning of the shoulder girdle. Analyses of external shape highlight the interplay between genetic regulation and biomechanical influences in producing changes in external clavicular shape. Additionally, since the release of the upper limb from strictly locomotor demands likely decreased the magnitude of strain habitually faced by the clavicle, any modification in clavicular morphology reflective of this transition would be expected in the internal structure of the bone long before any changes in external shape. In sum, this research has provided novel insight into the nature and degree of arboreality in *Australopithecus*, supporting arboreal behaviors as a critical component of daily life and highlighting the variation in upper limb loading even between relatively contemporaneous hominins. Most importantly, the results presented here provide evolutionary context for the similarity between modern human and chimpanzee clavicular morphology, allowing for a better interpretation of the fossil material moving forward

Appendix: Details of the Extant Sample

Supplementary Table S.1. The specimen number, genus and species names, assigned age bin, side of the clavicle, sex of the specimen (if known), locality of the specimen, measurements from the clavicle, humerus, and femur, and the micro-CT scanning details of each extant specimen included in the dissertation.

Specimen	Genus	Species	Age	Side	Sex	Locality	Clavicle Length	Humeral Head	Humerus Length	Femur Length	Voxel Size (um)	Voltage (kV)	Current (uA)	Timing (ms)	Projections	Averaging	Skipped Frames	Filter
AMNH_M_0284	*Pongo*	*pygmaeus*	Inf.	R	?	Indonesia	86	25.4	195	141	49.632	100	250	250	600	3	1	0.1 mm Cu
AMNH_M_114217	*Gorilla*	*gorilla*	Inf.	R	?	West Africa	62.4	24.3	143	122	36.843	100	250	250	700	3	1	0.1 mm Cu
AMNH_M_140426	*Pongo*	*pygmaeus mori*	Adult	R	M	Indonesia	186.5	N/A	N/A	N/A	70.188	100	250	250	1450	3	1	0.2 mm Cu
AMNH_M_145600	*Gorilla*	*gorilla*	Adult	L	M	Africa	161	66.8	422	362	85.068	100	250	250	600	3	1	0.2 mm Cu
AMNH_M_147176	*Gorilla*	*gorilla*	Juv.	R	M	Africa	73.6	31.9	211	179	39.808	100	250	250	700	3	1	0.1 mm Cu
AMNH_M_150285	*Gorilla*	*gorilla*	Juv.	R	?	Africa	74.4	33.4	196.5	171	41.794	100	250	250	700	3	1	0.2 mm Cu
AMNH_M_167335	*Gorilla*	*gorilla gorilla*	Adult	R	M	Cameroon	165	69.7	454	372.5	88.391	100	250	250	600	3	1	0.2 mm Cu
AMNH_M_167336	*Gorilla*	*gorilla gorilla*	Adult	L	M	Cameroon	165	68.1	403	356	60.072	100	250	250	800	3	1	0.2 mm Cu
AMNH_M_167338	*Gorilla*	*gorilla gorilla*	Adult	R	M	Cameroon	180	73.2	454	394	60.072	100	250	250	800	3	1	0.2 mm Cu
AMNH_M_167339	*Gorilla*	*gorilla gorilla*	Adult	L	F	Cameroon	120	50	369.5	305.5	65.307	100	250	250	600	3	1	0.2 mm Cu

Table S.1. Continued

AMNH_M_167341	*Pan*	*troglodytes*	Adult	R	M	Cameroon	137.5	49.9	319.5	318	73.358	100	250	250	600	3	1	0.2 mm Cu
AMNH_M_167344	*Pan*	*troglodytes*	Adult	L	M	Cameroon	124	44.8	279	274	64.141	100	250	250	600	3	1	0.2 mm Cu
AMNH_M_167345	*Pan*	*troglodytes*	Adol.	R	?	Cameroon	103	37.1	264.5	268	55.916	100	270	250	600	3	1	0.1 mm Cu
AMNH_M_167430	*Gorilla*	*gorilla gorilla*	Adult	L	F	Cameroon	131	60.1	384	321	72.280	100	250	250	600	3	1	0.2 mm Cu
AMNH_M_170362	*Gorilla*	*gorilla gorilla*	Adol.	R	?	Cameroon	131.5	59.2	355	295	73.015	100	250	250	600	3	1	0.1 mm Cu
AMNH_M_174860	*Pan*	*troglodytes troglodytes*	Adult	R	F	Equatorial Guinea	122	46.9	300	297.5	72.28	100	250	250	600	3	1	0.2 mm Cu
AMNH_M_18010	*Pongo*	*pygmaeus*	Adol.	R	F	Indonesia	125	37.4	272	N/A	65.515	100	250	250	600	3	1	0.2 mm Cu
AMNH_M_200899	*Pongo*	*pygmaeus*	Inf.	R	F	Indonesia	82	22	185.5	134.5	45.613	100	250	250	700	3	1	0.1 mm Cu
AMNH_M_201457	*Gorilla*	*gorilla gorilla*	Inf.	R	F	Cameroon	57.1	21	115	100	32.768	100	250	250	700	3	1	none
AMNH_M_201460	*Gorilla*	*gorilla gorilla*	Adult	L	M	Cameroon	177	71.9	454	372	65.352	100	250	250	1000	3	1	0.2 mm Cu
AMNH_M_201469	*Pan*	*troglodytes troglodytes*	Adult	R	F	Cameroon	130	43.8	292	293	69.441	100	250	250	600	3	1	0.2 mm Cu
AMNH_M_201471	*Gorilla*	*gorilla gorilla*	Adult	L	M	Cameroon	151	72.5	442	377.5	82.949	100	250	250	750	3	1	0.2 mm Cu
AMNH_M_201475	*Pan*	*troglodytes schweinfurthii*	Adol.	R	?	DRC	95	38.1	225	231	52.459	100	250	250	700	3	1	0.2 mm Cu
AMNH_M_202932	*Gorilla*	*beringei graueri*	Adult	L	M	DRC	181	71.7	467.5	401	64.136	100	250	250	850	3	1	0.2 mm Cu
AMNH_M_214103	*Gorilla*	*gorilla gorilla*	Adult	R	M	DRC	149	N/A	N/A	N/A	80.066	100	250	250	600	3	1	0.2 mm Cu

Table S.1. Continued

AMNH_M_28252	*Pongo*	*pygmaeus*	Adult	R	M	Indonesia	200	46.8	380	288	64.136	100	250	250	650	3	1	0.2 mm Cu
AMNH_M_28253	*Pongo*	*pygmaeus*	Adult	R	M	Indonesia	155.5	45.6	342	N/A	60.923	100	250	250	700	3	1	0.2 mm Cu
AMNH_M_51201	*Pan*	*troglodytes schweinfurthii*	Juv.	L	F	DRC	69.3	26.3	155	159.5	39.045	100	250	250	800	3	1	0.1 mm Cu
AMNH_M_51202	*Pan*	*troglodytes schweinfurthii*	Adult	R	M	DRC	122	42.5	305	302.5	65.515	100	250	250	600	3	1	0.2 mm Cu
AMNH_M_51206	*Pan*	*troglodytes schweinfurthii*	Inf.	R	M	DRC	49.7	18.4	107	104	28.625	100	250	250	700	3	1	0.1 mm Cu
AMNH_M_51211	*Pan*	*troglodytes schweinfurthii*	Adol.	R	F	DRC	107	35.3	254	241.5	61.512	100	250	250	600	3	1	0.1 mm Cu
AMNH_M_51278	*Pan*	*troglodytes schweinfurthii*	Adult	R	M	DRC	111.5	46.4	267	N/A	63.026	100	250	250	600	3	1	0.2 mm Cu
AMNH_M_51377	*Pan*	*troglodytes schweinfurthii*	Adult	R	M	DRC	130	44.7	323.5	320	71.258	100	250	250	700	3	1	0.2 mm Cu
AMNH_M_51378	*Pan*	*troglodytes schweinfurthii*	Adol.	R	F	DRC	113.5	40.7	282.5	285.5	61.251	100	270	250	700	3	1	0.1 mm Cu
AMNH_M_51387	*Pan*	*troglodytes schweinfurthii*	Inf.	R	F	DRC	64.8	21.5	145	144	36.843	100	250	250	700	3	1	0.1 mm Cu
AMNH_M_51388	*Pan*	*troglodytes schweinfurthii*	Juv.	R	F	DRC	79.1	27.9	191	191	43.371	100	250	250	700	3	1	0.2 mm Cu
AMNH_M_51389	*Pan*	*troglodytes schweinfurthii*	Juv.	R	M	DRC	73.1	31.1	179	171	40.849	100	250	250	700	3	1	0.2 mm Cu
AMNH_M_51391	*Pan*	*troglodytes schweinfurthii*	Juv.	R	M	DRC	86	28.5	188.5	193	49.123	100	250	250	700	3	1	0.2 mm Cu
AMNH_M_51392	*Pan*	*troglodytes schweinfurthii*	Adol.	L	F	DRC	114.5	38.2	266	270	61.512	100	250	250	600	3	1	0.1 mm Cu
AMNH_M_54089	*Gorilla*	*beingei beringei*	Adult	L	M	Wild-origin, Africa	182	69.2	407	386	60.072	100	250	250	800	3	1	0.2 mm Cu

Table S.1. Continued

AMNH_M_54091	*Gorilla*	*beingei beringei*	Adult	R	F	DRC	144	53.3	342	312.5	75.949	100	250	250	600	3	1	0.2 mm Cu
AMNH_M_54092	*Gorilla*	*beingei beringei*	Adult	R	F	DRC	154	54.6	358	329	60.511	100	250	250	700	3	1	0.2 mm Cu
AMNH_M_54327	*Gorilla*	*gorilla gorilla*	Adult	L	F	Cameroon	130	57.6	345	293	73.728	100	250	250	600	3	1	0.2 mm Cu
AMNH_M_54328	*Gorilla*	*gorilla gorilla*	Juv.	R	M	Cameroon	86.5	36.3	211	186	49.595	100	250	250	700	3	1	0.1 mm Cu
AMNH_M_54329	*Gorilla*	*gorilla gorilla*	Inf.	L	M	Cameroon	48.1	19.9	109	94	27.384	100	250	250	700	3	1	none
AMNH_M_54356	*Gorilla*	*gorilla gorilla*	Adult	R	F	Cameroon	149.5	55.7	381.5	326	61.452	100	250	250	700	3	1	0.2 mm Cu
AMNH_M_86855	*Pan*	*paniscus*	Inf.	L	M	DRC	48.7	20.5	130	125	27.668	100	250	250	700	3	1	0.2 mm Cu
AMNH_M_86857	*Pan*	*paniscus*	Adult	R	F	DRC	93	34.1	248	262	50.171	100	250	250	600	3	1	0.1 mm Cu
AMNH_M_89351	*Pan*	*troglodytes verus*	Adult	L	F	Cote D'Ivoire	114	43.2	276	275.5	63.026	100	250	250	600	3	1	0.2 mm Cu
AMNH_M_89352	*Pan*	*troglodytes verus*	Adult	R	M	Cote D'Ivoire	106	34.4	261	254	61.512	100	250	250	700	3	1	0.1 mm Cu
AMNH_M_89353	*Pan*	*troglodytes verus*	Adult	R	M	Cote D'Ivoire	128	45.6	320	320	73.015	100	250	250	600	3	1	0.1 mm Cu
AMNH_M_89354	*Pan*	*troglodytes verus*	Adult	R	F	Cote D'Ivoire	110	41	288	284	61.251	100	270	250	700	3	1	0.1 mm Cu
AMNH_M_89355	*Pan*	*troglodytes verus*	Adult	R	M	Cote D'Ivoire	119	43.2	277	288.5	65.296	100	270	250	700	3	1	0.1 mm Cu
AMNH_M_89356	*Pan*	*troglodytes verus*	Inf.	L	F	Cote D'Ivoire	66.3	23.1	148	141	36.532	100	250	250	700	3	1	0.2 mm Cu
AMNH_M_89425	*Pan*	*troglodytes verus*	Inf.	L	M	Liberia	74.9	28.7	191	178	42.481	100	250	250	700	3	1	0.1 mm Cu

Table S.1. Continued

AMNH_M_89426	*Pan*	*troglodytes verus*	Adult	R	M	Liberia	109	39.5	278.5	282	59.297	100	270	250	700	3	1	0.1 mm Cu
AMNH_M_89427	*Pan*	*troglodytes verus*	Inf.	R	F	Liberia	49.9	18.9	98.5	93.5	30.094	100	250	250	700	3	1	none
AMNH_M_90191	*Pan*	*troglodytes troglodytes*	Adult	R	F	West Africa	127	41.4	293.5	289	68.772	100	250	250	600	3	1	0.2 mm Cu
AMNH_M_90194	*Gorilla*	*gorilla gorilla*	Adult	R	M	Cameroon	159	68.7	446	391	88.659	100	250	250	600	3	1	0.1 mm Cu
AMNH_M_90289	*Gorilla*	*gorilla gorilla*	Adult	R	M	Cameroon	170	66.3	400	349.5	58.176	100	250	250	800	3	1	0.2 mm Cu
AMNH_M_90290	*Gorilla*	*gorilla gorilla*	Adult	R	M	Cameroon	155	68.9	422	359	85.504	100	250	250	600	3	1	0.1 mm Cu
CMNH_HTB_0162	*Hylobates*	*concolor*	Juv.	R	?	BORNEO	56.75	16.05	167	150	29.406	100	280	250	700	3	1	0.2mm Cu
CMNH_HTB_0346	*Pan*	*troglodytes*	Adol.	R	M?	NO DATA	111.33	40.46	269	272	59.265	110	250	250	800	3	1	0.2 mm Cu
CMNH_HTB_0347	*Pan*	*troglodytes*	Adol.	R	M?	NO DATA	107.64	42.93	250	248	56.835	110	250	250	800	3	1	0.2 mm Cu
CMNH_HTB_0753	*Pan*	*troglodytes*	Inf.	R	M?	GABOON	60.02	19.34	127	127	31.455	100	250	250	700	3	1	0.2 mm Cu
CMNH_HTB_0830	*Pan*	*troglodytes*	Juv.	L	M	NO DATA	73.4	24.88	149	152	38.427	100	250	250	700	3	1	0.2 mm Cu
CMNH_HTB_0880	*Pan*	*troglodytes*	Juv.	R	F	FRENCH CONGO	77.26	27.63	189	157	34.561	100	250	250	700	3	1	0.2 mm Cu
CMNH_HTB_1024	*Pongo*	*pygmaeus*	Juv.	R	?	SUMATRA	107.82	28.96	235		55.927	100	250	250	700	3	1	0.2 mm Cu
CMNH_HTB_1030	*Pongo*	*pygmaeus*	Adult	R	F	PONTIANAK, SUMATRA	159	39.4	316	246	83.387	100	250	250	650	3	1	0.2mm Cu
CMNH_HTB_1055	*Pongo*	*pygmaeus*	Adult	R	F ?	PONTIANAK, SUMATRA	157	42.43	306	241	79.883	100	250	250	650	3	1	0.2mm Cu
CMNH_HTB_1168	*Pongo*	*pygmaeus*	Adult	L	F	SUMATRA	154	44.87	320	248.5	80.778	100	250	250	650	3	1	0.2mm Cu

Table S.1. Continued

CMNH_HTB_1169	*Pongo*	*pygmaeus*	Adol.	R	M?	SUMATRA	116.54	37.16	261		61.732	100	250	250	700	3	1	0.2 mm Cu
CMNH_HTB_1176	*Pan*	*troglodytes*	Inf.	R	?	FRENCH WEST AFRICA	63.24	25.31	159	161	35.74	100	250	250	700	3	1	0.2 mm Cu
CMNH_HTB_1423	*Gorilla*	*gorilla*	Adult	R	F	EBOLWA, CAMEROON	146	58.24	398	323	77.881	100	250	250	650	3	1	0.2mm Cu
CMNH_HTB_1424	*Gorilla*	*gorilla*	Juv.	R	F?	EBOLWA, CAMEROON	86.09	36.05	238	235	49.198	100	250	250	700	3	1	0.2 mm Cu
CMNH_HTB_1442	*Pongo*	*pygmaeus*	Inf.	R	M	SUMATRA	77.12	22.35	172		41.4	100	250	250	700	3	1	0.2 mm Cu
CMNH_HTB_1704	*Gorilla*	*gorilla*	Adult	R	F	EBOLWA, CAMEROON	128	54.21	375.5	316	70.214	100	250	250	650	3	1	0.2mm Cu
CMNH_HTB_1716	*Pan*	*troglodytes*	Juv.	L	F	EBOLWA, CAMEROON	87.66	33.6	222	186	50.727	100	300	500	850	3	1	0.2mm Cu
CMNH_HTB_1718	*Pan*	*troglodytes*	Adult	R	M	EBOLWA, CAMEROON	129.34	48.9	300	301	67.884	100	250	250	650	3	1	0.2mm Cu
CMNH_HTB_1719	*Pan*	*troglodytes*	Adult	R	F	EBOLWA, CAMEROON	129.4	43.88	288.75	295.5	67.241	100	250	250	700	3	1	0.2mm Cu
CMNH_HTB_1720	*Pan*	*troglodytes*	Adult	R	F	EBOLWA, CAMEROON	120.9	42.54	294	295.5	64.805	100	250	250	700	3	1	0.2mm Cu
CMNH_HTB_1721	*Pan*	*troglodytes*	Adult	R	F	EBOLWA, CAMEROON	120.9	39.85	271	275	62.834	100	250	250	700	3	1	0.2mm Cu
CMNH_HTB_1722	*Pan*	*troglodytes*	Adult	R	M	EBOLWA, CAMEROON	137.5	46.37	320	307.5	74.049	100	250	250	650	3	1	0.2mm Cu
CMNH_HTB_1724	*Pan*	*troglodytes*	Adult	R	F	EBOLWA, CAMEROON	130.5	44.42	314	303.5	68.875	100	250	250	700	3	1	0.2mm Cu
CMNH_HTB_1725	*Gorilla*	*gorilla*	Adult	R	F	EBOLWA, CAMEROON	134	52.9	342.5	315.5	70.775	100	250	250	700	3	1	0.2mm Cu
CMNH_HTB_1727	*Gorilla*	*gorilla*	Juv.	R	F	EBOLWA, CAMEROON	100.42	47.96	294.5	252	53.926	100	250	250	800	3	1	0.2 mm Cu
CMNH_HTB_1729	*Gorilla*	*gorilla*	Adult	R	M	EBOLWA, CAMEROON	170.5	70.77	405.5	355	62.141	100	250	250	1000	3	1	0.2mm Cu
CMNH_HTB_1730	*Gorilla*	*gorilla*	Adult	R	M	EBOLWA, CAMEROON	179	71.98	439.5	367.5	62.141	100	250	250	1000	3	1	0.2mm Cu
CMNH_HTB_1777	*Pan*	*troglodytes*	Adol.	R	M	EBOLWA, CAMEROON	111.5	41.08	271	267	59.852	110	250	250	800	3	1	0.2 mm Cu
CMNH_HTB_1783	*Gorilla*	*gorilla*	Adol.	R	F	EBOLWA, CAMEROON	108.55	43.83	303	267	58.889	110	250	250	800	3	1	0.2 mm Cu

Table S.1. Continued

CMNH_HTB_1798	*Gorilla*	*gorilla*	Adult	R	F	EBOLWA, CAMEROON	130	53.44	366	304.5	68.056	100	250	250	650	3	1	0.2mm Cu
CMNH_HTB_1799	*Gorilla*	*gorilla*	Inf.	R	?	EBOLWA, CAMEROON	71.97	30.09	193.09	174.5	38.793	100	250	250	700	3	1	0.2mm Cu
CMNH_HTB_1800	*Pan*	*troglodytes*	Adol.	R	F	EBOLWA, CAMEROON	119.64	45.4	280	257	54.518	100	250	250	700	3	1	0.2 mm Cu
CMNH_HTB_1806	*Gorilla*	*gorilla*	Adult	R	F	EBOLWA, CAMEROON	138.5	56.95	376	308.5	72.242	100	250	250	650	3	1	0.2mm Cu
CMNH_HTB_1843	*Pan*	*troglodytes*	Adult	R	F	EBOLWA, CAMEROON	129	44.62	314	299	67.938	100	250	250	700	3	1	0.2mm Cu
CMNH_HTB_1844	*Gorilla*	*gorilla*	Juv.	R	M?	EBOLWA, CAMEROON	115.28	53.49	319.5	283	61.938	110	250	250	800	3	1	0.2 mm Cu
CMNH_HTB_1845	*Gorilla*	*gorilla*	Adol.	R	M	EBOLWA, CAMEROON	122.67	49.34	326.5	284	64.945	100	250	250	700	3	1	0.2 mm Cu
CMNH_HTB_1848	*Pan*	*troglodytes*	Inf.	L	F?	EBOLWA, CAMEROON	67.58	25.33	160	117	31.776	100	250	250	700	3	1	0.2mm Cu
CMNH_HTB_1854	*Gorilla*	*gorilla*	Adult	R	F	EBOLWA, CAMEROON	146.5	57.6	400	331	77.428	100	250	250	650	3	1	0.2mm Cu
CMNH_HTB_1855	*Pan*	*troglodytes*	Adol.	R	M	EBOLWA, CAMEROON	96.69	37.5	241.25	285	63.681	110	250	250	800	3	1	0.2 mm Cu
CMNH_HTB_1857	*Gorilla*	*gorilla*	Adult	R	M	EBOLWA, CAMEROON	170	71.92	434	374	62.141	100	250	250	1000	3	1	0.2mm Cu
CMNH_HTB_1858	*Gorilla*	*gorilla*	Inf.	L	?	EBOLWA, CAMEROON	72.85	28.64	188	159.5	38.793	100	250	250	800	3	1	0.2mm Cu
CMNH_HTB_1731	*Gorilla*	*gorilla*	Adult	R	M	EBOLWA, CAMEROON	178	69.21	435	373.5	70.57	100	250	250	1000	3	1	0.2mm Cu
CMNH_HTB_1732	*Gorilla*	*gorilla*	Adult	R	M	EBOLWA, CAMEROON	157	72.83	428	375	63.229	100	250	250	900	3	1	0.2mm Cu
CMNH_HTB_1733	*Gorilla*	*gorilla*	Adult	R	M	EBOLWA, CAMEROON	175	75.82	462	390	62.141	100	250	250	1000	3	1	0.2mm Cu
CMNH_HTB_1734	*Gorilla*	*gorilla*	Adol.	R	M	EBOLWA, CAMEROON	126.98	55.01	334	291.25	69.887	100	250	250	700	3	1	0.2 mm Cu
CMNH_HTB_1738	*Pan*	*troglodytes*	Adult	R	M	EBOLWA, CAMEROON	140.5	48.1	308	304.5	73.009	100	250	250	650	3	1	0.2mm Cu
CMNH_HTB_1744	*Pan*	*troglodytes*	Adult	R	F	EBOLWA, CAMEROON	117.7	43.75	289.5	295	63.107	100	250	250	650	3	1	0.2mm Cu
CMNH_HTB_1753	*Gorilla*	*gorilla*	Juv.	R	F	EBOLWA, CAMEROON	109.6	43.17	298.5	259.5	57.978	100	250	250	700	3	1	0.2 mm Cu

Table S.1. Continued

CMNH_HTB_1756	*Gorilla*	*gorilla*	Adult	R	F	EBOLWA, CAMEROON	130.5	54.25	354	290	69.045	100	250	250	650	3	1	0.2mm Cu
CMNH_HTB_1757	*Pan*	*troglodytes*	Juv.	R	F	EBOLWA, CAMEROON	102.24	35.41	255.25	221	45.907	100	250	250	600	3	1	0.2mm Cu
CMNH_HTB_1758	*Pan*	*troglodytes*	Adult	R	M	EBOLWA, CAMEROON	112.7	45.35	317.5	314	60.106	100	250	250	700	3	1	0.2mm Cu
CMNH_HTB_1760	*Gorilla*	*gorilla*	Juv.	R	F?	EBOLWA, CAMEROON	97.3	32.78	226	202	50.732	110	250	250	800	3	1	0.2 mm Cu
CMNH_HTB_1771	*Pan*	*troglodytes*	Adol.	R	F?	EBOLWA, CAMEROON	91.07	33.43	227	224.5	47.05	100	250	250	700	3	1	0.2 mm Cu
CMNH_HTB_1772	*Gorilla*	*gorilla*	Inf.	R	?	EBOLWA, CAMEROON	74.71	25.99	166.12	139	40.334	100	250	250	700	3	1	0.2mm Cu
CMNH_HTB_1773	*Pan*	*troglodytes*	Juv.	R	F?	EBOLWA, CAMEROON	92.04	34.95	223	229	48.925	100	250	250	700	3	1	0.2 mm Cu
CMNH_HTB_1859	*Gorilla*	*gorilla*	Adult	R	M	EBOLWA, CAMEROON	165	74.41	450.5	375.5	62.141	100	250	250	1000	3	1	0.2mm Cu
CMNH_HTB_1860	*Gorilla*	*gorilla*	Adol.	R	M	EBOLWA, CAMEROON	128.11	55.56	357.5	319	68.712	100	250	250	700	3	1	0.2 mm Cu
CMNH_HTB_1880	*Pan*	*troglodytes*	Adult	R	F	EBOLWA, CAMEROON	131	49.43	295.5	305.5	69.176	100	250	250	700	3	1	0.2mm Cu
CMNH_HTB_1881	*Pan*	*troglodytes*	Juv.	R	F	EBOLWA, CAMEROON	59.57	19.09	122	231	55.728	100	320	500	700	3	1	0.2mm Cu
CMNH_HTB_1928	*Gorilla*	*gorilla*	Adol.	R	F	ABONG MBONG, FRENCH CAMEROONS	125.25	54.98	354	309.5	66.979	100	250	250	700	3	1	0.2 mm Cu
CMNH_HTB_1935	*Gorilla*	*gorilla*	Adol.	R	F?	ABONG MBONG, FRENCH CAMEROONS	115.15	57.05	361	316.5	64.394	110	250	250	800	3	1	0.2 mm Cu
CMNH_HTB_2026	*Pan*	*troglodytes*	Adult	R	M	EBOLWA, CAMEROON	137	50.6	305	304	68.875	100	250	250	700	3	1	0.2mm Cu
CMNH_HTB_2747	*Pan*	*troglodytes*	Adult	R	M	ABONG MBONG, FRENCH CAMEROONS	133	45.54	294	287	69.236	100	250	250	700	3	1	0.2mm Cu
CMNH_HTB_2822	*Gorilla*	*gorilla*	Juv.	R	M?	ABONG MBONG, FRENCH CAMEROONS	101.62	46.74	293	252	56.45	110	250	250	800	3	1	0.2 mm Cu

Table S.1. Continued

CMNH_HTB_3540	*Pan*	*troglodytes*	Juv.	R	M?	ABONG MBONG, DJAPOSTEN, CAMEROONS, WEST A	81.97	31.8	195	201	42.909	100	250	250	700	3	1	0.2 mm Cu
CMNH_HTB_3552	*Pan*	*troglodytes*	Adult	R	M	ABONG MBONG, DJAPOSTEN, CAMEROONS, WEST A	138.5	49.15	282	290	73.156	100	250	250	700	3	1	0.2mm Cu
CMNH_HTB_3553	*Pan*	*troglodytes*	Adol.	R	M?	ABONG MBONG, DJAPOSTEN, CAMEROONS, WEST A	107.93	39.77	253	263	57.559	110	250	250	800	3	1	0.2 mm Cu
CMNH_HTB_3881	*Hylobates*	*lar*	Adult	R	M	CHAMPE, CHIENGMSIAM	88.8	21.46	256	212	48.381	100	250	250	700	3	1	0.2mm Cu
CMNH_HTB_3882	*Hylobates*	*lar*	Adol.	R	M	CHAMPE, CHIENGMSIAM	62.31	17.63	192.5	170	32.749	100	280	250	600	3	1	0.2mm Cu
CMNH_HTB_3883	*Hylobates*	*lar*	Adult	R	M	CHAMPE, CHIENGMSIAM SIAM	89	21.77	240.5	219	47.099	100	250	250	700	3	1	0.2mm Cu
CMNH_HTB_3884	*Hylobates*	*lar*	Adult	R	M	CHAMPE, CHIENGMSIAM SIAM	79.6	17.88	216	192	43.84	100	250	250	700	3	1	0.2mm Cu
CMNH_HTB_3886	*Hylobates*	*lar*	Adult	R	M	CHAMPE, CHIENGMSIAM	90.8	21.6	250	220	48.228	100	250	250	750	3	1	0.2mm Cu
CMNH_HTB_3887	*Hylobates*	*lar*	Adult	R	M	CHAMPE, CHIENGMSIAM	92.3	21.9	247	205	50.595	100	250	250	750	3	1	0.2mm Cu
CMNH_HTB_3888	*Hylobates*	*lar*	Adult	R	M	CHAMPE, CHIENGMSIAM	87.83	20.89	235	199	48.12	100	250	250	850	3	1	0.2mm Cu
CMNH_HTB_3891	*Hylobates*	*lar*	Adol.	R	M	CHAMPE, CHIENGMSIAM	72.16	19.74	210.25	177.6	39.568	100	280	250	600	3	1	0.2mm Cu
CMNH_HTB_3899	*Hylobates*	*lar*	Adult	R	F ?	CHAMPE, CHIENGMSIAM	89.22	21.34	221.5	202	48.12	100	250	250	700	3	1	0.2mm Cu
CMNH_HTB_3900	*Hylobates*	*lar*	Adult	R	F ?	CHAMPE, CHIENGMSIAM	89.53	21.48	247	218	48.12	100	250	250	724	3	1	0.2mm Cu

Table S.1. Continued

CMNH_HTB_3901	*Hylobates*	*lar*	Adult	R	F ?	CHAMPE, CHIENGMSIAM	97.31	21.91	248.5	225	53.1	100	250	250	724	3	1	0.2mm Cu
CMNH_HTB_3902	*Hylobates*	*lar*	Adult	R	F ?	CHAMPE, CHIENGMSIAM	79.25	19.4	226.5	195	43.877	100	250	250	600	3	1	0.2mm Cu
CMNH_HTB_3903	*Hylobates*	*lar*	Adult	R	F ?	CHAMPE, CHIENGMSIAM	88.6	21.23	235	203.5	48.371	100	250	250	700	3	1	0.2mm Cu
CMNH_HTB_3912	*Hylobates*	*lar*	Adult	R	F	CHAMPE, CHIENGMSIAM	82.55	20.34	236	207.5	44.69	100	250	250	700	3	1	0.2mm Cu
CMNH_HTH_0128	*Homo*	*sapiens*	Adult	R	F	N/A	136.49	47.25	296	421	71.722	100	250	250	700	3	1	0.2 mm Cu
CMNH_HTH_0291	*Homo*	*sapiens*	Adult	R	M	N/A	149.57	51.55	330	448	78.459	100	250	250	600	3	1	0.2mm Cu
CMNH_HTH_0315	*Homo*	*sapiens*	Adult	R	F	N/A	131.16	46.33	277	405	71.722	100	250	250	800	3	1	0.2 mm Cu
CMNH_HTH_0404	*Homo*	*sapiens*	Juv.	R	M	N/A	112.4	39.67	270.5	387.5	61.787	100	250	250	600	3	1	0.2mm Cu
CMNH_HTH_0548	*Homo*	*sapiens*	Adol.	R	M	N/A	146.65	53.28	354	512.5	77.62	100	250	250	650	3	1	0.2mm Cu
CMNH_HTH_0569	*Homo*	*sapiens*	Adult	R	M	N/A	143.84	52.53	316.5	448	75.66	100	250	250	600	3	1	0.2mm Cu
CMNH_HTH_0576	*Homo*	*sapiens*	Adol.	R	F	N/A	138.02	44.7	299.75	440.5	72.857	100	250	250	600	3	1	0.2mm Cu
CMNH_HTH_0589	*Homo*	*sapiens*	Adult	R	F	N/A	139.04	46.76	312	421	73.542	100	250	250	700	3	1	0.2 mm Cu
CMNH_HTH_0632	*Homo*	*sapiens*	Juv.	R	F	N/A	93.04	32.04	199	281	48.249	100	250	250	600	3	1	0.2mm Cu
CMNH_HTH_0673	*Homo*	*sapiens*	Adult	R	F	N/A	138.37	51.45	311	435.5	72.393	100	250	250	700	3	1	0.2 mm Cu
CMNH_HTH_0846	*Homo*	*sapiens*	Adult	R	M	N/A	163.19	53.26	330.5	472	84.884	100	250	250	600	3	1	0.2mm Cu
CMNH_HTH_0872	*Homo*	*sapiens*	Juv.	R	F	N/A	106.54	38.4	222	345	55.605	100	250	250	600	3	1	0.2mm Cu
CMNH_HTH_0933	*Homo*	*sapiens*	Adult	R	F	N/A	141.69	46.9	302	442	74.839	100	250	250	600	3	1	0.2mm Cu
CMNH_HTH_1070	*Homo*	*sapiens*	Adult	R	F	N/A	136.06	43.82	302.75	431.5	71.722	100	250	250	700	3	1	0.2 mm Cu

Table S.1. Continued

CMNH_HTH_1074	*Homo*	*sapiens*	Inf.	R	F	N/A	90.89	31.68	206	299.5	47.597	100	250	250	600	3	1	0.2mm Cu
CMNH_HTH_1115	*Homo*	*sapiens*	Inf.	R	F	N/A	81.78	25.2	164.75	218	42.718	100	250	250	600	3	1	0.2mm Cu
CMNH_HTH_1115	*Homo*	*sapiens*	Inf.	R	F	N/A	81.78	25.2	164.75	218	42.728	100	250	250	600	3	1	0.2mm Cu
CMNH_HTH_1208	*Homo*	*sapiens*	Adult	R	F	N/A	135.35	44.61	291	429	71.44	100	250	250	900	3	1	0.2 mm Cu
CMNH_HTH_1232	*Homo*	*sapiens*	Adol.	L	F	N/A	125.23	41.01	298	446	65.341	100	250	250	700	3	1	0.2mm Cu
CMNH_HTH_1271	*Homo*	*sapiens*	Adult	R	M	N/A	153.91	51.44	321	394	79.915	100	250	250	600	3	1	0.2mm Cu
CMNH_HTH_1385	*Homo*	*sapiens*	Inf.	R	M	N/A	64.3	21.1	121.75	162	33.434	100	250	250	700	3	1	0.2mm Cu
CMNH_HTH_1557	*Homo*	*sapiens*	Inf.	R	M	N/A	74.38	27.35	121	155.5	38.89	100	250	250	700	3	1	0.2mm Cu
CMNH_HTH_1589	*Homo*	*sapiens*	Adol.	R	M	N/A	107.27	45.93	267	411	57.213	100	250	250	700	3	1	0.2mm Cu
CMNH_HTH_1784	*Homo*	*sapiens*	Inf.	R	M	N/A	95.07	33.62	203	267	49.348	100	250	250	600	3	1	0.2mm Cu
CMNH_HTH_1785	*Homo*	*sapiens*	Adult	R	F	N/A	136.06	47.48	308	435	71.722	100	250	250	700	3	1	0.2 mm Cu
CMNH_HTH_1834	*Homo*	*sapiens*	Juv.	R	M	N/A	102.91	34.24	232	332	53.271	100	250	250	600	3	1	0.2mm Cu
CMNH_HTH_1876	*Homo*	*sapiens*	Adult	R	M	N/A	142.2	55.34	324	455.5	75.66	100	250	250	600	3	1	0.2mm Cu
CMNH_HTH_1949	*Homo*	*sapiens*	Adol.	R	F	N/A	131.88	44.27	302.5	454.75	68.791	100	250	250	600	3	1	0.2mm Cu
CMNH_HTH_2041	*Homo*	*sapiens*	Adult	R	F	N/A	155.32	45.57	327	489	81.456	100	250	250	600	3	1	0.2mm Cu
CMNH_HTH_2091	*Homo*	*sapiens*	Adult	R	M	N/A	144.45	54.38	299.5	412	75.641	100	250	250	600	3	1	0.2mm Cu
CMNH_HTH_2115	*Homo*	*sapiens*	Adult	R	F	N/A	152.87	45.54	346.5	481.5	78.133	100	250	250	600	3	1	0.2mm Cu
CMNH_HTH_2135	*Homo*	*sapiens*	Juv.	R	F	N/A	139.09	41.62	289	413.25	71.767	100	250	250	600	3	1	0.2mm Cu
CMNH_HTH_2562	*Homo*	*sapiens*	Adult	R	M	N/A	169.73	54.79	339.5	481.25	89.203	100	250	250	600	3	1	0.2mm Cu
CMNH_HTH_2659	*Homo*	*sapiens*	Adult	R	M	N/A	152.6	54.04	327	459	82.057	100	250	250	700	3	1	0.2 mm Cu

Table S.1. Continued

CMNH_HTH_2714	*Homo*	*sapiens*	Inf.	R	F	N/A	60.74	18.75	102	128.5	31.583	100	250	250	600	3	1	0.2mm Cu
CMNH_HTH_2829	*Homo*	*sapiens*	Adult	R	M	N/A	157.18	51.98	352	513	83.062	100	250	250	600	3	1	0.2mm Cu
CMNH_HTH_3049	*Homo*	*sapiens*	Adult	R	M	N/A	137.22	46.24	309.5	443	71.722	100	250	250	700	3	1	0.2 mm Cu
CMNH_HTH_3112	*Homo*	*sapiens*	Adol.	R	M	N/A	129.64	45.58	268	371.5	68.964	100	250	250	600	3	1	0.2mm Cu
FMNH_M_127164	*Pan*	*troglodytes*	Inf.	R	N/A	Wild-origin, Africa	62.3	N/A	N/A	N/A	34.677	100	250	250	700	3	1	0.1 mm Cu
FMNH_M_26065	*Gorilla*	*gorilla beringei*	Adult	R	N/A	Wild-origin, Africa	187.1	N/A	N/A	N/A	69.109	100	250	250	900	3	1	0.2 mm Cu
FMNH_M_27529	*Pan*	*troglodytes schweinfurthii*	Adult	R	N/A	Wild-origin, Africa	121.4	N/A	N/A	N/A	65.84	100	250	250	600	3	1	0.2 mm Cu
FMNH_M_27542	*Pan*	*troglodytes*	Adult	R	N/A	Wild-origin, Africa	119	N/A	N/A	N/A	64.997	100	250	250	700	3	1	0.2 mm Cu
FMNH_M_27551	*Gorilla*	*gorilla beringei*	Adult	R	N/A	Wild-origin, Africa	170.9	N/A	N/A	N/A	73.4	100	250	250	600	3	1	0.2 mm Cu
FMNH_M_27552	*Pan*	*troglodytes*	Adult	R	N/A	Wild-origin, Africa	126	N/A	N/A	N/A	69.107	100	250	250	600	3	1	0.2 mm Cu
FMNH_M_33532	*Pongo*	*pygmaeus pygmaeus*	Adol.	R	N/A	Wild-origin, Africa	126.89	N/A	N/A	N/A	70.129	100	250	250	800	3	1	0.2 mm Cu
FMNH_M_33533	*Pongo*	*pygmaeus pygmaeus*	Adult	L	N/A	Wild-origin, Africa	166.46	N/A	N/A	N/A	73.4	100	250	250	700	3	1	0.2 mm Cu
FMNH_M_33534	*Pongo*	*pygmaeus pygmaeus*	Juv.	R	N/A	Wild-origin, Africa	64.95	N/A	N/A	N/A	37.28	100	250	250	700	3	1	0.1 mm Cu
FMNH_M_33535	*Pongo*	*pygmaeus pygmaeus*	Adult	L	N/A	Wild-origin, Africa	177.34	N/A	N/A	N/A	73.4	100	250	250	700	3	1	0.2 mm Cu
FMNH_M_33536	*Pongo*	*pygmaeus pygmaeus*	Adult	R	N/A	Wild-origin, Africa	159.62	N/A	N/A	N/A	64.04	100	250	250	600	3	1	0.2 mm Cu
FMNH_M_34905	*Pan*	*troglodytes*	Juv.	R	N/A	Wild-origin, Africa	81.9	N/A	N/A	N/A	47.248	100	250	250	600	3	1	0.1 mm Cu

Table S.1. Continued

FMNH_M_42582	*Pan*	*troglodytes troglodytes*	Inf.	R	N/A	Wild-origin, Africa	68.3	N/A	N/A	N/A	52.119	100	250	250	1800	3	1	0.1 mm Cu
FMNH_M_42582	*Pan*	*troglodytes troglodytes*	Inf.	R	N/A	Wild-origin, Africa	68.3	N/A	N/A	N/A	71.79	100	250	250	2024	3	1	0.1 mm Cu
FMNH_M_42692	*Pan*	*troglodytes verus*	Juv.	R	N/A	Wild-origin, Africa	82.3	N/A	N/A	N/A	54.356	100	250	250	1800	3	1	0.2 mm Cu
FMNH_M_46497	*Hylobates*	*concolor gabriellae*	Adult	R	N/A	Wild-origin, Asia	90.6	N/A	N/A	N/A	47.624	120	250	333	1400	3	1	none
FMNH_M_46498	*Hylobates*	*concolor gabriellae*	Adult	R	N/A	Wild-origin, Asia	98.8	N/A	N/A	N/A	51.818	120	250	333	1400	3	1	none
FMNH_M_46499	*Hylobates*	*concolor gabriellae*	Adult	R	N/A	Wild-origin, Asia	88.2	N/A	N/A	N/A	47.831	120	250	333	1200	3	1	none
FMNH_M_57202	*Gorilla*	*gorilla gorilla*	Adult	R	N/A	Wild-origin, Africa	161.6	N/A	N/A	N/A	68.422	100	250	250	700	3	1	0.2 mm Cu
FMNH_M_99740	*Hylobates*	*lar entelloides*	Adult	R	N/A	Wild-origin, Asia	87.2	N/A	N/A	N/A	47.215	120	250	333	1200	3	1	none
FMNH_M_99761	*Hylobates*	*lar entelloides*	Adult	R	N/A	Wild-origin, Asia	74.4	N/A	N/A	N/A	39.595	120	250	333	1000	3	1	none
MCZ_M_35456	*Hylobates*	*lar*	Inf.	R	F	Siam	42.5	12.2	119.2	103.1	24.33318	120	200	250	2000	1	N/A	none
MCZ_M_35458	*Hylobates*	*lar*	Inf.	R	F	Siam	33.4	10.8	95.7	87.6	20.14407	120	200	250	2000	1	N/A	none
MCZ_M_36380	*Hylobates*	*lar*	Inf.	R	M	Siam	49.4	11.5	127.2	112.5	27.58306	120	200	250	2000	1	N/A	none
MCZ_M_37358	*Pongo*	*pygmaeus*	Adol.	R	M	Borneo	126.8	43.3	316	231	68.94491	120	200	250	2000	1	N/A	none
MCZ_M_37361	*Pongo*	*pygmaeus*	Adol.	L	M	Borneo	143.6	44.5	314	241	78.81033	120	200	250	2000	1	N/A	none
MCZ_M_37364	*Pongo*	*pygmaeus*	Adol.	R	F	Borneo	135.9	42.9	319.5	238	72.56037	120	200	250	2000	1	N/A	none
MCZ_M_37375	*Hylobates*	*lar*	Adol.	R	M	Borneo	64.9	17.1	192	170	35.53766	120	200	250	2000	1	N/A	none
MCZ_M_37376	*Hylobates*	*lar*	Juv.	L	M	Borneo	52.4	14.2	146.9	138.4	28.68074	120	200	250	2000	1	N/A	none
MCZ_M_37377	*Hylobates*	*lar*	Adol.	R	M	Borneo	72.2	18.9	211	196	39.40564	120	200	250	2000	1	N/A	none
MCZ_M_37384	*Hylobates*	*lar*	Adol.	R	M	Borneo	59.4	17.2	186	168.5	34.32807	120	200	250	2000	1	N/A	none
MCZ_M_41422	*Hylobates*	*lar*	Inf.	R	F	Siam	64.6	16.3	178.1	153.2	34.32807	120	200	250	2000	1	N/A	none

Table S.1. Continued

MCZ_M_41425	*Hylobates*	*lar*	Juv.	R	F	Siam	60.3	16.7	185.3	160.7	32.92261	120	200	250	2000	1	N/A	none
MCZ_M_41432	*Hylobates*	*lar*	Adol.	R	F	Siam	71.1	18.6	217.5	188	40.46948	120	200	250	2000	1	N/A	none
MCZ_M_41435	*Hylobates*	*lar*	Adol.	L	M	Siam	77.2	19.7	224	195	42.60918	120	200	250	2000	1	N/A	none
MCZ_M_41437	*Hylobates*	*lar*	Adol.	R	F	Siam	72.5	19	218	191	40.53936	120	200	250	2000	1	N/A	none
MCZ_M_41438	*Hylobates*	*lar*	Adol.	L	F	Siam	64.1	17.2	184.5	165	35.8478	120	200	250	2000	1	N/A	none
MCZ_M_41442	*Hylobates*	*lar*	Adult	R	F	Siam	89.9	20.3	246.2	215.5	50.34855	120	200	250	2000	1	N/A	none
MCZ_M_41443	*Hylobates*	*lar*	Juv.	R	F	Siam	48.2	14.1	145.6	129.2	26.73741	120	200	250	2000	1	N/A	none
MCZ_M_41444	*Hylobates*	*lar*	Juv.	L	M	Siam	54.9	16.2	159.4	140.9	30.69611	120	200	250	2000	1	N/A	none
MCZ_M_41452	*Hylobates*	*lar*	Juv.	R	F	Siam	64.8	18.6	195.5	168.5	36.83577	120	200	250	2000	1	N/A	none
MCZ_M_41455	*Hylobates*	*lar*	Adult	R	F	Siam	85.6	20.8	245	208	46.06048	120	200	250	2000	1	N/A	none
MCZ_M_41457	*Hylobates*	*lar*	Adult	R	M	Siam	88.2	20.3	229	201.5	48.53936	120	200	250	2000	1	N/A	none
MCZ_M_41458	*Hylobates*	*lar*	Adult	R	F	Siam	83.1	20.1	232	203	45.63477	120	200	250	2000	1	N/A	none
MCZ_M_41459	*Hylobates*	*lar*	Adult	R	M	Siam	87.8	21.9	236	208.5	47.093	120	200	250	2000	1	N/A	none
MCZ_M_41460	*Hylobates*	*lar*	Adult	R	F	Siam	89.5	19.4	245	207	48.248	120	200	250	2000	1	N/A	none
MCZ_M_41461	*Hylobates*	*lar*	Adol.	L	M	Siam	73.9	19.1	220	193	41.76924	120	200	250	2000	1	N/A	none
MCZ_M_41462	*Hylobates*	*lar*	Inf.	R	F	Siam	37.8	10.8	113.6	98.6	21.99077	120	200	250	2000	1	N/A	none
MCZ_M_41463	*Hylobates*	*lar*	Adult	R	F	Siam	90.9	19.6	224	200	49.48822	120	200	250	2000	1	N/A	none
MCZ_M_41464	*Hylobates*	*lar*	Adult	R	M	Siam	87.4	19.7	247.5	211	48.82868	120	200	250	2000	1	N/A	none
MCZ_M_41465	*Hylobates*	*lar*	Adult	R	M	Siam	83.1	19.7	227	196	45.51926	120	200	250	2000	1	N/A	none
MCZ_M_41466	*Hylobates*	*lar*	Inf.	R	F	Siam	38.8	11.1	101.3	89.3	21.86464	120	200	250	2000	1	N/A	none
MCZ_M_41467	*Hylobates*	*lar*	Adol.	R	M	Siam	69.8	18.8	208.5	186.5	39.22064	120	200	250	2000	1	N/A	none
MCZ_M_41468	*Hylobates*	*lar*	Adult	R	M	Siam	86.3	19.9	222	193	47.87666	120	200	250	2000	1	N/A	none

Table S.1. Continued

MCZ_M_41469	*Hylobates*	*lar*	Adult	L	F	Siam	88.1	20.3	257	216	47.87662	120	200	250	2000	1	N/A	none
MCZ_M_41470	*Hylobates*	*lar*	Inf.	R	M	Siam	38.3	10.1	109.6	94.7	29.7464	120	200	250	2000	1	N/A	none
MCZ_M_41473	*Hylobates*	*lar*	Adol.	R	F	Siam	65.3	17.8	189	173	35.75566	120	200	250	2000	1	N/A	none
MCZ_M_41482	*Hylobates*	*lar*	Inf.	R	F	Siam	49.3	14.4	137.1	124.5	28.02317	120	200	250	2000	1	N/A	none
MCZ_M_41488	*Hylobates*	*lar*	Juv.	R	F	Siam	56.2	14.9	162	140.5	31.5666	120	200	250	2000	1	N/A	none
MCZ_M_41491	*Hylobates*	*lar*	Adol.	R	M	Siam	66.8	18.7	205	179	37.64561	120	200	250	2000	1	N/A	none
MCZ_M_41498	*Hylobates*	*lar*	Juv.	R	M	Siam	56.4	15.9	172	150	32.30085	120	200	250	2000	1	N/A	none
MCZ_M_41499	*Hylobates*	*lar*	Adol.	R	M	Siam	75.6	19.1	219.5	197	42.4286	120	200	250	2000	1	N/A	none
MCZ_M_41502	*Hylobates*	*lar*	Juv.	R	F	Siam	54.8	14.8	163	146	31.4985	120	200	250	2000	1	N/A	none
MCZ_M_41535	*Hylobates*	*lar*	Adol.	R	F	Siam	65.8	18.7	202	180	37.12728	120	200	250	2000	1	N/A	none
MCZ_M_41537	*Hylobates*	*lar*	Adol.	R	M	Siam	67.4	19	208.5	184.5	37.64503	120	200	250	2000	1	N/A	none
MCZ_M_41539	*Hylobates*	*lar*	Inf.	R	M	Siam	44.6	13.7	129.5	113	24.75076	120	200	250	2000	1	N/A	none
MCZ_M_41542	*Hylobates*	*lar*	Juv.	R	M	Siam	65.9	16.9	178.5	165	37.9327	120	200	250	2000	1	N/A	none
MCZ_M_41544	*Hylobates*	*lar*	Inf.	R	M	Siam	37.5	9.2	92.2	85.4	21.77218	120	200	250	2000	1	N/A	none
MCZ_M_41548	*Hylobates*	*lar*	Juv.	L	?	Siam	59.2	16.4	158	141	34.04625	120	200	250	2000	1	N/A	none
MCZ_M_41549	*Hylobates*	*lar*	Juv.	R	M	Siam	62.9	17.9	180	162	35.29254	120	200	250	2000	1	N/A	none
MCZ_M_41550	*Hylobates*	*lar*	Adol.	R	M	Siam	71.1	19.7	223	196	41.34537	120	200	250	2000	1	N/A	none
MCZ_M_50959	*Pongo*	*pygmaeus*	Juv.	R	M	Sumatra	109.1	26.7	245.5	189	58.22099	120	200	250	2000	1	N/A	none
MPITC_06_10	*Pan*	*troglodytes verus*	Juv.	R	M	Tai Forest, Ivory Coast	91.2	N/A	N/A	N/A	24.7278	130	150	400	3716	2	N/A	0.5mm Brass
MPITC_06_13	*Pan*	*troglodytes verus*	Adult	R	M	Tai Forest, Ivory Coast	117.9	N/A	N/A	N/A	32.9898	130	150	400	3615	2	N/A	0.5mm Brass

Table S.1. Continued

MPITC_06_15	*Pan*	*troglodytes verus*	Adol.	R	F	Tai Forest, Ivory Coast	104.4	N/A	N/A	N/A	32.9898	130	150	400	3201	2	N/A	0.5mm Brass
MPITC_06_21	*Pan*	*troglodytes verus*	Juv.	R	M	Tai Forest, Ivory Coast	85.7	N/A	N/A	N/A	24.7278	130	150	400	3521	2	N/A	0.5mm Brass
MPITC_06_31	*Pan*	*troglodytes verus*	Adol.	R	F	Tai Forest, Ivory Coast	108.4	N/A	N/A	N/A	32.9703	130	150	400	3318	2	N/A	0.5mm Brass
MPITC_06_37	*Pan*	*troglodytes verus*	Juv.	R	?	Tai Forest, Ivory Coast	75.9	N/A	N/A	N/A	24.7278	130	150	400	3112	2	N/A	0.5mm Brass
MPITC_06_46	*Pan*	*troglodytes verus*	Adol.	R	M	Tai Forest, Ivory Coast	89.9	N/A	N/A	N/A	32.9898	130	150	400	2760	2	N/A	0.5mm Brass
MPITC_06_50	*Pan*	*troglodytes verus*	Adol.	R	F	Tai Forest, Ivory Coast	101.4	N/A	N/A	N/A	32.9703	130	150	400	3062	2	N/A	0.5mm Brass
MPITC_06_54	*Pan*	*troglodytes verus*	Juv.	R	?	Tai Forest, Ivory Coast	86.3	N/A	N/A	N/A	24.7278	130	150	400	3521	2	N/A	0.5mm Brass
MPITC_06_64	*Pan*	*troglodytes verus*	Juv.	R	M	Tai Forest, Ivory Coast	82.1	N/A	N/A	N/A	24.7278	130	150	400	3280	2	N/A	0.5mm Brass
MPITC_08_63	*Pan*	*troglodytes verus*	Adult	R	M	Tai Forest, Ivory Coast	123.7	N/A	N/A	N/A	40.3208	130	150	400	3095	2	N/A	0.5mm Brass
MPITC_11_04	*Pan*	*troglodytes verus*	Adult	R	M	Tai Forest, Ivory Coast	119.3	N/A	N/A	N/A	40.3208	130	150	400	2995	2	N/A	0.5mm Brass
USNM_M_113419	*Hylobates*	*lar*	Inf.	R	?	N/A	46	N/A	N/A	N/A	75.65	100	220	N/A	N/A	N/A	N/A	N/A
USNM_M_143593	*Pongo*	*abelii*	Adult	R	M	Indonesia	188	53.3	418	300	58.205	100	180	150	1600	3	1	0.2mm Cu
USNM_M_143594	*Pongo*	*abelii*	Adult	R	M	Indonesia	173	47.3	366	274	57.651	100	180	150	1000	3	1	0.2mm Cu
USNM_M_143596	*Pongo*	*abelii*	Adult	L	F	Indonesia	154	43.2	341	255	50.274	100	180	150	1400	3	1	none
USNM_M_143597	*Pongo*	*abelii*	Adult	R	F	Indonesia	153	42.4	330	261	50.274	100	180	150	900	3	1	none
USNM_M_143598	*Pongo*	*abelii*	Adult	R	F	Indonesia	142	42.8	326	246	76.723	100	180	150	700	3	1	0.2mm Cu

Table S.1. Continued

USNM_M_143599	*Pongo*	*abelii*	Juv.	R	F	Indonesia	99.5	30.4	224	173	56.414	100	180	150	1000	3	1	0.2 mm Cu
USNM_M_143600	*Pongo*	*abelii*	Adult	L	F	Indonesia	152	39.5	330	230	61.51	100	180	150	700	3	1	0.2 mm Cu
USNM_M_145304	*Pongo*	*pygmaeus*	Adult	R	M	Indonesia	176	55.6	358	275	57.143	100	180	150	1200	3	1	0.2 MM Cu
USNM_M_145305	*Pongo*	*pygmaeus*	Adult	R	M	Indonesia	192	50.9	363	289	69.751	100	180	150	1200	3	1	0.2 mm Cu
USNM_M_145306	*Pongo*	*pygmaeus*	Adult	R	F	Indonesia	168	43.8	336	256	50.507	100	180	150	1000	3	1	0.2 mm Cu
USNM_M_145307	*Pongo*	*pygmaeus*	Adol.	L	M	Indonesia	128	44.8	320	237	47.044	100	180	150	800	3	1	none
USNM_M_145308	*Pongo*	*pygmaeus*	Adult	R	F	Indonesia	170	42.9	323	248	53.174	100	180	150	1200	3	1	none
USNM_M_145309	*Pongo*	*pygmaeus*	Adult	R	F	Indonesia	163	42.1	324	258	50.274	100	180	150	900	3	1	none
USNM_M_145310	*Pongo*	*pygmaeus*	Adult	R	M	Indonesia	193	51.6	343	283	65.714	100	180	150	1000	3	1	0.2 mm Cu
USNM_M_153805	*Pongo*	*pygmaeus*	Adult	R	F	Indonesia	141	40.9	297	233	61.51	100	180	150	700	3	1	0.2 mm Cu
USNM_M_153821	*Pongo*	*pygmaeus*	Adol.	L	F	Indonesia	140	40.4	304	241	62.76	100	180	150	700	3	1	0.2 mm Cu
USNM_M_153822	*Pongo*	*pygmaeus*	Adult	R	F	Indonesia	154	39.2	306	230	54.717	100	200	150	1000	3	1	0.2 mm Cu
USNM_M_153823	*Pongo*	*pygmaeus*	Adult	R	M	Indonesia	196	53.1	384	302	59.754	100	200	150	1000	3	1	0.2 mm Cu
USNM_M_153824	*Pongo*	*pygmaeus*	Adol.	R	F	Indonesia	150	43.9	338	253	50.642	100	200	150	1000	3	1	0.2 mm Cu
USNM_M_154411	*Hylobates*	*mulleri*	Inf.	R	?	N/A	37.6	N/A	N/A	N/A	55.2	110	220	N/A	N/A	N/A	N/A	N/A
USNM_M_174697	*Gorilla*	*gorilla gorilla*	Adol.	R	F	Gabon	103.7	36.1	314	281	56.152	100	180	150	1000	3	1	none
USNM_M_220066	*Pan*	*troglodytes*	Adol.	L	M	Gabon	111.3	36.2	272	271	60.724	100	180	150	1000	3	1	none

Table S.1. Continued

USNM_M_220067	*Pan*	*troglodytes*	Juv.	L	M	Gabon	80.6	29.5	186	180	44.182	100	180	150	1000	3	1	none
USNM_M_220068	*Pan*	*troglodytes*	Inf.	R	M	Gabon	72.3	20.4	160.1	158.5	41.617	100	180	150	1000	3	1	0.2 mm Cu
USNM_M_220324	*Gorilla*	*gorilla gorilla*	Adult	L	M	Gabon	168	63.6	451	392	87.17	100	180	150	1000	3	1	none
USNM_M_236972	*Pan*	*troglodytes*	Juv.	R	F	Uganda	83.4	23.3	167.3	164.3	47.044	100	180	150	800	3	1	none
USNM_M_239883	*Gorilla*	*beringei beringei*	Adult	L	M	Congo, Democratic Rep. Of	189	71.6	437	390	69.79	100	180	150	1000	3	1	none
USNM_M_239884	*Gorilla*	*beringei beringei*	Inf.	L	M	Congo, Democratic Rep. Of	74.32	28.7	198	164	45.676	100	180	150	900	3	1	none
USNM_M_260590	*Hylobates*	*lar carpenteri*	Adult	R	F	Thailand	82.1	19.9	235	210	49.173	100	180	250	600	3	1	0.1 mm Cu
USNM_M_260591	*Hylobates*	*lar*	Inf.	R	?	N/A	19.7	N/A	N/A	N/A	33.5	100	220	N/A	N/A	N/A	N/A	N/A
USNM_M_271047	*Hylobates*	*lar vestitus*	Adult	R	F	Indonesia	86.8	19.8	231	198	49.963	100	180	150	1000	3	1	0.2 mm Cu
USNM_M_317197	*Pongo*	*pygmaeus*	Inf.	L	M	Malaysia	59.6	16.2	106.4	78.4	34.142	100	200	150	700	3	1	none
USNM_M_320788	*Hylobates*	*concolor*	Inf.	R	?	N/A	27.1	N/A	N/A	N/A	23.61	110	220	N/A	N/A	N/A	N/A	N/A
USNM_M_395636	*Gorilla*	*beringei beringei*	Adult	R	M	Rwanda	193	66.9	426	366	63.104	100	180	150	1000	3	1	none
USNM_M_396936	*Gorilla*	*beringei beringei*	Adol.	R	F	Rwanda	134	51.9	370	N/A	74.424	100	180	150	1000	3	1	none
USNM_M_396937	*Gorilla*	*beringei beringei*	Adult	L	F	Rwanda	152	55.4	357	N/A	81.717	100	180	150	1000	3	1	none
USNM_M_396942	*Gorilla*	*beringei beringei*	Adult	R	M	Rwanda	176	62.8	422	N/A	59.848	100	180	150	1000	3	1	none
USNM_M_397351	*Gorilla*	*beringei beringei*	Adult	R	M	Rwanda	175	69.1	427	377	58.205	100	180	150	1200	3	1	0.2 mm Cu
USNM_M_397352	*Gorilla*	*beringei beringei*	Adult	L	M	Rwanda	179	N/A	N/A	N/A	58.205	100	180	150	1200	3	1	0.2 mm Cu
USNM_M_397353	*Gorilla*	*beringei beringei*	Adult	R	F	Rwanda	157	N/A	N/A	N/A	58.205	100	180	150	1200	3	1	0.2 mm Cu

Table S.1. Continued

USNM_M_398409	*Gorilla*	*beringei beringei*	Inf.	R	?	Rwanda	37.1	12.8	69.5	65.2	21.75	100	180	150	800	3	1	none
USNM_M_49463	*Hylobates*	*lar entelloides*	Adult	R	?	Thailand	89.3	21.2	235	201	50.076	100	180	150	1000	3	1	none
USNM_M_49768	*Pongo*	*pygmaeus*	Adult	R	F	Indonesia	161	40.2	333	256	63.353	100	180	150	1000	3	1	none
USNM_M_49769	*Pongo*	*pygmaeus*	Adult	R	F	Indonesia	150	44	323	253	79.437	100	180	150	1000	3	1	none
USNM_M_49849	*Pongo*	*abelii*	Juv.	R	M	Indonesia	110.9	32.4	246	180	59.717	100	180	150	1000	3	1	none
USNM_M_49850	*Pongo*	*abelii*	Adult	R	M	Indonesia	137	44.2	333	243	73.420	100	180	150	1000	3	1	none
USNM_M_49855	*Pongo*	*abelii*	Adult	L	M	Indonesia	182	52.1	370	291	64.427	100	180	150	1000	3	1	none
USNM_M_49856	*Pongo*	*abelii*	Adol.	R	M	Indonesia	137	40.6	285	221	73.629	100	180	150	1000	3	1	none
USNM_M_49857	*Pongo*	*abelii*	Adult	R	F	Indonesia	147	42.2	322	239	50.642	100	200	150	1000	3	1	0.2 mm Cu
USNM_M_49861	*Pongo*	*abelii*	Adult	L	F	Indonesia	155	41.3	332	254	59.473	100	200	150	900	3	1	0.2 mm Cu
USNM_M_49862	*Pongo*	*abelii*	Adol.	R	F	Indonesia	139	36.7	316	247	46.261	100	200	150	1000	3	1	0.2 mm Cu
USNM_M_49864	*Pongo*	*abelii*	Adult	L	M	Indonesia	159	45.2	347	263	63.161	100	180	150	1000	3	1	none
USNM_M_49893	*Pan*	*troglodytes*	Inf.	R	M	Unknown Locality	60.9	22.7	143.7	147.4	34.792	100	180	150	700	3	1	none
USNM_M_49957	*Pongo*	*pygmaeus*	Adult	L	F	Indonesia	141	39.3	313	243	77.987	100	180	150	1000	3	1	none
USNM_M_49958	*Pongo*	*pygmaeus*	Adult	R	M	Indonesia	211	55.7	387	296	57.288	100	180	150	1000	3	1	none
USNM_M_49959	*Pongo*	*pygmaeus*	Adult	R	F	Indonesia	150	42.5	317	253	82.084	100	180	150	1000	3	1	none
USNM_M_49972	*Pongo*	*pygmaeus*	Inf.	R	M	Indonesia	50.6	15.7	82.2	61	41.596	100	180	150	2000	3	1	none
USNM_M_545039	*Gorilla*	*beringei beringei*	Adult	L	M	Rwanda	196	68.8	413	362	50.274	100	180	150	900	3	1	none
USNM_M_545040	*Gorilla*	*beringei beringei*	Adult	L	M	Rwanda	184	69.2	423	N/A	60.111	100	180	150	1200	3	1	none
USNM_M_545043	*Gorilla*	*beringei beringei*	Adult	L	F	Rwanda	133	52.3	355	N/A	74.836	100	180	150	700	3	1	0.2 mm Cu

Table S.1. Continued

USNM_M_545044	*Gorilla*	*beringei beringei*	Inf.	R	M	Rwanda	54.8	18.7	124.8	108.1	32.746	100	180	150	800	3	1	none
USNM_M_545045	*Gorilla*	*beringei beringei*	Adult	R	F	Rwanda	150	54.7	355	312	59.237	100	180	150	700	3	1	0.2 mm Cu
USNM_M_545047	*Gorilla*	*beringei beringei*	Adult	L	F	Rwanda	146	N/A	N/A	N/A	53.611	100	200	150	1000	3	1	0.2 mm Cu
USNM_M_599169	*Gorilla*	*gorilla gorilla*	Inf.	R	M	Equatorial Guinea	73.6	27.7	166.2	140.3	41.617	100	180	150	1000	3	1	0.2 mm Cu
USNM_M_49861	*Pongo*	*abelii*	Adult	L	F	Indonesia	155	41.3	332	254	59.473	100	200	150	900	3	1	0.2 mm Cu
USNM_M_49862	*Pongo*	*abelii*	Adol.	R	F	Indonesia	139	36.7	316	247	46.261	100	200	150	1000	3	1	0.2 mm Cu
USNM_M_49864	*Pongo*	*abelii*	Adult	L	M	Indonesia	159	45.2	347	263	63.161	100	180	150	1000	3	1	none
USNM_M_49893	*Pan*	*troglodytes*	Inf.	R	M	Unknown Locality	60.9	22.7	143.7	147.4	34.792	100	180	150	700	3	1	none
USNM_M_49957	*Pongo*	*pygmaeus*	Adult	L	F	Indonesia	141	39.3	313	243	77.987	100	180	150	1000	3	1	none
USNM_M_49958	*Pongo*	*pygmaeus*	Adult	R	M	Indonesia	211	55.7	387	296	57.288	100	180	150	1000	3	1	none
USNM_M_49959	*Pongo*	*pygmaeus*	Adult	R	F	Indonesia	150	42.5	317	253	82.084	100	180	150	1000	3	1	none
USNM_M_49972	*Pongo*	*pygmaeus*	Inf.	R	M	Indonesia	50.6	15.7	82.2	61	41.596	100	180	150	2000	3	1	none
USNM_M_545039	*Gorilla*	*beringei beringei*	Adult	L	M	Rwanda	196	68.8	413	362	50.274	100	180	150	900	3	1	none
USNM_M_545040	*Gorilla*	*beringei beringei*	Adult	L	M	Rwanda	184	69.2	423	N/A	60.111	100	180	150	1200	3	1	none
USNM_M_545043	*Gorilla*	*beringei beringei*	Adult	L	F	Rwanda	133	52.3	355	N/A	74.836	100	180	150	700	3	1	0.2 mm Cu
USNM_M_545044	*Gorilla*	*beringei beringei*	Inf.	R	M	Rwanda	54.8	18.7	124.8	108.1	32.746	100	180	150	800	3	1	none
USNM_M_545045	*Gorilla*	*beringei beringei*	Adult	R	F	Rwanda	150	54.7	355	312	59.237	100	180	150	700	3	1	0.2 mm Cu
USNM_M_545047	*Gorilla*	*beringei beringei*	Adult	L	F	Rwanda	146	N/A	N/A	N/A	53.611	100	200	150	1000	3	1	0.2 mm Cu

Table S.1. Continued

USNM_M_599169	*Gorilla*	*gorilla gorilla*	Inf.	R	M	Equatorial Guinea	73.6	27.7	166.2	140.3	41.617	100	180	150	1000	3	1	0.2 mm Cu

References

Adams, D., Collyer, M., Kaliontzopoulou, A., Baken, E., 2020. Geomorph: geometric morphometric analyses of 2D/3D landmark data. R package version 3.2. 1.

Ahrens, J., Geveci, B., Law, C., 2005. ParaView: An End-User Tool for Large Data Visualization. In: Visualization Handbook. Elesvier.

Alemseged, Z., 2023. Reappraising the palaeobiology of Australopithecus. Nature. 617, 45–54.

Alemseged, Z., Spoor, F., Kimbel, W.H., Bobe, R., Geraads, D., Reed, D., Wynn, J.G., 2006. A juvenile early hominin skeleton from Dikika, Ethiopia. Nature. 443, 296–301.

Ashton, E.H., Oxnard, C.E., 1964. Functional Adaptations in the Primate Shoulder Girdle. Proceedings of the Zoological Society of London. 142, 49–66.

Augat, P., Schorlemmer, S., 2006. The role of cortical bone and its microstructure in bone strength. Age and Ageing. 35, ii27–ii31.

Barak, M.M., Lieberman, D.E., Hublin, J.-J., 2011. A Wolff in sheep's clothing: Trabecular bone adaptation in response to changes in joint loading orientation. Bone. 49, 1141–1151.

Barak, M.M., Weiner, S., Shahar, R., 2008. Importance of the integrity of trabecular bone to the relationship between load and deformation of rat femora: an optical metrology study. Journal of Materials Chemistry. 18, 3855–3864.

Barros, A.P., 2014. Ontogeny, phylogeny and functional morphology of the hominoid shoulder girdle (Doctoral). Doctoral thesis, UCL (University College London). UCL (University College London).

Berger, L.R., 1994. Functional morphology of the hominoid shoulder, past and present. University of the Witwatersrand, Johannesburg, South Africa.

Berger, L.R., de Ruiter, D.J., Churchill, S.E., Schmid, P., Carlson, K.J., Dirks, P.H.G.M., Kibii, J.M., 2010. Australopithecus sediba: A New Species of Homo-Like Australopith from South Africa. Science. 328, 195–204.

Berthaume, M., Grosse, I.R., Patel, N.D., Strait, D.S., Wood, S., Richmond, B.G., 2010. The effect of early hominin occlusal morphology on the fracturing of hard food items. Anatomical Record (Hoboken, N.J.: 2007). 293, 594–606.

Biewener, A.A., 1982. Bone Strength in Small Mammals and Bipedal Birds: Do Safety Factors Change With Body Size? Journal of Experimental Biology. 98, 289–301.

Biewener, A.A., Fazzalari, N.L., Konieczynski, D.D., Baudinette, R.V., 1996. Adaptive changes in trabecular architecture in relation to functional strain patterns and disuse. Bone. 19, 1–8.

Bird, E.E., Kivell, T.L., Skinner, M.M., 2022. Patterns of internal bone structure and functional adaptation in the hominoid scaphoid, lunate, and triquetrum. American Journal of Biological Anthropology. 177, 266–285.

Black, S., Scheuer, L., 1996. Age Changes in the Clavicle: from the Early Neonatal Period to Skeletal Maturity. International Journal of Osteoarchaeology. 6, 425–434.

Bookstein, F.L., 1997. Landmark methods for forms without landmarks: morphometrics of group differences in outline shape. Medical Image Analysis. 1, 225–243.

Bowland, L.A., Scott, J.E., Kivell, T.L., Patel, B.A., Tocheri, M.W., Orr, C.M., 2021. Homo naledi pollical metacarpal shaft morphology is distinctive and intermediate between that of australopiths and other members of the genus *Homo*. Journal of Human Evolution. 158, 103048.

Burgess, M.L., Schmitt, D., Zeininger, A., McFarlin, S.C., Zihlman, A.L., Polk, J.D., Ruff, C.B., 2016. Ontogenetic scaling of fore limb and hind limb joint posture and limb bone cross-sectional geometry in vervets and baboons. American Journal of Physical Anthropology. 161, 72–83.
Burr, D.B., Ruff, C.B., Johnson, C., 1989. Structural adaptations of the femur and humerus to arboreal and terrestrial environments in three species of macaque. American Journal of Physical Anthropology. 79, 357–367.
Cant, J.G.H., 1987. Effects of sexual dimorphism in body size on feeding postural behavior of Sumatran orangutans (Pongo pygmaeus). American Journal of Physical Anthropology. 74, 143–148.
Carlson, K.J., 2005. Investigating the form-function interface in African apes: Relationships between principal moments of area and positional behaviors in femoral and humeral diaphyses. American Journal of Physical Anthropology. 127, 312–334.
Carlson, K.J., 2006. Muscle architecture of the common chimpanzee (Pan troglodytes): perspectives for investigating chimpanzee behavior. Primates. 47, 218–229.
Carlson, K.J., Green, D.J., Jashashvili, T., Pickering, T.R., Heaton, J.L., Beaudet, A., Stratford, D., Crompton, R., Kuman, K., Bruxelles, L., Clarke, R.J., 2021. The pectoral girdle of StW 573 ('Little Foot') and its implications for shoulder evolution in the Hominina. Journal of Human Evolution. 158, 102983.
Carter, D., Orr, T., Fyhrie, D.P., 1989. Relationships between loading history and femoral cancellous bone architecture. Journal of biomechanics. 22, 231–244.
Chan, L.K., 2008. The range of passive arm circumduction in primates: Do hominoids really have more mobile shoulders? American Journal of Physical Anthropology. 136, 265–277.
Chirchir, H., Kivell, T.L., Ruff, C.B., Hublin, J.-J., Carlson, K.J., Zipfel, B., Richmond, B.G., 2015. Recent origin of low trabecular bone density in modern humans. Proceedings of the National Academy of Sciences. 112, 366–371.
Chirchir, H., Zeininger, A., Nakatsukasa, M., Ketcham, R.A., Richmond, B.G., 2017. Does trabecular bone structure within the metacarpal heads of primates vary with hand posture? Comptes Rendus Palevol, Hominin biomechanics, virtual anatomy and inner structural morphology: From head to toe. A tribute to Laurent Puymerail. 16, 533–544.
Churchill, S.E., Green, D.J., Feuerriegel, E.M., Macias, M.E., Mathews, S., Carlson, K.J., Schmid, P., Berger, L.R., 2018. Special Issue: Australopithecus sediba The Shoulder, Arm, and Forearm of Australopithecus sediba. PaleoAnthropology. 234–281.
Churchill, S.E., Holliday, T.W., Carlson, K.J., Jashashvili, T., Macias, M.E., Mathews, S., Sparling, T.L., Schmid, P., de Ruiter, D.J., Berger, L.R., 2013. The Upper Limb of Australopithecus sediba. Science. 340, 1233477.
Churchill, S.E., Trinkaus, E., 1990. Neandertal scapular glenoid morphology. American Journal of Physical Anthropology. 83, 147–160.
Ciochon, R.L., 1987. Hominoid Cladistics and the Ancestry of Modern Apes and Humans. In: Primate Evolution and Human Origins. Routledge.
Corrigan, G.E., 1960. The Neonatal Clavicle. Neonatology. 2, 79–92.
Corruccini, R.S., Ciochon, R.L., 1976. Morphometric affinities of the human shoulder. American Journal of Physical Anthropology. 45, 19–37.
Cosnefroy, Q., Marchal, F., Bellaiche, L., Carlier, R., Cazeau, C., Lamberton, F., Perrier, A., Theil, J.-C., Berillon, G., 2022. Do femoral biomechanical properties follow locomotor

changes in primates? An ontogenetic study of olive baboons (Papio anubis). American Journal of Biological Anthropology. 179, 609–623.
Cost, I.N., Middleton, K.M., Sellers, K.C., Echols, M.S., Witmer, L.M., Davis, J.L., Holliday, C.M., 2020. Palatal Biomechanics and Its Significance for Cranial Kinesis in Tyrannosaurus rex. The Anatomical Record. 303, 999–1017.
Cotter, M.M., Simpson, S.W., Latimer, B.M., Hernandez, C.J., 2009. Trabecular microarchitecture of hominoid thoracic vertebrae. The Anatomical Record: Advances in Integrative Anatomy and Evolutionary Biology: Advances in Integrative Anatomy and Evolutionary Biology. 292, 1098–1106.
Cowgill, L.W., 2007. Humeral torsion revisited: A functional and ontogenetic model for populational variation. American Journal of Physical Anthropology. 134, 472–480.
Cronskär, M., Rasmussen, J., Tinnsten, M., 2015. Combined finite element and multibody musculoskeletal investigation of a fractured clavicle with reconstruction plate. Computer Methods in Biomechanics and Biomedical Engineering. 18, 740–748.
Currey, J.D., 2002. Bones: Structure and Mechanics. Princeton University Press.
Currey, J.D., Dean, M.N., Shahar, R., 2017. Revisiting the links between bone remodelling and osteocytes: insights from across phyla. Biological Reviews. 92, 1702–1719.
Daegling, D.J., 2002. Estimation of torsional rigidity in primate long bones. Journal of Human Evolution. 43, 229–239.
Daegling, D.J., 2007. Morphometric estimation of torsional stiffness and strength in primate mandibles. American Journal of Physical Anthropology. 132, 261–266.
Dainton, M., Macho, G.A., 1999. Did knuckle walking evolve twice? Journal of Human Evolution. 36, 171–194.
Davis, J., Santana, S., Dumont, E., Grosse, I., 2010. Predicting bite force in mammals: two-dimensional versus three-dimensional lever models. Journal of Experimental Biology. 213, 1844–1851.
Demes, B., Jungers, W.L., Selpien, K., 1991. Body size, locomotion, and long bone cross-sectional geometry in indriid primates. American Journal of Physical Anthropology. 86, 537–547.
Diogo, R., Potau, J.M., Pastor, J.F., 2013a. Photographic and descriptive musculoskeletal atlas of chimpanzees: with notes on the attachments, variations, innervation, function and synonymy and weight of the muscles. CRC Press.
Diogo, R., Potau, J.M., Pastor, J.F., Paz, F.J. de, Barbosa, M., Ferrero, E.M., Bello, G., Aziz, M.A., Arias-Martorell, J., Wood, B., 2013b. Photographic and Descriptive Musculoskeletal Atlas of Orangutans: with notes on the attachments, variations, innervations, function and synonymy and weight of the muscles. CRC Press.
Diogo, R., Wood, B., 2011. Soft-tissue anatomy of the primates: phylogenetic analyses based on the muscles of the head, neck, pectoral region and upper limb, with notes on the evolution of these muscles. Journal of Anatomy. 219, 273–359.
Diogo, R., Wood, B.A., 2012. Comparative Anatomy and Phylogeny of Primate Muscles and Human Evolution. CRC Press.
Dirks, P.H., Roberts, E.M., Hilbert-Wolf, H., Kramers, J.D., Hawks, J., Dosseto, A., Duval, M., Elliott, M., Evans, M., Grün, R., Hellstrom, J., Herries, A.I., Joannes-Boyau, R., Makhubela, T.V., Placzek, C.J., Robbins, J., Spandler, C., Wiersma, J., Woodhead, J.,

Berger, L.R., 2017. The age of Homo naledi and associated sediments in the Rising Star Cave, South Africa. eLife. 6, e24231.
Dirks, P.H.G.M., Kibii, J.M., Kuhn, B.F., Steininger, C., Churchill, S.E., Kramers, J.D., Pickering, R., Farber, D.L., Mériaux, A.-S., Herries, A.I.R., King, G.C.P., Berger, L.R., 2010. Geological Setting and Age of Australopithecus sediba from Southern Africa. Science. 328, 205–208.
Doran, D.M., 1992. The ontogeny of chimpanzee and pygmy chimpanzee locomotor behavior: a case study of paedomorphism and its behavioral correlates. Journal of Human Evolution. 23, 139–157.
Doran, D.M., 1993. Comparative locomotor behavior of chimpanzees and bonobos: The influence of morphology on locomotion. American Journal of Physical Anthropology. 91, 83–98.
Doran, D.M., 1997. Ontogeny of locomotion in mountain gorillas and chimpanzees. Journal of Human Evolution. 32, 323–344.
Doube, M., Conroy, A.W., Christiansen, P., Hutchinson, J.R., Shefelbine, S., 2009. Three-Dimensional Geometric Analysis of Felid Limb Bone Allometry. PLOS ONE. 4, e4742.
Doube, M., Kłosowski, M.M., Wiktorowicz-Conroy, A.M., Hutchinson, J.R., Shefelbine, S.J., 2011. Trabecular bone scales allometrically in mammals and birds. Proceedings of the Royal Society B: Biological Sciences. 278, 3067–3073.
Dunmore, C.J., Bachmann, S., Synek, A., Pahr, D.H., Skinner, M.M., Kivell, T.L., 2023. The deep trabecular structure of first metacarpals in extant hominids. American Journal of Biological Anthropology. 1–18.
Dunmore, C.J., Skinner, M.M., Bardo, A., Berger, L.R., Hublin, J.-J., Pahr, D.H., Rosas, A., Stephens, N.B., Kivell, T.L., 2020. The position of Australopithecus sediba within fossil hominin hand use diversity. Nature Ecology & Evolution. 4, 911–918.
Dunmore, C.J., Wollny, G., Skinner, M.M., 2018. MIA-Clustering: a novel method for segmentation of paleontological material. PeerJ. 6, e4374.
Ehrlich, P.J., Lanyon, L.E., 2002. Mechanical strain and bone cell function: a review. Osteoporosis international: a journal established as result of cooperation between the European Foundation for Osteoporosis and the National Osteoporosis Foundation of the USA. 13, 688–700.
Eriksen, E.F., 1986. Normal and pathological remodeling of human trabecular bone: three dimensional reconstruction of the remodeling sequence in normals and in metabolic bone disease. Endocrine reviews. 7, 379–408.
Eriksen, E.F., 2010. Cellular mechanisms of bone remodeling. Reviews in Endocrine and Metabolic Disorders. 11, 219–227.
Evans, F.G., Krahl, V.E., 1945. The torsion of the humerus: a phylogenetic survey from fish to man. American Journal of Anatomy. 76, 303–337.
Fajardo, R.J., Desilva, J.M., Manoharan, R.K., Schmitz, J.E., Maclatchy, L.M., Bouxsein, M.L., 2013. Lumbar vertebral body bone microstructural scaling in small to medium-sized strepsirhines. The Anatomical Record. 296, 210–226.
Fannin, L.D., Joy, M.S., Dominy, N.J., McGraw, W.S., DeSilva, J.M., 2023. Downclimbing and the evolution of ape forelimb morphologies. Royal Society Open Science. 10, 230145.

Farrell, H.N., Alemseged, Z., 2023. Ontogenetic shape changes in the hominoid clavicle and the morphology of the Australopithecus afarensis juvenile DIK-1-1. Presented at the 92nd Annual Meeting of the American Association of Biological Anthropologists, Reno, NV.
Feuerriegel, E.M., Green, D.J., Walker, C.S., Schmid, P., Hawks, J., Berger, L.R., Churchill, S.E., 2017. The upper limb of Homo naledi. Journal of Human Evolution. 104, 155–173.
Feuerriegel, E.M., Voisin, J.-L., Churchill, S.E., Haeusler, M., Mathews, S., Schmid, P., 2019. Upper Limb Fossils of Homo naledi from the Lesedi Chamber, Rising Star System, South Africa. 40.
Fleagle, J., 2013. Primate Adaptation and Evolution. Academic Press.
Foote, M., 1993. Contributions of Individual Taxa to Overall Morphological Disparity. Paleobiology. 19, 403–419.
Garvin, H.M., Elliott, M.C., Delezene, L.K., Hawks, J., Churchill, S.E., Berger, L.R., Holliday, T.W., 2017. Body size, brain size, and sexual dimorphism in *Homo naledi* from the Dinaledi Chamber. Journal of Human Evolution. 111, 119–138.
Gebo, D.L., 1996. Climbing, brachiation, and terrestrial quadrupedalism: historical precursors of hominid bipedalism. American Journal of Physical Anthropology: The Official Publication of the American Association of Physical Anthropologists. 101, 55–92.
Georgiou, L., Kivell, T.L., Pahr, D.H., Skinner, M.M., 2018. Trabecular bone patterning in the hominoid distal femur. PeerJ. 6, e5156.
Gibson, L., 1985. The mechanical behaviour of cancellous bone. Journal of biomechanics. 18, 317–328.
Gibson, L.J., 2005. Biomechanics of cellular solids. Journal of biomechanics. 38, 377–399.
Gittins, S.P., 1983. Use of the Forest Canopy by the Agile Gibbon. Folia Primatologica. 40, 134–144.
Goldstein, S.A., Goulet, R., McCubbrey, D., 1993. Measurement and significance of three-dimensional architecture to the mechanical integrity of trabecular bone. Calcified Tissue International. 53, S127–S133.
Gómez, M., Casado, A., de Diego, M., Pastor, J.F., Potau, J.M., 2022. Anatomical and molecular analyses of the deltoid muscle in chimpanzees (Pan troglodytes) and modern humans (Homo sapiens): Similarities and differences due to the uses of the upper extremity. American Journal of Primatology. 84, e23390.
Gordon, J.E., 2009. Structures: Or Why Things Don't Fall Down. Hachette Books.
Grabowski, M., Hatala, K.G., Jungers, W.L., Richmond, B.G., 2015. Body mass estimates of hominin fossils and the evolution of human body size. Journal of Human Evolution. 85, 75–93.
Granatosky, M.C., 2018. A Review of locomotor diversity in mammals with analyses exploring the influence of substrate use, body mass and intermembral index in primates. Journal of Zoology. 306, 207–216.
Green, D., 2013. Ontogeny of the hominoid scapula: The influence of locomotion on morphology. American Journal of Physical Anthropology. 152, 239–260.
Green, D., Alemseged, Z., 2012. Australopithecus afarensis Scapular Ontogeny, Function, and the Role of Climbing in Human Evolution. Science. 338, 514–517.
Green, D.J., 2020. Scapula, clavicle, and proximal humerus. In: Zipfel, B., Richmond, B.G., Ward, C.V. (Eds.), Hominin Postcranial Remains from Sterkfontein, South Africa, 1936-1995. Oxford University Press, p. 0.

Griffin, N.L., 2008. Bone architecture of the hominin second proximal pedal phalanx: a preliminary investigation. Journal of Human Evolution. 54, 162–168.
Gross, T., Kivell, T., Skinner, M., Nguyen, N., Pahr, D., 2014. A CT-image-based framework for the holistic analysis of cortical and trabecular bone morphology. Palaeontologia Electronica.
Gunz, P., Mitteroecker, P., Bookstein, F.L., 2005. Semilandmarks in three dimensions. Modern morphometrics in physical anthropology. 73–98.
Gunz, P., Neubauer, S., Falk, D., Tafforeau, P., Le Cabec, A., Smith, T.M., Kimbel, W.H., Spoor, F., Alemseged, Z., 2020. Australopithecus afarensis endocasts suggest ape-like brain organization and prolonged brain growth. Science Advances.
Habib, M.B., Ruff, C.B., 2008. The effects of locomotion on the structural characteristics of avian limb bones. Zoological Journal of the Linnean Society. 153, 601–624.
Haile-Selassie, Y., Latimer, B.M., Alene, M., Deino, A.L., Gibert, L., Melillo, S.M., Saylor, B.Z., Scott, G.R., Lovejoy, C.O., 2010. An early Australopithecus afarensis postcranium from Woranso-Mille, Ethiopia. Proceedings of the National Academy of Sciences. 107, 12121–12126.
Hanna, J.B., Granatosky, M.C., Rana, P., Schmitt, D., 2017. The evolution of vertical climbing in primates: evidence from reaction forces. Journal of Experimental Biology. 220, 3039–3052.
Haramati, N., Cook, R.A., Raphael, B., McNamara, T.S., Staron, R.B., Feldman, F., 1994. Coraco-clavicular joint: normal variant in humans. Skeletal Radiology. 23, 117–119.
Harcourt-Smith, W.E.H., Aiello, L.C., 2004. Fossils, feet and the evolution of human bipedal locomotion. Journal of Anatomy. 204, 403–416.
Harrington, M.A., Keller, T.S., Seiler, J.G., Weikert, D.R., Moeljanto, E., Schwartz, H.S., 1993. Geometric properties and the predicted mechanical behavior of adult human clavicles. Journal of Biomechanics. 26, 417–426.
Harrison, T., 1987. The phylogenetic relationships of the early catarrhine primates: a review of the current evidence. Journal of Human Evolution. 16, 41–80.
Hatala, K.G., Gatesy, S.M., Falkingham, P.L., 2023. Arched footprints preserve the motions of fossil hominin feet. Nature Ecology & Evolution. 7, 32–41.
Hayes, W., Gerhart, T.N., 1985. Biomechanics of bone: Applications for assessment of bone strength. Bone and Mineral Research. 3, 259–294.
Henderson, K., Pantinople, J., McCabe, K., Richards, H.L., Milne, N., 2017. Forelimb bone curvature in terrestrial and arboreal mammals. PeerJ. 5, e3229.
Hildebrand, T., Rüegsegger, P., 1997. A new method for the model-independent assessment of thickness in three-dimensional images. Journal of Microscopy. 185, 67–75.
Hodgskinson, R., Currey, J., 1990. Effects of structural variation on Young's modulus of non-human cancellous bone. Proceedings of the Institution of Mechanical Engineers, Part H: Journal of Engineering in Medicine. 204, 43–52.
Howell, A.B., 1937. Morphogenesis of the Shoulder Architecture. Part VI. Therian Mammalia. The Quarterly Review of Biology. 12, 440–463.
Hunt, K.D., 1991. Positional behavior in the Hominoidea. International Journal of Primatology. 12, 95–118.
Inouye, S.E., 1992. Ontogeny and allometry of African ape manual rays. Journal of Human Evolution. 23, 107–138.

Inouye, S.E., 1994. Ontogeny of knuckle-walking hand postures in African apes. Journal of Human Evolution. 26, 459–485.
Irish, J.D., Guatelli-Steinberg, D., Legge, S.S., de Ruiter, D.J., Berger, L.R., 2013. Dental Morphology and the Phylogenetic "Place" of Australopithecus sediba. Science. 340, 1233062.
Isler, K., 2005. 3D-kinematics of vertical climbing in hominoids. American Journal of Physical Anthropology. 126, 66–81.
Ito, M., Nishida, A., Koga, A., Ikeda, S., Shiraishi, A., Uetani, M., Hayashi, K., Nakamura, T., 2002. Contribution of trabecular and cortical components to the mechanical properties of bone and their regulating parameters. Bone. 31, 351–358.
Jacobs, C.R., 2000. The mechanobiology of cancellous bone structural adaptation. Journal of rehabilitation research and development. 37, 209–216.
Johanson, D.C., Lovejoy, C.O., Kimbel, W.H., White, T.D., Ward, S.C., Bush, M.E., Latimer, B.M., Coppens, Y., 1982. Morphology of the Pliocene partial hominid skeleton (A.L. 288-1) from the Hadar formation, Ethiopia. American Journal of Physical Anthropology. 57, 403–451.
Judex, S., Garman, R., Squire, M., Donahue, L.-R., Rubin, C., 2004. Genetically based influences on the site-specific regulation of trabecular and cortical bone morphology. Journal of Bone and Mineral Research. 19, 600–606.
Jungers, W.L., 1982. Lucy's limbs: skeletal allometry and locomotion in Australopithecus afarensis. Nature. 297, 676–678.
Jungers, W.L., Grabowski, M., Hatala, K.G., Richmond, B.G., 2016. The evolution of body size and shape in the human career. Philosophical Transactions of the Royal Society B: Biological Sciences. 371, 20150247.
Jungers, W.L., Minns, R.J., 1979. Computed tomography and biomechanical analysis of fossil long bones. American Journal of Physical Anthropology. 50, 285–290.
Jungers, W.L., Stern, J.T., 1983. Body proportions, skeletal allometry and locomotion in the hadar hominids: a reply to Wolpoff. Journal of Human Evolution. 12, 673–684.
Kamibayashi, L.K., Richmond, F.J.R., 1998. Morphometry of Human Neck Muscles. Spine. 23, 1314.
Kappelman, J., Ketcham, R.A., Pearce, S., Todd, L., Akins, W., Colbert, M.W., Feseha, M., Maisano, J.A., Witzel, A., 2016. Perimortem fractures in Lucy suggest mortality from fall out of tall tree. Nature. 537, 503–507.
Keaveny, T.M., Morgan, E.F., Niebur, G.L., Yeh, O.C., 2001. Biomechanics of trabecular bone. Annual review of biomedical engineering. 3, 307–333.
Kilbourne, B.M., Hutchinson, J.R., 2019. Morphological diversification of biomechanical traits: mustelid locomotor specializations and the macroevolution of long bone cross-sectional morphology. BMC Evolutionary Biology. 19, 37.
Kivell, T.L., 2016. A review of trabecular bone functional adaptation: what have we learned from trabecular analyses in extant hominoids and what can we apply to fossils? Journal of Anatomy. 228, 569–594.
Kivell, T.L., Davenport, R., Hublin, J.-J., Thackeray, J.F., Skinner, M.M., 2018. Trabecular architecture and joint loading of the proximal humerus in extant hominoids, Ateles, and Australopithecus africanus. American Journal of Physical Anthropology. 167, 348–365.

Kivell, T.L., Deane, A.S., Tocheri, M.W., Orr, C.M., Schmid, P., Hawks, J., Berger, L.R., Churchill, S.E., 2015. The hand of Homo naledi. Nature Communications. 6, 8431.
Kivell, T.L., Schmitt, D., 2009. Independent evolution of knuckle-walking in African apes shows that humans did not evolve from a knuckle-walking ancestor. Proceedings of the National Academy of Sciences. 106, 14241–14246.
Koh, S.-W., Cavanaugh, J.M., Leach, J.P., Rouhana, S.W., 2004. Mechanical properties of the shoulder ligaments under dynamic loading. SAE Technical Paper.
Langenderfer, J., Jerabek, S.A., Thangamani, V.B., Kuhn, J.E., Hughes, R.E., 2004. Musculoskeletal parameters of muscles crossing the shoulder and elbow and the effect of sarcomere length sample size on estimation of optimal muscle length. Clinical biomechanics. 19, 664–670.
Lanyon, L.E., 1980. The influence of function on the development of bone curvature. An experimental study on the rat tibia. Journal of Zoology. 192, 457–466.
Lanyon, L.E., Goodship, A.E., Pye, C.J., MacFie, J.H., 1982. Mechanically adaptive bone remodelling. Journal of Biomechanics. 15, 141–154.
Larson, S.G., 1988. Subscapularis function in gibbons and chimpanzees: implications for interpretation of humeral head torsion in hominoids. American Journal of Physical Anthropology. 76, 449–462.
Larson, S.G., 2007. Evolutionary transformation of the hominin shoulder. Evolutionary Anthropology: Issues, News, and Reviews. 16, 172–187.
Larson, S.G., 2013. Shoulder Morphology in Early Hominin Evolution. In: Reed, K.E., Fleagle, J.G., Leakey, R.E. (Eds.), The Paleobiology of Australopithecus, Vertebrate Paleobiology and Paleoanthropology. Springer Netherlands, Dordrecht, pp. 247–261.
Larson, S.G., Stern, J.T., 1986. EMG of scapulohumeral muscles in the chimpanzee during reaching and "arboreal" locomotion. The American Journal of Anatomy. 176, 171–190.
Larson, S.G., Stern, J.T., 1987. EMG of chimpanzee shoulder muscles during knuckle-walking: problems of terrestrial locomotion in a suspensory adapted primate. Journal of Zoology. 212, 629–655.
Larson, S.G., Stern, J.T., 2013. Rotator cuff muscle function and its relation to scapular morphology in apes. Journal of Human Evolution. 65, 391–403.
Larson, S.G., Stern, J.T., Jungers, W.L., 1991. EMG of serratus anterior and trapezius in the chimpanzee: Scapular rotators revisited. American Journal of Physical Anthropology. 85, 71–84.
Latimer, B., Lovejoy, C.O., 1989. The calcaneus of Australopithecus afarensis and its implications for the evolution of bipedality. American Journal of Physical Anthropology. 78, 369–386.
Latimer, B., Ohman, J.C., Lovejoy, C.O., 1987. Talocrural joint in African hominoids: Implications for Australopithecus afarensis. American Journal of Physical Anthropology. 74, 155–175.
Laudicina, N.M., Cartmill, M., 2023. Clavicle length and shoulder breadth in hominoid evolution. The Anatomical Record. 306, 2090–2101.
Le Gros Clark, W.E., 1959. The Antecedents of Man. Edinburgh University Press, Edinburgh.
Ledogar, J.A., Benazzi, S., Smith, A.L., Weber, G.W., Carlson, K.B., Dechow, P.C., Grosse, I.R., Ross, C.F., Richmond, B.G., Wright, B.W., Wang, Q., Byron, C., Carlson, K.J., De Ruiter, D.J., Pryor Mcintosh, L.C., Strait, D.S., 2017. The Biomechanics of Bony Facial

"Buttresses" in South African Australopiths: An Experimental Study Using Finite Element Analysis. The Anatomical Record. 300, 171–195.
Levangie, P., Norkin, C., 2011. Joint Structure and Function: A Comprehensive Analysis. All PTHMS Faculty Publications.
Lieberman, D.E., 1996. How and why humans grow thin skulls: Experimental evidence for systemic cortical robusticity. American Journal of Physical Anthropology. 101, 217–236.
Lieberman, D.E., Devlin, M.J., Pearson, O.M., 2001. Articular area responses to mechanical loading: effects of exercise, age, and skeletal location. American Journal of Physical Anthropology. 116, 266–277.
Lieberman, D.E., Polk, J.D., Demes, B., 2004. Predicting long bone loading from cross-sectional geometry. American Journal of Physical Anthropology. 123, 156–171.
Ljunggren, A.E., 1979. Clavicular Function. Acta Orthopaedica Scandinavica. 50, 261–268.
Lovejoy, C.O., 1988. Evolution of Human Walking. Scientific American. 259, 118–125.
Lovejoy, C.O., Heiple, K.G., Burstein, A.H., 1973. The gait of Australopithecus. American Journal of Physical Anthropology. 38, 757–779.
Lovejoy, C.O., Johanson, D.C., Coppens, Y., 1982. Hominid upper limb bones recovered from the Hadar formation: 1974–1977 collections. American Journal of Physical Anthropology. 57, 637–649.
Lovejoy, C.O., McCollum, M.A., Reno, P.L., Rosenman, B.A., 2003. Developmental Biology and Human Evolution*. Annual Review of Anthropology. 32, 85–109.
MacLean, K., 2018. Development of a Probabilistic Chimpanzee Glenohumeral Model: Implications for Human Function (Doctoral Thesis). University of Waterloo.
MacLean, K.F.E., Dickerson, C.R., 2020. Development of a comparative chimpanzee musculoskeletal glenohumeral model: implications for human function. Journal of Experimental Biology. 223.
Marinescu, R., Daegling, D.J., Rapoff, A.J., 2005. Finite-element modeling of the anthropoid mandible: the effects of altered boundary conditions. The Anatomical Record. Part A, Discoveries in Molecular, Cellular, and Evolutionary Biology. 283, 300–309.
Martin, L., 1986. Relationships among great apes and humans. Major topics in primate and human evolution.
Martin, M.L., Travouillon, K.J., Fleming, P.A., Warburton, N.M., 2020. Review of the methods used for calculating physiological cross-sectional area (PCSA) for ecological questions. Journal of Morphology. 281, 778–789.
Mehlman, P.T., Doran, D.M., 2002. Influencing Western Gorilla Nest Construction at Mondika Research Center. International Journal of Primatology. 23, 1257–1285.
Melillo, S., Gunz, P., Coqueugniot, H., Reske, S., Hublin, J.-J., 2019. Structural effects of variation in the human clavicle. American Journal of Physical Anthropology. 168, 687–704.
Melillo, S.M., 2016. The Shoulder Girdle of KSD-VP-1/1. In: Haile-Selassie, Y., Su, D.F. (Eds.), The Postcranial Anatomy of Australopithecus Afarensis: New Insights from KSD-VP-1/1. Springer Netherlands, Dordrecht, pp. 113–141.
Milne, N., 2016. Curved bones: An adaptation to habitual loading. Journal of Theoretical Biology. 407, 18–24.
Milne, N., Granatosky, M.C., 2021. Ulna Curvature in Arboreal and Terrestrial Primates. Journal of Mammalian Evolution. 28, 897–909.

Mitteroecker, P., Gunz, P., Bernhard, M., Schaefer, K., Bookstein, F.L., 2004. Comparison of cranial ontogenetic trajectories among great apes and humans. Journal of Human Evolution. 46, 679–698.
Mivart, St.G., Huxley, T.H., 1867. XIII. On the appendicular skeleton of the primates. Philosophical Transactions of the Royal Society of London. 157, 299–429.
Morimoto, N., Nakatsukasa, M., Ponce de León, M.S., Zollikofer, C.P.E., 2018. Femoral ontogeny in humans and great apes and its implications for their last common ancestor. Scientific Reports. 8, 1930.
Nalley, T.K., Scott, J.E., McGechie, F., Grider-Potter, N., 2024. Comparative ontogeny of functional aspects of human cervical vertebrae. American Journal of Biological Anthropology. 183, e24788.
Nalley, T.K., Scott, J.E., Ward, C.V., Alemseged, Z., 2019. Comparative morphology and ontogeny of the thoracolumbar transition in great apes, humans, and fossil hominins. Journal of Human Evolution. 134, 102632.
Ogata, S., Uhthoff, H.K., 1990. The early development and ossification of the human clavicle--an embryologic study. Acta Orthopaedica Scandinavica. 61, 330–334.
O'Higgins, P., 2000. The study of morphological variation in the hominid fossil record: biology, landmarks and geometry. The Journal of Anatomy. 197, 103–120.
Oishi, M., Ogihara, N., Endo, H., Ichihara, N., Asari, M., 2009. Dimensions of forelimb muscles in orangutans and chimpanzees. Journal of Anatomy. 215, 373–382.
oqton, 2023. Geomagic Design X.
O'Rahilly, R., Gardner, E., 1972. The initial appearance of ossification in staged human embryos. American Journal of Anatomy. 134, 291–307.
Oxnard, C.E., 1969. Evolution of the human shoulder: some possible pathways. American Journal of Physical Anthropology. 30, 319–331.
Panagiotopoulou, O., Iriarte-Diaz, J., Mehari Abraha, H., Taylor, A.B., Wilshin, S., Dechow, P.C., Ross, C.F., 2020. Biomechanics of the mandible of Macaca mulatta during the power stroke of mastication: Loading, deformation, and strain regimes and the impact of food type. Journal of Human Evolution. 147, 102865.
Panagiotopoulou, O., Iriarte-Diaz, J., Wilshin, S., Dechow, P.C., Taylor, A.B., Abraha, H.M., Aljunid, S.F., Ross, C.F., 2017. In vivo bone strain and finite element modeling of a rhesus macaque mandible during mastication. Zoology (Jena, Germany). 124, 13–29.
Panagiotopoulou, O., Rankin, J.W., Gatesy, S.M., Hutchinson, J.R., 2016. A preliminary case study of the effect of shoe-wearing on the biomechanics of a horse's foot. PeerJ. 4, e2164.
Parsi-Pour, P., Kilbourne, B.M., 2020. Functional Morphology and Morphological Diversification of Hind Limb Cross-Sectional Traits in Mustelid Mammals. Integrative Organismal Biology. 2, obz032.
Partridge, T.C., Granger, D.E., Caffee, M.W., Clarke, R.J., 2003. Lower Pliocene Hominid Remains from Sterkfontein. Science. 300, 607–612.
Pattin, C.A., Caler, W.E., Carter, D.R., 1996. Cyclic mechanical property degradation during fatigue loading of cortical bone. Journal of Biomechanics. 29, 69–79.
Pickford, M., Senut, B., Gommery, D., Treil, J., 2002. Bipedalism in Orrorin tugenensis revealed by its femora. Comptes Rendus Palevol. 1, 191–203.

Pitfield, R., Miszkiewicz, J.J., Mahoney, P., 2017. Cortical Histomorphometry of the Human Humerus During Ontogeny. Calcified Tissue International. 101, 148–158.
Pollock, T.I., Panagiotopoulou, O., Hocking, D.P., Evans, A.R., 2022. Taking a stab at modelling canine tooth biomechanics in mammalian carnivores with beam theory and finite-element analysis. Royal Society Open Science. 9, 220701.
Porro, L.B., Metzger, K.A., Iriarte-Diaz, J., Ross, C.F., 2013. In vivo bone strain and finite element modeling of the mandible of Alligator mississippiensis. Journal of Anatomy. 223, 195–227.
Preuschoft, H., 2002. What does" arboreal locomotion" mean exactly and what are the relationships between" climbing", environment and morphology? Zeitschrift für Morphologie und Anthropologie. 171–188.
Preuschoft, H., Hohn, B., Scherf, H., Schmidt, M., Krause, C., Witzel, U., 2010. Functional Analysis of the Primate Shoulder. International Journal of Primatology. 31, 301–320.
Profico, A., Bondioli, L., Raia, P., O'Higgins, P., Marchi, D., 2021. morphomap: An R package for long bone landmarking, cortical thickness, and cross-sectional geometry mapping. American Journal of Physical Anthropology. 174, e24140.
Püschel, T.A., Sellers, W.I., 2016. Standing on the shoulders of apes: Analyzing the form and function of the hominoid scapula using geometric morphometrics and finite element analysis. American Journal of Physical Anthropology. 159, 325–341.
R Core Team, 2023. R: A Language and Environment for Statistical Computing.
Ratcliffe, R.J., Holt, K.G., 1997. Low frequency shock absorption in human walking. Gait & Posture. 5, 93–100.
Rayfield, E.J., 2007. Finite Element Analysis and Understanding the Biomechanics and Evolution of Living and Fossil Organisms. Annual Review of Earth and Planetary Sciences. 35, 541–576.
Richmond, B.G., 1998. Ontogeny and biomechanics of phalangeal form in primates (Ph.D.). State University of New York at Stony Brook, United States -- New York.
Richmond, B.G., Begun, D.R., Strait, D.S., 2001. Origin of human bipedalism: The knuckle-walking hypothesis revisited. American Journal of Physical Anthropology. 116, 70–105.
Richmond, B.G., Strait, D.S., 2000. Evidence that humans evolved from a knuckle-walking ancestor. Nature. 404, 382–385.
Richmond, B.G., Wright, B.W., Grosse, I., Dechow, P.C., Ross, C.F., Spencer, M.A., Strait, D.S., 2005. Finite element analysis in functional morphology. The Anatomical Record Part A: Discoveries in Molecular, Cellular, and Evolutionary Biology. 283A, 259–274.
Roach, N.T., Lieberman, D.E., Gill, T.J., Palmer, W.E., Gill, T.J., 2012. The effect of humeral torsion on rotational range of motion in the shoulder and throwing performance. Journal of Anatomy. 220, 293–301.
Roach, N.T., Richmond, B.G., 2015. Clavicle length, throwing performance and the reconstruction of the Homo erectus shoulder. Journal of Human Evolution. 80, 107–113.
Roach, N.T., Venkadesan, M., Rainbow, M.J., Lieberman, D.E., 2013. Elastic energy storage in the shoulder and the evolution of high-speed throwing in Homo. Nature. 498, 483–486.
Roberts, D., 1974. Structure and function of the primate scapula. Primate locomotion. 171–200.
Robinson, J.T., 1972. Early hominid posture and locomotion. (No Title).
Ross, C.F., 2005. Finite element analysis in vertebrate biomechanics. The Anatomical Record Part A: Discoveries in Molecular, Cellular, and Evolutionary Biology. 283A, 253–258.

Rothman, J.M., Pell, A.N., Dierenfeld, E.S., Mccann, C.M., 2006. Plant choice in the construction of night nests by gorillas in the Bwindi Impenetrable National Park, Uganda. American Journal of Primatology. 68, 361–368.
Rubin, C., Turner, A., Mallinckrodt, C., Jerome, C., McLeod, K., Bain, S., 2002. Mechanical strain, induced noninvasively in the high-frequency domain, is anabolic to cancellous bone, but not cortical bone. Bone. 30, 445–452.
Rubin, C., Turner, A.S., Bain, S., Mallinckrodt, C., McLeod, K., 2001. Low mechanical signals strengthen long bones. Nature. 412, 603–604.
Ruff, C., 2003. Ontogenetic adaptation to bipedalism: age changes in femoral to humeral length and strength proportions in humans, with a comparison to baboons. Journal of Human Evolution. 45, 317–349.
Ruff, C., 2009. Relative limb strength and locomotion in Homo habilis. American Journal of Physical Anthropology. 138, 90–100.
Ruff, C., Holt, B., Trinkaus, E., 2006. Who's afraid of the big bad Wolff?: "Wolff's law" and bone functional adaptation. American Journal of Physical Anthropology. 129, 484–498.
Ruff, C.B., 2000. Body size, body shape, and long bone strength in modern humans. Journal of Human Evolution. 38, 269–290.
Ruff, C.B., 2006. Gracilization of the Modern Human Skeleton: The latent strength in our slender bones teaches lessons about human lives, current and past. American Scientist. 94, 508–514.
Ruff, C.B., Burgess, M.L., Bromage, T.G., Mudakikwa, A., McFarlin, S.C., 2013. Ontogenetic changes in limb bone structural proportions in mountain gorillas (Gorilla beringei beringei). Journal of Human Evolution. 65, 693–703.
Ruff, C.B., Burgess, M.L., Junno, J.-A., Mudakikwa, A., Zollikofer, C.P.E., Ponce de León, M.S., McFarlin, S.C., 2018. Phylogenetic and environmental effects on limb bone structure in gorillas. American Journal of Physical Anthropology. 166, 353–372.
Ruff, C.B., Burgess, M.L., Ketcham, R.A., Kappelman, J., 2016. Limb Bone Structural Proportions and Locomotor Behavior in A.L. 288-1 ("Lucy"). PLOS ONE. 11, e0166095.
Ruff, C.B., Hayes, W.C., 1983. Cross-sectional geometry of Pecos Pueblo femora and tibiae—A biomechanical investigation: I. Method and general patterns of variation. American Journal of Physical Anthropology. 60, 359–381.
Ruff, C.B., Runestad, J.A., 1992. Primate Limb Bone Structural Adaptations. Annual Review of Anthropology. 21, 407–433.
Ruff, C.B., Trinkaus, E., Walker, A., Larsen, C.S., 1993. Postcranial robusticity in Homo. I: Temporal trends and mechanical interpretation. American Journal of Physical Anthropology. 91, 21–53.
Rusovici, R., Pendergast, M., O'Brien, J.T., Ghita, I., 2013. Finite element modeling of human clavicle under dynamic loading. Biomed. Eng. 10, 531–537.
Ryan, T.M., Shaw, C.N., 2013. Trabecular bone microstructure scales allometrically in the primate humerus and femur. Proceedings of the Royal Society B: Biological Sciences. 280, 20130172.
Ryan, T.M., Shaw, C.N., 2015. Gracility of the modern Homo sapiens skeleton is the result of decreased biomechanical loading. Proceedings of the National Academy of Sciences. 112, 372–377.

Ryan, T.M., van Rietbergen, B., 2005. Mechanical significance of femoral head trabecular bone structure in Loris and Galago evaluated using micromechanical finite element models. American Journal of Physical Anthropology. 126, 82–96.
Samuel, D.S., Nauwelaerts, S., Stevens, J.M.G., Kivell, T.L., 2018. Hand pressures during arboreal locomotion in captive bonobos (Pan paniscus). Journal of Experimental Biology. 221, jeb170910.
Saparin, P., Scherf, H., Hublin, J.-J., Fratzl, P., Weinkamer, R., 2011. Structural adaptation of trabecular bone revealed by position resolved analysis of proximal femora of different primates. The Anatomical Record: Advances in Integrative Anatomy and Evolutionary Biology. 294, 55–67.
Sarmiento, E., 1994. Terrestrial traits in the hands and feet of gorillas. Am. Mus. Novit. 3091, 1–56.
Sarmiento, E.E., 1985. Functional differences in the skeleton of wild and captive orangutans and their adaptive significance. New York University.
Sarringhaus, L.A., MacLatchy, L.M., Mitani, J.C., 2014. Locomotor and postural development of wild chimpanzees. Journal of Human Evolution. 66, 29–38.
Schulte, F.A., Ruffoni, D., Lambers, F.M., Christen, D., Webster, D.J., Kuhn, G., Müller, R., 2013. Local Mechanical Stimuli Regulate Bone Formation and Resorption in Mice at the Tissue Level. PLOS ONE. 8, e62172.
Schultz, A.H., 1930. The Skeleton of the Trunk and Limbs of Higher Primates. Human Biology. 2, 303–438.
Schultz, A.H., 1937. Proportions, Variability and Asymetries of the Long Bones of the Limbs and the Clavicles in Man and Apes. Human Biology. 9, 281–328.
Sellers, K.C., Middleton, K.M., Davis, J.L., Holliday, C.M., 2017. Ontogeny of bite force in a validated biomechanical model of the American alligator. Journal of Experimental Biology. 220, 2036–2046.
Senut, B., 1985. Functional aspects of Plio-Pleistocene hominid limb bones: implications for taxonomy and phylogeny. Ancestors: The Hard Evidence. 193–201.
Shaw, C.N., Ryan, T.M., 2012. Does skeletal anatomy reflect adaptation to locomotor patterns? cortical and trabecular architecture in human and nonhuman anthropoids. American Journal of Physical Anthropology. 147, 187–200.
Simons, E.L.R., Hieronymus, T.L., O'Connor, P.M., 2011. Cross sectional geometry of the forelimb skeleton and flight mode in pelecaniform birds. Journal of Morphology. 272, 958–971.
Skedros, J.G., Knight, A.N., Farnsworth, R.W., Bloebaum, R.D., 2012. Do regional modifications in tissue mineral content and microscopic mineralization heterogeneity adapt trabecular bone tracts for habitual bending? Analysis in the context of trabecular architecture of deer calcanei. Journal of Anatomy. 220, 242–255.
Smith, A.L., Benazzi, S., Ledogar, J.A., Tamvada, K., Smith, L.C.P., Weber, G.W., Spencer, M.A., Dechow, P.C., Grosse, I.R., Ross, C.F., Richmond, B.G., Wright, B.W., Wang, Q., Byron, C., Slice, D.E., Strait, D.S., 2015a. Biomechanical Implications of Intraspecific Shape Variation in Chimpanzee Crania: Moving Toward an Integration of Geometric Morphometrics and Finite Element Analysis. The Anatomical Record. 298, 122–144.
Smith, A.L., Benazzi, S., Ledogar, J.A., Tamvada, K., Smith, L.C.P., Weber, G.W., Spencer, M.A., Lucas, P.W., Michael, S., Shekeban, A., Al-Fadhalah, K., Almusallam, A.S.,

Dechow, P.C., Grosse, I.R., Ross, C.F., Madden, R.H., Richmond, B.G., Wright, B.W., Wang, Q., Byron, C., Slice, D.E., Wood, S., Dzialo, C., Berthaume, M.A., Casteren, A. van, Strait, D.S., 2015b. The Feeding Biomechanics and Dietary Ecology of Paranthropus boisei. The Anatomical Record. 298, 145–167.

Smith, A.L., Robinson, C., Taylor, A.B., Panagiotopoulou, O., Davis, J., Ward, C.V., Kimbel, W.H., Alemseged, Z., Ross, C.F., 2021. Comparative biomechanics of the Pan and Macaca mandibles during mastication: finite element modelling of loading, deformation and strain regimes. Interface Focus. 11, 20210031.

Smith, B.H., Crummett, T.L., Brandt, K.L., 1994. Ages of eruption of primate teeth: A compendium for aging individuals and comparing life histories. American Journal of Physical Anthropology. 37, 177–231.

Spadaro, J.A., Werner, F.W., Brenner, R.A., Fortino, M.D., Fay, L.A., Edwards, W.T., 1994. Cortical and trabecular bone contribute strength to the osteopenic distal radius. Journal of Orthopaedic Research. 12, 211–218.

Squyres, N., DeLeon, V.B., 2015. Clavicular curvature and locomotion in anthropoid primates: A 3D geometric morphometric analysis. American Journal of Physical Anthropology. 158, 257–268.

Stamos, P.A., Alemseged, Z., 2023. Hominin locomotion and evolution in the Late Miocene to Late Pliocene. Journal of Human Evolution. 178, 103332.

Stamos, P.A., Weaver, T.D., 2020. Ontogeny of the distal femoral metaphyseal surface and its relationship to locomotor behavior in hominoids. American Journal of Physical Anthropology. 172, 462–474.

Stauber, M., Rapillard, L., van Lenthe, G.H., Zysset, P., Müller, R., 2006. Importance of individual rods and plates in the assessment of bone quality and their contribution to bone stiffness. Journal of Bone and Mineral Research. 21, 586–595.

Stephens, N.B., Kivell, T.L., Pahr, D.H., Hublin, J.-J., Skinner, M.M., 2018. Trabecular bone patterning across the human hand. Journal of Human Evolution. 123, 1–23.

Stern, J.T., 2000. Climbing to the top: A personal memoir of Australopithecus afarensis. Evolutionary Anthropology: Issues, News, and Reviews. 9, 113–133.

Stern, J.T., Susman, R.L., 1983. The locomotor anatomy of Australopithecus afarensis. American Journal of Physical Anthropology. 60, 279–317.

Strait, D.S., Richmond, B.G., Spencer, M.A., Ross, C.F., Dechow, P.C., Wood, B.A., 2007. Masticatory biomechanics and its relevance to early hominid phylogeny: An examination of palatal thickness using finite-element analysis. Journal of Human Evolution, Homoplasy in Primate and Human Evolution. 52, 585–599.

Stratovan Corporation, 2018. Checkpoint.

Sugardjito, J., Hooff, J.A.R.A.M. van, 1986. Age-Sex Class Differences in the Positional Behaviour of the Sumatran Orang-Utan (Pongo pygmaeus abelii) in the Gunung Leuser National Park, Indonesia. Folia Primatologica. 47, 14–25.

Swan, K.R., Ives, R., Wilson, L.A.B., Humphrey, L.T., 2020. Ontogenetic changes in femoral cross-sectional geometry during childhood locomotor development. American Journal of Physical Anthropology. 173, 80–95.

Swartz, S.M., 1990. Curvature of the forelimb bones of anthropoid primates: Overall allometric patterns and specializations in suspensory species. American Journal of Physical Anthropology. 83, 477–498.

Swartz, S.M., Parker, A., Huo, C., 1998. Theoretical and empirical scaling patterns and topological homology in bone trabeculae. Journal of Experimental Biology. 201, 573–590.
Swindler, D.R., Wood, C.D., 1973. An atlas of primate gross anatomy: baboon, chimpanzee, and man. University of Washington Press, Seattle.
Thompson, N.E., Rubinstein, D., Larson, S.G., 2018. Great ape thorax and shoulder configuration—An adaptation for arboreality or knuckle-walking? Journal of Human Evolution. 125, 15–26.
Thorpe, S.K.S., Crompton, R.H., 2005. Locomotor ecology of wild orangutans (Pongo pygmaeus abelii) in the Gunung Leuser Ecosystem, Sumatra, Indonesia: A multivariate analysis using log-linear modelling. American Journal of Physical Anthropology. 127, 58–78.
Thorpe, S.K.S., Crompton, R.H., 2006. Orangutan positional behavior and the nature of arboreal locomotion in Hominoidea. American Journal of Physical Anthropology. 131, 384–401.
Thorpe, S.K.S., Crompton, R.H., Günther, M.M., Ker, R.F., Alexander, R.M., 1999. Dimensions and moment arms of the hind- and forelimb muscles of common chimpanzees (Pan troglodytes). American Journal of Physical Anthropology. 110, 179–199.
Toussaint, M., Tobias, P.V., Hughes, A.R., Macho, G.A., Partridge, T.C., 2003. The third partial skeleton of a late Pliocene hominin (Stw 431) from Sterkfontein, South Africa : research articles. South African Journal of Science. 99, 215–223.
Trinkaus, E., Ruff, C.B., 1999. Diaphyseal cross-sectional geometry of Near Eastern Middle Palaeolithic humans: The femur. Journal of Archaeological Science. 26, 409–424.
Trinkaus, E., Ruff, C.B., 2012. Femoral and Tibial Diaphyseal Cross-Sectional Geometry in Pleistocene Homo. PaleoAnthropology. 2012, 12–62.
Tsegai, Z.J., Kivell, T.L., Gross, T., Nguyen, N.H., Pahr, D.H., Smaers, J.B., Skinner, M.M., 2013. Trabecular Bone Structure Correlates with Hand Posture and Use in Hominoids. PLOS ONE. 8, e78781.
Tsegai, Z.J., Skinner, M.M., Gee, A.H., Pahr, D.H., Treece, G.M., Hublin, J.-J., Kivell, T.L., 2017. Trabecular and cortical bone structure of the talus and distal tibia in Pan and Homo. American Journal of Physical Anthropology. 163, 784–805.
Tsegai, Z.J., Skinner, M.M., Pahr, D.H., Hublin, J.-J., Kivell, T.L., 2018. Ontogeny and variability of trabecular bone in the chimpanzee humerus, femur and tibia. American Journal of Physical Anthropology. 167, 713–736.
Tseng, Z.J., Garcia-Lara, S., Flynn, J.J., Holmes, E., Rowe, T.B., Dickson, B.V., 2023. A switch in jaw form–function coupling during the evolution of mammals. Philosophical Transactions of the Royal Society B: Biological Sciences. 378, 20220091.
Tuttle, R.H., Basmajian, J.V., 1978. Electromyography of pongid shoulder muscles. III. Quadrupedal positional behavior. American Journal of Physical Anthropology. 49, 57–69.
Visualizations Sciences Group, 2017. Avizo Lite.
Voisin, J., 2015. Australopithecines shoulders: new remains for old debate. Recent discoveries and Perspectives in Human Evolution, Bar International Series S. 2719, 11–21.
Voisin, J.-L., 2006a. Clavicle, a neglected bone: Morphology and relation to arm movements and shoulder architecture in primates. The Anatomical Record Part A: Discoveries in Molecular, Cellular, and Evolutionary Biology. 288A, 944–953.

Voisin, J.-L., 2006b. Krapina and Other Neanderthal Clavicles : A Peculiar Morphology? Periodicum Biologorum. 108, 331.
Voisin, J.-L., 2008. The Omo I hominin clavicle: Archaic or modern? Journal of Human Evolution, Paleoanthropology of the Kibish Formation, Southern Ethiopia. 55, 438–443.
Voisin, J.-L., Feuerriegel, E.M., Churchill, S.E., Berger, L.R., 2020. The Homo naledi shoulder girdle: an adaptation to bouldering. The Anthropology. 124, 102783.
Wang, F., Metzner, F., Osterhoff, G., Zheng, L., Schleifenbaum, S., 2022. The role of bone marrow on the mechanical properties of trabecular bone: a systematic review. BioMedical Engineering OnLine. 21, 80.
Ward, C.V., 2002. Interpreting the posture and locomotion of Australopithecus afarensis: Where do we stand? Yearbook of Physical Anthropology. 45, 185–215.
Ward, C.V., 2013. Postural and Locomotor Adaptations of Australopithecus Species. In: Reed, K.E., Fleagle, J.G., Leakey, R.E. (Eds.), The Paleobiology of Australopithecus, Vertebrate Paleobiology and Paleoanthropology. Springer Netherlands, Dordrecht, pp. 235–245.
Wilken, A.T., Middleton, K.M., Sellers, K.C., Cost, I.N., Holliday, C.M., 2019. The roles of joint tissues and jaw muscles in palatal biomechanics of the savannah monitor (Varanus exanthematicus) and their significance for cranial kinesis. Journal of Experimental Biology. 222, jeb201459.
Williams, S.A., 2010. Morphological integration and the evolution of knuckle-walking. Journal of Human Evolution. 58, 432–440.
Young, N.M., 2008. A comparison of the ontogeny of shape variation in the anthropoid scapula: functional and phylogenetic signal. American Journal of Physical Anthropology. 136, 247–264.
Zawin, J., Jaramillo, D., 1993. Conversion of bone marrow in the humerus, sternum, and clavicle: changes with age on MR images. Radiology. 188, 159–164.
Zelditch, M.L., Swiderski, D., Sheets, H.D., 2012. Geometric Morphometrics for Biologists: A Primer, 2nd edition. ed. Academic Press, Amsterdam.
Zipfel, B., Richmond, B.G., Ward, C.V., 2020. Hominin Postcranial Remains from Sterkfontein, South Africa, 1936-1995. Oxford University Press.